The Durability of Fly Ash Geopolymer and Alkali-Activated Slag Concretes

Arie Wardhono
B.Sc, M. Em., M.Eng

School of Civil Environmental and Chemical Engineering

College of Science Engineering and Health

RMIT University

January 2015

DECLARATION

I certify that except where due acknowledgement has been made, the work is that of the author alone; the work has not been submitted previously, in whole or in part, to qualify for any other academic award; the content of the thesis is the result of work which has been carried out since the official commencement date of the approved research program; any editorial work, paid or unpaid, carried out by a third party is acknowledged; and, ethics procedures and guidelines have been followed.

Arie Wardhono

15 January 2015

ACKNOWLEDGMENTS

I would like to express my sincerest gratitude to my senior supervisor, A./Prof. Thomas C.K. Molyneaux and my second supervisor, Dr. David W. Law, for their invaluable support, guidance and suggestion throughout this research.

I would also like to express my gratitude to the Ministry of National Education Indonesia for the DIKTI scholarship and the support from my home institution, State University of Surabaya (Universitas Negeri Surabaya) Indonesia, for the opportunity to come to Australia to study as a full-time post-graduate research student. I am very grateful for all the support that I received throughout my candidature.

I really appreciate the support from Pavel Rijkov as Civil Engineering laboratory coordinator and Peg Gee Chang as Chemical Engineering laboratory coordinator for giving me access to all facilities in civil and chemical engineering laboratories of RMIT University. In addition, I would like to thank the support from Civil Engineering laboratory staffs (i.e. Saravanan Mani, Xiang Gao, Kevin Dung Le, Ramesh Dilipsingh, Bao Thach Nguyen and Kee Kong Wong), Chemical Engineering laboratory staffs (i.e. Cameron Crombie, Sandro Longano and Muthu Pannirselvam) and Mike Allan from Rheology & Materials Processing Centre (RMCP) in preparing equipment and facilities to conduct my laboratory experiments. In addition, I express my appreciation to Phillip Francis, Peter Rummel and the staff of RMIT Microscopy & Microanalysis Facility at RMIT University who trained me very well, helped and gave me access to conduct the micro-structure analysis throughout my candidature. I would like also to thank Daniel Kong for the discussion and providing the solution regarding the casting of fly ash geopolymer concrete. Further, I would like to thank to Cement Australia, Independence Cement and PQ Australia for supplying the materials for this research.

I also appreciate the assistance of the administrative staff at School of Civil, Chemical and Environmental Engineering (SCECE) of RMIT University. I wish to particularly acknowledge Marlene Mannays, Nhol Kao, Sharon Taylor, Louise Cini, Michael Jacobi and Charles Welcome who ably minded post-graduates

welfare and provided me with comfortable and conducive working environment at RMIT University during my candidature.

My family has been a dependable source of support. My deepest gratitude is for my wife, Enny Kurniawati, for her love, support, patience and encouragement, especially in difficult times. My parents, Bapak Suwarno and Ibu Endang Ariadi, and my mother-in-law, Ibu Siti Mudjiatun, for their endless love and prayers. My brother, Adie Prabowo & his family, and my brother-in-law, Kurniawan & his family, for their supports. I cannot conclude without mentioning the Indonesian communities in Melbourne, Victoria, who made my family and I have felt very much at home.

The last and the most important, all the achievement is made possible only because of the mercy of Allah Lord of world, all praise is due to Allah Lord of world.

ABSTRACT

The implementation of sustainable development in civil engineering society has led to the use of new materials with low environmental impact. Traditionally Ordinary Portland cement (OPC) is the primary material used in the production of concrete. However, the manufacture of OPC has led to environmental concerns over the energy needed to produce the material, the depletion of the quarried resources and the production of CO_2. This has led to the use of fly ash and slag, waste products, as cement replacement materials due to their characteristic pozzolanic and latent hydraulic properties. Recent research has shown that it is possible to develop concrete based solely on fly ash and slag activated directly by alkali solution, without the presence of OPC, known as fly ash geopolymer and alkali-activated slag (AAS). A major benefit is that the greenhouse gas emissions produced by fly ash geopolymer and AAS are reduced compared to those of OPC, which depends on the limestone calcination process and produces around 5% of worldwide greenhouse emissions.

In this research, the mechanical and durability properties of fly ash geopolymer and AAS concretes have been studied. The study has focussed on the relationship between durability and the mechanical properties of fly ash geopolymer and AAS concretes over the long term. The micro-structure was also studied to support the analysis. The existing concrete codes and standards (Australian Standard, and Concrete Institute of Australia recommended practice for fly ash geopolymer concrete) have also been studied to assess their validity when predicting material properties for these new materials.

The results show that fly ash geopolymer and AAS concretes exhibit a comparable compressive strength, lower modulus of elasticity but higher tensile strength compared to OPC concrete. In terms of mechanical properties, the short term behaviour of AAS concrete is better than fly ash geopolymer concrete, however fly ash geopolymer concrete shows

a better performance in the long term. The AAS concrete exhibits a reduction in strength over time due to the development of micro-cracks which leads to inferior strength in the long term, while the fly ash geopolymer concrete strength shows an improvement in strength with age due to the slow formation of the geopolymeric network. In terms of durability properties (permeation, resistance to chloride and carbonation), AAS concrete demonstrates a better performance compared to fly ash geopolymer concrete. However in the longer term the growth of the micro-cracks with time raises a question about the long term performance of AAS concrete. The existing Australian Standard should not be applied to AAS concretes due to the reduction in performance over time. However in the case of fly ash geopolymer concrete, the standard may conservatively be applied to the prediction of tensile strength but not to the prediction of modulus of elasticity which the standard over-predicts.

LIST OF PUBLICATIONS

Content of the thesis has been published in the following papers.

Wardhono, D.W. Law and T.C.K Molyneaux, 2012, "*Strength of alkali activated slag and fly ash-based geopolymer mortars*", in Proceeding of the Microdurability "The 2nd International Conference on Microstructural-related Durability of Cementitious Composites", in Amsterdam, The Netherlands, 11-13 April 2012.

Arie Wardhono, David W. Law and Thomas C.K. Molyneaux, 2013, "*Durability and mechanical properties of alkali activated slag concrete in long term performance*" in Proceedings of the ICCS13 "The 1st International Conference on Concrete Sustainability", in Tokyo, Japan, 27-29 May 2013.

Arie Wardhono, David W. Law and Thomas C.K. Molyneaux, 2014, "*The mechanical properties of fly ash geopolymer as cement replacement in long term performance*" in the CIC 2014 "Concrete Innovation Conference, in Oslo, Norway, 11-13 June 2014.

Arie Wardhono, David W. Law and Thomas C.K. Molyneaux, 2015, "*Mechanical properties of alkali activated slag concrete in long term performance*", Journal of Advance Concrete Technology (ACT) (*accepted paper).*

Arie Wardhono, David W. Law and Thomas C.K. Molyneaux, 2015, "*The effect of silicate of fly ash geopolymer strength development*", ACI Materials Journal (*submitted paper).*

TABLE OF CONTENTS

LIST OF FIGURES

LIST OF TABLES

LIST OF TERMS AND ABBREVIATIONS

AAS	Alkali-activated slag
C-S-H	Calcium Silicate Hydrate
C	The carbonation rate coefficient
C_s	Chloride surface concentration
D_a	Chloride diffusion coefficient
EDX	Energy Dispersive X-ray Spectroscopy
FA	Fly ash
GGBS	Ground Granulated Blast Furnace-Slag
HM	Hydration Modulus
Kb	Basicity coefficient
Ms	Modulus of activator
OPC	Ordinary Portland Cement
RH	Room humidity
SEM	Scanning Electron Microscopy
SSD	Saturated Surface Dry
UPV	Ultrasonic Pulse Velocity
w/b	Water to binder ratio
w/s	Water to solid ratio
X	Depth of carbonation

1. INTRODUCTION

1.1. Background

The drive by society for sustainable development has led to the use of new construction materials with low environmental impact. Historically concrete has been the most widely used construction material in civil engineering projects. The production of traditional concrete involves the use of the ordinary Portland cement (OPC) as the primary binder with OPC being approximately 10% – 15% by mass of concrete. However, there are well established environmental concerns regarding the production of OPC.

The annual global production of OPC was estimated to be 3.5 billion metric ton in 2005 and predicted to increase, due to global demand, particularly due to the growth in the developing countries, to 4.1 billion by 2013 (Freedonia Group, 2010) while by 2050, it was predicted to be three times the demand in 2005 (Humphreys & Mahasenan, 2002). The increasing demand of OPC production has led to environmental problems over the CO_2 emissions with approximately 0.7 – 1 ton of CO_2 produced per 1 ton of OPC (Davidovits, 1994, Berry et al., 2009). In addition, this OPC production also impacts on the environment due to the depletion of natural quarries (i.e. limestone). Another issue is the implementation of carbon tax regulations coming into effect in a number of countries which has encouraged the search for more environmentally viable alternative materials.

The use of low calcium fly ash (class F fly ash) and ground granulated blast furnace slag (GGBS), the most commonly used industrial by-products as replacement for OPC, has contributed to a reduction in environmental impact (Davidovits, 1994). The utilisation of fly ash in concrete has helped to enhance the mechanical and chemical properties of concretes, while GGBS has been used as cement replacement materials to provide higher durability (Swamy, 1986). Recent research has also shown that it is possible to develop a concrete based on low calcium fly ash and GGBS activated directly by alkali solution utilising sodium silicate (Na_2SiO_4), sodium hydroxide (NaOH), waterglass or sodium carbonate (Na_2CO_3) as the activator without the presence of OPC (Talling & Brandstetr, 1989, Roy, 1999, Bakharev et al., 1999a, Hardjito et al.,

2004, Adam et al., 2007, Wardhono et al., 2012). A major benefit is that the greenhouse gas emission produced is reduced compared to Portland cement production (PC), which depends on the limestone calcination process and produces around 5% of worldwide greenhouse emissions (Gartner, 2004).

The development and properties of fly ash geopolymer and alkali-activated slag (AAS) concretes have been investigated in a number of papers. In terms of mechanical properties, the properties of concrete strength are normally represented by compressive strength, tensile strength and modulus of elasticity (AS 3600, 2009). Recent research has shown that fly ash geopolymer and AAS concretes can achieve a comparable strength and display similar characteristics in their mechanical properties over shorts periods of time.

Fly ash geopolymer concrete has been observed to have a comparable compressive strength and modulus of elasticity compared to OPC concrete. It has also been found that fly ash geopolymer concrete can develop similar flexural strength behaviour to that of OPC concrete. Most of the studies, however, have been focussed on the short term behaviour of fly ash geopolymer, and only limited studies have been conducted on the long term performance. This similar behaviour compared to OPC concrete has indicated that existing concrete regulations for OPC concrete might be applicable for fly ash geopolymer concrete (Hardjito et al., 2004, Hardjito & Rangan, 2005, Fernandez-Jimenez et al., 2006, Rangan et al., 2006, Sumajouw & Rangan, 2006, Adam, 2009, Sagoe-Crentsil et al., 2010, Diaz-Loya et al., 2011, Neupane et al., 2014). However, it should be noted that the strength development of fly ash geopolymer depends on the impact of the initial silicate aluminate ratio (Si/Al ratio) on the geopolymerisation reaction. The strength achieved being a result of the reaction between the raw fly ash material and the alkaline activators used. An increase in the Si/Al ratio tends to reduce the strength and to prolong the setting time due to the increase of the silicate content availability and the condensation rate of the polymeric structures (Fletcher et al., 2005, Silva et al., 2007).

For AAS concrete, it was found that AAS concrete developed a comparable compressive strength and a higher flexural strength to that OPC concrete over short periods of time. The behaviour of AAS concrete was also shown to have a comparable strength to OPC concrete up to 180 days. Moreover, in comparison with fly ash geopolymer concrete, AAS concrete exhibited much higher

compressive strength for the same mixing condition. However, other research has found visible micro-cracks on the AAS surface which indicate a considerably higher total porosity for AAS concrete. These micro-cracks could lead to inferior compressive strength over long periods of time (Collins & Sanjayan, 1999, Bakharev et al., 1999a, Collins & Sanjayan, 2001, Adam, 2009, Yang et al., 2009, Bernal et al., 2012).

The durability of concrete has been considered as important as material strength since the failures of concrete structures are not only caused by excessive force, but also due to the deterioration of structural components. In long term performance, the permeation properties are highly important in controlling the durability of concrete in order to resist the ingression of deleterious substances into the concrete (Basheer et al., 2001). The corrosion of embedded steel reinforcement as the result of the ingress of moisture or aggressive ions into a concrete has been considered as the major cause of the deterioration mechanism in concrete (Miranda et al., 2005). Further, it was also demonstrated by other researcher that the main source of concrete deterioration was caused by carbonation and chloride attack which has led to the corrosion of the steel reinforcement (Basheer et al., 1996).

The durability resistance of fly ash geopolymer and AAS concretes to aggressive agents, such as chloride and carbonation attack, has been widely studied. The research has shown that fly ash geopolymer and AAS concretes have a satisfactory performance in the short term and could be suitable alternative materials to OPC concretes (Bakharev et al., 2001, Miranda et al., 2005, Law et al., 2012).

In order to be a potential alternative to traditional concrete replacement, fly ash geopolymer and AAS concretes must demonstrate comparable durability properties in resisting the attack and ingression from aggressive agents in the long term. However, research has shown that the fly ash geopolymer concrete can exhibit a numbers of small pores due to the un-reacted fly ash (Collins & Sanjayan, 2001, Kong et al., 2007) raising questions about the long term performance. Thus questions remain concerning the long term performance of both fly ash geopolymer concrete and AAS concrete which need investigating prior to their adoption as an alternative construction material to traditional concrete.

1.2. Aim of the research

The aim of the research is to evaluate the long term performance of fly ash geopolymer and AAS concretes with regard to their mechanical and durability properties. In addition, the evaluation of the application of existing concrete standards in Australia towards the use of fly ash geopolymer and AAS concretes will be examined.

1.3. Research objectives

The objectives of the research are listed below:

1) Evaluation of the long term performance of fly ash geopolymer and AAS concretes in terms of mechanical and durability properties.
2) Comparison of the use of two different materials (i.e. fly ash and slag), as 100% cement replacement materials in fly ash geopolymer and AAS concretes.
3) Evaluation of the existing concrete standard (i.e. Australian Standard) with regard to the use of fly ash geopolymer and AAS concretes in terms of engineering properties.

1.4. Scope of the thesis

To study the long term performance of the mechanical and durability properties of fly ash geopolymer and AAS concretes.

Initially a series of mortar experiments were carried out, as preliminary research, to establish the type of activator, the dosage and the modulus of alkaline activator. The preliminary research was based on the previous research project carried out at RMIT University on the short term performance of fly ash-based geopolymer and AAS concretes (Adam, 2009). The best results of fly ash geopolymer and AAS mortars from the preliminary research were used to develop fly ash geopolymer and AAS concretes for the long term tests.

In the next stage, the research investigated the long term performance of the mechanical properties of the fly ash geopolymer and AAS concretes. The properties investigated were compressive strength, modulus of elasticity, modulus of rupture and indirect tensile strength. The appropriateness of the existing concrete standards (i.e. Australian Standard and Concrete Institute

Australia recommended practice for geopolymer concrete) for fly ash geopolymer and AAS concretes have also been assessed.

The durability properties of fly ash geopolymer and AAS concretes were investigated by testing the porosity, the water absorption, the water permeability, the density, the resistivity, the chloride diffusion characteristics and the carbonation resistance. Furthermore, the microstructure of the fly ash geopolymer and AAS concretes was assessed using Scanning Electron Microscopy (SEM) and Energy Dispersive X-Ray Spectroscopy (EDX) analysis.

1.5. Outline of the thesis

The thesis is organised into seven chapters, as describes below:

Chapter one describes the rationale for investigating the long term performance of the mechanical and durability properties of fly ash geopolymer and AAS concretes. In addition, the aim, objectives and the scope of this research are also presented.

Chapter two presents the information from the existing literature on the impact of OPC production on the environment, the use of fly ash and slag in concrete as cement replacement materials, the history of alkali activation of cementitious material, the reaction mechanism and properties of fly ash geopolymer and AAS concretes, the type of material (i.e. fly ash and slag) suitable for alkali-activated binder for fly ash geopolymer and AAS concretes and the mechanical and the durability properties of fly ash geopolymer and AAS.

Chapter three describes the materials which are used to produce the fly ash geopolymer and AAS concretes. In addition, the experimental methods of concrete testing of the mechanical and durability properties are also presented.

Chapter four explores the feasibility of using fly ash and slag as 100% cement replacement material. The discussion of the experimental studies on the strength development of fly ash geopolymer and AAS mortars as preliminary research is also reported.

Chapter five elaborates the result of the mechanical and durability properties test of fly ash geopolymer concrete in long term performance. The mechanical properties comprise of compressive strength, modulus of elasticity, flexural tensile strength and indirect tensile strength. In addition, the discussion on the

long term performance of the mechanical properties of fly ash geopolymer concrete is also presented. While, the durability test comprises of porosity, water absorption, water permeability, density, ultrasonic pulse velocity, resistivity, chloride diffusion and depth of carbonation.

Chapter six discusses the result of the mechanical and durability properties test of AAS concrete in long term performance. The same mechanical and durability properties test procedures as used for fly ash geopolymer concrete are applied for AAS concrete.

Chapter seven discusses the result of the microstructure analysis of fly ash geopolymer and AAS concretes based on the Scanning Electron Microscopy (SEM) and Energy Dispersive X-Ray Spectroscopy (EDX) analysis. The discussion of the relationship between the microstructure and the mechanical and durability properties is also reported.

Chapter eight summarises the main findings and presents conclusions of the research in regard to the durability of fly ash geopolymer and AAS concretes in long term performance. This chapter also presents recommendations for further research.

2. LITERATURE REVIEW

2.1. Environmental issues related to concrete production

Approximately 80% of total embodied greenhouse gas emissions in concrete is attributable to the production of Portland cement (Flower & Sanjayan, 2007). The contribution of Portland cement production to worldwide greenhouse gas emissions is 1.6 billion tons or estimated to be about 7% (Mehta, 2001, Berry et al., 2009). This is directly as a result of the calcination of limestone in the kiln during the manufacturing process and fossil fuel combustion (Roy, 1999). In addition, the process of Portland cement manufacture is an energy intensive process (Berry et al., 2009). In Australia, the total greenhouse gas emissions from the production of Portland cement increased by 5.2% between 1990 and 2005 (Australian Greenhouse Office, 2007).

Global cement production is expected to rise 4.1% yearly through 2013 and expected to reach 3.5 billion metric tons, with the Asia/Pacific accounting for 69%, Africa/Middle East 12%, Western Europe 6%, North America 5% and other regions 8% (Freedonia Group, 2010). The highest growth of demand is expected to be in Asian countries where investment in infrastructure is still lagging behind other regions. According to the U.S. Geological Survey (U.S. Geological Survey, 2012), China accounted for 56% of global cement consumption in 2010, approximately 28 times the consumption of the U.S. The cement consumption in China alone accounts for as much as the combined consumption of the other top ten countries as shown in **Figure 2.1**. It is even exceeding India, which has a comparable population to China, possibly due to the deficit of the availability of raw materials.

The need to reduce the environmental impact of concrete production has been recognised by the industry. The U.S. concrete industry has developed plans to address these issues in a report “Vision 2030: A Vision for the U.S. Concrete Industry” (Mehta, 2001). The report states that ‘*concrete technologists are faced with the challenge of leading future development in a way that protects environmental quality while projecting concrete as a construction material of choice. Public concern will be responsibly addressed regarding climate change resulting from the increased concentration of global warming gases*’. In this

report, strategies to maintain concrete as a construction material and simultaneously to consider the impact of concrete on the environment are discussed (Mehta, 2001, Plenge, 2001).

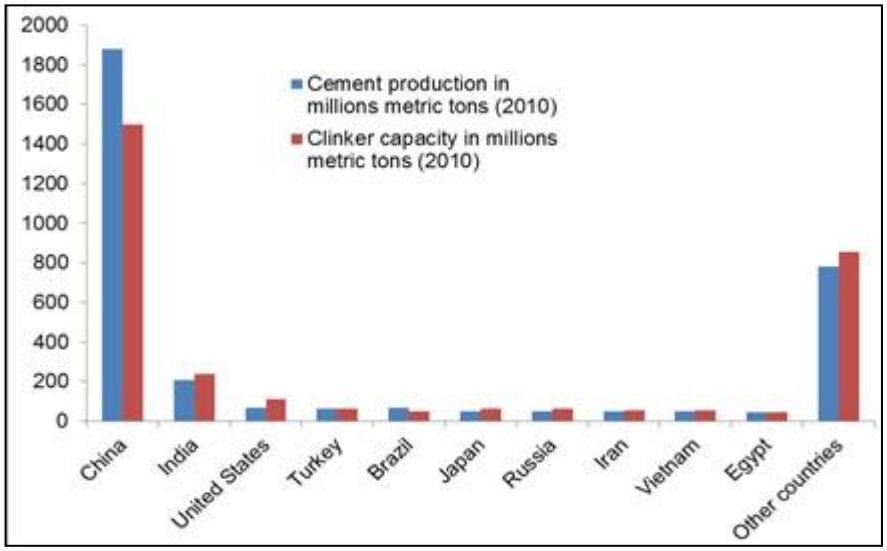

Source: (U.S. Geological Survey, 2012)

Figure 2.1 Top 10 countries in cement production

In order to reduce the environmental impact of the concrete industry, Mehta (2002) suggests two approaches, a short term and a long term approach. The short term approach would be to practise "*industrial ecology*" which involves the use of industrial by-products as cement replacement materials. The long term approach would be to lower the rate of material consumption. The environmental impact of the concrete industry may also be reduced by improving the durability of concrete products and by conserving materials and energy in concrete production (Mehta, 2002).

Likewise, in order to meet the environmental challenge in concrete production, Meyer (2009) suggests replacing as much Portland cement as possible with supplementary cementitious materials, especially those that are by-products of industrial processes, such as fly ash, ground granulated blast furnace slag, and silica fume. In addition, McCaffrey (2001) proposed three mechanisms to reduce the amount of carbon dioxide (CO_2) emissions by the cement industries, i.e. to decrease the proportion of calcined material in cement, to decrease the

proportion of cement in concrete, and to decrease the number of buildings using cement.

2.2. The use of fly ash and slag in concrete

The use of fly ash as a binder in concrete has led to many advantages in concrete properties, both in fresh concrete and hardened concrete (Onera et al., 2005). The advantages in fresh concrete are an increase in the workability, a reduction in the water requirement, reduced bleeding, and retarded time to set. In hardened concrete, fly ash contributes in continuing the pozzolanic activity of hardened concrete to gain higher strength at later ages. This is due to the reaction of fly ash with the $Ca(OH)_2$ after it releases from the hydration process of Portland cement. In terms of durability properties, concrete incorporating fly ash demonstrates improved durability characteristics due to the combined action of the increase in cementitious compounds and the reduction in permeability which leads to a better performance in sulphate attack and chloride ingression (Neville, 2011).

The advantages of using fly ash in concrete are not only in achieving high strength and high performance, but also in reducing the carbon dioxide (CO_2) released to the atmosphere during production.

Ground granulated blast-furnace slag (GGBS), a waste product from the steel manufacturing process, is used as a cement replacement material due to its latent hydraulic properties. The advantages in fresh concrete are improved workability and lower heat of hydration. A lower heat of hydration reduces the risk of thermal cracking in large pours. In hardened concrete, the advantages of using GGBS are improved micro-structure leading to increased long term strength and durability. This improvement is due to the reaction between GGBS with the excess $Ca(OH)_2$ to form a finely dispersed gel which fills the larger pores in the concrete. The result is a hardened cement paste, which contains fewer $Ca(OH)_2$ crystals and thus fewer large capillary pores. The reduction in free $Ca(OH)_2$ makes concrete chemically more stable, and the finer pore structure limits the ability of aggressive chemicals to diffuse through the concrete which contributes to the high resistance to chloride ingress, sulphate attack and alkali-silica reaction (Neville, 2011).

The benefits offered by fly ash or GGBS coupled with the concern of environmental issues in the construction industry have led to intensive study on the activation of fly ash or GGBS with alkaline solutions, such as sodium silicate and sodium hydroxide, which produces a binding material similar to cement (Hardjito, 2005). This new type of binder has brought forth the production of concrete without the use of Portland cement.

2.3. Alkali-activated cementitious materials

The history of alkali-activated cement is summarised in **Table 2.1** (Roy, 1999). Alkali-activated cements research started with the work of Feret in 1939 and Purdon in 1940. In 1959, Glukhovsky published the term “soil cements” for the binders and “soil silicates” for the concrete. Based on the starting materials, the alkaline cements were categorized into two groups: an alkaline binding system Me_2O-Me_2O_3-SiO_2-H_2O and an alkaline-earth alkali binding system Me_2O-MeO-Me_2O_3-SiO_2-H_2O. In 1979, a new type of binder, a mixture between alkalis and kaolinite, limestone and dolomite, similar to the alkaline binding system was introduced by Davidovits. As the product of the binder was more polymer than the other alkali-activated binding system, the term of “geopolymer” was adopted to emphasize the polymerisation reaction (Davidovits, 1991, Davidovits, 1994b, Roy, 1999, Shi et al., 2006).

Table 2.1 Bibliography of alkali-activated cements

Author(s)	Year	Significance
Feret	1939	Slags used for cement
Purdon	1940	Alkali-slag combinations
Glukhovsky	1959	Theoretical basis and development of alkaline cements
Glukhovsky	1965	First called “alkaline cements”
Davidovits	1979	“Geopolymer” term – emphasizes greater polymerization
Krivenko	1986	D.Sc. Thesis, R_2O-RO-R_2O_3-SiO_2-H_2O
Davidovits	1987	Ancient and modern concrete compared
Talling and Brandstetr	1989	Alkali-activated slag
Wu et al.	1990	Activation of slag cement
Roy and Malek	1993	Slag cements
Glukhovsky	1994	Ancient, modern and future concretes
Krivenko	1994	Alkaline cements

Source: Table 1 page 250 (Roy, 1999)

The term alkali activation is used to imply that alkali or alkali earth ions have been used as activators to stimulate the pozzolanic reaction or release the latent cementitious properties of finely divided inorganic materials using industrial by-products consisting mainly of silicates, alumina-silicates and calcium (Jiang, 1997).

Palomo et al. (1999) classifies the models of alkali activation into two different models. First, the activation of slag, containing primarily silicate (Si) and calcium (Ca), involving a low to mild alkali solution and second, the activation of fly ash, containing primarily silicate (Si) and aluminates (Al), using a high concentration alkali solution. The main hydration product of the first approach is a calcium silicate hydrate (C-S-H) gel, similar to that formed in OPC, however with a low Ca/Si ratio (Wang & Scrivener, 1995, Brough & Atkinson, 2002). The second mechanism involves the formation of an inorganic cementitious like material through a polymerisation process designated as a geopolymer reaction (Barbosa et al., 2000, Xu, 2002). The mechanism of geopolymerisation involves the polycondensation reaction of alumino-silicate oxide as a precursor, with alkali polysialates producing polymeric Si-O-Al bonds (Pacheco-Torgal et al., 2008). The term geopolymer was coined by Davidovits (Davidovits, 1991) and is used to differentiate the geopolymer reaction from other types of alkali-activated material (e.g. alkali-activated slag) since the hydration product is more polymer than C-S-H gel.

2.4. Fly ash geopolymer

2.4.1. Introduction to fly ash

According to ASTM C618-03 (2003), fly ash is defined as “the finely divided residue that results from the combustion of ground or powdered coal and that is transported by flue gasses”. In a power plant, fly ash is removed by the dust collection system as fine particles, predominantly spherical glassy particles, before they would be released into the atmosphere. The diameter of fly ash particles range from 1 μm – 150 μm and the size is affected by the type of dust collection system and is generally finer than that of ordinary Portland cement (Siddique, 2008).

The major chemical composition of fly ash is silica (SiO_2), alumina (Al_2O_3) and ferric oxide (Fe_2O_3). Other minor constituents of fly ash are oxides of calcium

(CaO), magnesium (MgO), sulphur (SO_3), alkaline (Na_2O, K_2O), phosphorus (P_2O_5), manganese (Mn_2O_3) and titanium (TiO_2). ASTM C618-03 categorises fly ash into three types based on the major chemical substances, i.e. class N, class F and class C as shown in **Table 2.2**. The minimum requirement of SiO_2, Al_2O_3 and Fe_2O_3 is 70% for class N and class F fly ashes, while in class C, the minimum amount of SiO_2, Al_2O_3 and Fe_2O_3 is between 50% – 70%. Furthermore, the CaO content in class N and class F fly ashes are low, whereas class C fly ash may content CaO higher than 10% (ASTM C618-03, 2003).

Table 2.2 Chemical requirements of fly ash (ASTM C618-03, 2003)

Requirements	Class		
	N	F	C
Silicon dioxide (SiO_2) plus aluminum oxide (Al_2O_3) plus iron oxide (Fe_2O_3), min, %	70.0	70.0	50.0
Sulfur trioxide (SO_3), max, %	4.0	5.0	5.0
Moisture content, max, %	3.0	3.0	3.0
Loss on ignition, max, %	10.0	6.0	6.0

Class F and class C fly ashes are the product of burning coal in power plants. Class F fly ash is typically generated from burning anthracite or bituminous coal and has pozzolanic properties due to the high content of SiO_2 and Al_2O_3 with a low content of CaO. On the other hand, class C fly ash is generally produced from lignite or sub-bituminous coal and has both pozzolanic and cementitious properties as the result of a high content of CaO with a low SiO_2 and Al_2O_3 content (Ramachandran, 1995).

2.4.2. Research on alkali-activated alumino-silicate

The research on alkali-activated alumina-silicate was started in the 1950's by Glukhovsky who first introduced the use of alkali alumina-silicates (Shi et al., 2006). However, the research on the alkali-activated alumino-silicate materials became a major interest after the term "geopolymer" was introduced by Davidovits (1991). As a new type of binder, the name "geopolymer" was established by Davidovits (1994b) to distinct geopolymer from alkali-activated alumino-silicate. However, most researchers prefer the name "geopolymer" to

name all the alkali-activated siliceous-aluminous binders. Geopolymers are formed when alumino-silicates dissolve in a strong base, reorganize and precipitate in a hardened state (Davidovits, 1991, Duxson et al., 2007a). The properties of geopolymers are very similar to Portland cement when formed under suitable conditions (Sofi et al., 2007).

Xu & Deventer (2000) found that naturally occurring Al-Si minerals could be a source materials for geopolymers. However, it was also found that the reaction mechanism of the geopolymer process involving the dissolution, gel formation, setting and hardening phases are extremely complex and require a great deal of further research. It is still not possible to predict quantitatively whether or not a specific Si-Al mineral will indeed be suitable for geopolymerisation.

Many researchers have used metakaolin as a source material of alumino-silicate for geopolymer production due to its pure alumino-silicate content (Davidovits, 1991, Barbosa et al., 2000, Xu & Deventer, 2000, Alonso & Palomo, 2001, Barbosa & MacKenzie, 2003, Wang et al., 2005, Duxson et al., 2006, Duxson et al., 2007b, Silva et al., 2007, Yip et al., 2008). Slavik et al. (2008) also demonstrates that coal bottom ash can be used to produce geopolymer material with an acceptable durability towards freeze-thaw and wet-dry tests. However, due to a limited availability and a high cost of metakaolin, most of the recent research on geopolymer materials has focussed on fly ash due to its wide and plentiful availability (Palomo et al., 1999, Swanepoel & Strydom, 2002, Hardjito et al., 2004, Hardjito, 2005, Hardjito & Rangan, 2005, Steveson & Sagoe-Crentsil, 2005, Fernandez-Jimenez et al., 2005a, Sun, 2005, Rangan et al., 2006, Sumajouw & Rangan, 2006, Song, 2007, Adam, 2009, Diaz-Loya et al., 2010).

2.4.3. Hydration product and reaction mechanism

The term “geopolymer” was first created and applied by Davidovits in reference to alumina-silicate polymers with an amorphous microstructure. He also suggested the term of poly(sialate) for the chemical designation of geopolymer based on silico-aluminates (Davidovits, 2002). Sialate is the abbreviation for silicon-oxo-aluminate in which the alkali is sodium (Na^+), potassium (K^+), lithium (Li^+) or calcium (Ca^{2+}). Polysialates are chain and ring polymers with Si^{4+} and Al^{3+} in IV-fold coordination with oxygen and range from amorphous to semi-crystalline (Davidovits, 1994b). Polysialates have the empirical formula:

$$M_n(-(SiO_2)_z-AlO_2)_n.wH_2O \qquad (2.1)$$

where (M) is a cation and (n) is a degree of polycondensation. The amorphous to semi-crystalline three dimensional silico-aluminate structures are defined as "geopolymer" and categorised based on the ratio of Si/Al as shown in **Figure 2.2** (Davidovits, 2002).

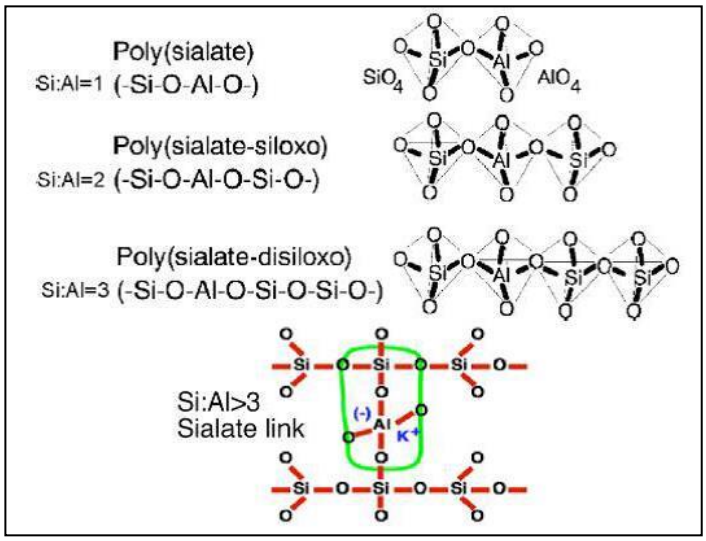

Figure 2.2 The chemical structures of polysialates (Davidovits, 2002)

Instead of hydration process as in the case of OPC based binders, the hardening process of geopolymer normally occurs through a polymerisation process. The complete step-by-step reaction kinetics involved in the geopolymerisation reaction in hardening process is still being studied by most researchers.

In the 1950's, Glukhovsky proposed a general mechanism for the alkali activation of materials containing primarily silica and reactive alumina (Li et al., 2010). In this model, the geopolymerisation process is divided into three stages:

- Destruction – coagulation stage
- Coagulation – condensation stage
- Condensation – crystallisation stage

The first stage of the geopolymer reaction involves the breakdown of the covalent bonds of Si-O-Si and Al-O-Si, and produces a colloid phase. in the next stage,

the accumulation of the breakdown products interact among themselves forming a coagulate structure which lead to the final stage of generation of a condensed structure and crystallisation (Li et al., 2010).

Duxson et al. (2007a) proposed another reaction mechanism model for geopolymerisation reaction (**Figure 2.3**). The model outlines the main processes in the transformation of a solid alumina-silicate source into a synthetic alkali alumina-silicate which consist of:

- Dissolution,
- Special equilibrium,
- Gelation,
- Reorganization, and
- Polymerization and hardening

In the geopolymerisation reaction, the dissolution mechanism starts with an initial attack by the alkaline solution on the fly ash particles (Fernandez-Jimenez et al., 2005a). The reaction products are generated both inside and outside the shell of the sphere, until the fly ash particles are completely or almost completely consumed (**Figure 2.4a-c**). The precipitation process occurs simultaneously with the dissolution process, as the alkaline solutions penetrate and react with the smaller fly ash particles inside the larger spheres and fill up the interior space with reaction product, forming a dense matrix (**Figure 2.4c**). However, due to the massive precipitations of reaction products, some portions of the smaller fly ash spheres are covered with a layer of the reaction products. This layer provides a crust (**Figure 2.4e**) which prevents the contact of fly ash with the alkaline medium resulting in un-reacted fly ash particles which leads to the reduction of the reaction rate. This process is not uniform but varies locally in the geopolymer matrix, depending on the particle size distribution and the local chemistry. The result is several morphologies existing in a single paste of geopolymer comprising un-reacted particles, particles attacked by the alkaline solution but which maintain their spherical shape and reaction product, as shown in **Figure 2.4d** (Fernandez-Jimenez et al., 2005a).

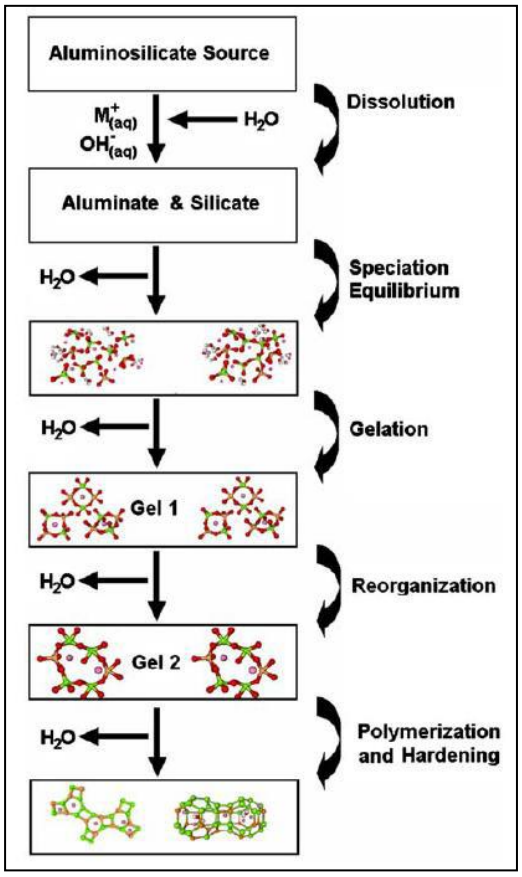

Figure 2.3 Conceptual models for geopolymerisation (Duxson et al., 2007a)

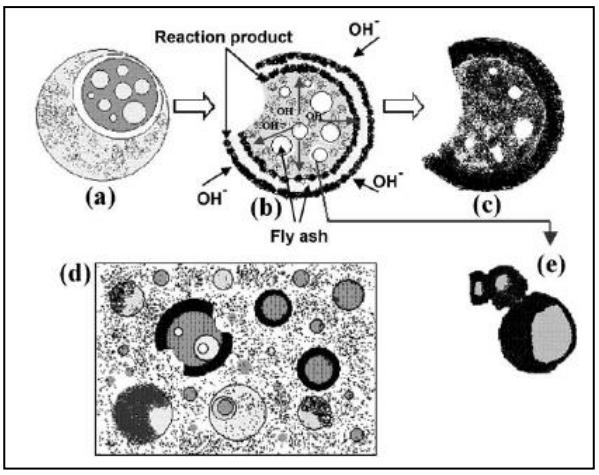

Figure 2.4 Descriptive model of the alkali activation of fly ash (Fernandez-Jimenez et al., 2005a)

Xu (2002) proposed a reaction scheme for the polycondensation process of the geopolymerisation reaction from the alumino-silicate materials by taking into

account the differences between zeolites and geopolymers products on its crystalline structures, as follows:

$$\text{Al-Si materials (s)} + \text{MOH (aq)} + Na_2SiO_3 \text{ (s or aq)} \quad (2.2)$$

$$\downarrow$$

$$\text{Al-Si materials (s)} + (M_z(AlO_2)_x(SiO_2)_y.nMOH.mH_2O) \text{ gel} \quad (2.3)$$

$$\downarrow$$

$$\text{Al-Si materials (s)}.(M_a((AlO_2)_a(SiO_2)_b).nMOH._mH2O) \quad (2.4)$$

Geopolymers with amorphous structure

In reactions 2.2 (**Equation 2.2**) and 2.3 (**Equation 2.3**), the extent of Al-Si material involved depends on the particle size, the extent of dissolution and the concentration of the alkaline solution. The formation of a $(M_z(AlO_2)_x(SiO_2)_y.nMOH.mH_2O)$ gel is a dominant step in the geopolymerisation process and essentially relies on the extent of dissolution of the alumina-silicate materials (Xu, 2002).

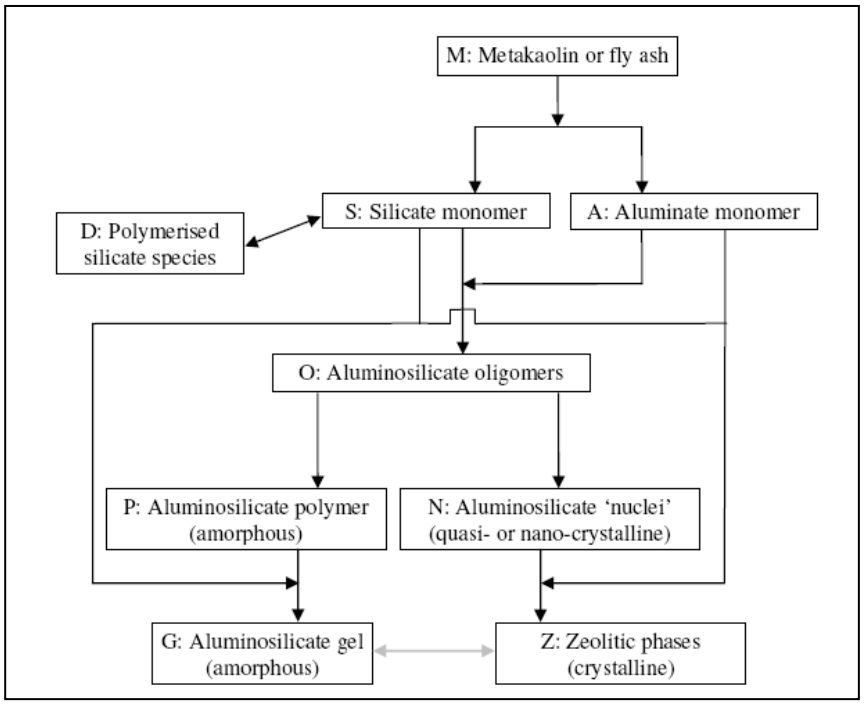

Figure 2.5 The proposed reaction sequence of geopolymerisation (Provis, 2006)

Another simplified model of the geopolymerisation reaction of metakaolin or fly ash has been proposed by Provis (2006) by considering the difference of the geopolymers and zeolites in the reaction products as shown in **Figure 2.5**.

In addition, the process of the geopolymerisation reaction involves the chemical reaction between alumino-silicate oxides (Si_2O_5, Al_2O_2) and the alkali polysilicates resulting in polymeric Si-O-Al bonds. The following equation (**Equation 2.5**) shows an example of the polycondensation reaction of alkali into poly(sialate-siloxo) (Davidovits, 1991, Jaarsveld & Deventer, 1996, Wallah & Rangan, 2006).

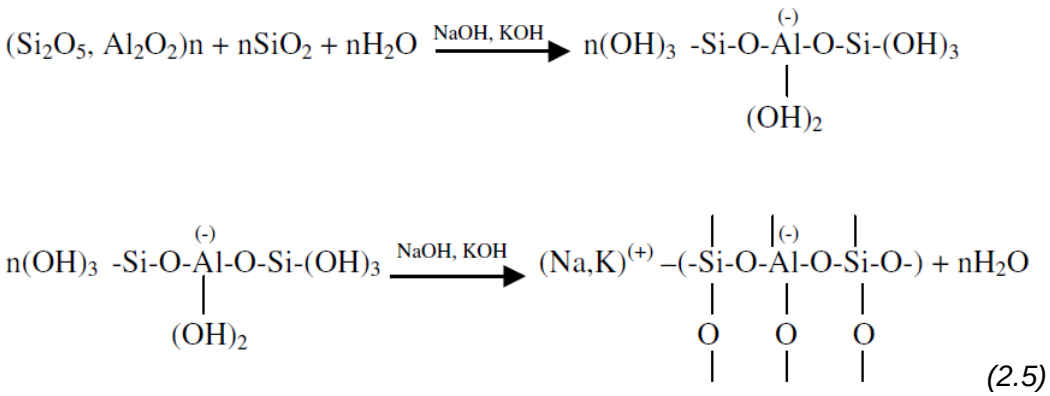

(2.5)

According to Rangan (2010), the 2nd equation on **Equation 2.5** reveals that the water in a geopolymer mixture plays no role in the chemical reaction and only contributes to the workability of the mixture during the handling process. The water is expelled from the geopolymer matrix during the curing and further drying periods This is in contrary to the chemical reaction of water in an OPC based concrete mixture during the hydration process.

2.4.4. Microstructure of fly ash geopolymer

The microstructure of fly ash based geopolymer has been studied by several researchers using SEM analysis. According to Fernandez-Jimenez & Palomo (2005b), the micro-structures contains primarily an amorphous alumino-silicate gel (**Figure 2.6A, points 4 and 5**) and un-reacted spheres of fly ash (**Figure 2.6A, point 3**). Some crystalline material with higher Si and lower Al content has also been identified. These materials probably attribute to a more developed alumino-silicate gel (**Figure 2.6B, point 6**). Fly ash spheres partially covered with

reaction product are also visible (**Figure 2.6C**). In addition, a little group of bright particles which were believed to be zeolite crystals are apparent. (**Figure 2.6D, points 7 and 8**).

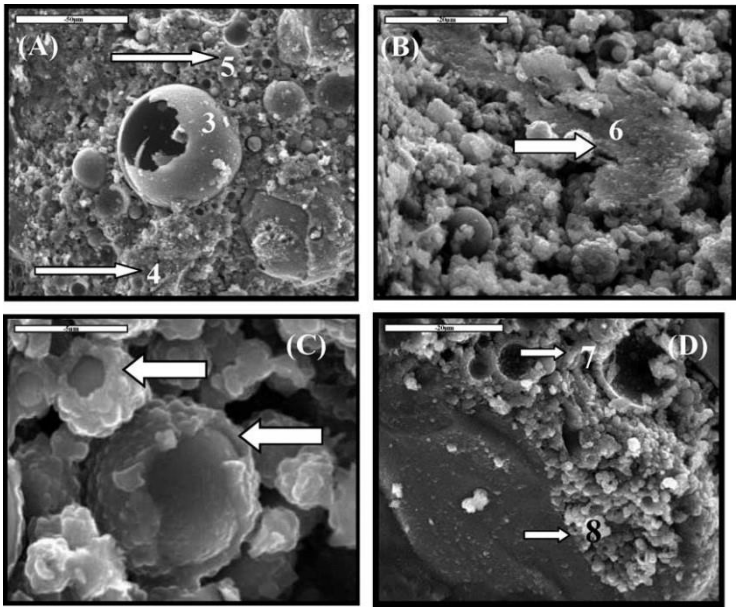

Figure 2.6 Microstructure of fly ash geopolymer mortar (Fernandez-Jimenez & Palomo, 2005b)

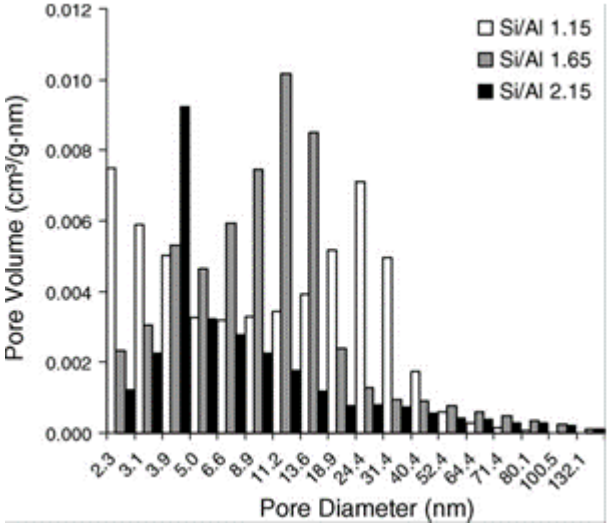

Figure 2.7 Pore volume distribution of geopolymers (Duxson et al., 2005)

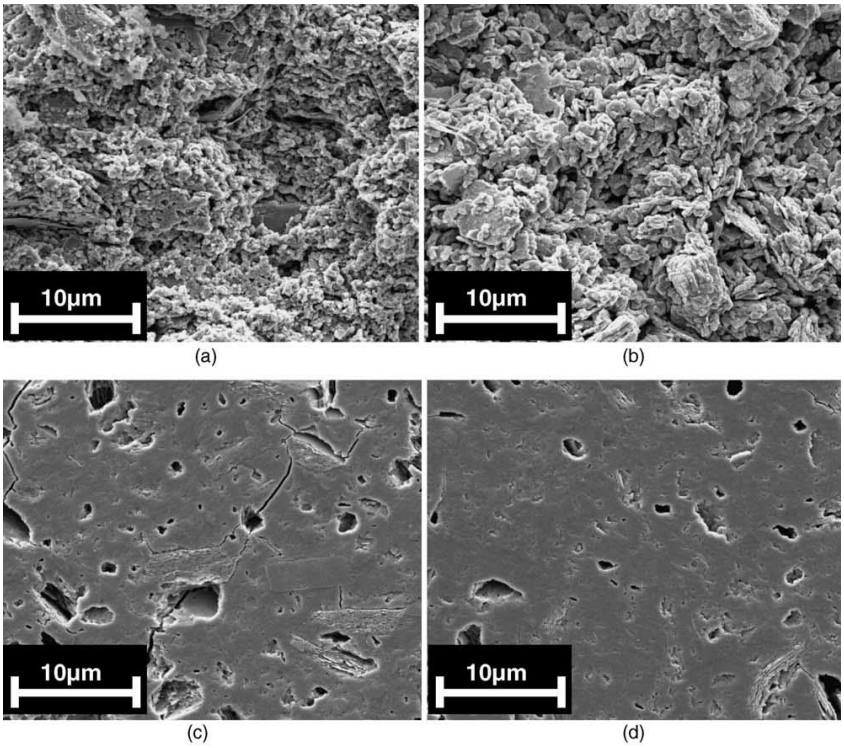

Figure 2.8 SEM micrographs of Na-geopolymers: Si/Al ratio of (a) 1.15, (b) 1.40, (c) 1.65 and (d) 1.90 (Duxson et al., 2005)

Duxson et al. (2005) found that the Si/Al ratio affects the microstructure of geopolymers. Specimens with a Si/Al ratio $\leq$ 1.4 exhibit a microstructure comprising clustered dense particulates with large interconnected pores. Specimens with a Si/Al ratio $\geq$ 1.65 appear homogeneous with porosity distributed in small pores. The authors also found that the pore volume distribution shifts towards smaller pores as the Si/Al ratio increases as shown in **Figure 2.7**. The SEM analysis in **Figure 2.8** shows a reduction of the pore volume along with the increase of Si/Al ratio (Duxson et al., 2005).

2.4.5. Fly ash requirement as geopolymer

As a precursor material for geopolymers, a high proportion of silica (SiO_2) and alumina (Al_2O_3) is required to ensure a sufficient potential reactive glassy constituent.

According to Sindhunata (2006), class F fly ash, an industrial by-product material, is much preferred in cement and geopolymer applications due to the high content of amorphous alumino-silicate and greater workability.

Further, according to Diaz-Loya et al. (2010), although silicate and aluminate are the main contributors to the geopolymer reaction, a high content of CaO and a high percentage of fine particles of fly ash below 5 μm affect the properties of the geopolymer. They suggest that a CaO content higher than 20% is not recommended for geopolymers due to its rapid setting.

In addition, Motorwala et al. (2013) suggest that the key characteristics required of a fly ash in producing geopolymers are the loss on ignition (LOI), fineness and uniformity. LOI is a measurement of un-burnt carbon remaining in the fly ash, while the finer gradation of fly ash generally results in a more reactive fly ash and contains less carbon. ASTM C618-03 (2003) limits the maximum LOI and SO_3 contained in fly ash that is used as a concrete binder. The maximum permissible limit of LOI is 6% with the aim of avoiding an increase of water demand, reducing the pozzolanic activity and reducing the fineness, while SO_3 is limited to a maximum of 5% to maintain the concrete stability and durability.

2.5. Alkali-Activated Slag (AAS)

2.5.1. Introduction to slag

Slags are a waste product from the pig iron manufacturing process consisting mainly of calcium-magnesium alumino-silicate glass. The structure, properties and chemical composition vary depending on the raw materials and the industrial process (Bakharev et al., 1999a). The most commonly used slags are blast-furnace slag. According to the ASTM Standard, blast-furnace slag is a non-metallic product that consists mainly of silicates and alumina-silicates of calcium that is produced in a blast-furnace in a molten condition with iron (ASTM C989-99, 2003). Ground granulated blast-furnace slag (GGBS) is obtained by quenching molten blast-furnace slag to produce a glassy material called granulated blast-furnace slag (GBS), which is then ground into a fine powder referred to as ground granulated blast-furnace slag.

The major constituents of GGBS are calcium oxide (CaO), silica (SiO_2), alumina (Al_2O_3) and magnesium oxide (MgO). Other minor constituents include sulphur

(SO_3), iron (Fe_2O_3), alkaline (Na_2O, K_2O), manganese (Mn_2O_3), phosphorus (P_2O_5) and titanium (TiO_2) oxides.

2.5.2. Research on AAS

Research on the use of slag as an alternative to cement was started when Feret first described such use in 1939. Purdon also described the reaction of alkalis on slag in 1940, but it was not until the works of Glukhovsky in the late 1950's that the idea became widespread (Roy, 1999, Pacheco-Torgal et al., 2008).

Ground granulated blast-furnace slag (GGBS) is an ideal material for alkali activated cement due to its latent hydraulic properties. The adoption of alkali-activated slag (AAS) has been used in construction projects. The industrial manufacture of cement based on the alkali activation of GGBS was started in Ukraine in the 1960's driven by ecological pressures (Fernandez-Jimenez et al., 1999). Most of the application of AAS has taken place in the former Soviet Union, China and Scandinavian countries due to environmental issues driving a search for an alternative binder for concrete (Talling & Brandstetr, 1989, Douglas & Brandstetr, 1990, Douglas et al., 1991, Wang et al., 1994, Shi, 1996, Fernandez-Jimenez & Puertas, 1997, Collins & Sanjayan, 1999, Bakharev, 2000, Yongde & Yao, 2000, Brough & Atkinson, 2002, Al-Otaibi, 2008, Escalante-Garcia et al., 2003).

In the early 1990's, a preliminary investigation on the activation of alkali-activated ground granulated blast-furnace slag with sodium silicate (waterglass) found that there was good potential as a replacement for Portland cement with satisfactory workability and comparable strength properties to Portland cement based concrete (Douglas & Brandstetr, 1990, Douglas et al., 1991).

According to Wang et al. (1994), the most important factors that affect the strength development of alkali-activated slag are the type of alkaline activator, the means of adding the activator, the dosage of alkali, the type and fineness of slag, the ratio of SiO_2/Na_2O (modulus, Ms) when using waterglass solution, curing temperature, and the ratio of liquid/slag or water/slag. They also concluded that waterglass (sodium silicate) is the best activator for the activation of alkali-activated slag.

2.5.3. Hydration product and reaction mechanism of AAS

The hydration product of alkali-activated slag (AAS) is very different from that of the fly ash geopolymer described in **Section 2.4.3**. The main hydration product of AAS is a calcium silicate hydrate (C-S-H) gel, similar to that formed in OPC. As observed in many experiments, hydrated calcium silicate (C-S-H) is the major component of hardened AAS pastes (I.G.Richardson et al., 1994, Wang & Scrivener, 1995, Bakharev, 2000, Brough & Atkinson, 2002, Escalante-Garcia et al., 2003, Wang & Scrivener, 2003). The ratio of Ca/Si in the C-S-H generally resembles that of the un-hydrated slag. However, it is much lower than the ratio of Ca/Si in C-S-H from the hydration of general Portland cement (Chen & Brouwers, 2007, Wang & Scrivener, 1995).

According to Taylor (1997), the type of C-S-H gel that forms in AAS concrete is different to that of general Portland cement concrete. The type of C-S-H gel in AAS is C-S-H(I) with the ratio of Ca/Si below 1.5, while OPC has C-S-H gel type II (C-S-H(II)) with a Ca/Si ratio of approximately 2. Furthermore, Brough & Atkinson (2002) observed two regions within the C-S-H gel. They found that the inner regions of the AAS hydrates contained a C-S-H gel with a Ca/Si ratio of approximately 0.9 with high Mg, while the outer regions had a Ca/Si ratio of approximately 0.7 with low Mg. However, they could not ascertain whether this high Mg was due to unreacted slag or hydrotalcite ($Mg_6Al_2CO_3(OH)_{16}.4H_2O$)).

Puertas et al. (2004) have also reported the presence of other mineral side products on GGBS activated with NaOH. Using XRD analysis, they identified the presence of hydrotalcite, calcite ($CaCO_3$) and C-S-H. In addition, Sakulich (2009) has also shown that C-S-H, the same binding materials that is produced in ordinary Portland cement, has been produced during the hydration process of AAS concrete. He also identified a number of mineral side products, such as hydrotalcite, which are unlikely to play an active role in providing strength.

The mechanism of alkali activation of GGBS is very different from that of fly ash geopolymer as described in **Section 2.4.3** due to the significant presence of calcium and low aluminium content.

According to Krivenko (1994), the alkali cations play a significant role as a catalyst in the early stages of the hydration process. This process involves an interchange with Ca^{2+} cations. However, in the later stages they are combined into the structures forming zeolite-like phases. Similarly to Krivenko, Jiang (1997)

also found that the alkali hydroxides play multiple roles in the hydration process, i.e. to provide OH^- ions at the initial stage and to become part of the reaction products in later stages.

Wang & Scrivener (1995) also suggest that during the hydration of alkali-activated slag, the dissolution and precipitation mechanism during the early stage is followed later by a solid state mechanism.

However, Taylor (1997) states that the role of alkalis in alkali-activated slag is similar to that in blended slag and OPC cements which is to maintain the supply of OH^- anions in the system. During the hydration process, the coating formed on the slag grains would prevent further hydration, hence an alkaline environment is required to break down this layer. In blended slag with OPC, this alkaline environment will be maintained by the $Ca(OH)_2$ as the result of the hydration of the OPC. However, as the level of OPC replacement increases, the quantity of $Ca(OH)_2$ is insufficient to maintain the alkaline environment, therefore an external source of alkali is needed.

The study by Krizan & Zivanovic (2002) has also indicated that the hydration process of alkali-slag cements are similar to that of OPC, but the mechanisms of hydration are different. The hydration process of alkali-slag cements was found to be influenced by the sodium content and the silica modulus (M_s). According to these authors, the hydration process begins with a destruction of the slag bonds Ca–O, Mg–O, Si–O–Si, Al–O–Al and Al–O–Si, and then a Si–Al layer is formed over the surface of the slag grains and, finally, formation of the hydration products.

2.5.4. Microstructure of AAS

The microstructure study AAS has been studied by several researchers who mainly report the existence of micro-cracks. According to Brough & Atkinson (2002), the microstructure of AAS gel consists of a homogeneous gel with considerable micro-cracking at the aggregate interface (**Figure 2.9**). The authors presumed that the micro-cracking was caused by drying shrinkage during the specimen preparation. However, the degree of drying shrinkage cracking was much reduced when fully hydration occurred at later ages. The inner product regions were generally darker than the outer products which were observed as

rims around partially reacted anhydrous grains and in the gel where smaller slag grains had fully hydrated.

The existence of micro-cracking was also investigated by Escalante-Garcia et al. (2009). According to the authors, despite the fact that there are substantial cracks in the AAS matrix compared to an OPC matrix, the AAS is relatively dense with any un-reacted slag grains being smaller than 100 μm (**Figure 2.10**), thus indicating that the slag has reacted by a dissolution-precipitation mechanism. Song et al. (2000) also found that the microstructure of AAS was a very smooth, homogeneous and interconnected-solid in all samples. The authors stated that the pores between grains looked very tortuous, and some of them appeared isolated from others. Higher alkaline concentration, however, gave a higher degree of reaction and resulted in more filled pores, therefore, a less porous microstructure.

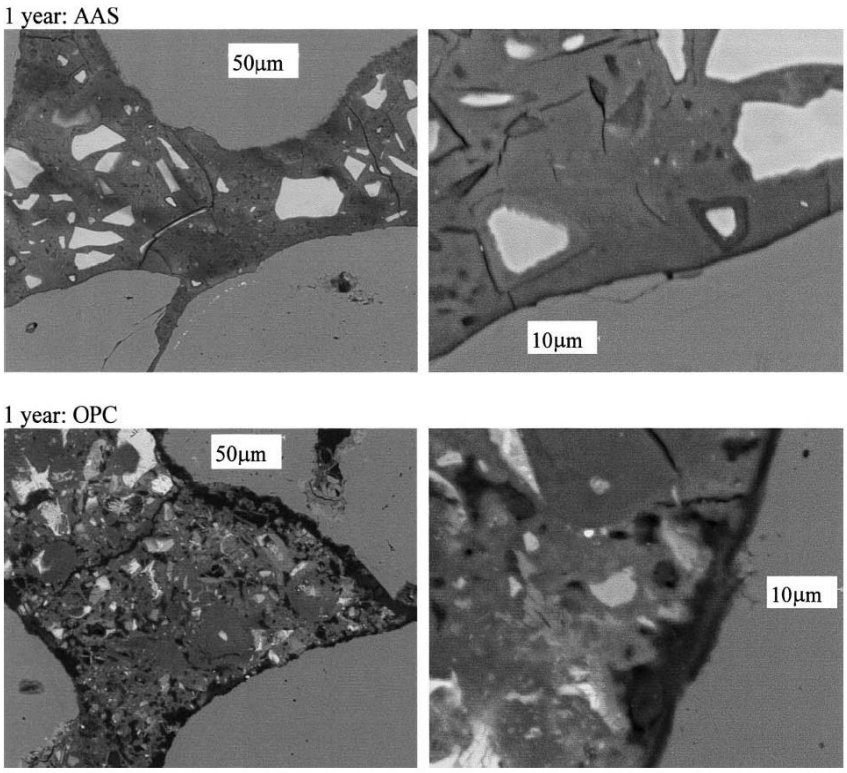

Figure 2.9 Backscattered electron images of samples of OPC and of sodium silicate-activated slag mortars hydrated at room temperature at 1 year (Brough & Atkinson, 2002)

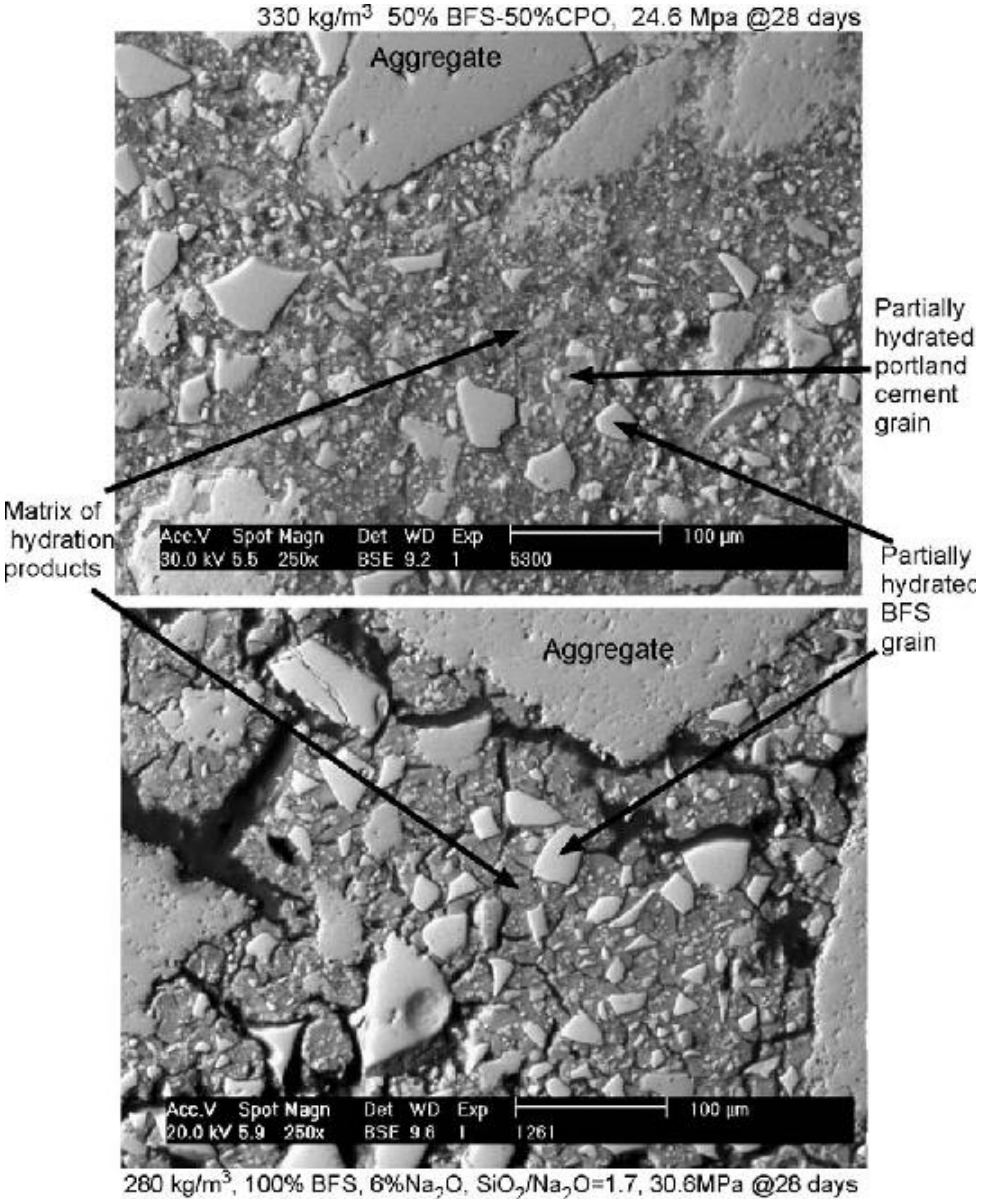

Figure 2.10 Scanning electron microscopy microstructures of polished samples of concretes of OPC-BFS and activated BFS, images obtained by backscattered electron images (Escalante-Garcia et al., 2009)

The pore structure development of alkali-activated slag mortar was also observed by Shi (1996). According to the author, the pore structure of the mortar was affected by the type of activator used. The slag activated by sodium silicate was less porosity than OPC, however, the porosity of alkali-activated slag is higher when activated by sodium hydroxide (**Figure 2.11**). Collins & Sanjayan (2000)

also investigated the pore size distribution of alkali-activated slag activated by sodium silicate (**Figure 2.12**). They found that alkali-activated slag paste has a much higher proportion of pore size within the mesopore limits than general OPC paste. The higher total volume of mesopores in alkali-activated slag paste could explain the higher magnitude of drying shrinkage of alkali-activated slag concrete.

The same authors Collins & Sanjayan (2001) also found that the network of interconnected micro-cracks within the alkali-activated slag concrete become progressively larger with increasing age. This indicates the possibility of a compressive strength reduction of alkali-activated slag concrete over time.

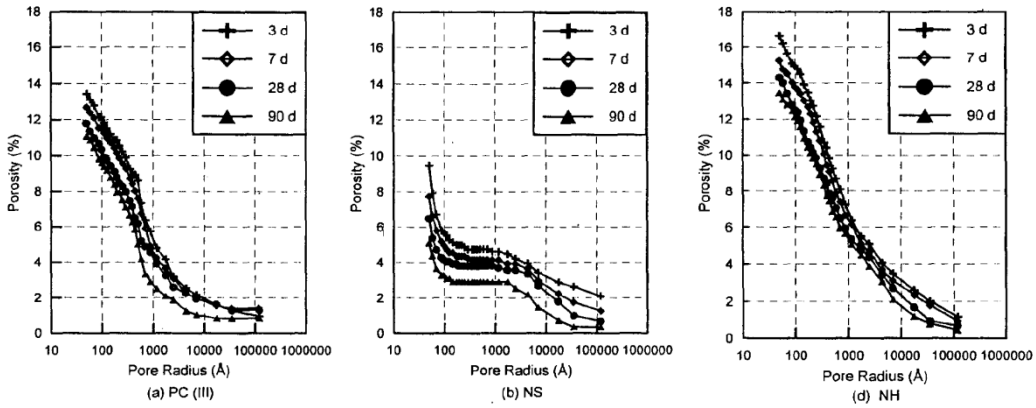

Figure 2.11 Cumulative pore volume of alkali-activated slag and Portland cement mortars (Shi, 1996)

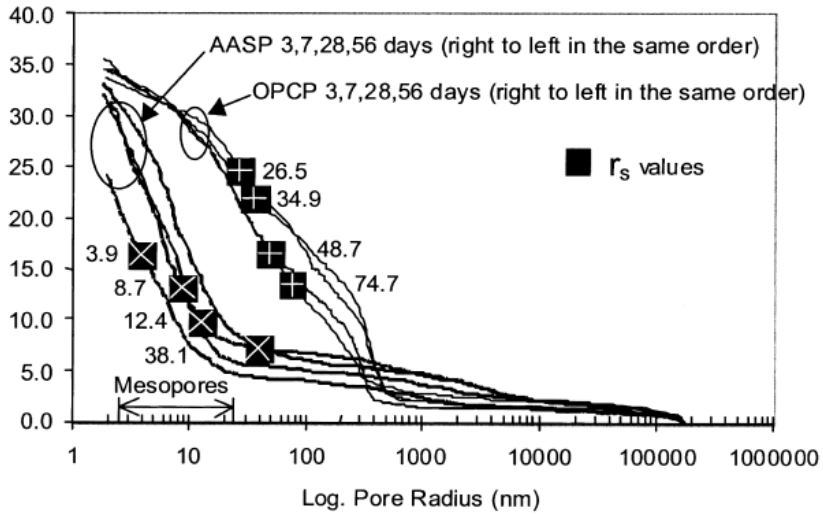

Figure 2.12 Cumulative pore size distribution of OPCP and AASP at 3, 7, 28, and 56 days (Collins & Sanjayan, 2000)

2.5.5. Slag requirement as AAS binder

The hydraulic activity of slag can be determined by using the basicity coefficient measurement. According to McGannon (1971), the basicity of a slag material is the ratio between the total content of basic constituents and total content of acidic constituents as given in **Equation 2.6**.

$$Kb = \frac{CaO + MgO + Fe_2O_3 + K_2O + Na_2O}{SiO_2 + Al_2O_3} \quad (2.6)$$

However, due the minor contents in the GGBS (less than 1%), the Fe_2O_3, K_2O and Na_2O have been omitted by several authors in calculating the basicity of slag (Bakharev, 2000, Wang et al., 1994, Yongde & Yao, 2000) as given in **Equation 2.7**.

$$Kb = \frac{CaO + MgO}{SiO_2 + Al_2O_3} \quad (2.7)$$

According to the basicity coefficient as given in **Equation 2.6** and **Equation 2.7**, the slag can be divided into three groups: acid (Kb < 1), neutral (Kb = 1) and basic (Kb > 1). Basic slag is the most active and produces the highest strength, while acid slag is more difficult to activate and generally do not develop a high strength (Bakharev, 2000).

Furthermore, according to Talling & Brandstetr (1989), a granulated slag can be used as a successful alkali-activated slag binder material with a CaO/SiO_2 ratio between 0.5 and 2.0 and an Al_2O_3/SiO_2 ratio between 0.1 and 0.6. In addition, Chang (2003) has also demonstrated that the hydration modulus (HM) of a granulated slag which is defined in **Equation 2.8** should exceed 1.4 to ensure good hydration properties.

$$HM = \frac{CaO + MgO + Al_2O_3}{SiO_2} \quad (2.8)$$

2.6. Alkaline activators

The alkaline activators are classified into six groups according to their chemical compositions (Glukhovsky et al., 1980):

(1) Caustic alkalis: MOH

(2) Non-silicate weak acid salts: M_2CO_3, M_2SO_3, M_3PO_4, MF, etc.

(3) Silicates: $M_2O.nSiO_2$

(4) Aluminates: $M_2O.nAl_2O_3$

(5) Alumino-silicates: $M_2O.nAl_2O_3.(2\text{-}6)SiO_2$

(6) Non-silicate strong acid salts: M_2SO_4

Researchers have widely found that activation with sodium silicate or sodium silicate blended with NaOH has given the best strength for fly ash geopolymer and AAS specimens. NaOH, Na_2CO_3 and Na_2SO_4 are also used by others as activators (**Table 2.3** and **2.4**). A blended sodium silicate and sodium hydroxide activator is selected for this study as this has been the most widely reported successful strategy.

Table 2.3 Strength of fly ash geopolymer activated by different type of activators

Authors	Specimen	Activators	28-days strength (MPa)
Bakharev (2005a)	Paste	NaOH (8%Na)	45.0
		Sodium silicate (8%Na)	52.0
Fernandez-Jimenez & Palomo (2005b)	Mortar	NaOH+Na_2CO_3 (14.98.68% Na_2O)	35.9
		NaOH (13.67% Na_2O)	70.4
		NaOH + sodium silicate (14.09% Na_2O)	91.6

The dosage of activator (in terms of $\%Na_2O$) is defined as the ratio of the Na_2O content of the alkaline activator to the mass of the binder (fly ash for fly ash geopolymer and GGBS for AAS), while the activator modulus (M_s) is the mass ratio of the SiO_2 to the Na_2O in the alkaline activator as follows:

$$\%Na_2O = \%Na_2O \text{ in sodium silicate and NaOH / mass of binder} \quad (2.9)$$

$$M_s = SiO_2 \text{ (activator) / } Na_2O \quad (2.10)$$

For fly ash geopolymer specimens, several authors have proposed that the activator concentration (in terms of NaOH molarity) in the fly ash geopolymer binder is an important parameter (Hardjito & Rangan, 2005, Park & Kang, 2006, Weng & Sagoe-Crentsil, 2007). However, when the activator concentration contains both sodium hydroxide and sodium silicate, it cannot reflect the effect of

the concentration of Na^+ ion in the mixture. Adam (2009) suggested the use of the activator dosage in terms of the mass ratio of total Na_2O in the activator solution to fly ash as the main indicator of the Na concentration. The purpose of this method was to take into account the effect of the alkali concentration in the mix. A similar approach was also adopted by Bakharev (2005a) using an activator dosage in terms of the mass ratio of Na to fly ash. According to the author, the mass ratio of Na_2O in the activator solution to fly ash for the sodium silicate based activator is more suitable since the grade of sodium silicate solution is usually specified by the ratio of SiO_2 to Na_2O which makes the mix calculation easier. Therefore, a similar approach with the work of Adam (2009) is adopted for this study.

Table 2.4 Strength of AAS activated by different type of activators

Authors	Specimen	Activators	28-days strength (MPa)
Bakharev (2000)	Paste	Na_2CO_3 (7%Na)	26.0
		NaOH (7%Na)	20.9
		Na_3PO_4 (7%Na)	12.0
		Sodium silicate (6%Na, Ms = 1.25)	30.0
Wang et al. (1994)	Mortar	Na_2SO_4 (2M)	20.0
		NaOH (4M)	22.9
		Na_2CO_3 (2M)	35.5
		Sodium silicate (2M, Ms = 1)	85.0
Shi (1996)	Mortar	NaOH (6%Na_2O)	13.0
		Na_2CO3 (6%Na_2O)	33.0
		Sodium silicate (6%Na_2O)	62.0
Escalante-Garcia et al. (2003)	Mortar	NaOH (6%Na_2O)	29.8
		Sodium silicate (6%Na_2O)	46.1
Fernandez-Jimenez et al. (2003)	Mortar	Na_2CO_3	40.0
		NaOH	28.0
		Sodium silicate	100.0

For AAS specimens, according to Wang et al. (1994), both the Na_2O dosage and activator modulus have significant influence on the strength development of AAS mortar. However, there is a certain value of Na_2O dosage above which there will be no further significant increase in strength. Moreover, in blended sodium silicate and sodium hydroxide, there is a competing effect of the Na_2O dosage and the activator modulus which results in an optimum value for both the Na_2O dosage and that of the activator modulus (M_s).

Wang et al. (1994) suggested that the optimum dosage of Na_2O should be within the range of 3.0% – 5.5% Na_2O by slag weight to avoid detrimental properties such as efflorescence and brittleness due to the effect of free alkali at higher dosage. Similar to Shi et al. (2006), it was found that under normal curing, the optimum Na_2O dosage depend on the requirement for high early strength design. They also recommended optimum limits for the activator modulus. This optimum value was varied depends on the type of slag, i.e. 0.75 – 1.25 for acid slag, 0.90 – 1.30 for neutral slag, and 1.00 – 1.50 for basic slag. Similar conclusions were also drawn by Krizan & Zivanovic (2002) who found an activator modulus between 0.60 – 1.50 resulted in higher ultimate strength compared to traditional Portland cement.

Table 2.5 Typical Na_2O dosage and sodium silicate based activator for geopolymer

Authors	Specimen	Na_2O dosage (%)	Modulus (M_s)
Fernandez-Jimenez & Palomo (2005b)	Mortar	5.55 – 14.90	0.037 – 1.23
Yang et al. (2009)	Mortar	8.90 – 16.40	0.90
Adam (2009)	Mortar	10.0 – 15.0	1.00 – 1.50
Hardjito & Rangan (2005)	Concrete	5.30 – 5.70	1.31 – 1.36
Wallah & Rangan (2006)	Concrete	5.70	1.31
Sumajouw & Rangan (2006)	Concrete	6.80	1.09
Adam (2009)	Concrete	7.50	0.75 – 1.25

The typical Na_2O dosage and activator modulus (M_s) for fly ash geopolymer and AAS specimens adopted by several authors are presented in **Table 2.5** and **Table 2.6**, respectively. It can be seen that a higher dosage of Na_2O was

required for fly ash geopolymer (5.3% – 16.3%) than that for AAS specimens (3% – 7%). This is attributed to the polymerisation process which requires highly alkaline solutions to dissolve the silica and alumina ions in the fly ash precursor. The extent of dissolution of Si and the Si/Al ratio in fly ash are significant factors in the geopolymerisation reaction (Davidovits, 1991).

Table 2.6 Typical Na_2O dosage and sodium silicate based activator for AAS

Authors	Specimen	Na_2O dosage (%)	Modulus (M_s)
Bakharev et al. (1999a)	Paste	4.8 – 12.0	0.87 – 1.30
Puertas et al. (2004)	Paste	4.0	1.50
Wang et al. (1994)	Mortar	3.0 – 5.5	0.75 – 1.50
Talling (1989)	Mortar	3.0 – 5.0	N/A
Shi (1996)	Mortar	6.0	1.50
Fernandez-Jimenez & Puertas (1997)	Mortar	4.0	1.50
Krizan & Zivanovic (2002)	Mortar	3.0 – 4.0	0.60 – 1.50
Escalante-Garcia et al. (2003)	Mortar	6.0	2.00
Zivica (2007)	Mortar	3.0 – 7.0	1.13
Adam (2009)	Mortar	3.0 – 5.0	0.75 – 1.25
Douglas et al. (1991)	Concrete	3.41 – 3.63	1.36 – 1.47
Al-Otaibi (2008)	Concrete	4.0 – 6.0	1.00 – 1.65
Adam (2009)	Concrete	5.0	0.75 – 1.25

A further study of Na_2O dosage and activator modulus (M_s) of fly ash geopolymer and AAS mortars has been conducted by Adam (2009) as presented in **Table 2.7**. According to the author, a lower Na_2O dosage of 5% gives the best result for the strength properties of AAS mortars. On the other hand, fly ash geopolymer required a higher Na_2O dosage of 15% to provide good strength properties. Furthermore, both fly ash geopolymer and AAS mortars exhibit good strength with an activator modulus in the range of 1.00 – 1.25. Consequently, a 15% Na_2O dosage for fly ash geopolymer and 5% Na_2O dosage for AAS, as well as an

activator modulus of 1.00 and 1.25 for both fly ash geopolymer and AAS mortars are chosen for this study.

Table 2.7 Fly ash geopolymer and AAS specimens (Adam, 2009)

Specimen	Activators	Na_2O dosage (%)	Alkali Modulus (M_s)	28-days strength (MPa)
AAS mortar	NaOH + sodium silicate	3	0.75	15.09
	NaOH + sodium silicate	3	1.00	26.63
	NaOH + sodium silicate	3	1.25	22.93
	NaOH + sodium silicate	5	0.75	43.54
	NaOH + sodium silicate	5	1.00	52.27
	NaOH + sodium silicate	5	1.25	49.48
AAS concrete	NaOH + sodium silicate	5	0.75	36.60
	NaOH + sodium silicate	5	1.00	45.30
	NaOH + sodium silicate	5	1.25	43.50
Fly ash geopolymer mortar	NaOH + sodium silicate	10	1.00	57.04
	NaOH + sodium silicate	10	1.25	59.71
	NaOH + sodium silicate	10	1.50	61.03
	NaOH + sodium silicate	15	1.00	74.69
	NaOH + sodium silicate	15	1.25	79.26
	NaOH + sodium silicate	15	1.50	69.16
Fly ash geopolymer concrete	NaOH + sodium silicate	7.5	0.75	46.10
	NaOH + sodium silicate	7.5	1.00	53.60
	NaOH + sodium silicate	7.5	1.25	57.30

2.7. Mechanical properties of fly ash geopolymer and AAS concretes

In the framework of the development of fly ash geopolymer and AAS concretes, various explorations have been performed in order to determine the mechanical properties of fly ash geopolymer and AAS concretes, as well as their long term properties.

Studies on the mechanical properties have generally addressed the compressive strength, modulus of elasticity and tensile strength (Hardjito & Rangan, 2005, Collins & Sanjayan, 2001, Fernandez-Jimenez et al., 2006, Diaz-Loya et al., 2011, Neupane et al., 2014, Bernal et al., 2012, Concrete Institute Australia, 2011, Nath & Sarker, 2012, Deb et al., 2014).

Research on the mechanical properties in terms of compressive strength, modulus of elasticity and tensile strength of fly ash geopolymer concrete has been conducted by Hardjito & Rangan (2005). The authors found that the fly ash geopolymer concrete has a comparable compressive strength and lower modulus of elasticity to that of OPC concrete for up to 90 days of their investigation. They also concluded that the modulus of elasticity of fly ash geopolymer concrete is similar to that OPC concrete. However, the indirect tensile strength of fly ash geopolymer concrete was found to be higher than the values recommended by Australian Standard (AS 3600, 2009) for OPC concrete (Hardjito & Rangan, 2005).

A similar finding was also found by Fernandez-Jimenez et al. (2006) for fly ash geopolymer concrete. The authors found that fly ash geopolymer concrete developed a high compressive and flexural strength and had a lower modulus of elasticity in short term periods (up to 90 days). According to the authors, it might be possible that fly ash geopolymer concrete exhibits a similar behaviour to high-performance OPC concrete. The values of compression modulus of elasticity based on formulae proposed by different codes proved to be unreliable. This was attributed to the existence of variables which had not been taken into consideration in the formula, but nevertheless influenced the properties (Fernandez-Jimenez et al., 2006).

The correlation of mechanical properties in terms of modulus of elasticity and flexural strength of fly ash geopolymer concrete was also investigated by Diaz-Loya et al. (2011) using regression analysis. The authors found that fly ash geopolymer concrete seems to possess a similar mechanical behaviour to that of

OPC concrete and that the relationship between the flexural and compressive strength can be expressed using ACI standards intended for ordinary concrete. Furthermore, they also found that the relationship between the modulus of elasticity and the compressive strength is similar to that of ordinary concrete, however the relationship is linear while ordinary concrete follows a power curve relationship (Diaz-Loya et al., 2011).

Neupane et al. (2014) investigated the applicability of the Australian Standard concluded that the indirect tensile strength and flexural strength were higher than calculated by the Australian Standard (AS 3600). Using the relevant Australian Standard (i.e. AS 1012.10 for the indirect tensile strength and AS 1012.11 for flexural tensile strength), the authors found that the observed tensile strength of the fly ash geopolymer concrete was slightly higher than that of OPC concrete (at 28 days). They found that observed results were 8% (for indirect tensile strength) and 10% (for direct tensile strength) higher than those predicted by AS 3600. Hence, based on these results, they proposed that the Australian Standard (AS 3600) can be used to estimate the modulus of elasticity of fly ash geopolymer concrete (Neupane et al., 2014).

A similar finding was also found by Deb et al. (2014) for the tensile strength of fly ash geopolymer concrete. Using the inclusion of the ground granulated blast furnace slag in the geopolymer mixture, the authors found that the predictions of tensile strength of compressive strength of ambient-cured geopolymer concrete using the ACI 318 and AS 3600 codes tend to be similar to that for OPC concrete. According to them, the predictions of heat-cured geopolymer concrete are more conservative than for ambient-cured geopolymer concrete (Deb et al., 2014).

The long term performance of AAS concrete in terms of the micro-cracking and compressive strength development has been investigated by Collins & Sanjayan (2001). The strength development of AAS concrete was investigated for ages up to 360 days. The authors found that the strength development tended to reduce (**Figure 2.13**). Using water sorptivity tests, the authors found that the reduction of strength could be attributed to the growing of the existence of a network of interconnected micro-cracks within the AAS concrete with increasing age (Collins & Sanjayan, 2001).

The engineering properties of AAS concretes in long term performance has also been investigated by Bernal et al. (2012). The authors found that AAS concrete has a comparable compressive strength and higher flexural strength compared to OPC concrete as shown in **Figure 2.14**. An increase of Si/Al ratio also affects the compressive and flexural strengths of AAS concrete with higher Si/Al ratio producing a higher compressive and flexural strength. However, it was also found that higher a Si/Al ratio tended to reduce the strength of AAS concrete at later ages (Bernal et al., 2012).

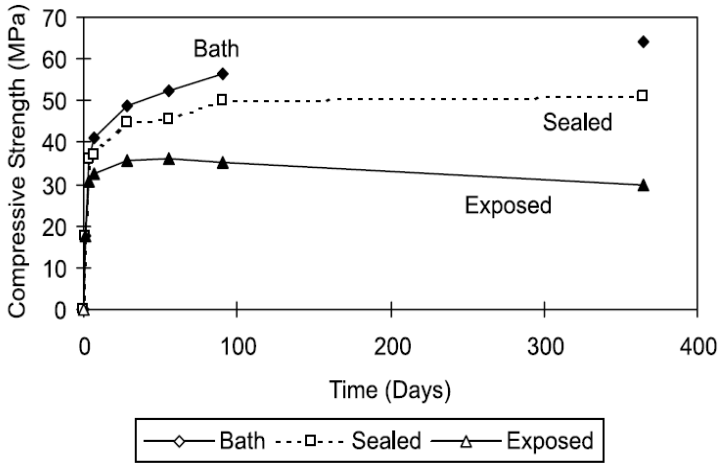

Figure 2.13 Effects of type of curing on compressive strength, AASC (Collins & Sanjayan, 2001)

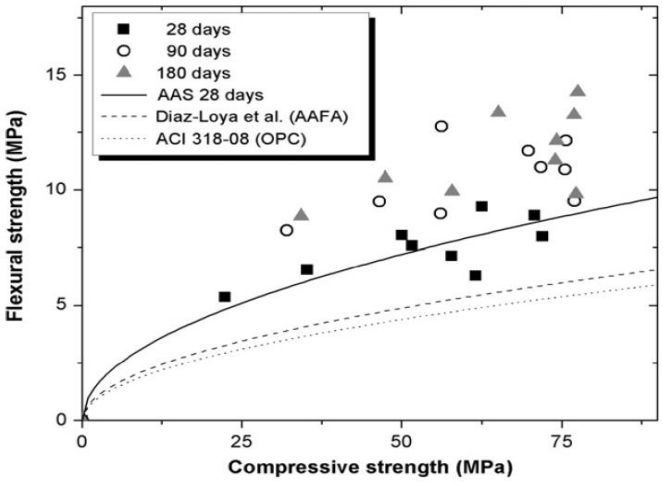

Figure 2.14 Compressive strength vs flexural strength of AAS concrete (Bernal et al., 2012)

In 2011, the Concrete Institute of Australia published a recommended practice for geopolymer concrete. This report states that the tensile and flexural strengths of geopolymer concrete is superior to that of OPC concrete so that the relationship proposed by the existing Australian Standard (AS 3600, 2009) can be applied to geopolymer concrete as well. Moreover, this report also states that the modulus of elasticity of geopolymer concrete is lower than OPC concrete. Thus a two phased model incorporating the Setunge model (**Equation 2.11**) and the Ng & Foster model (**Equation 2.12**), is proposed to calculate the modulus of elasticity of geopolymer concrete (Concrete Institute Australia, 2011).

(1) Setunge model (Setunge in Concrete Institute Australia (2011)

$$\frac{1}{E_c} = \frac{0.45}{V_a E_a + (1 - V_a) E_m} + 0.55\left(\frac{V_a}{E_a} + \frac{1 - V_a}{E_m}\right) \qquad (2.11)$$

(2) Ng & Foster model (Ng & Foster in Concrete Institute Australia (2011)

$$E_m = 3710\sqrt{f_{mm}} - 1280 (\text{MPa}) \qquad (2.12)$$

2.8. Factors affecting the mechanical properties of fly ash geopolymer and AAS concretes

Several factors have been identified as important parameters affecting the properties of fly ash geopolymer, i.e. the curing process, the fineness of fly ash precursors, the availability of silicate (Si) and aluminate (Al) as the ratio of Si/Al, as well as the CaO content in fly ash precursors.

According to Palomo et al. (1999), the curing temperature, the type of activators, and the curing time are the significant factors affecting the mechanical strength. Higher curing temperature and longer curing time resulted in higher compressive strength. While, alkaline activator that contained soluble silicates was found to increase the reaction rate of fly ash-based geopolymer compared to alkaline solutions that contained only hydroxide (Palomo et al., 1999). Similar results were found by Bakharev (2005a). According to this author, high strength fly ash geopolymer can be achieved by heat curing treatment. The author also suggested that long pre-curing at room temperature is important for strength

development of fly ash geopolymer materials prior to the application of heat curing treatment. Winnefeld et al. (2010) also concluded that heat curing treatment is significantly effective in developing the strength of fly ash geopolymer. The authors also proposed that 80^{O}C is the optimum curing temperature, while curing temperature above 80^{O}C decrease the compressive (**Figure 2.15**).

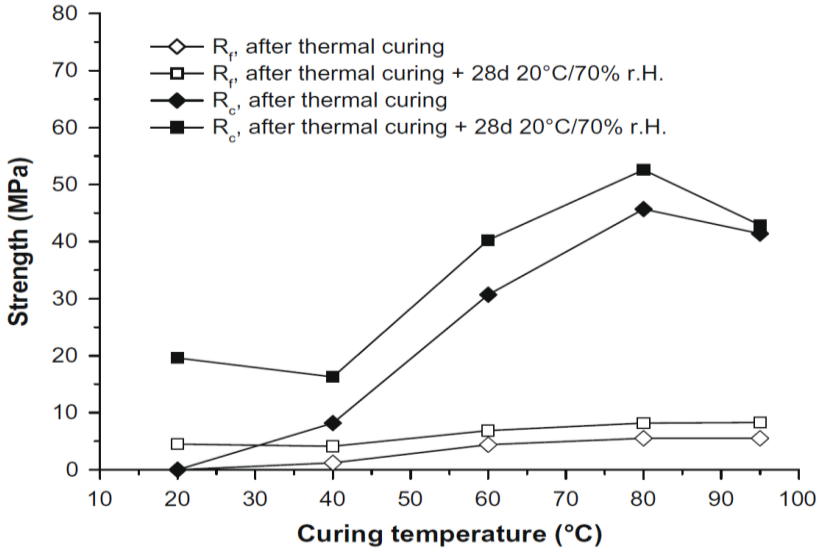

Figure 2.15 Influence of curing temperature on flexural (R_f) and compressive strength (R_c) of mortars based on low calcium fly ash (LCFA), water/binder ratio 0.27, activator concentration 7.3% Na_2O referred to fly ash (Winnefeld et al., 2010)

Research has shown that the strength properties of geopolymer are also significantly influenced by the availability of silicate (Si), aluminate (Al) and sodium (Na) on the fly ash precursors. According to Rowles & O'Connor (2003) the compressive strength of geopolymer is affected by the Si/Al and Na/Al molar ratio. It was found that Si/Al ratio of 2.5 and Na/Al ratio of 1.3 leads to better strength performance. The authors also suggested that the bonding network in the amorphous aluminosilicate alters systematically with the change of the composition. Similar finding were also demonstrated by Steveson & Sagoe-Crentsil (2005). According to these authors, high strength fly ash geopolymers have low porosity and a dense microstructure which can be achieved with a high silicate content with a Si/Al ratio of approximately 3.9 and a Na/Al ratio of approximately 1. They also concluded that the initial strength development can

be attributed to the charge-balancing role of the alkali cations in the fly ash formulations compared to the initial alkali dissolution reaction of the aluminosilicate fly ash particles.

The ratio of Si/Al also affects setting time of strength development of fly ash geopolymer concrete. According to Silva et al. (2007), the amount of Al available for the geopolymer reaction during synthesis appears to have a significant effect of controlling the setting time, with an increase in the Si/Al ratio leading to a longer setting time. This was considered to be due to the alteration of the properties of the geopolymer during condensation. Furthermore, Weng & Sagoe-Crentsil (2007) and Sagoe-Crentsil & Weng (2007) found that in a geopolymeric system with a high Si concentration, the condensation stage starts with formation of oligomeric silicates forming a poly(sialate)-siloxo or poly(sialate)-disiloxo 3D rigid polymeric structures, while in a low Si concentration a poly(sialate) polymer structure is formed. The poly(sialate) polymer structure is formed by the condensation and reaction between the aluminate and silicate species. However, an increase in the Si content creates oligomeric silicates (a condensation and reaction between silicate species) and forms poly(sialate)-siloxo or poly(sialate)-disiloxo. According to Silva et al. (2007), the rate of condensation between the silicate species themselves is slower than that between aluminate and silicate species.

Diaz-Loya et al. (2010) found that despite silicate and aluminate being the main contributors to the geopolymer reaction, CaO components from the fly ash precursors significantly affect the strength. The setting time was found to increase as the CaO content decreased below 20%, however the decrease in CaO was accompanied by a decline in the compressive strength of the resulting geopolymer. The authors suggested that CaO content in the range of 5% – 15% might be considered desirable for many applications.

Furthermore, Diaz-Loya et al. (2011) also found that the density of fly ash geopolymer is related to the fineness of the fly ash precursors. The activator solution demand rises as the fineness of fly ash decreases due to the need to fill larger voids among the coarse fly ash particles to achieve a workable material. However, a higher proportion of activator solution causes the overall density of the fly ash geopolymer to decrease which affects the modulus of elasticity and compressive strength of fly ash geopolymer concrete.

For AAS specimens, Wang et al. (1994) found that the strength properties are affected by several factors, i.e. the dosage of Na_2O, the alkali modulus (M_s), the type and the fineness of slag precursors. According to the authors, the best Na_2O dosage was within the range of 3.0% – 5.5%, with an alkali modulus of 0.75 – 1.5. The authors suggested that the fineness and the type of slag precursors (**Figure 2.16**) also play a significant role. Increasing the fineness of slag within its optimum range results in higher strength and the type of slag significantly affects the strength development at higher alkali modulus (M_s > 1.00).

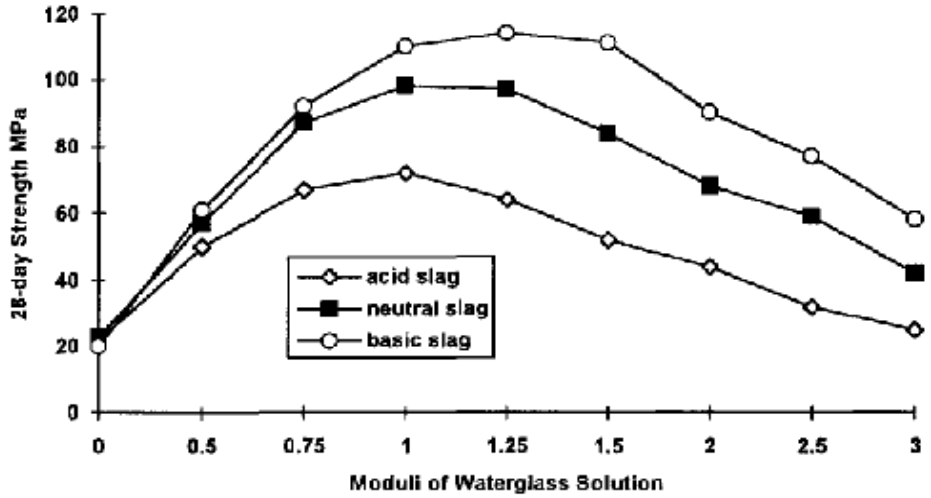

Figure 2.16 Moduli of waterglass solution vs 28-day strength for different type of slag (Wang et al., 1994)

Krizan & Zivanovic (2002) also found that the dosage of alkali modulus has a significant effect on the hydration process of alkali-slag cements. According to them, alkali-slag cements activated with sodium silicate with an alkali modulus between 0.6 and 1.5 results in a higher ultimate strength compared to Portland cement. However, it was also found that increasing the alkali modulus as well as the dosage of sodium silicate causes an increase on drying shrinkage. A similar finding was also observe by Adam (2009). The author found that Na_2O dosage and alkali modulus has significant effect on the strength development of AAS concrete. A Na_2O dosage of 5% and an alkali modulus (M_s) of 1.00 resulted in optimum strength with any further increase of alkali modulus tending to reduce the strength.

2.9. Durability of concrete

According to the ACI Committee 201 (ACI 201.2R-08, 2008), durability of ordinary Portland cement based concrete is determined by its ability to resist weathering action, chemical attack, abrasion or any other process of deterioration.

Isgor (2001) classified the deterioration of reinforced concrete structures into three main types (**Figure 2.17**):

1. Physical deterioration, due to cracking, frost attack, abrasion and fire.
2. Chemical deterioration, due to sulphate and acid attacks, biological, alkali aggregate reaction and leaching.
3. Reinforcement corrosion, due to carbonation and chloride attack.

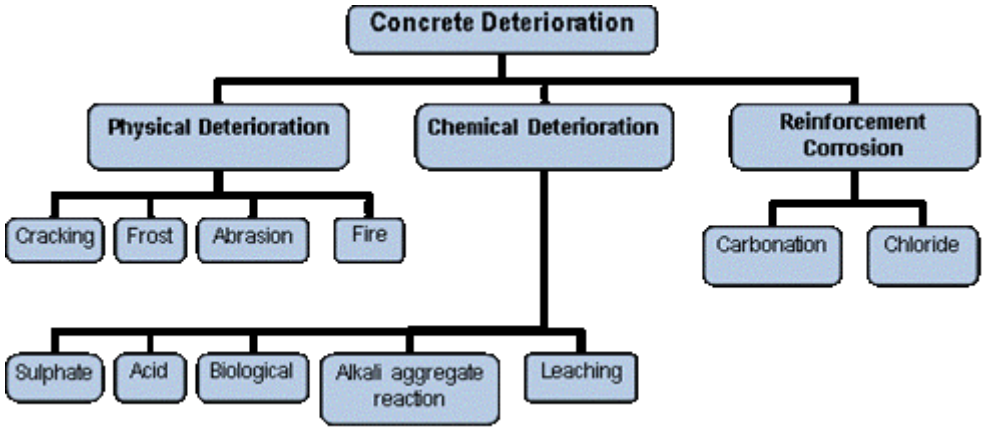

Figure 2.17 Deterioration of reinforce concrete structures (Isgor, 2001)

Based on a review of more than 400 published papers, Basheer et al. (1996) categorised the deterioration of reinforced concrete into two main types: the physical and the chemical mechanism. The authors also place carbonation and chloride attack as the main source of concrete deterioration (**Figure 2.18**).

Carbonation is caused by the dissolving of atmospheric carbon dioxide (CO_2) in concrete pore water. The reaction between the CO_2 and the calcium hydroxide forms an acidic solution which leads to the reduction of the pore solution's pH causing de-passivation of the steel and leading to corrosion. Chloride ions may

also be present in the mixing water, aggregates or accelerating admixtures. However, the most common issue is the ingression of chloride from outside the concrete, either from sea water for marine structures or due to the de-icing salts applied to highway structures. Both carbonation and chloride attack involves the presence of water as the CO_2 and chloride ions need to dissolve in water. According to Lees (1992), aggressive agents can penetrate concrete and react harmfully with the cement paste only when dissolved in water.

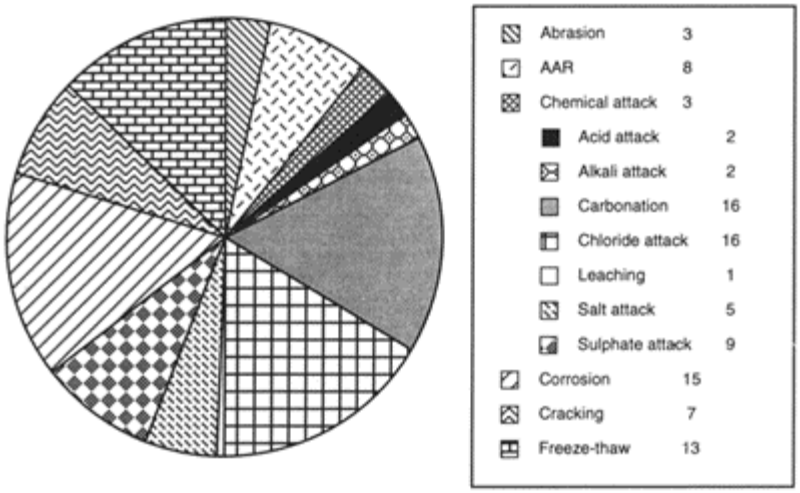

Figure 2.18 Reference to percentages assigned to the contribution of various mechanisms affecting durability (Basheer et al., 1996)

As carbonation and chloride attack are the main factors for the most common damage mechanisms related to reinforced concrete structures, the mechanism of chloride ingress and CO_2 diffusion from the environment, as well as the fluid transport mechanism into concrete plays a crucial role. The durability and the long term performance of concrete is significantly affected by these mechanisms (Basheer et al., 2001, Sagoe-Crentsil et al., 2010). Consequently, these mechanisms are the main focus of this durability study of fly ash geopolymer and AAS concrete.

2.9.1. Permeation properties of concrete

The permeation properties are defined as the ease with which fluids, both fluids and gases, can enter into or move through concrete (Ho, 2003). The permeation

properties are the crucial factors controlling the durability and the long term behaviour of concrete. The deterioration of concrete is most commonly caused either by the reaction between the penetrated aggressive agents such as water, carbon dioxide and chloride with the other aggressive agents which are already contained in the concrete, or by corrosion of the reinforcement which causes cracking of the concrete.

According to Basheer et al. (2001) and Ho (2003), the main transport processes which describe the movement of aggressive substances through concrete are distinguished as diffusion, absorption and permeability.

1. Diffusion is the process whereby a liquid, gas or ion migrates through concrete driven by a concentration gradient. The rate of diffusion is significantly affected by the characteristics of the penetrating substance and the chemistry of the concrete, as well as the concentration gradient and the size of capillary pores. The diffusion progress of a gas is very slow in saturated concrete, thus this property is a significant factor that need to be taken into account for a concrete in above-ground structures such as building or bridges, where concrete is in a partially dry condition.
2. Absorption is the transport of liquids in the pores of hardened cement paste due to surface tension capillary action under ambient conditions. The concrete takes in liquid by capillary suction to fill the pore space available. Capillary suction can occur in dry or partially dry concrete. This transport mechanism is particularly relevant to coastal structures where chloride salts are deposited on the concrete surface and then absorbed into the concrete.
3. Permeability is where a fluid flows through a concrete under the action of a pressure differential. The flow rate follows Darcy's law for laminar flow through a porous medium and depends on the pressure gradient and the size of interconnected pores. The concrete has to be in the saturated state with relevant pores being continuous and greater than 120 nm to allow the flow process. Permeability is a relevant property to assess the durability and service-ability of structures which have constant contact with water, such as dams, foundation and underground structures.

2.9.2. Chloride ion penetration

The penetration of chloride ions is the most significant problem related to OPC concrete exposed to marine environments or de-icing salts. In adequate concentration, chloride ions depassivate steel reinforcement and leads to corrosion, even under a high pH condition of concrete pore solution (Aitcin, 2004, Page, 2007) as shown in **Figure 2.19**.

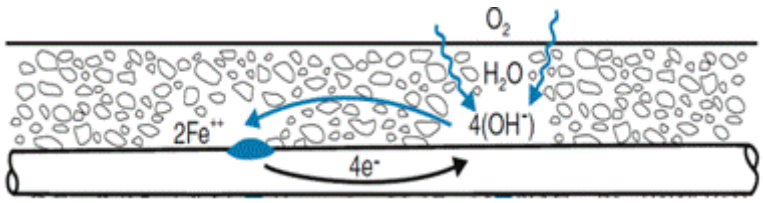

Figure 2.19 Reaction of corrosion (Cement Concrete & Aggregates Australia, 2009)

The reaction is divided into two reactions which are running simultaneously. The first reaction (anodic reaction, **Equation 2.13**) is an oxidation of iron to form ferrous ions, and the second reaction (cathodic reaction, **Equation 2.14**) is the forming of hydroxyl from the released electrons (from the oxidation of iron) which are consumed by oxygen.

Anodic reaction: $Fe \rightarrow Fe^{2+} + 2e^{-}$ *(2.13)*

Cathodic reaction: $O_2 + 2H_2O + 4e^{-} \rightarrow 4OH^{-}$ *(2.14)*

The state of reinforcement corrosion depending on the electrode potential and electrolytic pH of the corrosion cell can be illustrated by Pourbaix diagram as shown in **Figure 2.20**. These diagrams are based on equilibrium thermodynamics and defined as three regions in the potential-pH space which are: immunity region, corrosion region and passivity region (Markeset & Myrdal, 2008).

The transport process of chloride ions from sea water or de-icing salts into a concrete is a complex process which involves diffusion, capillary suction and convection (Elakneswaran et al., 2009). The most important characteristic related to the ingress of chloride ions is the pore structure of the cement past matrix which affects the porosity of concrete (Stanish et al., 1997). Lower porosity of a concrete leads to a reduction of the ingression of chloride ions into the concrete.

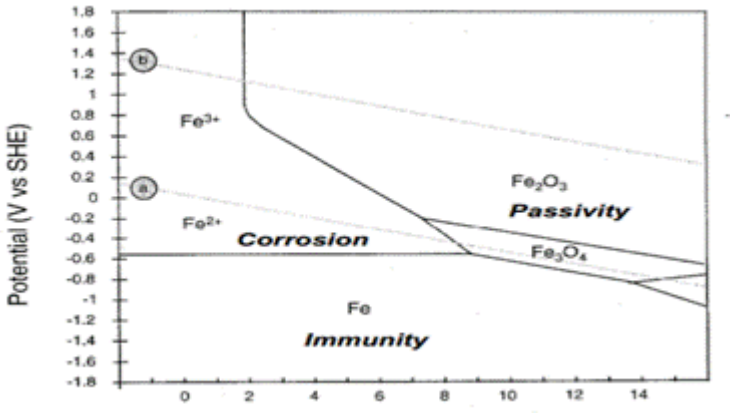

Figure 2.20 Simplified Pourbaix diagram for iron in water showing the most stable products at a given pH and potential (Markeset & Myrdal, 2008)

The accepted method to model the ingression of chloride ions due to diffusion is by applying Fick's first law as in **Equation 2.15** (Crank, 1975, Stanish et al., 1997). This equation can only strictly be applied under a steady state flow. This is a condition where the flow parameters, such as pressure, density and velocity are constant at a point of any time.

$$F = -D\frac{\partial C}{\partial x} \qquad (2.15)$$

where, F is the flux, C is the chloride concentration, D is the diffusion coefficient and x is the distance from the surface.

Fick's second law is applied to long term diffusion where the chloride flow is not steady. In this second law, the change in chloride ion content per unit time is equal to the change of the flux per unit length as in **Equation 2.16**.

$$\frac{\partial C}{\partial t} = -\frac{\partial F}{\partial x} \qquad (2.16)$$

2.9.3. Test method to evaluate chloride resistance of concrete

According to (Stanish et al., 1997), the resistance of concrete to the chloride ingression can be evaluated by using salt ponding test or a resistivity test. The resistivity test can also be used to determine the intensity of the initiated corrosion process of a concrete specimen (Song & Saraswathy, 2007).

The salt ponding test is a long term test for measuring the penetration of chloride ions into concrete in accordance with AASHTO T-259 (1997). The test set up is shown in **Figure 2.21**.

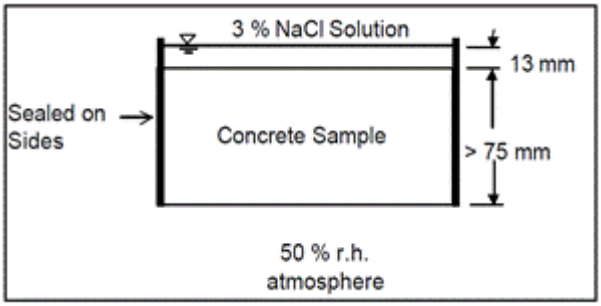

Figure 2.21 AASHTO T259 (salt ponding) test set up (Stanish et al., 1997)

The apparent chloride diffusion coefficient is found from the solution of **Equation 2.17** (Crank, 1975). This equation is applied to obtain the best fit curve to the chloride profile and the surface chloride concentration is determined from the intercept of the curve with the x=0 axis.

$$C_{x,t} = C_s\left[1 - erf\left[\frac{x}{2\sqrt{D_a t}}\right]\right] \qquad (2.17)$$

where, $C_{x,t}$ is the chloride concentration at depth x and time t, C_s is the chloride content at the surface, x is the depth, t is the time, D_a is the apparent diffusion coefficient and *erf* is an error function.

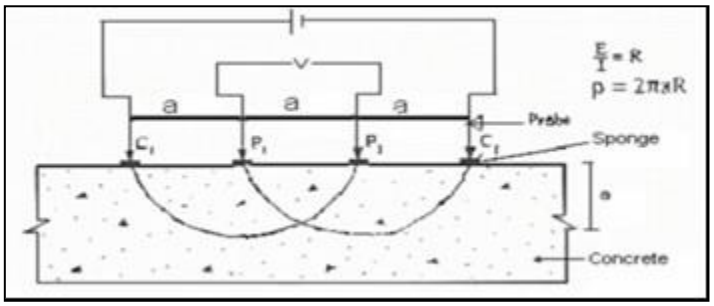

Figure 2.22 Circuit for electrical resistance (Song & Saraswathy, 2007)

The concrete resistivity is generally measured by using the Wenner array four probes method as shown in **Figure 2.22** (Song & Saraswathy, 2007, Stanish et al., 1997). The Wenner array probe test is a short term test to determine the

resistivity of concrete in situ, without removing cores of concrete. It consists of a set of four equally spaced probes. The current is applied through the two outer probes, while the two inner probes measure potential.

The resistivity of the concrete is calculated from the **Equation 2.18** (Song & Saraswathy, 2007, Stanish et al., 1997).

$$\rho = 2\pi a \frac{E}{I} \qquad (2.18)$$

where ρ is the resistivity of concrete, a is the distance between probes, E is the measured potential, and I is the applied current.

2.9.4 Carbonation of concrete

According to (Ho, 2003), carbonation is the process where carbon dioxide (CO_2) in air diffuses into concrete, dissolves in the pore solution, and then reacts with the hydroxides converting them to carbonates with a consequential drop of concrete pH to a value less than 9.

Carbonation of concrete is the reaction between the alkaline components in the cement paste and the CO_2 in the atmosphere which reduces concrete's pH to less than 9 (RILEM Recommendations, 1988). The decrease of a concrete's pH causes the depassivation of the steel reinforcement and permits corrosion. This deterioration particularly happens in urban environments with a high atmospheric CO_2 concentration.

The reaction between CO_2 and the $Ca(OH)_2$, a product of concrete hydration, produces $CaCO_3$, a calcium carbonate, which lowers the pH. According to Papadakis et al. (1989), the overall reaction between CO_2 and $Ca(OH)_2$ can be written as:

$$Ca(OH)_{2(s)} + CO_{2(g)} \rightarrow CaCO_{3(s)} + H_2O \qquad (2.19)$$

This reaction consists of elementary steps as shown in **Equation 2.20 – 2.24** (Papadakis et al., 1989). The dissolve of CO_2 in H_2O and the dissolution of calcium hydroxide in pore solution

$$CO_{2(g)} \rightarrow CO_{2(aq)} \qquad (2.20)$$

$$Ca(OH)_{2(s)} \rightarrow Ca^{2+}_{(aq)} + 2OH^{-}_{(aq)} \qquad (2.21)$$

The dissolved carbon dioxide reacts with hydroxide ions forming carbonate acid

$$CO_{2(aq)} + OH^-_{(aq)} \rightarrow HCO^-_{3(aq)} \quad (2.22)$$

The reaction between carbonate acid and hydroxide ions forms carbonate ions and water

$$HCO^-_{3(aq)} + OH^-_{(aq)} \rightarrow CO^{2-}_{3(aq)} + H_2O_{(aq)} \quad (2.23)$$

The reaction between Ca^{2+} and CO^{2-}_3 forms $CaCO_3$ the product of carbonation as in **Equation 2.24**.

$$Ca^{2+}_{(aq)} + CO^{2-}_{3(aq)} \rightarrow CaCO_{3(s)} \quad (2.24)$$

At high ambient relative humidity condition, all the pores of concrete are practically filled with water. The carbonation of $Ca(OH)_2$ in the presence of water can be written as:

$$CO_2 + H_2O \rightarrow H_2CO_3 \quad (2.25)$$

$$H_2CO_3 + Ca(OH)_2 \rightarrow CaCO_3 + 2H_2O \quad (2.26)$$

However, in a high concentration of hydroxyl ions, the solubility of $Ca(OH)_2$ significantly decreases (Houst & Wittmann, 2002). In this condition, the dissolved carbon dioxide reacts with sodium hydroxide producing sodium carbonate and releasing water (**Equation 2.27**). The sodium carbonate then reacts with calcium hydroxide forming calcium carbonate and release hydroxide ions as in **Equation 2.28**. These hydroxide ions will react again with carbon dioxide and continue as long as the calcium hydroxide is still available.

$$CO_2 + 2NaOH \rightarrow Na_2CO_3 + H_2O \quad (2.27)$$

$$Na_2CO_3 + Ca(OH)_2 \rightarrow CaCO_3 \downarrow + 2NaOH \quad (2.28)$$

The rate of carbonation is significantly affected by the moisture content of concrete. Low moisture content of concrete leads to the faster diffusion of CO_2, as the diffusion of gas in air is faster than in water. Contrary, if the moisture content is high, it will cause the pore of concrete to be fully filled with water and leads to a very low diffusion. However, the highest rate of carbonation occurs at a relative humidity between 50% - 70% as suggested by Neville (2011). Hence, the measurement of carbonation rate in an outdoor environment where the humidity varies is very difficult.

The depth of carbonation can be measured under a constant humidity as follows:

$$X = a + C\sqrt{t} \qquad (2.29)$$

where 'X' is the depth of carbonation, 'C' is the carbonation coefficient, 't' is the exposure period of accelerated carbonation, and 'a' is the empirical constant. The formulation in **Equation 2.29** has been agreed upon a numerous researchers (Houst & Wittmann, 2002, Sulapha et al., 2003, Sisomphon & Franke, 2007, Chang et al., 2004).

The carbonation of concrete can be detected using a phenolphthalein indicator solution which can be prepared by mixing a solution of 1% phenolphthalein and 70% ethyl alcohol as recommended by RILEM Recommendations (1988). The solution turns non-carbonated concrete into pink or violet colours and remains colourless in the carbonated region.

2.9.5 Autoclam water permeability test

The Autoclam permeability test system was developed by Montgomery and Adams and complemented with further research by Basheer and Long (Basheer et al., 2007).

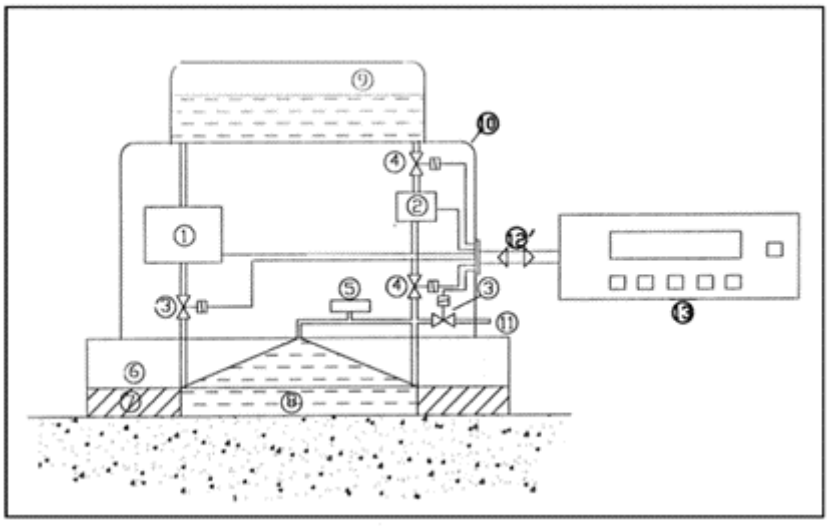

Figure 2.23 Schematic of Autoclam permeability system (Autoclam, 2010)

The experimental set-up for the test is shown in **Figure 2.23**. The transport mechanism of water into the capillary pores is considered to be due to the

absorption process rather than by the pressure induced flow from the Autoclam system. As water is absorbed by the capillary action, the pump and the control system maintain a constant pressure. The volume of water delivered into the concrete is measured and recorded by the equipment every minute, so that the total quantity of water which is absorbed is known. The result is represented by the water permeability index which can be determined by plotting the quantity of water flowing into the concrete against the square root of time. The slope between 5 and 15 minutes is used to specify the water permeability index in units of $m^3/\sqrt{min}$ (Basheer et al., 2007).

The Autoclam permeability system is highly suited to the study reported here as it can be applied on the same specimens at the same location for long periods of time without damaging the specimens.

2.10. Summary of chapter 2

Chapter 2 on literature review may be summarised as follows:

1) Fly ash and GGBS can be used as 100% cement replacement material in short term periods.
2) The mechanical properties of fly ash geopolymer and AAS concretes can be measured based on the compressive strength, modulus of elasticity and tensile strength.
3) The permeation properties are a significant factor to the concrete durability when the concrete is exposed to chloride environment and carbon in the atmosphere.
4) The modulus of elasticity of fly ash geopolymer concrete demonstrates lower performance compared to that OPC concrete. However, fly ash geopolymer concrete shows a comparable compressive strength and a better tensile strength compared to OPC concrete in the short term.
5) The compressive strength and tensile strength of AAS concrete is comparable to that OPC concrete in the short term. However, there are concerns over the long term performance due to the increase of sorptivity with time.

3. MATERIALS AND EXPERIMENTAL METHODS

3.1. Overview

This chapter presents the detail of the materials and the experimental methods for the development of fly ash geopolymer and alkali-activated slag (AAS) specimens. The properties and specifications of the materials and the mix proportion of the fly ash geopolymer and AAS specimens are described. The experimental methods for the specimens, the test program and the test parameters are explained.

3.2. Materials

3.2.1. Fly ash

The fly ash used to manufacture fly ash geopolymer was provided by Cement Australia Ltd Australia from Tarong power station. As comparison, fly ash supplied by Blue Circle Southern Cement Ltd Australia from Mt. Piper power station will be used. Both fly ashes were low calcium fly ash (class F fly ash) in accordance with Australian Standard (AS 3582.1, 1998). A Scanning Electron Microscope (SEM) image of Cement Australia fly ash (PFA1) and Blue Circle Southern Cement fly ash (PFA2) were shown in **Figure 3.1** and **Figure 3.2**, and the chemical compositions were presented in **Table 3.1**.

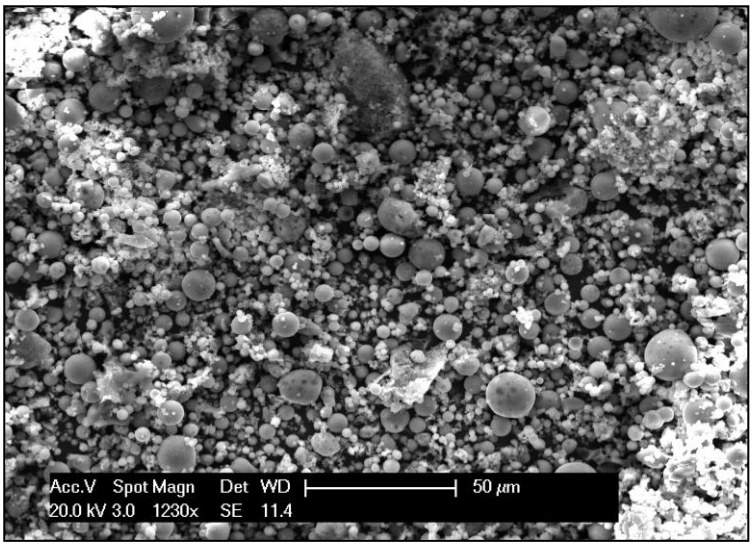

Figure 3.1 SEM images of Cement Australia fly ash (PFA1)

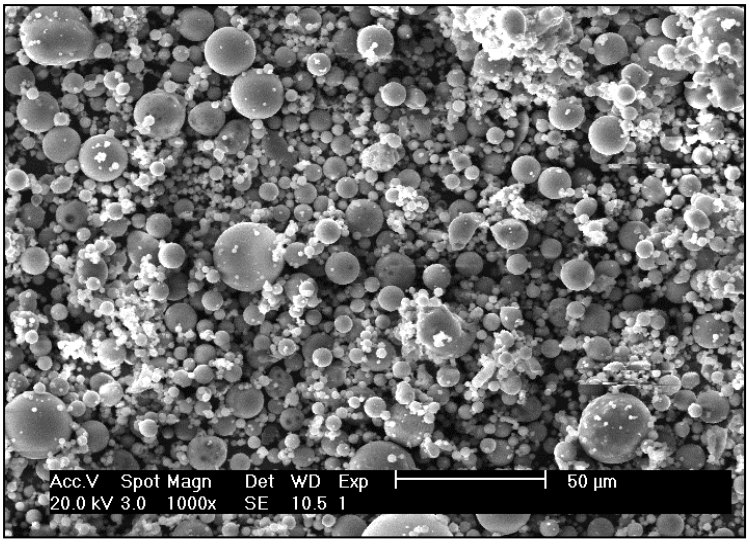

Figure 3.2 SEM images of Blue Circle Southern Cement fly ash (PFA2)

Both fly ashes used in this research were class F fly ash according to the requirement of ASTM standard (ASTM C618-03, 2003), as shown in **Table 3.2**. The lime (CaO) contained in both fly ashes was also less than 10%, i.e. PFA1 was 0.18% and PFA2 was 2.02%.

Table 3.1 Chemical compositions of fly ash (mass %)

Component	PFA1	PFA2
SiO_2	70.30	66.67
Al_2O_3	23.10	25.07
Fe_2O_3	1.40	1.69
CaO	0.18	2.02
MgO	0.56	NA
K_2O	0.91	1.00
Na_2O	0.35	0.38
TiO_2	2.60	1.24
P_2O_5	0.22	1.24
Mn_2O_3	NA	0.04
SO_3	0.26	0.63
LOI	2.00	1.53

Table 3.2 PFA1 and PFA2 in accordance with ASTM C618-03 (2003)

Components	$SiO_2+Al_2O_3+Fe_2O_3$ (%)	SO_3 (%)	Na_2O (%)	LOI (%)
ASTM C618	$\geq$ 70.00	$\leq$ 5.00	$\leq$ 1.50	$\leq$ 6.00
PFA1	94.80	0.26	0.35	2.00
PFA2	93.43	0.63	0.38	1.53

The XRD diffractograms of Cement Australia fly ash (PFA1) and Blue Circle Southern Cement fly ash (PFA2) are shown in **Figure 3.3** and **Figure 3.4**. These are both Class F fly ash with low calcium content with some quartz and mullite crystalline inclusions in a vitreous form. Quartz is found in small amounts and in some cases mullite is found as well. PFA1 was noted as having a higher quartz and mullite content than that of PFA2. The XRD analysis was performed using a Bruker D4 Endeavour machine with a scanning resolution of 1^O over a range starting at 6^O through to 90^O at 2θ scale and was carried out at the X-Ray facility, RMIT University, Melbourne, Australia.

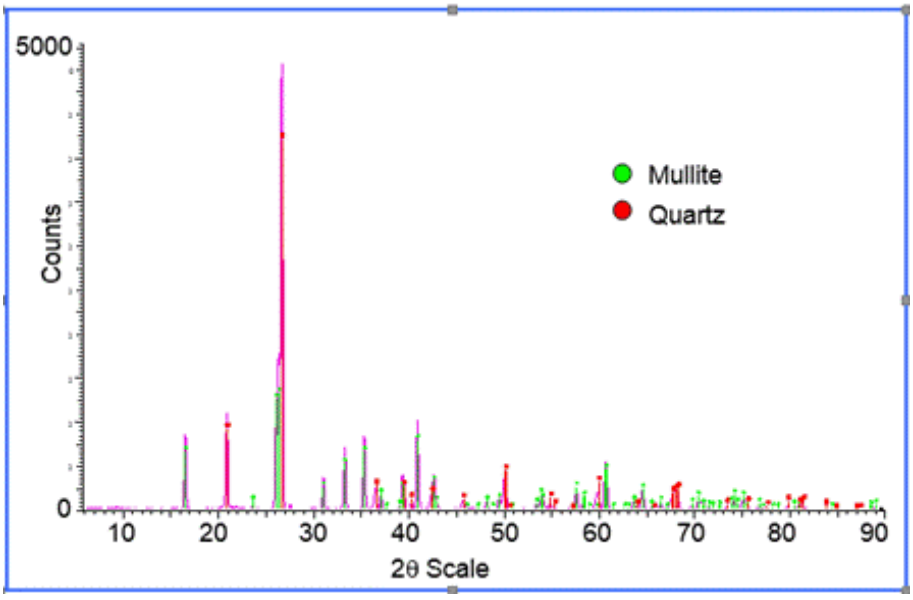

Figure 3.3 XRD diffractograms of PFA1

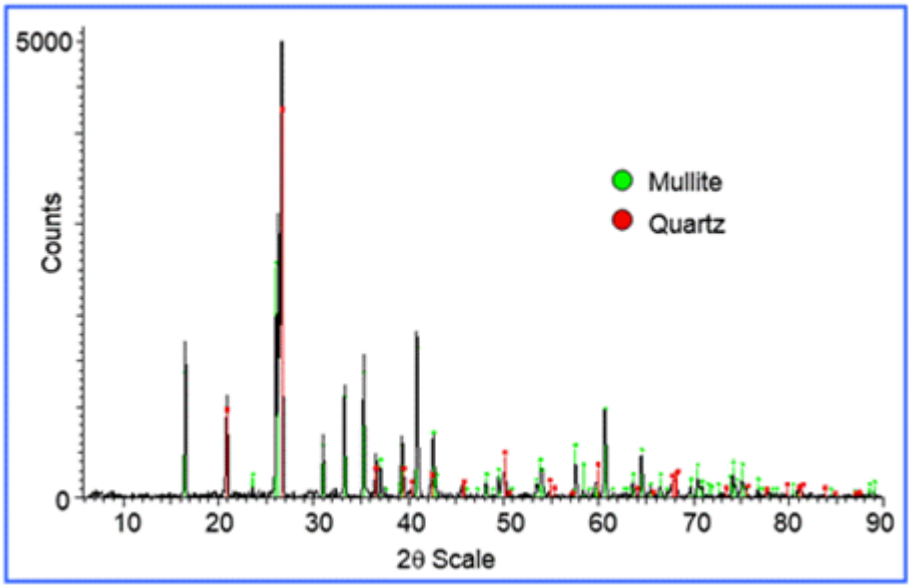

Figure 3.4 XRD diffractograms of PFA2

The fineness of the fly ashes was measured using a Malvern Particle Size Analyser (Mastersizer X) carried out at carried at the Rheology and Material Processing Centre (RMCP) facility, RMIT University, Melbourne, Australia. The fineness of the fly ashes was 64.78% for PFA1 and 72.85% for PFA2 passing 45 μm sieves, respectively.

3.2.2. Slag

The slag used to produce alkali-activated slag was ground granulated blast furnace slag (GGBS), a construction grade slag, supplied by Independence Cement & Lime Ltd Australia. The properties of this slag conformed to Australian Standard (AS 3582.2, 2001). A SEM image of slag is shown in **Figure 3.5** and the chemical composition is presented in **Table 3.3**.

The GGBS used for this mortar research was classified as acid slag ($K_b < 1$) with the basicity coefficient (K_b) of 0.811 and 0.803 as given in **Equation 2.6** and **Equation 2.7**, respectively. The GGBS has complied with the requirement of an AAS binder with a CaO/SiO_2 ratio of 0.976, an Al_2O_3/SiO_2 ratio of 0.386 and a hydration modulus (HM) of 1.499 as given in **Section 2.5.5**.

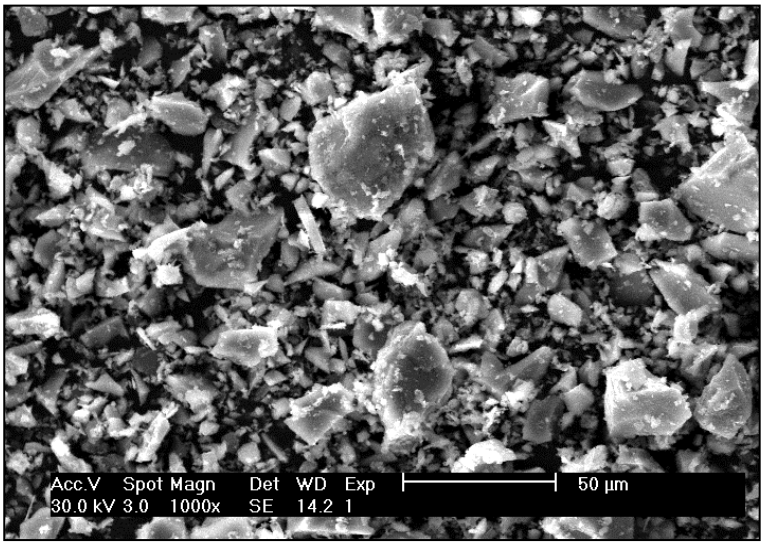

Figure 3.5 SEM images of GGBS

Table 3.3 Chemical compositions of GGBS (mass %)

Component	GGBS
SiO_2	36.87
Al_2O_3	14.23
Fe_2O_3	0.32
CaO	36.00
MgO	5.05
K_2O	0.05
Na_2O	0.01
TiO_2	0.63
P_2O_5	0.36
Mn_2O_3	0.39
SO_3	6.08
LOI	NA

The XRD diffractograms of GGBS with the scanning rate of 1^O from 6^O to 90^O at 2θ scale was given in **Figure 3.6**. The XRD diffractograms demonstrated that GGBS contained semi-crystalline and amorphous phased with low intensity peaks corresponding to gypsum. The fineness of the GGBS was 93.86% passing 45 μm sieves.

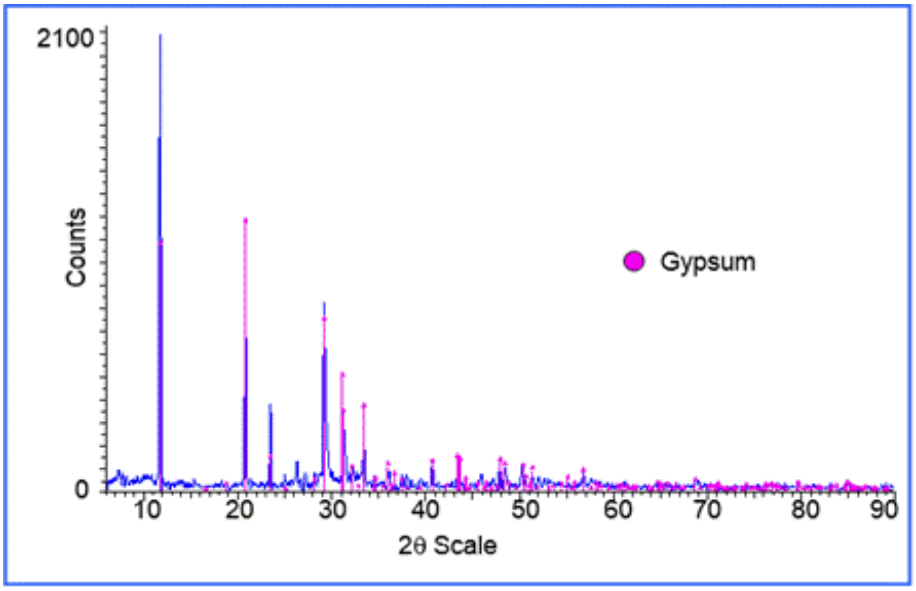

Figure 3.6 XRD diffractograms of GGBS

3.2.3. Alkaline activators

The activator contained a combination of sodium silicate (Na_2SiO_3) and sodium hydroxide (NaOH) solution. The Grade D sodium silicate (in solution form) was supplied by PQ Australia.

Table 3.4 Chemical and physical properties of liquid sodium silicate

Product Name	D™
Wt. Ratio SiO_2/Na_2O	2.00
$\%Na_2O$	14.7
$\%SiO_2$	29.4
Density @ 68°F(20°C) °Be'	50.5
Density @ 68°F(20°C) lb/gal	12.8
Density @ 68°F(20°C) g/cm^3	1.53
pH	12.8
Viscosity Centipoises	400
Characteristics	Clear to opalescent liquid

(Source: PQ Australia)

The chemical composition of the sodium silicate solution was 14.7% Na_2O and 29.4% SiO_2 with a SiO_2/Na_2O wt. ratio of approximately 2.00 and a density of 1.53 g/cm^3. The properties of the sodium silicate solution based on the MSDS of PQ Australia are shown in **Table 3.4**. Sodium hydroxide solutions were prepared by dissolving sodium hydroxide pellets with de-ionised water. A high alkaline solution of 15M NaOH was used for the fly ash geopolymer and a lower concentration of alkaline solution, 10M NaOH was used for the AAS.

3.2.4. Fine aggregates

The fine aggregate used for the production of fly ash geopolymer and AAS specimens was from Langwarrin source, Victoria, Australia, with the fineness modulus of 2.03 conforming to Australian Standard (AS 1141.5, 2000). Typical grading of the fine aggregate is shown in **Table 3.5**.

Table 3.5 Grading of the fine aggregate

Test sieve size	Retained (%)	Cumulative passing (%)	Specification passing (%)
4.75 mm	0.4	99.6	90 – 100
2.36 mm	4.6	95.0	85 – 97
1.18 mm	7.9	87.1	70 – 95
600 μm	13.2	74.0	45 – 80
300 μm	36.4	37.6	25 – 47
150 μm	34.4	3.2	0 – 15
75 μm	2.9	0.3	0 – 5
PAN	0.3	0.0	0

3.2.5. Combined aggregates

The fine and coarse aggregates used for the production of the fly ash geopolymer and AAS specimens were prepared in accordance with Australian Standards (AS 1141.5, 2000, AS 1141.6.1, 2000). The moisture condition of the coarse aggregates was saturated surface dry (SSD). The fine aggregate was from the Langwarrin source and the coarse aggregates were from the Mawson Lake Cooper quarry with a specific gravity of 2.99. The typical grading of the combined aggregate is shown in **Table 3.6**.

Table 3.6 Grading of the combined aggregate

Test sieve size	Aggregate			Combination *)
	Fine	7 mm	10 mm	
19.00 mm	100.0	100.0	100.0	100.00
9.50 mm	100.0	100.0	100.0	100.00
6.70 mm	100.0	96.0	100.0	99.24
4.75 mm	99.6	36.0	21.0	57.65
2.36 mm	95.0	3.0	2.0	42.18
1.18 mm	87.1	0.0	1.0	37.83
600 μm	74.0	1.0	0.0	32.01
300 μm	37.6	0.0	0.0	16.17
150 μm	3.2	0.0	0.0	1.38
75 μm	0.3	0.0	0.0	0.13
PAN	0.0	0.0	0.0	0.00

*) 43% (fine) + 19% (7 mm) + 38% (10 mm) (Adam, 2009)

3.3. Mix proportion

According to Wang et al. (1994), the dosage and the activator modulus played a significant role on the properties of the alkali-activated cementitious materials.

The dosage of activator was defined as the ratio of the Na_2O content of the alkaline activator to the mass of the binder. While, the activator modulus (AM) was the mass ratio of the SiO_2 to the Na_2O in the alkaline activator.

3.4. Notations

Specimen notations used for fly ash geopolymer and AAS specimens are as follows:

a) Fly ash geopolymer b) AAS

Figure 3.7 Notations for (a) fly ash geopolymer and (b) AAS specimens

'X' represents the specimen name with G = fly ash geopolymer and AAS = alkali-activated slag; 'a' represents the type of fly ash for fly ash geopolymer only, i.e. A = fly ash type 1 (PFA1) and B = fly ash type 2 (PFA2); 'b' represents the concentration level of Na_2O (%) which was 15% for the fly ash geopolymer and 5% for the AAS; while 'c' represents the activator modulus (M_s), i.e. M_s = 1.00 ; 1.125 ; 1.25.

3.5. Mechanical properties

Mechanical properties tests will cover the compressive strength test, the modulus of elasticity test, the flexural tensile strength (modulus of rupture test), the indirect tensile strength (splitting test), and the measurement of density.

3.5.1. Compressive strength test

The compressive strength test was carried out in accordance with Australian Standard (AS 1012.9, 1999). All compression tests were performed using the MTS machine with a loading capacity of 1000 kN as shown in **Figure 3.8**.

For fly ash geopolymer and AAS mortar specimens, three cube specimens were tested for compressive strength 3, 7, 14 and 28 days after casting for each mix design with a loading rate of 1 MPa/minute. The size of specimen was 50 mm cubes.

Figure 3.8 Compressive strength test

For fly ash geopolymer and AAS concrete specimens, three cylinder specimens (100 mm diameter x 200 mm long) were tested for compressive strength 28, 56, 90, 180, 360 and 540 days after casting for each mix design to determine the long term performance of the specimens. A loading rate of 20 $\pm$ 2 MPa/minute was adopted. The compressive strength was calculated from the applied load at the point of cylinder failure. The failure pattern of the crushed cylinders was recorded photographically. The average of the three tests of cylinder was reported.

The compressive strength of the specimen was calculated using AS 1012.9-1990 as follows:

$$\sigma = \frac{F}{A} \tag{3.1}$$

Where:

σ = the compressive strength (MPa)

F = the force applied (N)

A = the cross-sectional area (mm^2)

3.5.2. Modulus of elasticity

The static modulus of elasticity tests were performed on the MTS machine modified by the adoption of a Linear Variable Differential Transformer (LVDT) according to Australian Standard (AS 1012.17, 1997). The static elastic modulus was undertaken by subjecting cylinder specimens to uni-axial compression with a loading rate of 15 $\pm$ 2 MPa/min. The strain was measured by a compressometer with a gauge length of 100 mm and a 20.000 x 10^{-6} strain capacity. The compressometer utilised a pair of LVDTs on the opposite side of the concrete cylinder, as shown in **Figure 3.9**.

The test load was determined using method 1, of article 2.5.1 (a) AS 1012.17-1997, and represents the equivalent of 40% of the average compressive strength of no fewer than two specimens. A series of readings were taken and the stress-strain relationship was established. Three cylinders (100 mm diameter x 200 mm long) were tested for each data point. The first and second readings were discarded - used for the setting of the gauges. Tests were carried out at 28, 90, 180, 360 and 540 days after casting.

Figure 3.9 Modulus of elasticity test with compressometer

The static modulus of elasticity (E) of the specimen was calculated using AS 1012.17-1997 as follows:

$$E = \frac{(G_2 - G_1)}{(\varepsilon_2 - 0.00005)} \tag{3.2}$$

Where:

- E = the static modulus of elasticity (MPa)
- G_1 = the applied load at a strain of 50 x 10^{-6} m/m (MPa)
- G_2 = the test load divided by the cross-sectional area of the unloaded specimen (MPa),
- ε_2 = the deformation at test load divided by the gauge length (10^{-6} m/m).

The correlation between the modulus of elasticity of concrete and its compressive strength based on Australian Standard (AS 3600, 2009) clause 3.1.2 (a) was also presented as comparison. The modulus of elasticity of normal concrete can be calculated using AS 3600-2009 as follows:

(i) $E_{ci} = \left(\rho^{1.5}\right)$ x $\left(0.043\sqrt{f_{cmi}}\right)$ in MPa, when $f_{cmi} \leq 40$ MPa (3.3)

(ii) $E_{ci} = \left(\rho^{1.5}\right)$ x $\left(0.024\sqrt{f_{cmi}} + 0.12\right)$ in MPa, when $f_{cmi} > 40$ MPa (3.4)

(iii) $f_{cmi} = 90\% f_{cm}$ (3.5)

Where:

E_{ci} = the mean modulus of elasticity of concrete at appropriate age (MPa)

ρ = the density of concrete in accordance with AS 10.12.12.1 (kg/m^3)

f_{cmi} = the mean value of the in situ compressive strength (MPa)

f_{cm} = the mean value of the cylinder strength (MPa)

3.5.3. Flexural tensile strength

The flexural tensile strength (modulus of rupture test) (**Figure 3.10)** was carried out on the MTS machine in accordance with Australian Standard (AS 1012.11, 2000). The setup of the flexural tensile strength test followed a four point bending test as shown in **Table 3.7** conforming Table 1 AS 1012.11-2000.

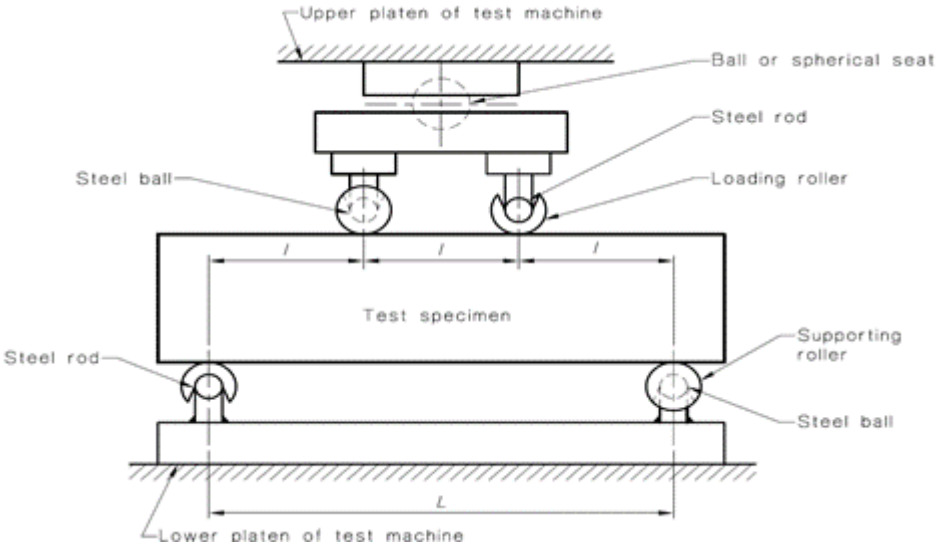

Figure 3.10 Flexural testing apparatus (AS 1012.11, 2000)

Table 3.7 Centre to centre distance of the supporting rollers

Nominal size of specimens mm	Centre to centre distance of rollers	
	Supporting rollers (*L*) Mm	Loading rollers (*l*) Mm
150 x 150 100 x 100	450 + 10, – 5 300 + 8, – 3	$\frac{L}{3} \pm 1$

The nominal size of specimens (**Figure 3.11)** was 100 x 100 mm with supporting rollers (L) at a span of 300 mm (overall length 350mm). A loading rate of 1 $\pm$ 0.1 MPa/min was adopted. Three prism specimens were tested for each data point. The test was undertaken 28, 56, 90, 180, 360 and 540 days after casting.

Figure 3.11 Flexural tensile strength test

The flexural tensile strength which was determined based on the modulus of rupture (f_{cf}) of the specimen was calculated using AS 1012.11-2000:

$$f_{cf} = \frac{PL(1000)}{BD^2} \tag{3.6}$$

Where:

- f_{cf} = the flexural tensile strength / modulus of rupture (MPa)
- P = the maximum applied force indicated by testing machine (kN)
- L = the span length (mm)
- B = the average width of specimen at the section of failure (mm)
- D = the average depth of specimen at the section of failure (mm)

The flexural tensile strength (f_{cf}) was used to assess the uniaxial tensile strength of the concrete. The correlation between the flexural tensile strength of concrete and uniaxial tensile strength (f_{ct}) was determined based on Australian Standard (AS 3600, 2009) article 3.1.1.3 (a) as follows:

$$f_{ct} = 0.6 f_{cf} \tag{3.7}$$

Where:

f_{ct} = the uniaxial tensile strength (MPa)

f_{cf} = the flexural tensile strength in accordance with AS 1012.11 (MPa)

3.5.4. Indirect tensile strength

The indirect tensile strength test was performed on the MTS machine in accordance with Australian Standard (AS 1012.10, 2000). The MTS machine was equipped with indirect tensile strength test equipment as shown in **Figure 3.12** and **Figure 3.13** with a loading rate of 1.5 $\pm$ 0.15 MPa/min. Three sets of cylinder specimens were tested 28, 56, 90, 180, 360 and 540 days after casting. The specimen was a 150 mm diameter x 300 mm long cylinder.

The indirect tensile strength (T) of the specimen was calculated using AS 1012.10-2000:

$$T = \frac{2000P}{\pi LD} \tag{3.8}$$

Where:

T = the indirect tensile strength (MPa)

P = the maximum applied force indicated by the testing machine (kN)

L = the length (mm)

D = the diameter (mm)

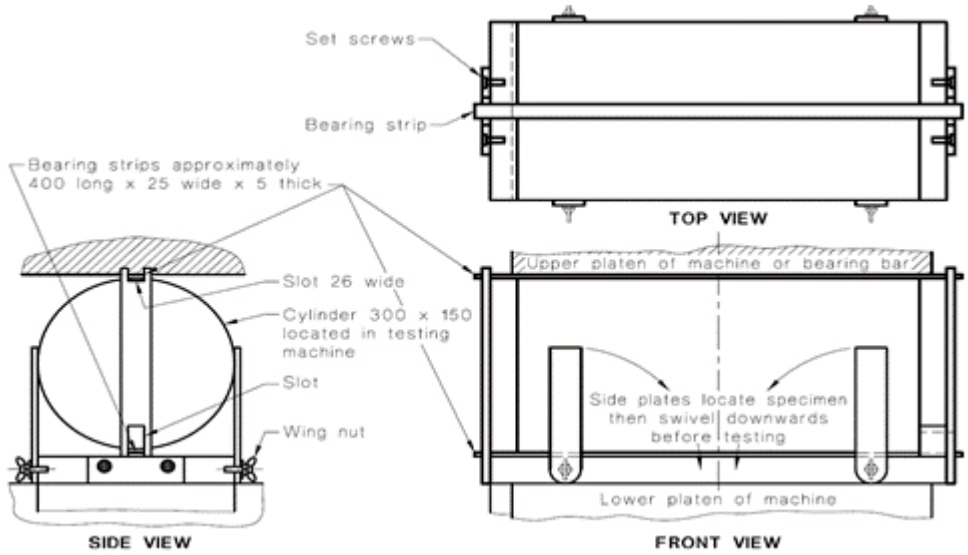

Figure 3.12 Indirect tensile strength apparatus (AS 1012.10, 2000)

Figure 3.13 Indirect tensile strength test

The indirect tensile strength was used to assess the tensile strength of the concrete. The correlation between the indirect tensile strength of concrete and uniaxial tensile strength (f_{ct}) was determined based on Australian Standard (AS 3600, 2009) clause 3.1.1.3 (b) as follows:

$$f_{ct} = 0.9 f_{ct.sp} \tag{3.9}$$

Where:

f_{ct} = the uniaxial tensile strength (MPa)

$f_{cf.sp}$ = T = the indirect tensile strength in accordance with AS 1012.10 (MPa)

3.5.5. Density

The density of the concrete specimens (100 mm diameter x 200 mm long cylinder) was estimated using rapid measuring method in accordance with Australian Standard (AS 10.12.12.1, 1998). Three sets of cylinder specimens were tested at 28, 56, 90, 180, 360 and 540 days after casting.

The density of hardened fly ash geopolymer and AAS concretes using the rapid measuring method was obtained by determining the mass of the specimen and the volume as calculated from the dimensions of the test specimens. The standard moisture condition of the concrete specimens was in the saturated surface-dry (SSD) condition.

The density of the specimen based on the rapid measuring method was calculated using AS 1012.12.1-1998 as follows:

$$\rho = \frac{m}{v} \tag{3.10}$$

Where:

ρ = the density of the specimen (kg/m^3)

m = the mass of the specimen (gram)

v = the volume of the specimen, determined from the measurement (m^3)

Note: The average density of a group of specimens shall be rounded off to the nearest 20 kg/m^3.

3.6. Durability properties

Durability tests will include the porosity test, the water absorption test, the water permeability test, the surface hardness test, the ultrasonic pulse velocity (UPV) test, the resistivity test, the chloride diffusion test and the carbonation test.

3.6.1. Porosity

The porosity or volumetric proportion of void test was undertaken in accordance with ASTM C642-97 (2003). The porosity test can be used to identify the possibility of micro-cracks on fly ash geopolymer and AAS concrete specimens. Three sets of cylinder specimens, 100 mm diameter x 200 mm long, were tested 28, 56, 90, 180, 360 and 540 days after casting. The procedure was as follows:

1) Dry the specimen in an oven at temperature of 100^{O}C to 110^{O}C for not less than 24 hours and record the mass of the specimen (*A*) in grams.
2) Store the specimen in water at a temperature of approximately 21^{O}C for not less than 48 hours. Then, boil the specimen in water for 5 hours.
3) Immerse in water at temperature of approximately 21^{O}C for approximately 1 hour. Then, weigh (*D*) the specimen (kg) while suspended in a tank of water.
4) Surface-dry the specimen and determine the mass of the specimen (*C*) in grams at the moisture condition of SSD.

The porosity of the specimen is calculated as follows:

$$\phi = \frac{(C - A)}{(C - D)} x100\% \quad (3.11)$$

Where:

ϕ = the porosity of the specimen (%)

A = the mass of the specimen from the oven (grams)

C = the mass of the specimen after immersion in SSD condition (grams)

D = the mass of the specimen during immersion in a water tank (grams)

According to Technical Report No.54 (2000), the relationship between the concrete quality and the porosity can be predicted as shown in **Table 3.8**.

Table 3.8 Classification of the quality of concrete based on porosity

Quality of concrete	Classification	Percentage volume of Penetrated voids
Good	Good or low porosity	< 10%
Average	Medium porosity	10% - 15%
Poor	Highly porous concrete	> 15%

3.6.2. Water absorption

The water absorption test was carried out in accordance with Australian Standard (AS 1012.21, 1999) to determine the immersed absorption. Immersed absorption (A_i) is the ratio (%) of the mass of water contained in a concrete specimen, and was used to determine the water absorption of fly ash geopolymer and AAS concrete specimens. The specimens of 100 mm diameter x 200 mm long cylinders were cut into four equal slices and the result were the average of the results for the four slices. The specimens were tested 28, 56, 90, 180, 360 and 540 days after casting.

The procedure of the immersed absorption (A_i) test in accordance with AS 1012.21-1999 articles 7.1 was as follows:

1) Weigh the specimen to the nearest 0.1 grams and dry in an oven at temperature of 100^{O}C to 110^{O}C for not less than 24 hours. After removing the specimen from the oven, allow it to be cool then determine the oven-

dry mass of the cooled specimen and record as M_1 to the nearest 0.1 grams.

2) After final drying, cooling and weighing, immerse the specimen in water at 23 $\pm$ 2^{O}C for not less than 48 hours.

3) Surface-dry the saturated specimen by removing the surface moisture and determine its mass M_{2i} to the nearest 0.1 grams.

The water absorption of the specimen based on immersed absorption method was calculated using AS 1012.21-1999 articles 8(a) as follows:

$$Ai = \frac{(M_{2i} - M_1)}{M_1} x100\% \quad (3.12)$$

Where:

A_i = the immersed absorption of the specimen (%)

M_{2i} = the mass of the specimen after immersion in SSD condition (grams)

M_1 = the mass of the specimen from the oven (grams)

3.6.3. Water permeability

The water permeability test was performed using the Autoclam Permeability System (Montgomery et al., 1993, Claisse et al., 2003, Basheer et al., 2007). The water permeability test was conducted 28, 90, 180, 360 and 540 days after casting for each mix design. Two cube specimens 300 mm x 300 mm x 100 mm were tested 28, 56, 90, 180, 360 and 540 days after casting for fly ash geopolymer and AAS concretes. The test was carried out at one location on each specimen.

Figure 3.14 AutoCLAM equipment for water permeability test

3.6.4. Ultrasonic Pulse Velocity (UPV)

The Ultrasonic Pulse Velocity (UPV) was measured in accordance with ASTM Standard (ASTM C597-02, 2003). The UPV test is also considered as a non-destructive testing (NDT) method and is used to determine the strength and quality of a material based on the speed of a stress wave passing through the medium which is related to the elasticity-density. According to the ASTM C597-02 (2003), the UPV testing apparatus shall consist of a pulse generator, a pair of transducers, a time measuring circuit, a time display unit and connecting cables as shown in **Figure 3.15** and **Figure 3.16**.

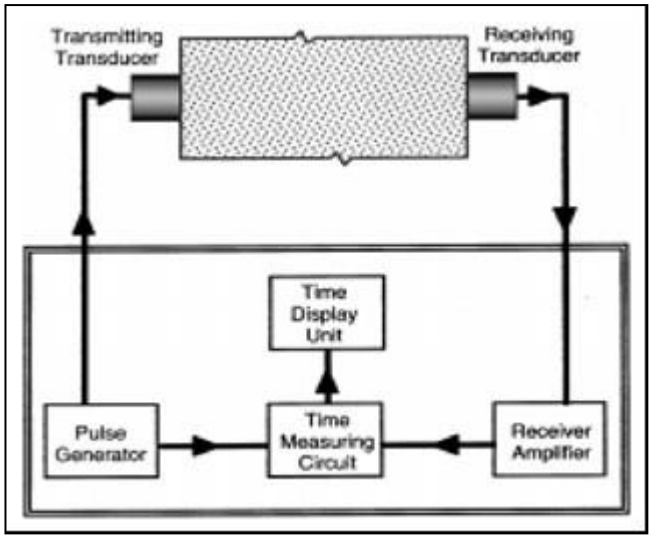

Figure 3.15 Schematic of pulse velocity apparatus (ASTM C597-02, 2003)

Figure 3.16 Ultrasonic Pulse Velocity (UPV) test equipment

All these tests were carried out using the TICO ultrasonic instrument from Proceq. Three cuboid specimens of 200 mm x 200 mm x 100 mm were tested 28, 90, 180, 360 and 540 days after casting for fly ash geopolymer and AAS concretes. The UPV was measured with a pulse of longitudinal vibration produced by an electro-acoustical transducer and received by another transducer after travelling a known path. The transit time (T) and the pulse velocity (V) was measured and calculated. The quality of the specimen can be predicted on the basis of pulse velocity (IAEA, 2002) as shown in **Table 3.9**.

Table 3.9 Classification of the quality of concrete based on velocity (IAEA, 2002)

Longitudinal pulse velocity (km/s.10^3)	Quality of concrete
> 4.5	Excellent
3.5 – 4.5	Good
3.0 – 3.5	Doubtful
2.0 – 3.0	Poor
< 2.0	Very poor

The testing procedure of UPV test was as follows:

- Set the instrument by connecting the transducers to the UPV equipment.
- Calibrate the instrument using the calibration cylinder. The transit time (T) reading should be approximately 20.5 μs.
- Put and hold transducers firmly against each end of specimens.
- Record the transit time (μs) and the pulse velocity (m/s) reading.
- Take at least 10 readings from the specimens.

The pulse velocity was calculated using ASTM C597-02 as follows:

$$V = \frac{L}{T} \tag{3.13}$$

Where:

V = the pulse velocity (m/s)

L = the distance between centres of transducer faces (m)

T = the transit time (seconds)

3.6.5. Resistivity

The resistivity test is designed to measure the electrical resistivity of the concrete specimen in an effective and non-destructive manner and is common practice within the field. The electrical resistivity of concrete is an important parameter in assessing the likelihood of corrosion having initiated. High electrical resistivity of a concrete will tend to slow the corrosion process compared to that of a concrete with a low resistivity (Song & Saraswathy, 2007). The resistivity test will be conducted using RESI resistivity meter from Proceq. The resistivity reading was in a scale of 0 – 100 kΩcm. Three cuboid specimens of 200 mm width x 200 mm length x 100 mm were tested at 28, 90, 180, 360 and 540 days after casting for fly ash geopolymer and AAS concretes.

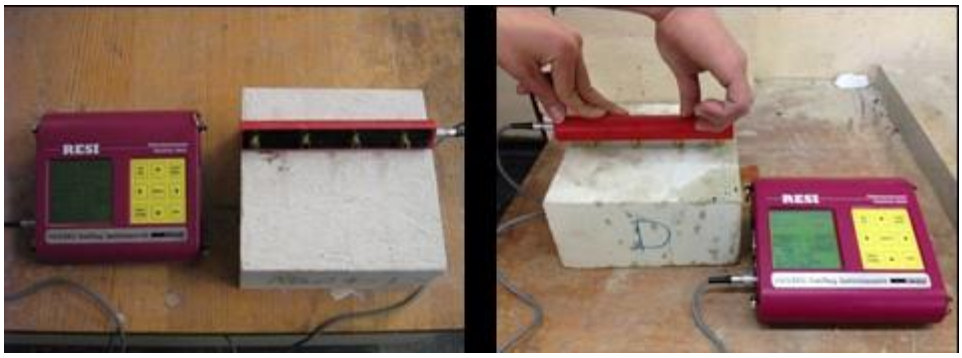

Figure 3.17 Resistivity test equipment

The relationship between the risk of corrosion and the resistivity measurements can be predicted (IAEA, 2002) and shown in **Table 3.10**.

Table 3.10 Corrosion risk from resistivity measurement (IAEA, 2002)

Resistivity (Ohm.cm)	Corrosion risk
Greater than 20,000	Negligible
10,000 to 20,000	Low
5,000 to 10,000	High
Less than 5,000	Very high

The testing procedure for the resistivity test was as follows:

- Calibrate the instrument using the calibration instrument. The actual reading should be 12 $\pm$ 1 kΩcm with the current at 100%.
- Put and hold the probe firmly on the surface of specimens.
- Record the actual resistivity (kΩcm) and the current (%) readings.
- Take at least 10 readings from the specimens.

3.6.6. Chloride diffusion

The chloride diffusion coefficient (D_a) and the surface concentration (C_s) were determined based on the chloride ponding test in accordance with AASHTO and ASTM standards (AASHTO T-259, 1997, ASTM C1543-02, 2003).

100 mm x 100 mm x 100 mm cast cubes were tested. All faces, except the bottom face, were painted with epoxy in order to make the chloride ingress uni-directional as demonstrated in **Figure 3.18**. This method facilitated the preparation of chloride specimens without the need for coring.

(a) Specimens with epoxy (b) Specimens in 3% NaCl solution

Figure 3.18 Salt ponding test (a) Coated specimen ; (b) NaCl solution

The test was carried out 90 days after casting. 3% NaCl solution was used as the chloride solution in accordance with ASTM C1543-02 (2003). The specimens were immersed into the solution for duration of 90 days. To prevent the evaporation of chloride solution, the container was closed and the solution renewed every 2 weeks.

After 90 days, the specimens were removed from the chloride solution and cut into three different thicknesses with the depth increments correspond to 0-20 mm, 20-40 mm and 40-100 mm. Each slice was then ground and pulverized using a ring mill machine to 150 μm and sent to an accredited laboratory to determine the chloride content according to AASHTO standard (AASHTO T-260, 1997). The chloride diffusion coefficient (D_a) and the surface concentration (C_s) were calculated by plotting the chloride profiles and determining the best fit curve using Fick's 2nd Law (Crank, 1975).

3.6.7. Carbonation

The carbonation test was carried out in order to assess the carbonation ingression in fly ash geopolymer and AAS concretes. Due to the long term reaction of the actual process of carbonation, the test was performed using a controlled environment, i.e. a purpose built accelerated carbonation chamber, as shown in **Figure 3.19**. The concrete specimens were exposed to CO_2 in an environment where the concentration, the temperature and the relative humidity was controlled. The procedure and the equipment were adopted from previous research at RMIT University (Adam, 2009). The specimens were 100 mm concrete cubes. In order to ensure unidirectional ingress, all faces of the specimen were painted with an epoxy except one. The test was performed at the age of 28, 90, 180 and 360 days.

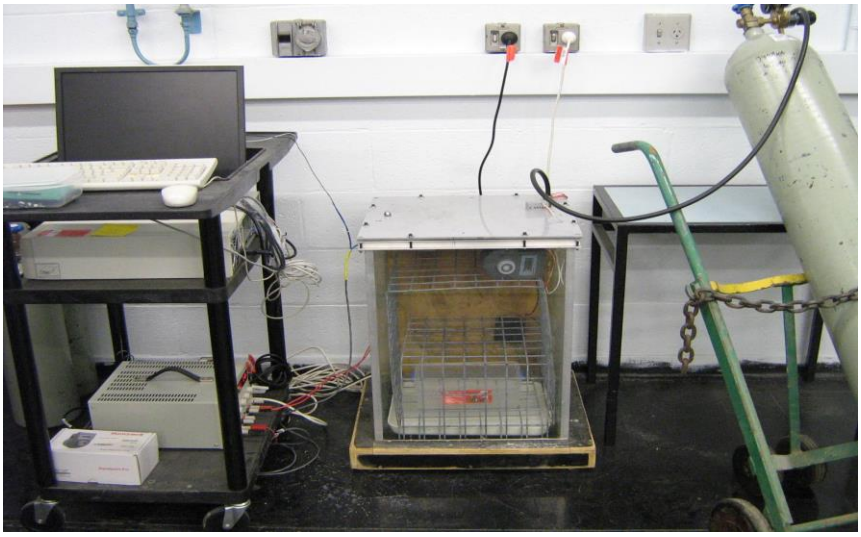

Figure 3.19 Accelerated carbonation chamber

The environment of accelerated carbonation chamber was set: the concentration of CO_2 was set to 20% $\pm$ 1%, the temperature was set to 20^{O}C $\pm$ 1^{O}C and the relative humidity was set to 70% $\pm$ 1%.

The depth of carbonation of fly ash geopolymer and AAS concrete specimens was measured by using a pH indicator on the surface of a sliced specimen. The pH indicator was prepared by mixing a 1% solution of phenolphthalein in water in accordance with RILEM standard (RILEM Recommendations, 1994).

The depth of carbonation was measured based on the change of colour on the surface of the specimen. The non-carbonated part of the specimens indicated by a purple-red colour (still highly alkaline), while, the carbonated part of the specimens was uncoloured due to the reduction of the alkalinity of the concrete during the carbonation process. An average depth of carbonation was taken.

3.7. Summary of chapter 3

C**hapter 3** on materials and experimental studies may be summarised as follows:

1) Fly ash type 1 (PFA1) from Tarong power station was used to produce fly ash geopolymer specimens. As a comparison, fly ash type 2 (PFA2) from Mt. Piper power station was used. All fly ashes were classified as class F fly ash. GGBS was used to prepare the AAS specimens.
2) The Na_2O dosage of 15% was used to prepare the fly ash geopolymer specimens, while AAS the specimens were prepared using 5% Na_2O dosage.
3) The alkaline activator moduli (M_s) of 1.00, 1.125 and 1.25 were adopted for both fly ash geopolymer and AAS mortar specimens.
4) For fly ash geopolymer and AAS concrete specimens, the activator modulus (M_s) was determined based on the result of preliminary research (**Chapter 4)**.
5) The mechanical properties of fly ash geopolymer and AAS specimens were measured using the compressive strength test, the modulus of elasticity test, the flexural tensile strength test, the indirect tensile strength test and the density measurement.

6) The durability properties of fly ash geopolymer and AAS specimens were determined using the porosity test, the water absorption test, the water permeability test, the ultrasonic pulse velocity (UPV) test, the resistivity test, the chloride diffusion test and the carbonation test.

4. FLY ASH GEOPOLYMER AND ALKALI-ACTIVATED SLAG MORTARS

4.1. Overview

Based on the literature review, there are three factors considered as influencing the material properties of fly ash geopolymer and alkali-activated slag (AAS) mortars, i.e. the type of the activator, the dosage and the modulus of alkaline activator. Previous research at RMIT University, Australia (Adam, 2009) showed that the use of a sodium silicate based solution combined with sodium hydroxide could be used to produce an optimum strength for fly ash geopolymer and AAS mortars. A higher dosage of 15% was required for the fly ash geopolymer and a lower dosage of 5% for AAS mortars, while an alkaline activator modulus of 1.00 and 1.25 gave the optimum result for the strength development. Heat curing also affected the rate of the activation of the binder in the strength development of the fly ash geopolymer mortar.

This chapter presents preliminary research in which mix designs are developed for fly ash geopolymer and AAS mortars by starting with the optimum mix design from the previous research at RMIT University (Adam, 2009). Fly ash from Tarong power station (PFA1) was used to produce fly ash geopolymer mortar. Fly ash from Mt. Piper power station (PFA2) with lower silicate content was used as a comparison. The AAS mortar was prepared using a standard commercially available construction grade GGBS. The Na_2O dosage of 15% and 5% was applied for fly ash geopolymer and AAS mortars, respectively. An alkaline activator modulus of 1.00, 1.125 and 1.25 was used for both fly ash geopolymer and AAS mortars. It is to be noted that fly ash geopolymer and AAS were used as 100% substitution to ordinary Portland cement (OPC).

4.2. Materials

4.2.1. Fly ash

Fly ash from Tarong power station (PFA1) was used to prepare the fly ash geopolymer mortar, while fly ash from Mt. Piper power station (PFA2) was used

as comparison data. The properties of fly ash PFA1 and PFA2 are described in **Chapter 3 Section 3.2.1**.

4.2.2. Slag

Ground granulated blast furnace slag (GGBS), a construction grade slag, was used to prepare the AAS mortar. The properties of slag are described in **Chapter 3 Section 3.2.2**.

4.2.3. Alkaline activators

Sodium silicate and sodium hydroxide were used to prepare the fly ash geopolymer and AAS mortars. The properties of the sodium silicate and sodium hydroxide are described in **Chapter 3 Section 3.2.3**.

4.2.4. Fine aggregate

Fine aggregate with a fineness modulus of 2.03 was used to prepare the fly ash geopolymer and AAS mortar specimens. The properties of fine aggregate are described in **Chapter 3 Section 3.2.4**.

4.3. Mix proportions

The mix designs of fly ash geopolymer and AAS mortars were adopted from previous research conducted at RMIT University, Melbourne, Australia (Adam, 2009). A range of Na_2O dosage and the alkaline modulus for fly ash geopolymer and AAS specimens has been reported in the literature (**Chapter 2 Section 2.6)** (Wang et al., 1994, Shi, 1996, Krizan & Zivanovic, 2002, Escalante-Garcia et al., 2003, Fernandez-Jimenez et al., 2003, Zivica, 2007, Fernandez-Jimenez & Puertas, 1997, Fernandez-Jimenez & Palomo, 2005b, Adam, 2009, Yang et al., 2009). It was found that a higher dosage of Na_2O (>7%) and an activator modulus of 1.0 – 1.5 were required to obtain a satisfactory strength for fly ash geopolymer specimens. For AAS specimens, it was found that the dosage range of 3% - 5% Na_2O and 0.75 – 1.25 for the activator modulus resulted in acceptable strength and good workability.

Adam (2009) conducted further experimental work on the Na_2O dosage and the activator modulus as reported in the literature review (**Chapter 2 Section 2.6 Table 2.7)**. According to Adam (2009), a higher dosage of 15% Na_2O for fly ash

geopolymer mortar and a lower activator dosage of 5% Na_2O for AAS mortar with the activator modulus of 1.00 – 1.25 provided the best performance of fly ash geopolymer and AAS mortars in terms of compressive strength and workability. Hence, it was decided to adopt these mix proportions for the fly ash geopolymer and AAS mortars for this research.

The detailed mix designs of the fly ash geopolymer and AAS mortars are summarized in **Table 4.1**. A blend of liquid sodium silicate and sodium hydroxide was prepared with the alkali modulus (mass ratio of SiO_2 to Na_2O) ranging from 1.00 to 1.25. An alkali modulus of 1.125 was also investigated for this research to obtain additional information on the impact of the alkali modulus (Adam's work adopted an alkali modulus of 1.00 and 1.25). Dosages of Na_2O of 15% and 5% by mass weight were investigated for the fly ash geopolymer and AAS mortar mixes, respectively.

Table 4.1 Details of fly ash geopolymer and AAS mortars

Mortar	Variables	
	Na_2O dosage	**Activator Modulus (M_s) Design**
AAS5-1.00	5%	1.00
AAS5-1.125	5%	1.125
AAS5-1.25	5%	1.25
G15-1.00	15%	1.00
G15-1.125	15%	1.125
G15-1.25	15%	1.25

Fly ash geopolymer and AAS mortars were prepared with a mass ratio of sand to binder of 2.75 (ASTM C109/C109M-07, 2008). The ratio of volume of fine aggregate to the total volume of mixture was maintained at 60% for fly ash geopolymer and 63% for AAS mortars. A water binder ratio (w/b) of 0.52 was used to prepare the AAS mortar, while a water solid ratio (w/s) of 0.41 was used to prepare the fly ash geopolymer mortar. Instead of using a w/b ratio, the w/s ratio was used for fly ash geopolymer mortar due to the high quantity of solid contained in the alkaline activator. This solid comprised Na_2O and SiO_2 and reduced the workability of fly ash geopolymer, especially at higher dosages of Na_2O. The reason for the use of the w/s ratio for fly ash geopolymer was to give a more consistent workability during the mixing process. The quantity of solid was

determined by the mass of fly ash or slag and the solid contained in the alkaline activator solution, while the quantity of water in the fly ash geopolymer and AAS mixes was taken as the sum of water contained in the sodium silicate, sodium hydroxide and the added water.

The absolute volume method (Neville, 2011) was used in determining the proportion of cementitious materials, fine aggregate, chemical activator, and water. The aim was to maintain the volume of material with the w/b or w/s ratio remaining constant. The calculation of the proportions by the absolute volume method for the fly ash geopolymer and AAS mortars was based on previous research (Adam, 2009).

Fly ash (FA) geopolymer mortar A (FG-A) was developed using fly ash type 1 (PFA1). As a comparison, fly ash geopolymer mortar B (FG-B) was prepared using fly ash type 2 (PFA2). The mix proportions of the fly ash geopolymer and AAS mortars are given in **Table 4.2, Table 4.3,** and **Table 4.4**.

Table 4.2 Mix design of FA geopolymer mortar A (FG-A) per litre mix (kg)

Mixture	Fly ash PFA1	Fine sand	Activator		Added Water
			Na_2SiO_3	NaOH 15M	
GA15-1.00	0.500	1.375	0.255	0.117	0.034
GA15-1.125	0.498	1.369	0.286	0.102	0.027
GA15-1.25	0.496	1.363	0.316	0.087	0.021

Table 4.3 Mix design of FA geopolymer mortar B (FG-B) per litre mix (kg)

Mixture	Fly ash PFA2	Fine sand	Activator		Added water
			Na_2SiO_3	NaOH 15M	
GB15-1.00	0.500	1.375	0.255	0.117	0.034
GB15-1.125	0.498	1.369	0.286	0.102	0.027
GB15-1.25	0.496	1.363	0.316	0.087	0.021

Table 4.4 Mix design of AAS mortar per litre mix (kg)

Mixture	GGBS	Fine sand	Activator		Added water
			Na_2SiO_3	NaOH 10M	
AAS5-1.00	0.525	1.445	0.089	0.056	0.173
AAS5-1.125	0.524	1.442	0.100	0.049	0.172
AAS5-1.25	0.523	1.439	0.111	0.042	0.172

For fly ash geopolymer specimens, the mix design ratio of water, sodium silicate and sodium hydroxide was maintained at 0.034, 0.255, and 0.117 respectively, based on the activator modulus (M_s design) = 1.00 for FG-A. This was analogous to the use of fly ash as a replacement material where the mix proportions are maintained irrespective of the source of the fly ash. For consistency similar labelling was used for PFA1 and PFA2, i.e. GA15-1.00 and GB15-1.00 for the same mix proportions.

For control and comparison, the data of ordinary Portland cement (OPC) and fly ash geopolymer mortar tests from previous research work at RMIT University were used (Adam, 2009).

4.4. Mixing

The procedure of mixing was developed based on previous research (Adam, 2009) as given in **Figure 4.1**. The mixing process for all specimens was carried out using a 5 litre Hobart mixer as shown in **Figure 4.2**. The sodium silicate and sodium hydroxide solutions were combined prior to the mixing process. The mixtures were poured into 50 x 50 x 50 mm^3 steel moulds and vibrated for 10 seconds to remove air bubbles.

4.5. Curing

The standard curing regime used for OPC concrete was also applied to the AAS specimens due to the similar characteristic of the hydration product, a C-S-H gel. The curing regime was 24 hours at room temperature prior to being demoulded and followed by water curing for 6 days at 20^{O}C.

The fly ash geopolymer specimens required a different curing regime to achieve structural integrity due to the slow setting at room temperature. Structural integrity of the specimens was not achieved to enable compressive strength testing using the curing regime applied to the ASS specimens. As such after being demoulded, the fly ash geopolymer specimens were left at room temperature for 24 hours then cured in the oven at 80^{O}C for 24 hours. The fly ash geopolymer specimens were wrapped with cling film to prevent water evaporation causing surface cracking during heating (**Figure 4.3** and **Figure 4.4)**. The specimens were then left at room temperature until testing.

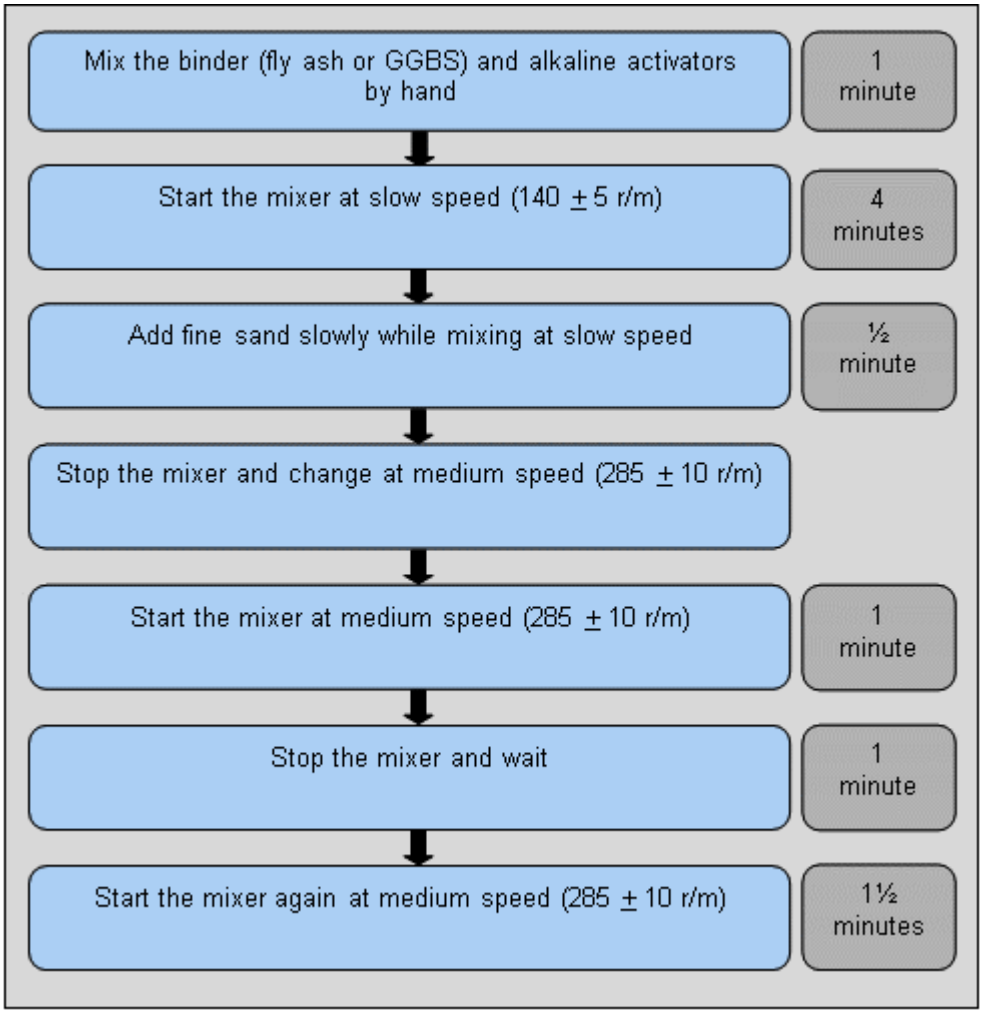

Figure 4.1 Mixing procedures of fly ash geopolymer and AAS mortars (Adam, 2009)

Figure 4.2 Hobart mixer and mixing process

Figure 4.3 Fly ash geopolymer and AAS mortars in steel moulds

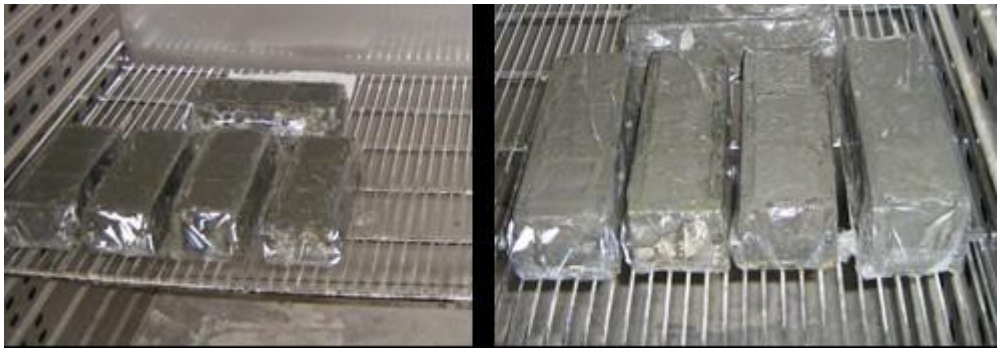

Figure 4.4 Oven curing for fly ash geopolymer wrapped in cling film

4.6. Result and discussion

4.6.1. Strength of fly ash geopolymer mortar

The strength development of the fly ash geopolymer mortar with PFA1 (FG-A) is shown in **Table 4.5** and **Figure 4.5**. The fly ash geopolymer mortar data with PFA2 (FG-B) is presented in **Table 4.6** and **Figure 4.6**.

The strength development of FG-A mortar demonstrated a lower compressive strength for all mixes compared to that of OPC mortar as shown in **Figure 4.5**. The highest compressive strength of the FG-A mortar, 30.21 MPa, was exhibited by the GA15-1.00 mix at 28 days. This was approximately half of the OPC mortar strength. However, the FG-A mortar showed further significant increase over time indicating that the hydration process had not completely finished and a higher ultimate strength could be expected.

Table 4.5 Compressive strength of FA geopolymer mortars FG-A

Mix	Activator Modulus (Ms)	Compressive strength (MPa)			
		3 days	7 days	14 days	28 days
GA15 – 1.00	1.00	12.33	19.89	23.68	30.21
GA15 – 1.125	1.125	9.19	11.85	17.11	28.88
GA15 – 1.25	1.25	5.98	11.00	14.77	28.61
OPC*	N/A	20.38	36.25	46.26	55.07

* as control (Adam, 2009)

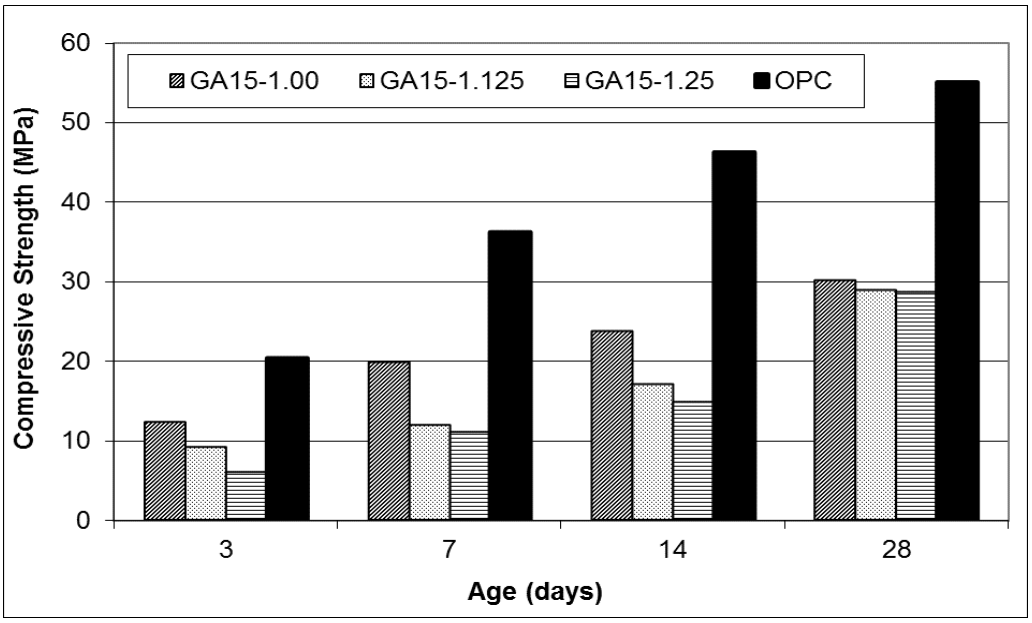

Figure 4.5 Strength of FA geopolymer mortar FG-A

In contrast, the strength development of FG-B was predominantly achieved within the first 3 – 7 days with little further development to 28 days as shown in **Figure 4.6**. The initial strength of FG-B mortar was higher than that of OPC mortar. The GB15-1.00 mix exhibited the highest initial strength compare to all mixes with 38.43 MPa at 3 days which is twice that of the OPC mortar. It also showed the highest compressive strength with 54.85 MPa at 28 days, equivalent to the OPC 28 days strength of 55.01 MPa.

Table 4.6 Compressive strength of FA geopolymer mortars FG-B

Mix	Activator Modulus (Ms)	Compressive strength (MPa)			
		3 days	7 days	14 days	28 days
GB15 – 1.00	1.00	38.43	45.92	49.97	54.85
GB15 – 1.125	1.125	32.15	37.89	43.82	45.83
GB15 – 1.25	1.25	28.90	34.89	37.84	40.24
OPC*	N/A	20.38	36.25	46.26	55.07

* as control (Adam, 2009)

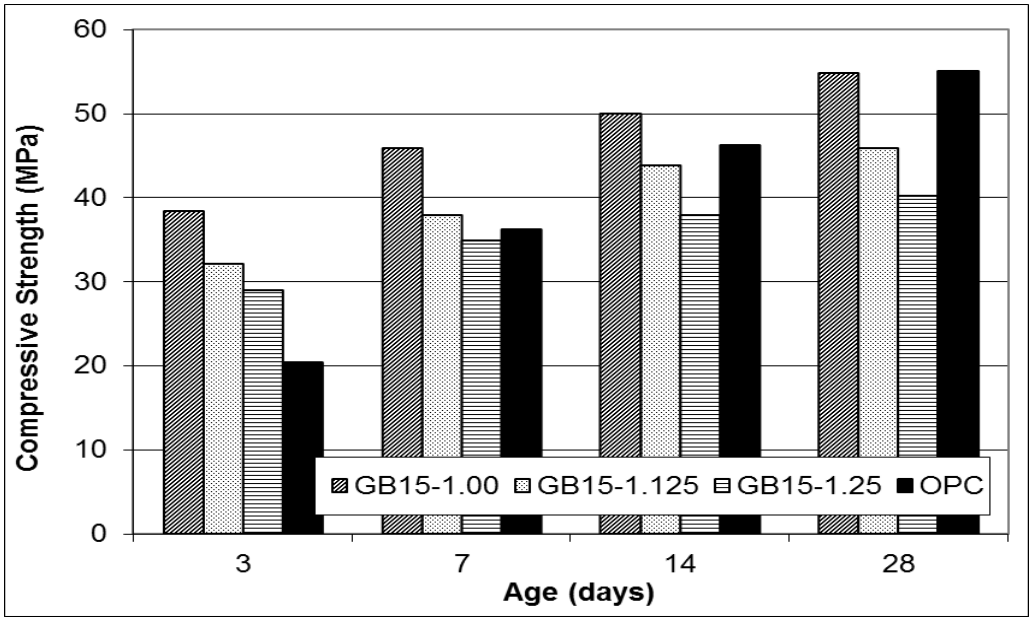

Figure 4.6 Strength of FA geopolymer mortar FG-B

4.6.2. Effect of alkali modulus on fly ash geopolymer mortar

The influence of alkali modulus (M_s) on compressive strength is presented in **Table 4.7, Figure 4.7** and **Figure 4.8**.

Table 4.7 Effect of alkali modulus (M_s) of FG-A and FG-B mortars

Days	Compressive strength (MPa) on activator modulus (M_s) of						OPC
	FG-A mortar			FG-B mortar			
	1.00	1.125	1.25	1.00	1.125	1.25	
3	12.33	9.19	5.98	38.43	32.15	28.90	20.38
7	19.89	11.85	11.00	45.92	37.89	34.89	36.25
28	30.21	28.88	28.61	54.85	45.83	40.24	55.07

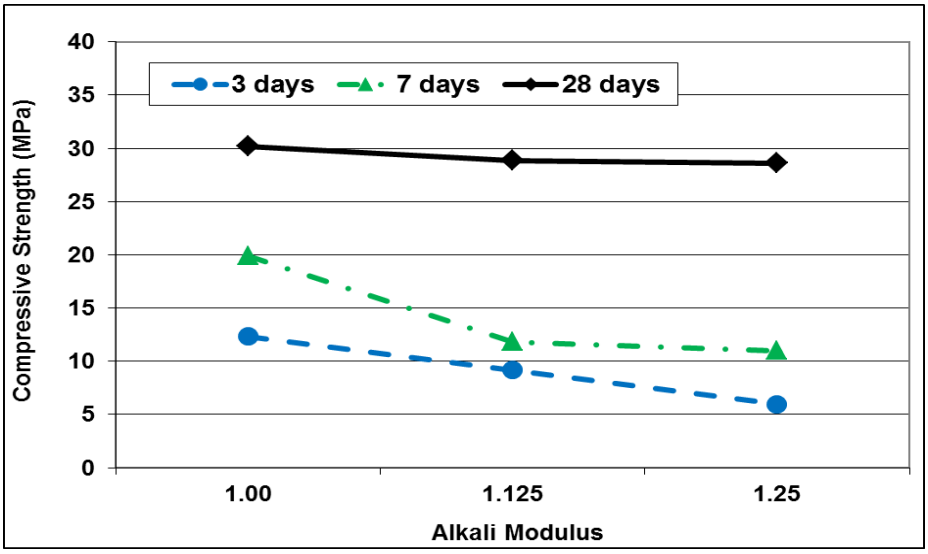

Figure 4.7 Effect of alkali modulus (M_s) of FG-A mortar

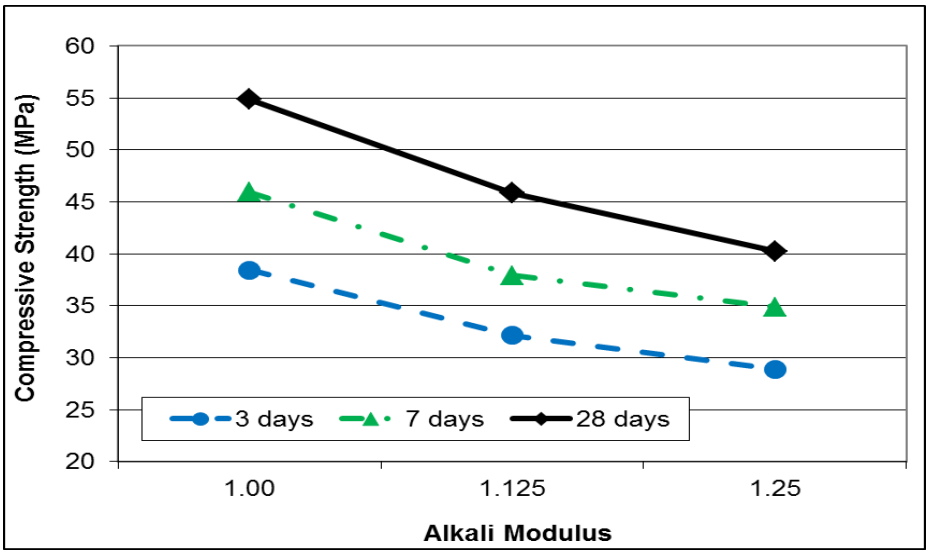

Figure 4.8 Effect of alkali modulus (M_s) of FG-B mortar

The SiO_2 content is influenced by the availability of SiO_2 in the alkaline solution. Fly ash from the previous research (Adam, 2009) was used as a basis to determine the alkali modulus (M_s). As the SiO_2 content in the fly ash precursor (PFA1 and PFA2) of FG-A and FG-B was significantly different from the previous research (FG-C) as shown in **Table 4.8**, the definition of M_s in this research was modified to explain the effect of M_s in the development of mortar strength.

Table 4.8 Change of alkali modulus (M_s) due to silicate (SiO_2) content on fly ash precursors

Mix	SiO_2 content in fly ash (%)	M_s Design (M_s)	M_s Specimen (M_{ss})	M_s Effective (M_{se})	Strength 28 days (MPa)
FG-A	70.30	1.00	1.033	5.875	30.21
	70.30	1.125	1.159	5.988	28.88
	70.30	1.25	1.282	6.088	28.61
FG-B	66.67	1.00	1.033	5.625	54.85
	66.67	1.125	1.159	5.739	45.83
	66.67	1.25	1.282	5.840	40.24
FG-C*	49.95	1.00	1.033	4.439	74.69
	49.95	1.25	1.282	4.663	79.26

* fly ash geopolymer data from the previous research as control (Adam, 2009)

The alkali modulus (M_s design) was determined (as previously) by considering the activators only without the influence of the effect of the SiO_2 in the fly ash precursors (**Equation 4.1**). However, due to the different percentage of SiO_2 in the fly ash precursors, the effective alkali modulus (M_{se}), which takes into account the SiO_2 content in the different fly ash compositions (**Equation 4.2**), was used as a comparison with the previous data (FG-C).

$$M_s \text{ design} = M_s \text{ specimen } (M_s) = SiO_2 \text{ (activator)} / Na_2O \quad (4.1)$$

$$M_s \text{ effective } (M_{se}) = SiO_2 \text{ (activator + fly ash)} / Na_2O \quad (4.2)$$

The alkali modulus of the activator solution has a significant impact on the strength development of the geopolymer specimens. In the geopolymer reaction, increasing the alkali modulus leads to an increase in the soluble silicate, which promotes an acceleration in the reaction rate due to the higher concentration of reactants. However, in order to keep the w/s ratio in balance, increasing the alkali modulus causes a reduction of the sodium hydroxide content which is used to dissolve the SiO_2 and the Al_2O_3 monomer from the fly ash grain. The role of the cations, i.e. Na^+ (from sodium hydroxide), is essential to maintain the electric neutrality in the geopolymeric matrix. Reducing the sodium hydroxide content will reduce the Na^+ cations and affects the electric neutrality of the Si-O-Al-O monomer in the geopolymeric matrix which leads to a lower strength at higher

alkali modulus. It has previously been noted that increasing the design alkali modulus beyond the ratio of 1.5 resulted in no further strength development (Hardjito & Rangan, 2005, Fernandez-Jimenez & Palomo, 2005b).

The strength of the FG-A and FG-B mortars is lower than the FG-C mortar. This is attributed to the change of M_{se} which is caused by the SiO_2 in the fly ash. The FG-A and FG-B mortars are made using the same mix design as the FG-C specimens. However, due to the higher amount of SiO_2 composition in the fly ash precursors of PFA1 and PFA2, the M_{se} increases by approximately 1.43 or 31% for FG-A mortar and 1.18 or 25% for FG-B mortar compared to FG-C mortar which is hypothesised as the cause of the low strength development of FG-A and FG-B.

4.6.3. The effect of Si/Al ratio on fly ash geopolymer mortar strength

The general formula of the three-dimensional (3D) amorphous geopolymeric network is $M_n(-(SiO_2)_z-AlO_2)_n,wH_2O$, where n is the degree of polymerization, z is 1, 2, 3, and M is the alkali cation. The most common types of geopolymer are polysialate (-Si-O-Al-O-), poly sialate-siloxo (-Si-O-Al-O-Si-O-) and poly sialate-disiloxo (-Si-O-Al-O-Si-O-Si-O-). This geopolymeric network structure is affected by the ratio of Si/Al. Polysialate is formed under an Si/Al ratio of 1, polysialate-siloxo is formed under an Si/Al ratio of 2, and polysialate-disiloxo is formed under an Si/Al ratio of 3 (Davidovits, 1994b).

Table 4.9 The Si/Al ratio of fly ash geopolymer mortars

Mix	M_s Design (M_s)	M_s Effective (M_{se})	Na	Al	Si	Si/Al ratio	Na/Al ratio	Strength 28d (MPa)
FG-A	1.00	5.875	6.3	10.8	70.4	6.5	0.6	30.21
	1.125	5.988	9.6	10.5	71.5	6.8	0.9	28.88
	1.25	6.088	19.9	7.4	67.1	9.1	2.7	28.61
FG-B	1.00	5.625	19.2	17.2	61.5	3.6	1.1	54.85
	1.125	5.739	16.4	15.8	63.8	4.0	1.0	45.83
	1.25	5.840	12.6	14.9	66.4	4.5	0.8	40.24

Note: Data was acquired using EDX analysis

The silicate (Si) and aluminate (Al) components which affected the fly ash geopolymer specimens were identified using EDX analysis. Based on **Table 4.9**, the matrix of the FG-A and FG-B mortars mainly comprised Si-Al-O as the ratio of Si/Al for FG-A was 6.5 – 9.1 and the Si/Al ratio of FG-B was 3.6 – 4.5 with the main geopolymeric matrix for both inferred to be (Si)-polysialate-disiloxo. The high Si/Al ratio in the FG-A specimen is hypothesised as the cause of the low strength development of FG-A.

The strength development of the geopolymer system is influenced by the presence of the Si and Al components. The highest strength of FG-B at 54.85 MPa is achieved with an M_{se} of 5.625 at an Si/Al ratio of 3.6 and an Na/Al ratio of 1.1 as presented in **Table 4.9**. However, the increasing of the Si/Al ratio tends to reduce the strength in the geopolymer. Increasing the Si/Al ratio to 6.5 causes the reduction of strength of FG-A (GA15-1.00 mix) to 30.21 MPa. A similar finding was also found by other researchers who found an optimum strength performance with a ratio of Si/Al of 3.0 – 3.8 and a Na/Al of approximately 1.0 (Rowles & O'Connor, 2003, Fletcher et al., 2005, Steveson & Sagoe-Crentsil, 2005).

The high Si/Al ratio of FG-A can be inferred as the cause of the slow reaction in forming geopolymer structure compared to the FG-B specimens. The increase of the Si/Al ratio which was found in both FG-A and FG-B mortars is assumed to cause the deferment of the geopolymer reaction time. An increase of the Si/Al ratio has been seen to affect the setting time of the geopolymer during the condensation stage. A condensation process between aluminates and silicates predominantly occurs in a mixture with a low Si/Al ratio (Si/Al ratio = 1) resulting mainly in (Si)-polysialate structures. However, the increase in Si/Al ratio (Si/Al > 1) will form oligomeric silicates, caused by the condensation process among the silicates themselves, and creating a 3D geopolymeric network of (Si)-polysialate-siloxo and (Si)-polysialate-disiloxo. It has been assumed that the rate of condensation between aluminates and silicates was faster than between silicates components (Sagoe-Crentsil & Weng, 2007, Weng & Sagoe-Crentsil, 2007, Silva et al., 2007).

4.6.4. The strength development of fly ash geopolymer mortar

A comparison of the FG-A and FG-B mortars is made with the fly ash geopolymer mortar from the previous research (Adam, 2009) (FG-C). The strength development of FG-A compared to FG-B and FG-C at the lower modulus (M_s of 1.00) and the higher modulus (M_s of 1.25) is shown in **Figure 4.9** and **Figure 4.10**, respectively.

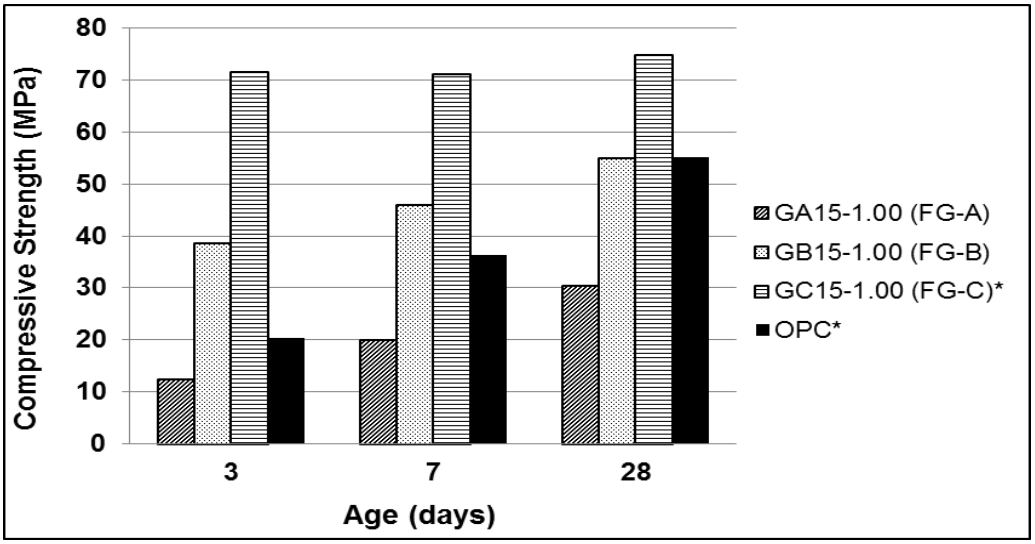

***** (Adam, 2009)

Figure 4.9 Comparison of FA geopolymer strength at Ms = 1.00

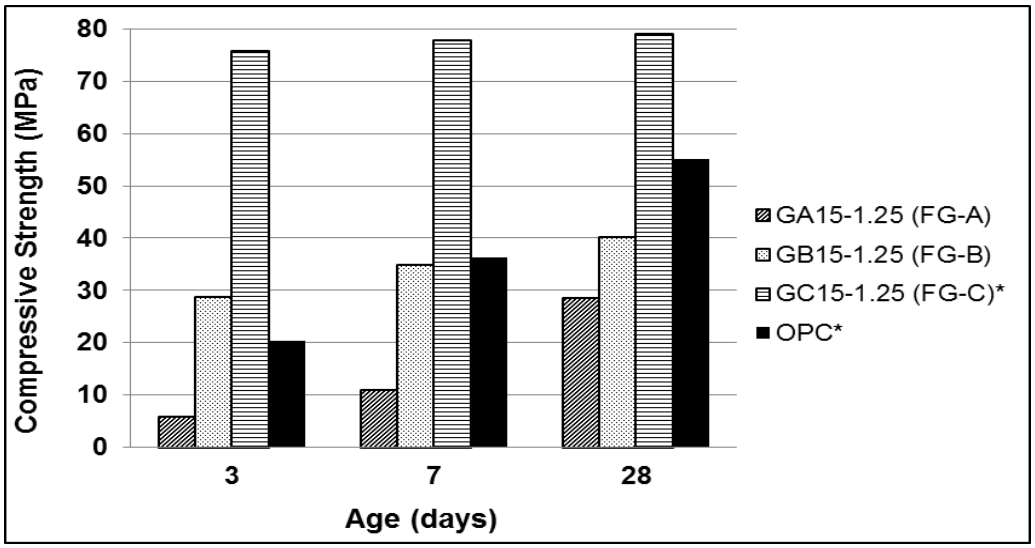

***** (Adam, 2009)

Figure 4.10 Comparison of FA geopolymer strength at Ms = 1.25

The FG-A displays the lowest compressive strength compared to all mixes. The highest 3 day strength of FG-A is achieved by the GA15-1.00 mix with only 12.33 MPa, which is only half of the OPC mortar strength. However, FG-A mixes do increase in strength by approximately 20 MPa from 3 to 28 days with the final strength being 30.21 MPa at 28 days. The 3 day compressive strength of geopolymer mortar FG-B and FG-C are higher than for the FG-A. The highest 3 day strength for the FG-C mix is achieved by the GC15-1.25 mix, with 75.92 MPa, 3-times higher than the OPC mortar. However, none of the FG-C mixes display any significant increase in strength after 3 days. While the FG-B has a lower initial strength than FG-C, the maximum value being 38.43 MPa for the GB15-1.00 mix, all the FG-B mixes do increase by 10 – 15 MPa up to 28 days.

It has been hypothesized that the strength development of fly ash geopolymer specimens is affected by the components of silicate (Si) and aluminate (Al) in the fly ash precursor (Diaz-Loya et al., 2011, Rowles & O'Connor, 2003, Steveson & Sagoe-Crentsil, 2005). However, despite silicate and aluminate concentrations being significant factors in the geopolymer reaction, there are other components that can affect the strength development of fly ash geopolymer specimens. According to Diaz-Loya et al. (2010), a high percentage of fine particles and a high content of CaO component in the fly ash precursor affect the strength properties of fly ash geopolymers.

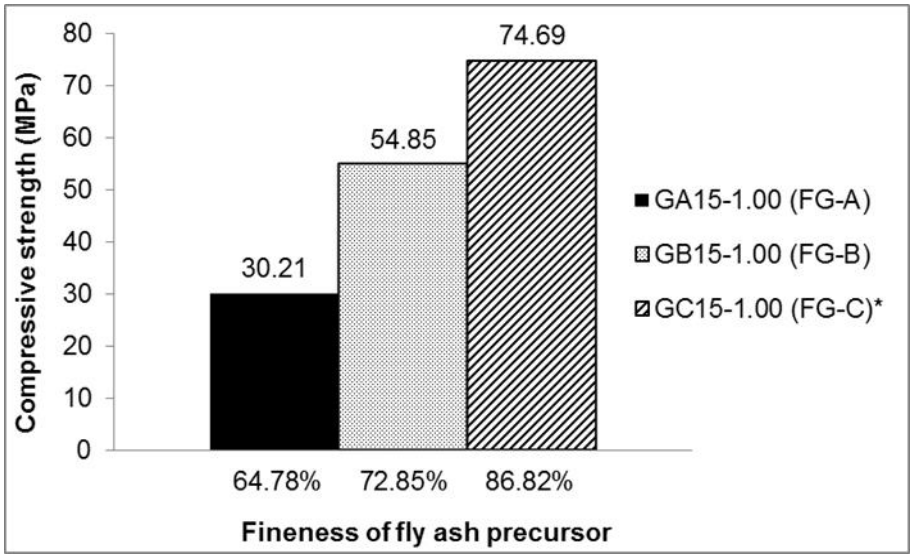

***** as comparison (Adam, 2009)

Figure 4.11 Strength properties of fly ash geopolymer based on fly ash fineness at 28 days age

Figure 4.11 shows the effect of fly ash fineness on the strength development of the FG-A and FG-B mortars, as well as the FG-C mortar from previous research (Adam, 2009). The FG-C mortar specimen demonstrates the highest strength 74.69 MPa compared to all specimens with the fineness of the fly ash precursor being 86.82%. Conversely, the low fineness of fly ash tends to produce a low strength geopolymer specimen. FG-A mortar with the lowest fineness of fly ash of 64.78% exhibits the lowest strength with only achieving 30.21 MPa at 28 days. A greater number of fine particles of fly ash precursor results in a higher surface area, and therefore higher reactivity, resulting in higher compressive strength as suggested by Diaz-Loya et al. (2010).

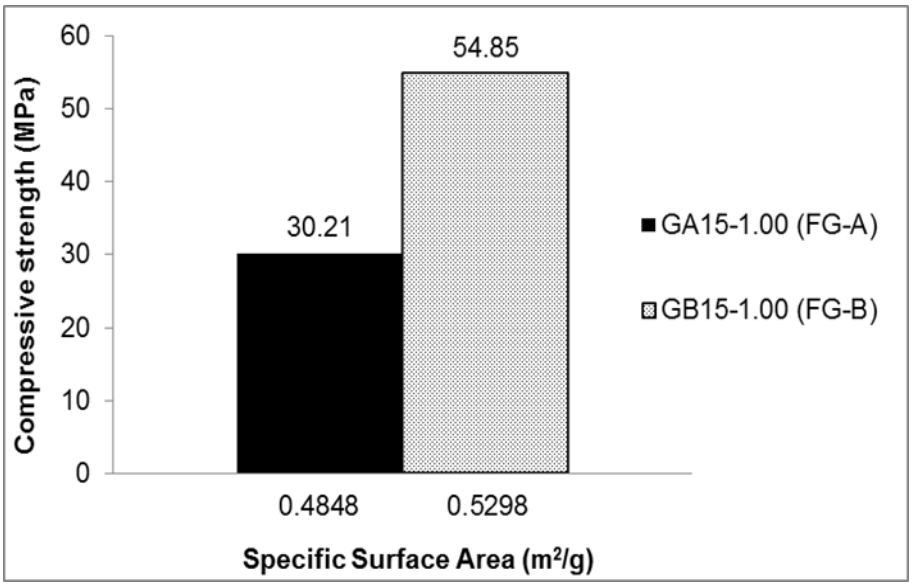

Figure 4.12 Strength properties of fly ash geopolymer based on fly ash specific surface area at 28 days age

Figure 4.12 displays the effect of the specific surface area on the strength of the fly ash geopolymer mortars of FG-A and FG-B. The FG-B mortar with a specific surface area of 0.5298 m^2/g demonstrates a better strength performance (54.85 MPa) compared to that of FG-A (30.21 MPa) with a lower specific surface area of 0.4848 m^2/g. This is attributed to the increase of the density of fly ash at higher specific surface area. A similar finding was also observed by (Quan, 2011). The authors performed a test on a blended concrete with fly ash and found that the compressive strength of blended concrete with fly ash increases with the increases of specific surface area of fly ash. Hence, it can be inferred that the

strength development of fly ash geopolymer is also affected by the specific surface of the fly ash precursors.

The strength development of fly ash geopolymer is also affected by the CaO content in fly ash precursors. **Figure 4.13** demonstrates the effect of the CaO content in fly ash precursors to the compressive strengths reported for this work compared to previously reported data (Adam, 2009), while **Table 4.10** gives the CaO, SiO_2 and Al_2O_3 contents of the respective fly ashes.

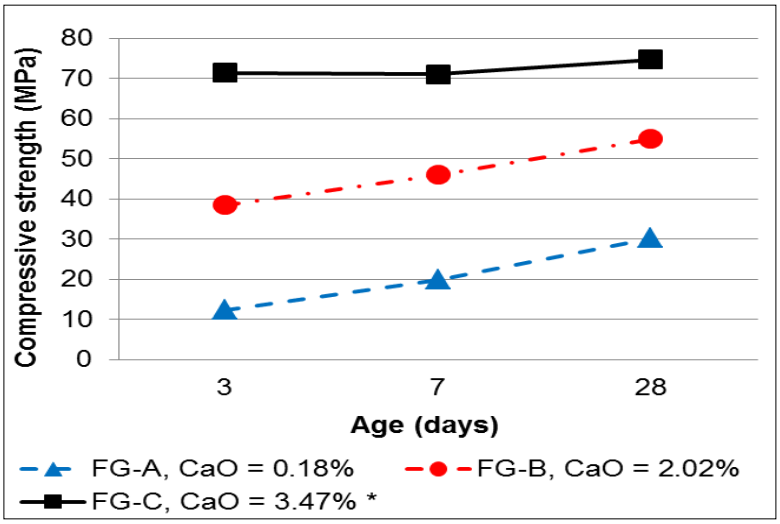

* Adam (2009)

Figure 4.13 Effect of CaO content on fly ash geopolymer

Table 4.10 Comparison of chemical composition of fly ash precursors

Components	FG-A	FG-B	FG-C*
	PFA1	PFA2	PFA3*
CaO	0.18%	2.02%	3.47%
SiO_2	70.30%	66.67%	49.45%
Al_2O_3	23.10%	25.07%	29.61%

* Adam (2009)

The data shows that the FG-A mortar demonstrates the lowest strength of all mortar specimens. This low strength is attributed to the low content of CaO in the fly ash precursor which is the lowest compared to the other fly ash geopolymer

specimens. Furthermore, an increase of CaO in the fly ash precursor tends to increase the strength of fly ash geopolymer. FG-B with a CaO content of 2.02% exhibits a better strength performance compared to that of the FG-A specimens, while the FG-C with the highest CaO content shows the highest strength compared to all fly ash geopolymer mortar specimens. Fly ash with high CaO content is more reactive with water and tends to form the calcium silicate hydrated (C-S-H) compounds that increase the early strength of the geopolymer specimen. It also increases the reaction rate between the fly ash and the alkaline solutions which leads to the high early strength of fly ash geopolymer (**Figure 4.13**). A similar finding was also reported by Diaz-Loya et al. (2010) who found that the setting time and the strength development of fly ash geopolymer is affected by the content of CaO in the fly ash precursor. According to the authors, this is attributed to the formation of calcium silicate hydrated compounds which formed at high calcium silicate content and increase the mechanical strength of the resultant geopolymer. Temuujin et al. (2009) also suggests that the addition of calcium compounds is likely to result in precipitation calcium silicate hydrate or calcium silicate aluminate hydrate phases and improve the dissolution of the fly ash in the alkaline which increases the mechanical properties of fly ash geopolymer specimens.

4.6.5. Strength of AAS mortar

The development of the compressive strength of AAS mortars up to the 28 days is shown in **Table 4.11** and **Figure 4.14**.

Table 4.11 Compressive strength of AAS mortars

Mix	Activator Modulus (Ms)	Compressive strength (MPa)			
		3 days	7 days	14 days	28 days
AAS5 – 1.00	1.00	31.44	39.38	47.07	47.93
AAS5 – 1.125	1.125	31.67	41.03	44.42	45.18
AAS5 – 1.25	1.25	35.93	48.55	46.88	42.34
OPC*	N/A	20.38	36.25	46.26	55.07

* as control (Adam, 2009)

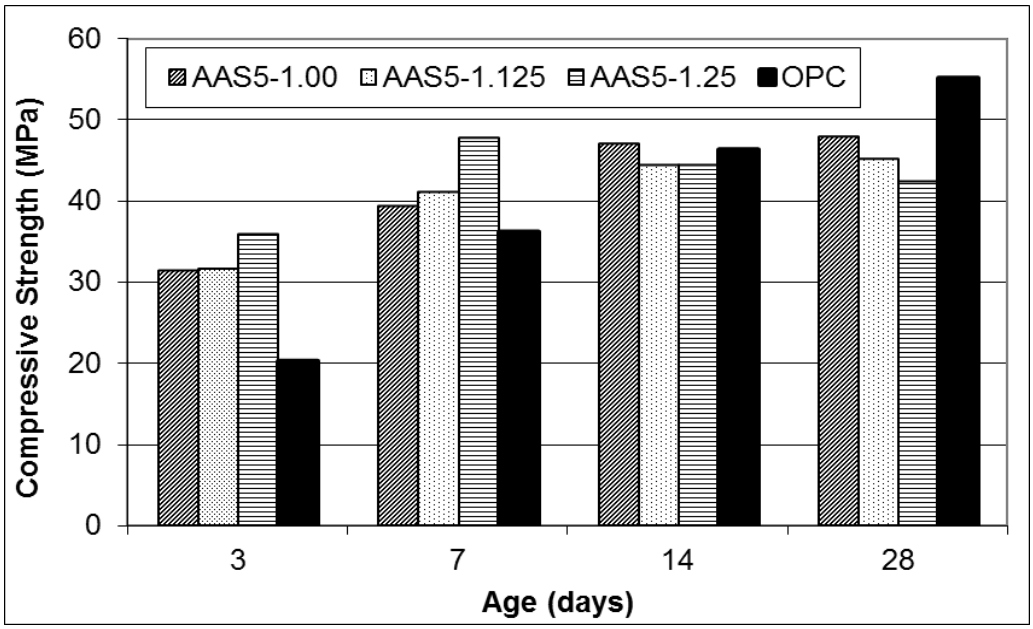

Figure 4.14 Strength of AAS mortars

The 3 and 7 days compressive strength for all the AAS mortar was superior to the OPC mortar, however by 28 days the strengths were lower than that of the OPC mortar. An increase of 10 – 18 MPa in the AAS mortar strength was observed from 3 to 14 days but no further strength development occurred from 14 to 28 days. Indeed a slight decrease in strength was noted for all AAS mortar from 14 to 28 days. The largest increase was observed for the AAS5-1.00 mix but the highest compressive strength for any AAS mix was achieved by the AAS5-1.25 with 48.55 MPa at the age of 7 days.

4.6.6. Effect of alkali modulus on AAS mortar

The influence of alkali modulus on compressive strength of AAS mortar is presented in **Table 4.12** and **Figure 4.15**. An increase of 4 – 9 MPa in the AAS mortar strength was noted between 3 and 7 days with the increasing of alkali modulus (M_s) from 1.00 to 1.25. However, by the age of 28 days there was a decrease of 6 MPa for AAS with M_s = 1.00 to 1.25. This behaviour can be attributed to classification of the slag as an acid slag in agreement with other authors (Wang et al., 1994).

Table 4.12 Effect of alkali modulus on AAS mortar

Days	Compressive strength (MPa) on activator modulus (M_s) of			OPC*
	1.00	**1.125**	**1.25**	
3	31.44	31.67	35.91	20.38
7	39.38	41.03	47.76	36.25
28	47.93	45.18	42.33	55.07

* Adam (2009)

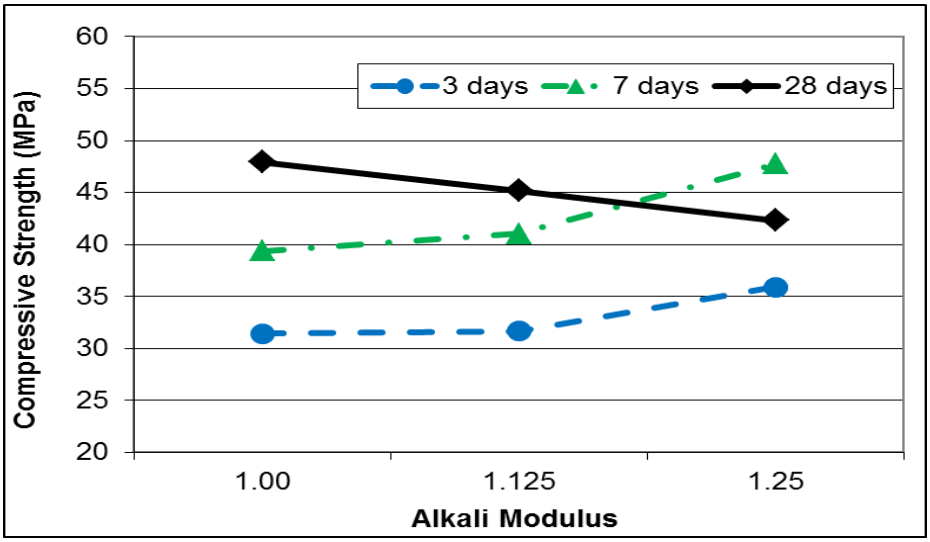

Figure 4.15 Effect of alkali modulus on AAS mortar

It was found that increasing the alkali modulus results in an initial increase in strength. However, this subsequently resulted in a reduction in strength at later ages. This was in agreement with the results from previous author's (Adam, 2009). Increasing the alkali modulus in the solution causes an increase of the anion concentration of sodium silicate. The anion in the sodium silicate reacts with Ca^{2+} dissolving from the surface of the slag grains and formed the primary C-S-H gel. This rapid formation of the C-S-H leads to the high initial strength. Increasing the M_s also increases the alkalinity of the solution which leads to the acceleration of the absorption of ions on the slag grains surface and induces an increase in the rate of initial reaction. Thus the high initial strength for AAS mortar at M_s = 1.25 is attributed to the high reaction rate during the formation of C-S-H gel. According to Shi & Li (1989), under the same dosage of Na_2O, increasing the alkali modulus shortens the setting time of AAS specimens.

The ultimate optimum strength of AAS mortar specimens at M_s = 1.00 indicated that either all the slag in the mix has been consumed, which means that the dissolution of the slag surface has stopped, or that the further reaction of C-S-H gel formation has been prevented by a protective crust as the result of the reaction of available slag, as suggested by Law et al. (2012).

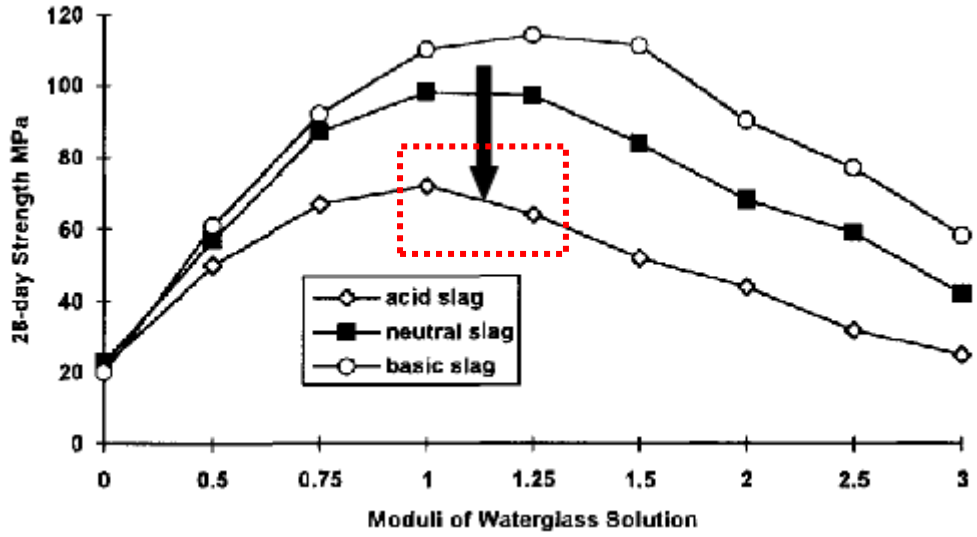

Figure 4.16 Moduli of sodium silicate solution to 28-day strength for different types of slag (Wang et al., 1994)

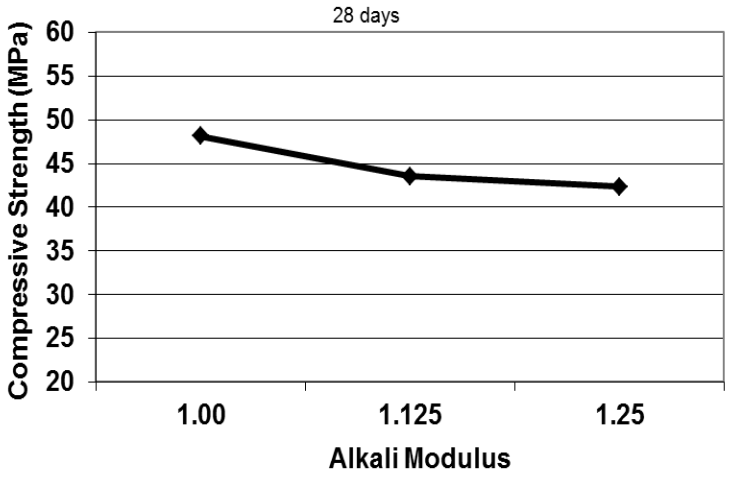

Figure 4.17 Effect of alkali modulus on AAS (acid slag) mortar

Furthermore, the optimum value of the AAS mortar is achieved at M_s = 1.00, in agreement with Wang et al. (1994) for acid slag as shown in **Figure 4.16**. It was found that the optimum alkali modulus value for acid slag is M_s = 1.00 and strength tend to decline at higher activator modulus. The declining behaviour of AAS mortar strength at 28 days strength, as shown in **Figure 4.17** is also similar to Wang's observation.

4.6.7. The strength development of AAS mortar

A comparison of the AAS mortars (AS-A) is made with the AAS mortar from the previous research (Adam, 2009) (AS-B). The strength development of AAS at the lower modulus (M_s = 1.00) and the higher modulus (M_s = 1.25) is shown in **Figure 4.18** and **Figure 4.19**, respectively.

Both AAS mortars, AS-A and AS-B, demonstrate a higher initial compressive strength compared to OPC concrete at an alkali modulus (M_s) of 1.00 (**Figure 4.18**). The highest initial strength of the AAS mortars is achieved by the AS-B1, with 35.19 MPa and AAS5-1.00, with 31.44 MPa at 3 days age. Both AAS mortars demonstrated an increase in strength with time. The final strength, at 28 days, being 47.93 MPa and 52.27 MPa for AAS5-1.00 and AS-B1, respectively. However, despite both mortars exhibiting a high initial strength, OPC mortar has the highest compressive strength with a final strength of 55.07 MPa. In addition, although AAS5-1.00 displays a significant increase in strength up to 14 days, the strength development tends to be constant afterwards and demonstrates the lowest strength at 28 days.

Furthermore, both AAS mortars also demonstrate the highest initial strength at a higher alkali modulus (M_s = 1.25), as shown in **Figure 4.19**. However, both AAS mortars show a significant decrease at later ages. AS-B2 exhibits a decrease in strength at 14 days with the final strength of 49.48 MPa at 28 days, while AAS5-1.00 demonstrates a significant decrease in strength at 7 days with the final strength being 42.31 MPa. The final strength of both mortars show a lower strength compared to OPC.

Increasing the alkali modulus in AAS mortars tended to reduce the strength as shown in **Figure 4.20**. The strength development of AAS mortar is assumed to be affected by the alkali modulus. The strength of AAS5 decreases from 47.93 (at

M_s = 1.00) to 42.31 MPa (at M_s = 1.25), while AS-B from previous work (Adam, 2009) shows a decrease from 52.27 (M_s = 1.00) to 49.48 (M_s = 1.25) as shown in **Table 4.13**. All AAS mortars demonstrate a similar behaviour in strength development over time. However, higher alkali modulus AAS mortar tends to have a reduction in compressive strength earlier than the lower alkali modulus mortars. Similar finding was also found by other researchers (Wang et al., 1994, Fernandez-Jimenez et al., 1999, Adam, 2009). They found that higher alkali modulus tends to reduce the strength of AAS specimens.

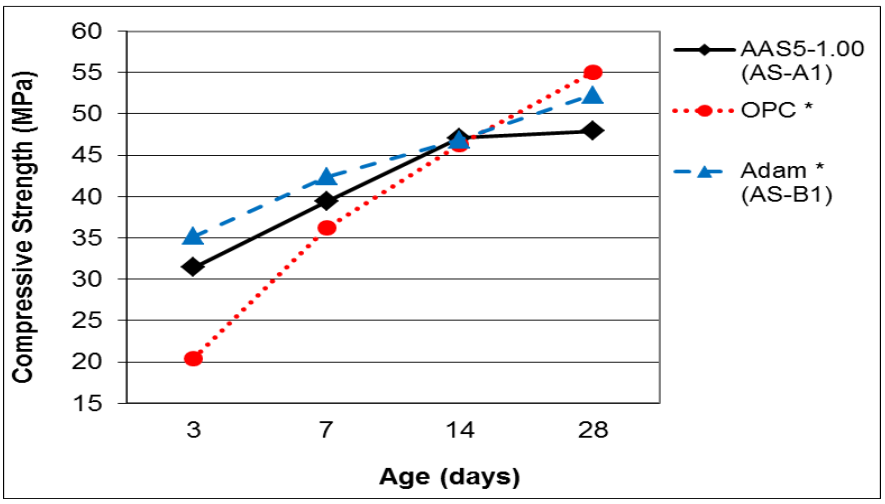

* Adam (2009)

Figure 4.18 Comparison of AAS strength at Ms = 1.00

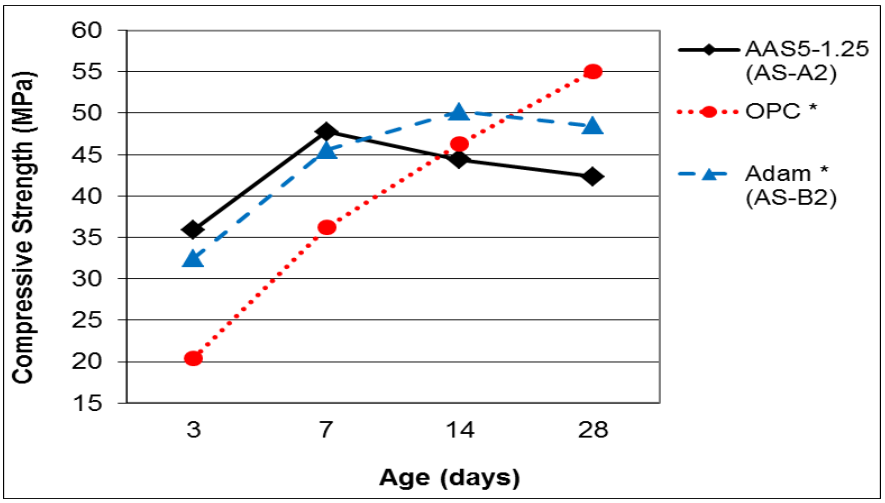

* Adam (2009)

Figure 4.19 Comparison of AAS strength at Ms = 1.25

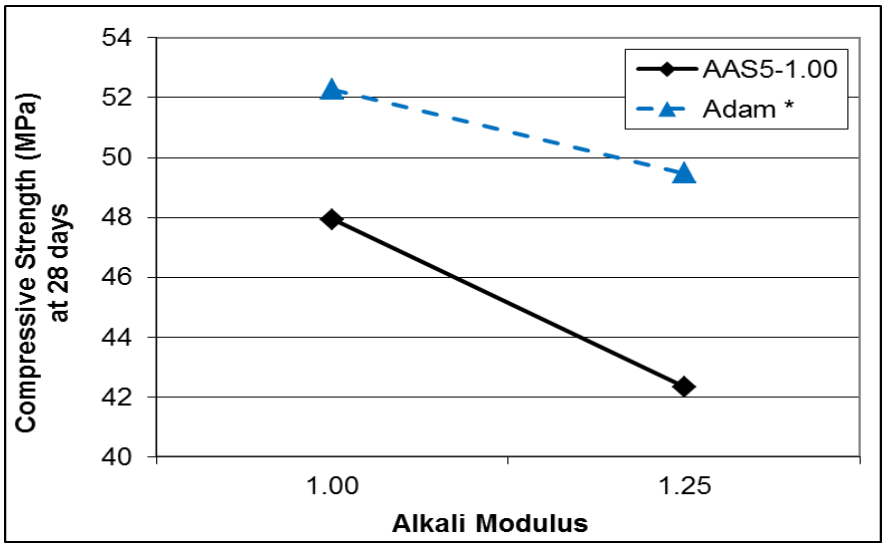

* Adam (2009)

Figure 4.20 Effect of alkali modulus at 28 days age

Table 4.13 Comparison of alkali modulus (M_s) at 28 days

Specimens	Compressive strength at Ms of (MPa)	
	1.00	**1.25**
AS-A (AAS5)	47.93	42.31
AS-B (Adam*)	52.27	49.48

* Adam (2009)
** Based on **Equation 2.6 (Chapter 2 Section 2.5.5)**
*** Based on **Equation 2.7 (Chapter 2 Section 2.5.5)**

Table 4.14 Classification of slags

Specimens	Basicity Coefficient (K_b)		Classification of slag
	K_b (Eq. 2.6) **	K_b (Eq. 2.7) ***	
AS-A (AAS5)	0.811	0.803	Acid
AS-B (Adam *)	1.030	1.020	Basic

* Adam (2009)
** Based on **Equation 2.6 (Chapter 2 Section 2.5.5)**
*** Based on **Equation 2.7 (Chapter 2 Section 2.5.5)**

The decrease of strength in AAS mortars is also attributed to the classification of the slag precursor. The classification of slag is determined based on the basicity coefficient which is calculated based on **Equation 2.6** and **Equation 2.7** (**Chapter 2 Section 2.5.5**) as shown in **Table 4.14**. The basicity coefficient (K_b) of AAS5 is 0.803 – 0.811 which is classified as acid slag ($K_b < 1$), while AS-B from previous work (Adam, 2009) is classified as basic slag with a basicity coefficient of 1.02 – 1.03 ($K_b = 1$). This behaviour was also reported by Wang et al. (1994)'s. They found that the optimum alkali modulus of acid slag is 1.00 and increasing the alkali modulus beyond $M_s = 1.00$ tends to decrease the strength.

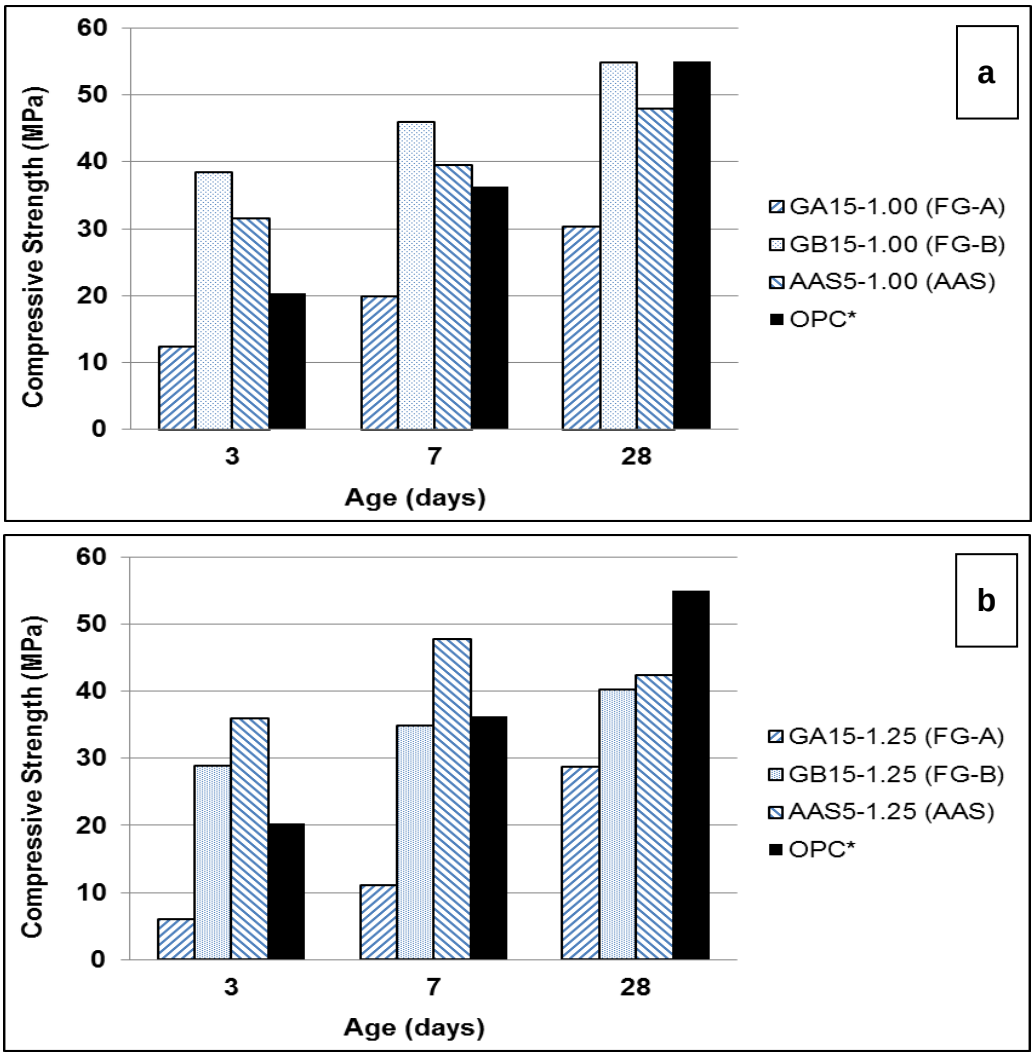

Figure 4.21 Comparison between FA geopolymer and AAS mortars for alkali modulus (Ms) = 1.00 (a) and 1.25 (b)

Overall, the 28 days strength of the FG-B and AAS mortars is comparable with that of Ordinary Portland cement (OPC) mortar, shown in **Figure 4.21**. A comparable strength performance is shown for both fly ash geopolymer and AAS mortars with the alkali modulus (M_s) = 1.00 (**Figure 4.21a**). However, a higher alkali modulus (M_s = 1.25) has a tendency to reduce the strength of both mortar specimens (**Figure 4.21b**).

4.7. Summary of chapter 4

The result of the investigation on the strength development of fly ash geopolymer and AAS mortars can be summarized as follows:

1. Fly ash and slag can be used as 100% cement replacement to produce fly ash geopolymer and AAS specimens, respectively.
2. Fly ash geopolymer B (FG-B) mortar demonstrated a better performance in strength development compared to fly ash geopolymer A (FG-A) mortar.
3. The FG-B mortar exhibited a comparable strength to traditional OPC, while the FG-A mortar showed a lower strength compared to OPC mortar. It was also found that increasing the alkali modulus lowered the strength of both the FG-A and FG-B mortars. A higher alkali modulus had a tendency to reduce the strength of fly ash geopolymer mortars.
4. The strength development of fly ash geopolymer mortar was affected by the fineness, specific surface area, silicate (Si) content, ratio of Si/Al, and CaO content of the fly ash precursors. While, the strength development of AAS mortar was influenced by the activator modulus and the dosage of concentration of the activator solution.
5. Greater fineness and specific surface area of fly ash will result in a higher reactivity resulting in higher compressive strength of fly ash geopolymer. FG-B mortar with a high fineness and specific surface area exhibited a higher strength than the FG-A mortar.
6. The strength development of fly ash geopolymer mortar was influenced by the concentration of Si in the fly ash precursors. A high concentration of Si concentration led to a change in the effective alkali modulus (M_{se}) and a

reduction in the compressive strength. FG-A mortar with high silicate demonstrated a lower strength compared to FG-B mortar due to the increase of the alkali modulus beyond 1.5.

7. The ratio of Si/Al significantly affected the strength development of fly ash geopolymer. Higher Si/Al ratios tended to delay the reaction time of fly ash geopolymer mortar. FG-A mortar with a higher Si/Al ratio demonstrated a slow strength development compared to FG-B mortar with a lower SI/Al ratio.
8. The strength development of fly ash geopolymer mortar was affected by the content of CaO in the fly ash precursors. A low CaO content in fly ash precursors slows the setting time resulting in a lower compressive strength of fly ash geopolymer. FG-A mortar with a very low content of CaO exhibited a low strength development compared to the FG-B mortar.
9. The early strength of the AAS mortar was higher than that of the traditional OPC, however at 28 days the strength tended to reduced and become less than that of the OPC.
10. Increasing the alkali modulus in the AAS mortar had minimal impact on the strength. The strength development of AAS mortar was significantly influenced by the dosage of the alkali modulus.
11. The reduced strength of AAS mortar at higher activator modulus was also attributed to the type of slag precursor which was acid slag in agreement with other authors.
12. Overall, the strength development of FG-B and AAS mortars was comparable to that OPC, while FG-A mortar has the lowest strength of all mortar specimens.

5. MECHANICAL AND DURABILITY PROPERTIES OF FLY ASH GEOPOLYMER CONCRETE

5.1. Overview

The previous investigation on the strength of fly ash geopolymer mortar in **Chapter 4** confirmed the possibility of producing concrete using 100% fly ash as a cement replacement.

Research in **Chapter 4** found that an activator modulus of 1.00 resulted in an optimum strength performance for fly ash geopolymer mortar. Furthermore, the strength development is influenced by the concentration of silicates, aluminates and CaO in the fly ash. A high concentration of silicates contributes to a change in the alkali modulus and a reduction in the compressive strength due to the change of the geopolymer matrix. The Si/Al ratio is also observed to play a major role in the strength development – with a high Si/Al ratio tending to delay the strength development. In contrast, it was found that a low CaO content results in a strength reduction. Fly ash type 2 (PFA2) gives better initial strength development compared to fly ash type 1 (PFA1). However, PFA1 fly ash shows a significant increase in strength over time indicating that the reaction is not completed in the short term. Based on these findings PFA1, with a high Si content, was selected with an Na_2O dosage of 15% and an activator modulus (M_s) of 1.00 to develop a fly ash geopolymer concrete for long term performance testing.

This chapter presents the experimental results of the long term performance of the mechanical properties of fly ash geopolymer concrete. The mechanical properties have been examined at 28, 56, 90, 180, 360 and 540 days. The testing included assessment of the compressive strength, the modulus of elasticity, the modulus of rupture, the indirect tensile strength, and the density. The durability properties of fly ash geopolymer concrete were also assessed by performing porosity, water absorption, water permeability, ultrasonic velocity tests, resistivity, chloride diffusion and carbonation tests.

5.2. Materials

5.2.1. Fly ash

PFA1 was used to prepare the fly ash geopolymer concrete specimens. The properties of fly ash type 1 are described in **Chapter 3 Section 3.2.1**.

5.2.2. Alkaline activators

The same alkaline activators of sodium silicate and sodium hydroxide as used for the mortar were used for the fly ash geopolymer concrete specimens. A high concentration alkaline solution of 15M NaOH was used. The properties of alkaline activators are described in **Chapter 3 Section 3.2.3**.

5.2.3. Aggregates

The properties of the fine and coarse aggregates are described in **Chapter 3 Section 3.2.5**. The moisture condition of the fine and coarse aggregates was saturated surface dry (SSD). The fine aggregate was from the Langwarrin source and the coarse aggregates were from the Mawson Lake Cooper quarry with a specific gravity of 2.03 and 2.99, respectively. The typical grading of the combined aggregate is shown in **Table 3.6 Chapter 3 Section 3.2.5**.

5.3. Mix proportions

The selection of the mixes was based on the standard compressive strength for concrete corresponding to grade B1 and B2 as defined in AS 3600, having a 28 days compressive strength of 40 $\pm$ 10 MPa (Adam, 2009). The rationale of the selection process for design strength was to investigate the performance of fly ash geopolymer concrete compared to a standard strength OPC concrete. An Na_2O dosage of 15% with an M_s of 1.00 was selected to achieve the target strength (based on the results in **Chapter 4).**

A water/solid (w/s) ratio of 0.41 was used to achieve workability during the mixing process. The volume of aggregates to the total volume of mixture was kept to 68%. The quantity of water has been taken as the sum of water contained in the sodium silicate, sodium hydroxide and the added water, while the quantity of solid

was determined by the mass of fly ash and the solid contained in the alkaline activator solution (Adam, 2009).

Table 5.1 summarizes the details for the fly ash geopolymer concrete. A blend of liquid sodium silicate and sodium hydroxide provides an M_s of 1.00. The Na_2O dosage (the ratio of Na_2O in alkaline solution to the mass of fly ash) is 15%.

Table 5.1 Mix design of fly ash geopolymer concrete (kg/m^3)

Mixture	Fly ash	Aggregate			Activator		Added water
		Sand	7 mm	10 mm	Na_2SiO_3	NaOH 10M	
G15-1.00	467	784	346	693	234	147	10

5.4. Mixing and curing process

The preparation of the fine and coarse aggregates was adopted from previous research (Adam, 2009). All aggregates were in SSD condition prior to mixing in order to stabilize the absorption. The liquid solutions of sodium silicate, sodium hydroxide and additional water were blended prior to mixing.

The mixing procedure was developed from the previous research at RMIT University (Adam, 2009) as shown in **Figure 5.1** and **Figure 5.2**. The mixing was carried out using a 120 litre mixer then poured into moulds as presented in **Table 5.2**.

Heat curing was adopted as the most suitable curing method. The specimens were left at room temperature for 24 hours after being de-moulded and then cured in the oven at 80^{O}C for another 24 hours. The specimens were wrapped with plastic to prevent the evaporation of the liquid (**Figure 5.3)** during heat curing treatment. The specimens were stored at room temperature prior to testing.

Table 5.2 Type of moulds for testing

No	Moulds	Size	Tests
1	Cylinder	100 mm diameter x 200 mm high	Compressive strength Elasticity modulus Density, Porosity Water absorption
2	Cylinder	150 mm diameter x 300 mm high	Indirect tensile
3	Prism	100 mm x 100 mm x 300 mm	Modulus of rupture
4	Block	300 mm x 300 mm x 100 mm	Water permeability
5	Block	200 mm x 200 mm x 100 mm	UPV Resistivity
6	Block	100 mm x 100 mm x 100 mm	Chloride diffusion Carbonation

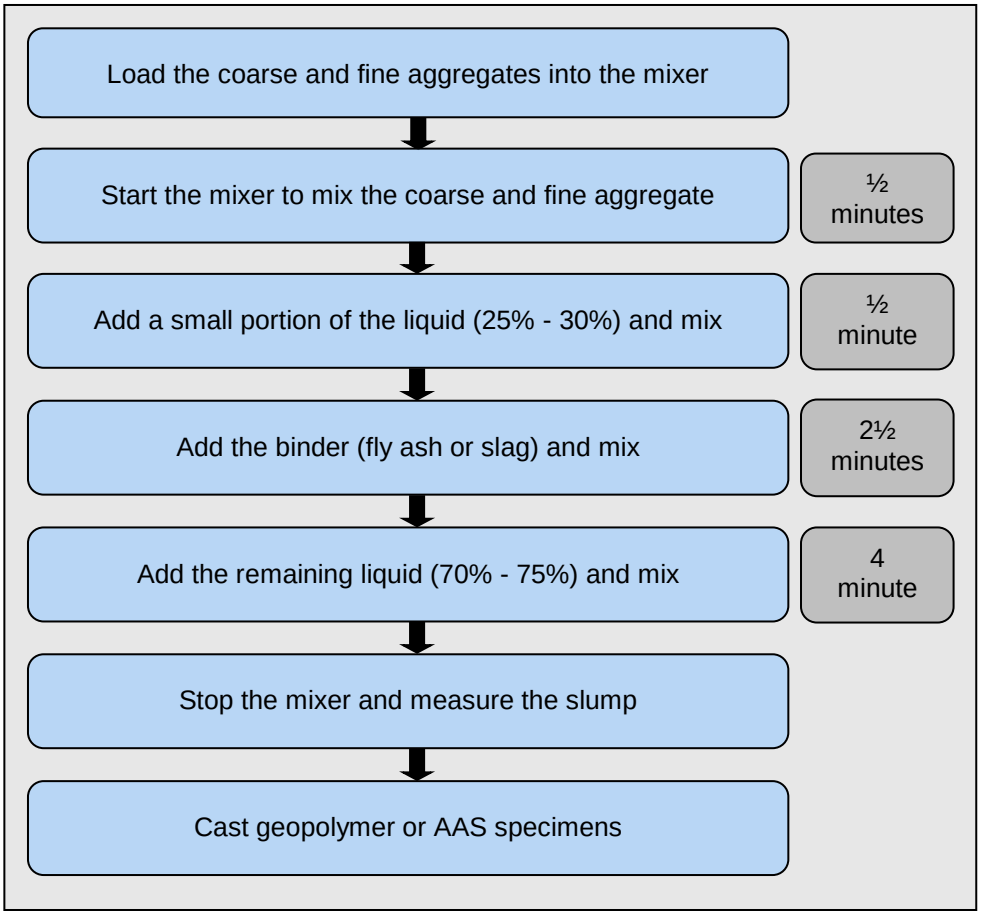

Figure 5.1 Mixing procedures of geopolymer concrete (Adam, 2009)

Figure 5.2 Casting process of fly ash geopolymer and AAS concretes

Figure 5.3 Heat curing for fly ash geopolymer concretes

5.5. Workability

The slump test is the most common workability test employed for fresh concrete (Mehta & Monteiro, 2006). ACI defines the workability as “that property of freshly mixed concrete or mortar that determines the ease with which it can be mixed, placed, consolidated, and finished to a homogenous condition” (ACI 116R-00, 2005).

The workability of the fly ash geopolymer concrete was measured using a slump test in accordance with Australian Standard (AS 1012.3.1, 1998). The test was performed using a truncated cone of 300 mm height, 100 mm diameter on top and 200 mm diameter on the bottom as shown in **Figure 5.4**.

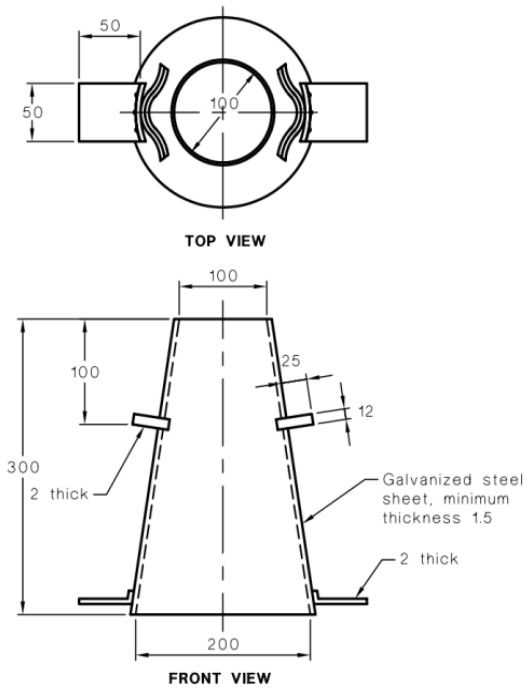

Figure 5.4 Truncated cone for slump test (AS 1012.3.1, 1998)

The result of the slump test is shown in **Figure 5.5**. It demonstrates that standard slump test is not a suitable measure as the liquid characteristic of the fly ash geopolymer concrete results in collapse as soon as slump cone is lifted. The water/solid ratio had been determined to achieve a workable mixing process.

Figure 5.5 Slump test of fresh fly ash geopolymer concrete

The collapse is attributed to the spherical shape of fly the ash particles (**Figure 3.1**) resulting in a high flow-ability for the material. Similar results have been reported by other authors (Atis & Karahan, 2009, Bouzoubaa et al., 1999). It is also hypothesised that a lubricant effect from the sodium silicate solution (Adam, 2009), coupled with the added water (**Table 5.1**) further contributed to the high slump. The fresh fly ash geopolymer concrete specimens also displayed highly sticky characteristics, again in accordance with the findings of other researchers (Adam, 2009, Rangan et al., 2006).

5.6. Density development

The density of the fly ash geopolymer concrete was measured using the rapid measurement method in accordance with Australian Standards (AS 10.12.12.1, 1998). The density development is shown in **Table 5.3**. The detailed calculation of the density of fly ash geopolymer concrete is provided in **Appendix C**.

Table 5.3 Density development of fly ash geopolymer concrete

Time (days)	Density (kg/m^3)
28	2302.4
56	2307.6
90	2310.9
180	2321.4
360	2324.2
540	2325.5
Average	2315.3
Density	2320

Note: The average density of a group of specimens is rounded to the nearest 20 kg/m^3 (AS 10.12.12.1, 1998).

The density tended to increase over time (**Figure 5.6**) with an initial density at 28 days of 2302.4 kg/m^3 increasing to a final density of 2325.5 kg/m^3 at 540 days. This suggests that the reaction process is not complete at 28 days. Overall an increase in density of 1.03% is observed between 28 and 540 days.

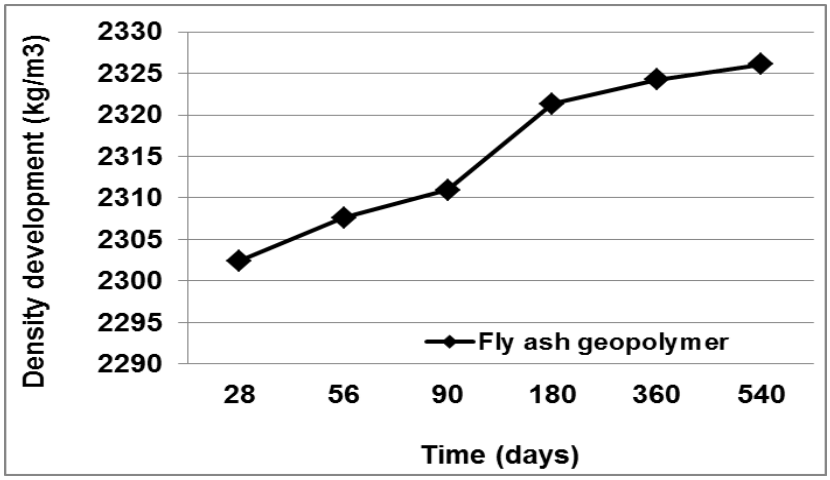

Figure 5.6 Density development of fly ash geopolymer concrete

Table 5.4 Density of fly ash geopolymer concrete compared to others

Researchers	Density (kg/m^3)
Swanepoel & Strydom (2002)	1500 – 1800
Hardjito & Rangan (2005)	2330 – 2430
Diaz-Loya et al. (2011)	1890 – 2371
Fly ash geopolymer (this research)	2305 – 2330

However, despite demonstrating a marginal increase over time, the density of fly ash geopolymer concrete is lower than OPC concrete (characteristically with a density of approximately 2400 kg/m^3) in accordance with AS 3600 (2009). This might be attributable to the specific gravity of the raw materials used to produce fly ash geopolymer concrete. The specific gravity of the fly ash is 2.1 (Cement Australia, 2011) which is lower than that of Portland cement with a specific gravity of 3.0 – 3.2 (Cement Australia, 2013). A similar finding was also found by other researchers (Swanepoel & Strydom, 2002, Hardjito & Rangan, 2005, Diaz-Loya et al., 2010) as shown in **Table 5.4**. They found that the density of fly ash geopolymer concrete is lower than OPC normal concrete with a density in the range 1500 – 2430 kg/m^3.

5.7. Long term mechanical properties of fly ash geopolymer concrete

5.7.1. The development of compressive strength

Compressive strength tests of the fly ash geopolymer concrete were carried out at 28, 56, 90, 180, 360 and 540 (as described in **Chapter 3 Section 3.5.1)**.

The compressive strength was calculated by dividing the maximum load to failure by the average cross sectional area (Kett, 2010). The compressive strength was calculated from an average of 3 specimens (calculations presented in **Appendix D)**. The strength development is shown in **Table 5.5** and **Figure 5.7**.

Table 5.5 Compressive strength of fly ash geopolymer concrete

Mix	Age					
	28 days	56 days	90 days	180 day	360 day	540 day
Compressive strength (MPa)	22.37	25.13	27.01	31.09	33.23	33.09
Standard deviation	0.56	0.66	0.71	1.15	1.50	0.87

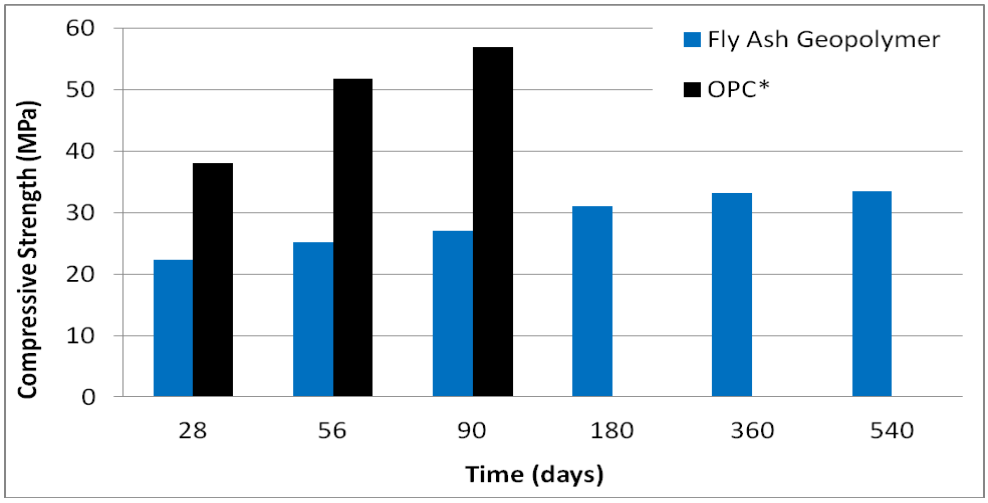

Note: * Adam (2009)

Figure 5.7 Strength development of fly ash geopolymer concrete

The fly ash geopolymer concrete exhibits a lower strength at 28 days compared to the OPC concrete. Indeed at 28 days the FAG concrete has only achieved a compressive strength of 22.37 MPa, and does not meet the design compressive

strength of 40 ± 10 MPa. However, the fly ash geopolymer concrete shows a significant increase in strength with further time, achieving 31.09 MPa at 180 days increasing to 33.23 MPa at 360 days and 33.09 MPa at 540 days. This would indicate that the reaction process is not complete at 28 days. Overall an increase in strength of 48.55% is observed between 28 and 360 days. In general, class F fly ash-based geopolymer concretes exhibit a slower setting and strength development at room temperature (Winnefeld et al., 2010) and higher strength can be achieved by adopting a heat curing treatment (Bakharev, 2005a). As such it is interesting to note that even with heat curing, strength development continues with time, indicating that the geoploymeric reaction is on-going with time despite the heat curing.

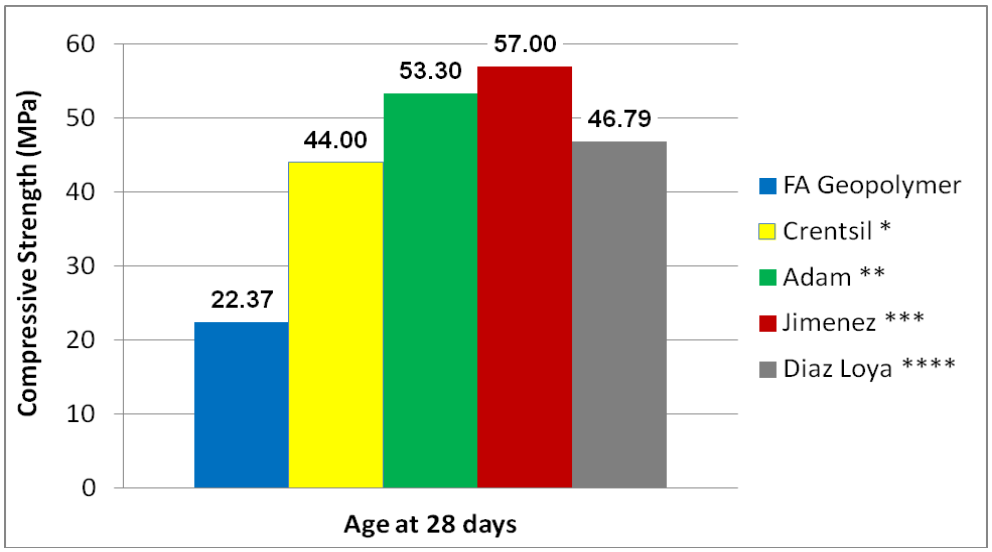

Note: * Sagoe-Crentsil et al. (Sagoe-Crentsil et al., 2010)
** Adam (Adam, 2009)
*** Fernandez-Jimenez et al. (Fernandez-Jimenez et al., 2006)
**** Diaz-Loya et al. (Diaz-Loya et al., 2011)

Figure 5.8 Comparison of strength development at 28 days

The results indicated that the strength development of the fly ash geopolymer concrete was affected by the availability of silicates, aluminates and CaO content in the fly ash precursors as discussed in the preliminary research (**Chapter 4 Section 4.6),** in agreement with other authors (Fletcher et al., 2005, Steveson & Sagoe-Crentsil, 2005, Rowles & O'Connor, 2003, Diaz-Loya et al., 2010). **Figure 5.8** shows the compressive strengths reported for this research compared to

previously reported data, while **Table 5.6** gives the CaO, SiO_2 and Al_2O_3 contents of the respective fly ashes used (Diaz-Loya et al., 2011, Sagoe-Crentsil et al., 2010, Adam, 2009, Fernandez-Jimenez et al., 2006).

Table 5.6 Comparison of chemical composition of fly ash precursor

Components	FA Geopolymer	Crentsil [1]	Adam [2]	Jimenez [3]	Diaz-Loya [4]
CaO	0.18	3.29	3.47	2.44	5.01
SiO_2	70.30	47.19	49.45	53.09	62.12
Al_2O_3	23.10	29.79	29.61	24.80	19.59
Si + Al	93.40	76.98	79.06	77.89	81.71
Si/Al ratio	3.04	1.58	1.67	2.14	3.14

Note: * Sagoe-Crentsil et al. (Sagoe-Crentsil et al., 2010)
** Adam (Adam, 2009)
*** Fernandez-Jimenez et al. (Fernandez-Jimenez et al., 2006)
**** Diaz-Loya et al. (Diaz-Loya et al., 2011)

The data shows that the fly ash geopolymer concrete has a higher total Si and Al (Si + Al = 93.40%) components compared to other specimens and has a similar Si/Al ratio to the Diaz-Loya specimens (Si/Al ratio of approximately 3.00). However, the compressive strength of the fly ash geopolymer concrete exhibits the lowest strength of all specimens at 22.37 MPa. This low strength is attributed to the low content of CaO (0.18%) in the fly ash precursors which was the lowest compared to other geopolymer specimens.

A high content of CaO in the fly ash allows the calcium silicate glass structure in the fly ash to react with the water and to form calcium silicate hydration compounds that improve the mechanical strength of the resultant geopolymer. Although, increasing the CaO content in the fly ash appears to have a positive effect on the compressive strength of the resulting geopolymer, the use of fly ash with a CaO content more than 20% is not recommended as source material for geopolymer due to its very rapid setting time according to Diaz-Loya et al. (2010).

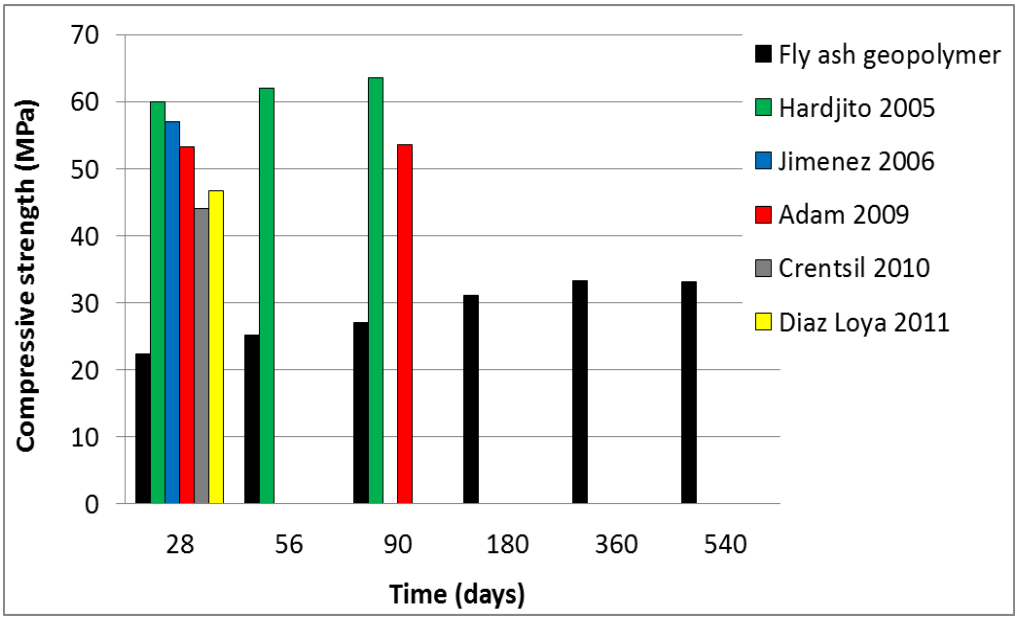

Note: 1 Hardjito & Rangan (2005)
2 Fernandez-Jimenez et al. (2006)
3 Adam (2009)
4 Sagoe-Crentsil et al. (2010)
5 Diaz-Loya et al. (2011)

Figure 5.9 Long term performance of fly ash geopolymer concrete

Figure 5.9 displays the long term performance of fly ash geopolymer concrete compared to other reported works (Diaz-Loya et al., 2011, Sagoe-Crentsil et al., 2010, Adam, 2009, Hardjito & Rangan, 2005, Fernandez-Jimenez et al., 2006). These generally show a high initial strength at 28 days with a further slight increase up to 90 days. The study reported here continues testing up to 540 days and again confirms the on-going reaction of fly ash geopolymer concrete with time.

5.7.2. The development of modulus of elasticity

The modulus of elasticity is a property of concrete that relates stress and elongation within the elastic limit. A higher modulus of elasticity indicates a better quality of concrete. The modulus of elasticity of the fly ash geopolymer concrete was assessed in accordance with AS 1012.17 (1997) as described in **Chapter 3 Section 3.5.2.** The test load was determined based on method 1, article 2.5.1(a) (AS 1012.17, 1997) and taken as equivalent to 40% of the average compressive

strength (**Appendix E**). The development with time of the modulus of elasticity is shown in **Table 5.7** and **Figure 5.10** (calculations shown in **Appendix E)**.

Table 5.7 Modulus of elasticity of fly ash geopolymer concrete

Age of concrete (days)	Compressive strength (MPa)	Modulus of elasticity (MPa)
28	22.37	8022
90	27.01	11541
180	31.09	14462
360	33.23	14779
540	33.09	15942

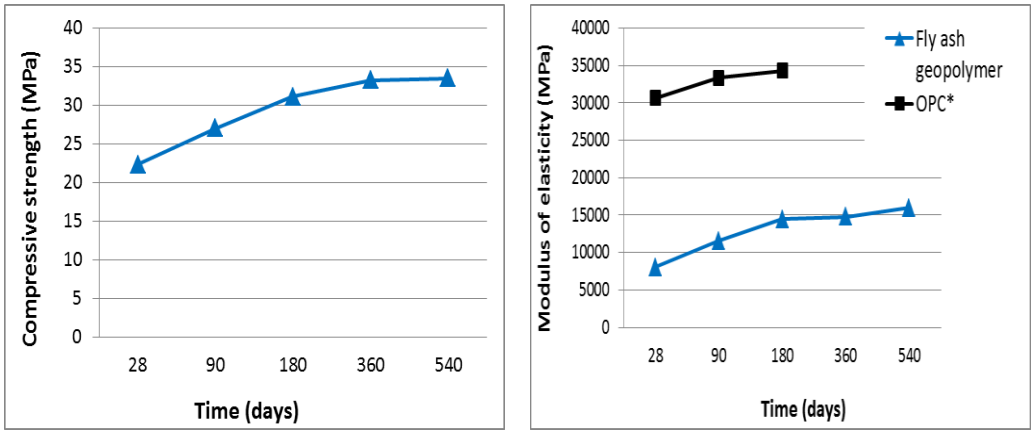

Note: * (Adam, 2009)

Figure 5.10 Compressive strength vs modulus of elasticity of fly ash geopolymer concrete

Similar to OPC concrete, the modulus of elasticity of fly ash geopolymer concrete appears to be affected by that of the geopolymer paste and the aggregate. For OPC concrete, the relationship between the modulus of elasticity and compressive strength follows a positive linear relationship in accordance with AS 3600 (2009).

The results demonstrate that the fly ash geopolymer concrete has a modulus of elasticity lower than that of OPC concrete. However, it was found that the change with time displays a similar pattern to the development of compressive strength. The modulus of elasticity increases as the compressive strength increases as

shown in **Figure 5.10**, with the relationship being positive linear as displayed by OPC concrete.

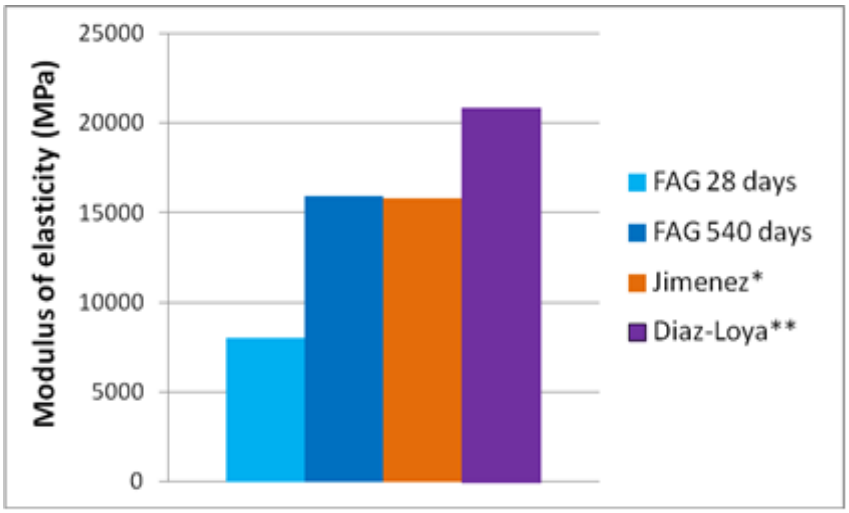

Note: * Fernandez-Jimenez et al. (2006)
** Diaz-Loya et al. (2011)

Figure 5.11 Comparison of modulus of elasticity of fly ash geopolymer concrete to other researchers

The modulus of elasticity of the fly ash geopolymer concrete was measured to be 8022 MPa at 28 days, lower than other reported results (**Figure 5.11**). However, the modulus of elasticity demonstrated a significant increase over time achieving a value of 15942 MPa at 540 days similar to the results reported by other authors (Diaz-Loya et al., 2011, Fernandez-Jimenez et al., 2006). This further indicates that the geopolymeric reaction is not complete at 28 days, in agreement with the compressive strength results reported above.

5.7.3. The development of flexural tensile strength

Although concrete is designed to achieve a specified compressive strength, tensile strength is also considered an important factor. While concrete is not designed to resist direct tension forces due the brittle nature of the material, the determination of tensile strength of concrete plays an important role due to the occurrence of cracking in concrete caused by the overloading under flexural conditions. These cracks may cause serviceability and durability issues.

According to the Australian Standard (AS 3600, 2009), the flexural tensile strength of concrete may be calculated using two different methods as follows:

(1) Based on the measured flexural tensile strength test (modulus of rupture test result), in accordance with Australian Standard (AS 1012.11, 2000).

(2) Based on the compressive strength test result in the absence of more accurate data, the characteristic of flexural tensile strength of concrete can be calculated using the equation: $f'_{ct} = 0.6\sqrt{f'_c}$ *(5.1)*

(3) The measured values for the compressive strength and flexural strength are the mean of three trials while the and predicted mean values are obtained by multiplying the characteristic values by 1.4

The development over time of the flexural tensile strength of fly ash geopolymer concrete, based on the modulus of rupture test results, is shown in **Table 5.8** and **Figure 5.12 (c**alculations in **Appendix F)**.

Table 5.8 Flexural tensile strength of fly ash geopolymer concrete

Age of concrete (days)	Compressive strength f'c (MPa)	Measured flexural tensile strength [1] $f_{ct.f}$ (Actual) (MPa)	Mean values flexural tensile strength from AS 3600 [2] $f_{ct} = 1.4\ (0.6)\ \sqrt{f'c}$ (Predicted) (MPa)	Flexural tensile strength ratio (measured / mean values)
28	22.37	4.73	3.97	1.19
56	25.13	5.33	4.21	1.27
90	27.01	5.78	4.37	1.32
180	31.09	6.62	4.68	1.41
360	33.23	7.01	4.84	1.45
540	33.47	7.23	4.86	1.49

For OPC concrete, the relationship between the flexural tensile strength and the compressive strength follows a positive linear relationship. An increase in the compressive strength of OPC concrete leads to an increase in the flexural tensile strength. The behaviour of the flexural tensile strength of the fly ash geopolymer concrete is seen to be similar to that of OPC concrete (**Figure 5.12**).

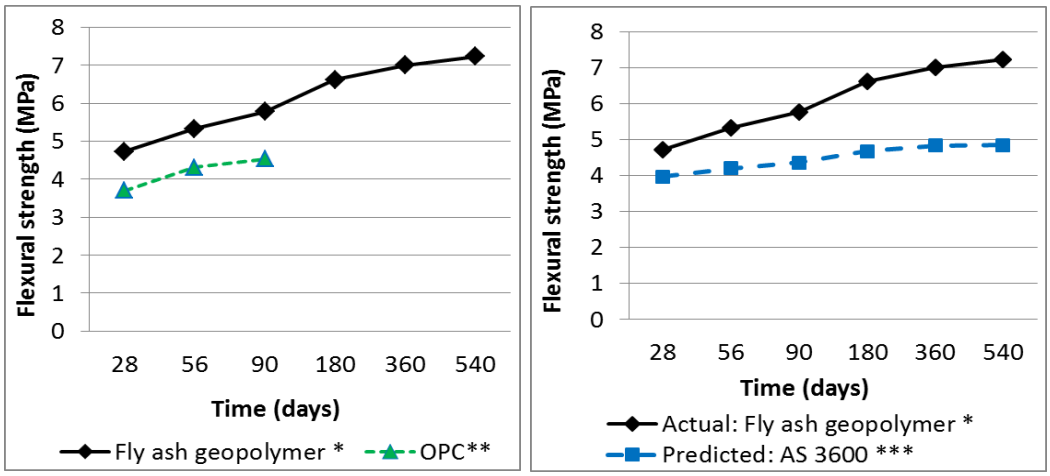

Note: * Actual, based on laboratory results, Australian Standard (AS 1012.11, 2000)
** Predicted, based on previous research (Adam, 2009, AS 3600, 2009)
*** Predicted, based on Australian Standard (AS 3600, 2009)

Figure 5.12 Measured flexural tensile strength of fly ash geopolymer concrete

The flexural tensile strength of the fly ash geopolymer concrete follows a positive linear relationship with increasing compressive strength, **Figure 5.12**. The predicted flexural tensile strength of fly ash geopolymer concrete is predicted (AS 3600, 2009) to be 3.97 MPa at 28 days and increases to 4.86 MPa at 540 days. However, the actual measured flexural tensile strength is found to be higher than the mean values flexural tensile strength predicted (**Table 5.8** and **Figure 5.12**). Hence AS 3600 is found to under-value the flexural tensile strength development of fly ash geopolymer concrete, indicating that the use of AS 3600 would be conservative to calculate the flexural tensile strength. This also indicates that the long term behaviour of fly ash geopolymer concrete is significantly better than the AS 3600 prediction.

Similar results have been found by other researchers (Fernandez-Jimenez et al., 2006, Diaz-Loya et al., 2011, Neupane et al., 2014), **Table 5.9**. These results show that the measured flexural tensile strengths of geopolymer concrete are higher than values predicted from AS 3600 (2009). The flexural tensile strength ratio, which is determined based on the ratio of the measured flexural tensile strength to the predicted AS 3600 value, shows that the measured flexural tensile strength is approximately 20% – 50% higher than that predicted by AS 3600.

Table 5.9 Flexural tensile strength of fly ash geopolymer concrete compared to other results at 28 days

Specimens	Compressive strength (MPa)	Measured flexural tensile strength (Actual) (MPa)	Mean values flexural tensile strength from AS 3600 (Predicted) (MPa)	Flexural tensile strength ratio (measured / AS 3600)
Fly ash geopolymer	22.37	4.73	3.97	1.19
Jimenez (1)	37.65	6.85	3.68	1.86
Diaz Loya (2)	36.17	4.27	3.61	1.18
Neupane (3)	60.30	6.50	4.66	1.39

Note: (1) Fernandez-Jimenez et al. (2006)
(2) Diaz-Loya et al. (2011)
(3) (Neupane et al., 2014)

According to Fernandez-Jimenez et al. (2006), this can be attributed to the micro-structural characteristic of fly ash geopolymer concrete. The 3D skeleton produced in the geopolymeric reaction affords exceptional physical solidity which is responsible for the mechanical behaviour observed.

According to Sofi et al. (2007), the higher flexural strength of geopolymer concrete compared to OPC concrete is attributed to the polycondensation reaction. The composition of the hardened fly ash geopolymer matrix is different to the pore structure of OPC concrete. Thus, the favourable flexural tensile strength results presented can be attributed to the type of matrix formed in the fly ash geopolymer materials (Sofi et al., 2007).

5.7.4. The development of uniaxial tensile strength

According to AS 3600 (2009), the uniaxial tensile strength of concrete may be calculated using three different methods:

(1) Based on the measured flexural tensile strength test (modulus of rupture test result) in accordance with AS 1012.11 (2000) and calculated using

$$f'_{ct} = 0.6\sqrt{f'_{ct.f}} \qquad (5.2)$$

(2) Based on the measured indirect tensile strength test (splitting test result)) in accordance with AS 1012.10 (2000) and calculated using

$$f'_{ct} = 0.9\sqrt{f'_{ct.sp}} \qquad (5.3)$$

(3) Based on the compressive strength test result in the absence of more accurate data, the characteristic values of uniaxial tensile strength of concrete can be calculated using $f'_{ct} = 0.36\sqrt{f'c}$, (5.4)

(4) The measured values for the compressive strength and uniaxial strength are the mean of three trials while the and predicted mean values are obtained by multiplying the characteristic values by 1.4

According to Neville (2011), the tensile strength determined in the indirect tensile strength test (splitting test) is believed to be close to the direct tensile strength of concrete. Thus, the indirect tensile strength test result was used to determine the uniaxial tensile strength of fly ash geopolymer and AAS concretes.

The development with time of the uniaxial tensile strength is shown in **Table 5.10** and **Figure 5.13**.

Table 5.10 Uniaxial tensile strength of fly ash geopolymer concrete

Age of concrete (days)	Compressive strength (MPa)	Measured indirect tensile strength $f_{ct.sp}$ (MPa)	Actual Uniaxial tensile strength from AS 3600 $f_{ct} = 0.9\sqrt{f'_{ct.sp}}$ (MPa)	Predicted Mean values uniaxial tensile strength from AS 3600 $f_{ct} = 1.4$ (0.36)$\sqrt{f'c}$ (MPa)	Uniaxial tensile strength ratio (measured / mean values)
28	22.37	2.12	1.91	2.38	0.80
56	25.13	2.43	2.19	2.53	0.87
90	27.01	2.80	2.52	2.62	0.96
180	31.09	3.36	3.03	2.81	1.08
360	33.23	3.82	3.44	2.91	1.18
540	33.47	4.13	3.72	2.92	1.27

Applying Australian Standard (AS 3600, 2009) to predict the long term performance found that the predicted uniaxial tensile strength follows a positive linear relationship with the increase of compressive strength with time (**Figure 5.13**). This behaviour is similar to that of OPC concrete.

The uniaxial tensile strength is predicted to be 2.38 MPa at 28 days and increase to 2.92 MPa after 540 days. However, the actual measured uniaxial tensile strength is found to be higher than that predicted by AS 3600. This indicates that

the use of AS 3600 equation to calculate the uniaxial tensile strength of fly ash geopolymer concrete would be conservative. Similar result has been found by Neupane et al. (2014). Their results show that the uniaxial tensile strength of fly ash geopolymer concrete is significantly higher than those predicted by Australian Standards (AS 3600, 2009) for OPC concrete.

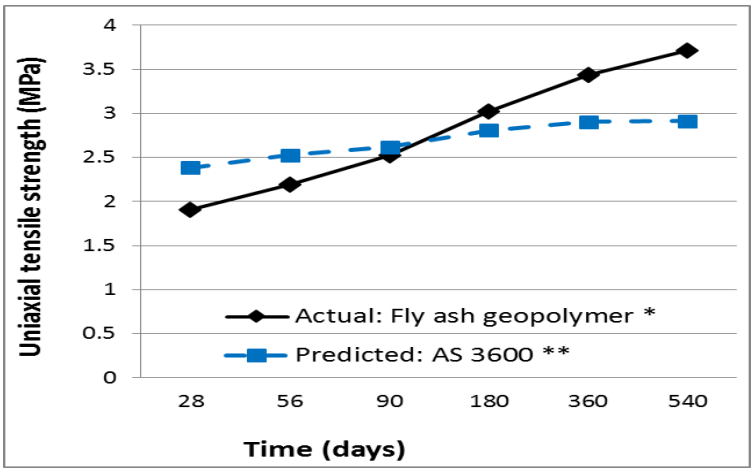

Note: * Actual, based on laboratory results, (AS 1012.10, 2000)
** Predicted, calculated based on article 3.1.1.3 (AS 3600, 2009)

Figure 5.13 Uniaxial tensile strength of fly ash geopolymer concrete

These observations are similar to the results for the flexural tensile strength tests. This corroborates the conclusion that the existing Australian standard (AS 3600, 2009) can be used to predicted the uniaxial tensile strength of fly ash geopolymer concrete. It also supports the findings that fly ash geopolymer concrete continues to gain strength over time due to the continuing geopolymeric reaction.

5.7.5. Correlation between compressive strength and the modulus of elasticity and tensile strength

A regression analysis is used to investigate the relationships between variables (Sykes, 1993). The coefficient of determination ($0 \leq R^2 \leq 1$) is also evaluated in this process, with a high value indicating a strong relationship between the variables. A regression analysis has been performed to investigate the relationships between the compressive strength to the modulus of elasticity, the compressive strength to the flexural tensile strength, and the compressive strength to the uniaxial tensile strength.

Correlation between compressive strength and modulus of elasticity

The comparison of the 28 day modulus of elasticity of fly ash geopolymer concrete to the existing Australian Standard (AS 3600, 2009) and the Ng & Foster model proposed by the Concrete Institute of Australia is shown in **Table 5.11** and **Figure 5.14**. The development of the modulus of elasticity of fly ash geopolymer concrete also gives a positive linear relationship with time, similar to the development of compressive strength, as shown in **Figure 5.14**.

Table 5.11 Comparison of modulus of elasticity of fly ash geopolymer concrete to the existing standards

Age of concrete (days)	Compressive strength (MPa)	Actual: Modulus of Elasticity (1) AS1012.17 (MPa)	Predicted 1: Modulus of Elasticity (2) AS3600 (MPa)	Predicted 2: Model Ng & Foster (3) (MPa)
28	22.37	8022	22403	16267
90	27.01	11541	24480	18001
180	31.09	14462	26147	19406
360	33.23	14779	26954	20106
540	33.09	15942	26853	20061

Note: (1) Based on laboratory results, Australian Standard (AS 1012.17, 1997)
(2) Australian Standard, Article 3.1.2(a) (AS 3600, 2009)
(3) Model proposed by Ng & Foster (Concrete Institute Australia, 2011)

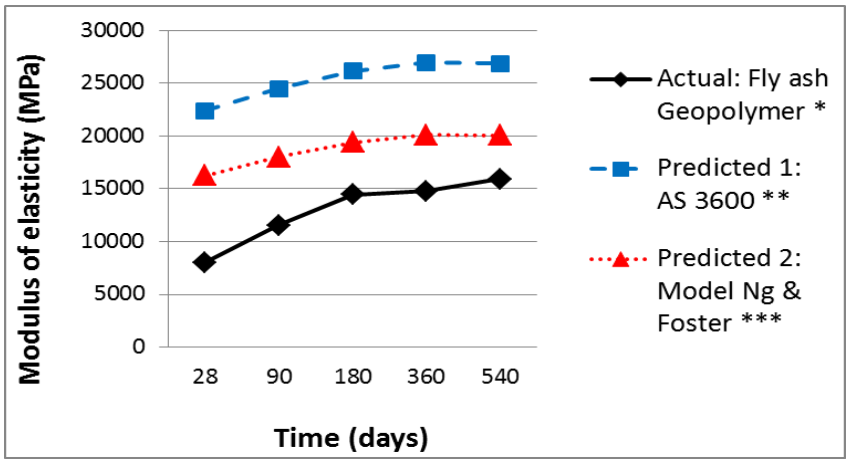

Note: * Actual, based on laboratory results, Australian Standard (AS 1012.17, 1997)
** Predict 1, Australian Standard, Article 3.1.2(a) (AS 3600, 2009)
*** Predict 2, Model proposed by Ng & Foster (Concrete Institute Australia, 2011)

Figure 5.14 Comparison of modulus of elasticity of fly ash geopolymer concrete to existing standards

However, it was found that the actual modulus of elasticity of fly ash geopolymer concrete is much lower than that predicted for OPC concrete in accordance with AS 3600 (2009). In the short term, it was found that the actual modulus of elasticity shows a lower value compared to the AS 3600 and the Ng & Foster model. However, the long term modulus of elasticity demonstrates a significant increase over time and achieved a comparable strength to the result proposed by the Ng & Foster model (Concrete Institute Australia, 2011) at 540 days. According to Fernandez-Jimenez et al. (2006) and Olivia & Nikraz (2012), it might be possible to use the formula proposed by different codes does not consider the existence of variables that affect the property such as the presence of soluble silicate in solution, microstructure characteristics and the content of silicate in fly ash precursors. This low value of the modulus of elasticity has also been attributed to the high Si/Al ratio and low content of CaO in fly ash precursors which leads to a slow geopolymeric reaction and low compressive strength (Silva et al., 2007, Diaz-Loya et al., 2010, Olivia & Nikraz, 2012).

Based on a regression analysis of the data a general regression model representing the correlation between static modulus of elasticity and compressive strength is suggested, **Figure 5.15**, gives the following equation:

$$E_c = 49.968(fc')^{1.6412} \qquad (5.4)$$

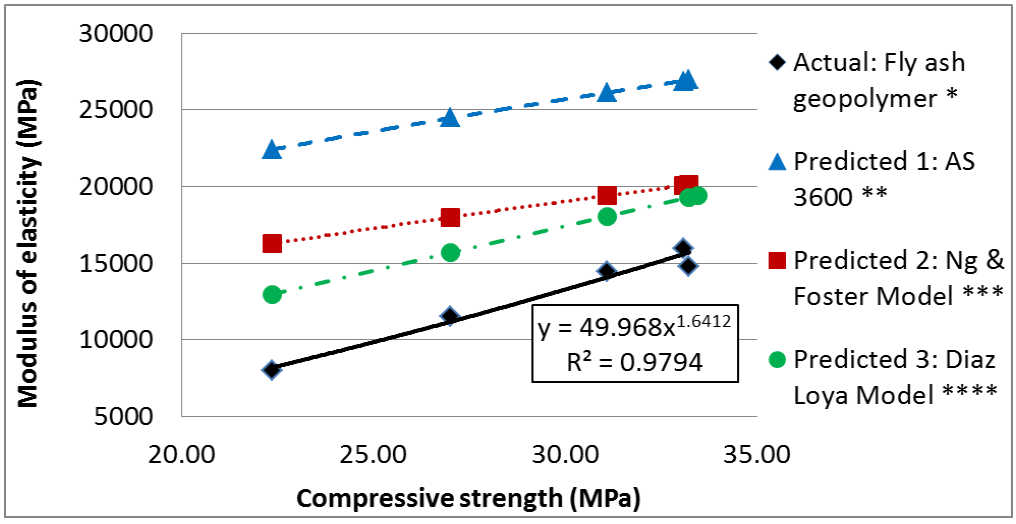

Note: * Actual, based on laboratory results, Australian Standard (AS 1012.17, 1997)
** Predicted 1, Australian Standard, Article 3.1.2(a) (AS 3600, 2009)
*** Predicted 2, model by Ng & Foster (Concrete Institute Australia, 2011)
**** Predicted 3, model proposed by Diaz-Loya (Diaz-Loya et al., 2011)

Figure 5.15 Correlation between modulus of elasticity and compressive strength of fly ash geopolymer concrete in time

where 'E_c' is the static modulus of elasticity and fc' is the compressive strength. It should be noted that this is based on a small sample size of data. The coefficient of determination of the correlation between modulus of elasticity and compressive strength was 98.13% which indicates that the model fits the data well. The equation suggests a similar trend to those developed by other authors (Diaz-Loya et al., 2011). However, although the trend is similar to that of OPC concrete, the model for fly ash geopolymer concrete predicts a lower modulus of elasticity compared to that of traditional OPC concrete (as found by other researchers, (Diaz-Loya et al., 2011, Fernandez-Jimenez et al., 2006, Hardjito & Rangan, 2005, Sofi et al., 2007).

Based on this finding, it can concluded that the use of the existing Australian standard (AS 3600, 2009) should not be applied to determine the modulus of elasticity for fly ash geopolymer concrete.

Correlation between compressive strength and flexural tensile strength

Table 5.12 presents a comparison of the flexural strength of fly ash geopolymer concrete based on AS 3600 and the models proposed by others (Diaz-Loya et al., 2011, Neupane et al., 2014, AS 3600, 2009).

Table 5.12 Comparison of flexural tensile strength of fly ash geopolymer concrete to the existing standards

Age of concrete (days)	Compressive strength f'c (MPa)	Actual: Measured flexural tensile strength (1) $f_{ct.f}$ (MPa)	Predicted 1 Mean values flexural tensile strength from AS 3600 (2) $f_{ct} = 1.4\ (0.6)\sqrt{f'_c}$ (MPa)	Predicted 2 Neupane model (3) $f_{ct.f} = 0.0421\ f'^{1.2358}_c$ (MPa)	Predicted 3 Diaz Loya model (4) $f_{ct} = 0.69\ \sqrt{f'_c}$ (MPa)
28	22.37	4.73	3.97	1.96	3.26
56	25.13	5.33	4.21	2.26	3.46
90	27.01	5.78	4.37	2.47	3.59
180	31.09	6.98	4.68	2.94	3.85
360	33.23	7.96	4.84	3.20	3.98
540	33.47	8.53	4.86	3.22	3.99

Note : (1) Based on laboratory results, (AS 1012.11, 2000)
(2) Australian Standard, Article 3.1.1.3 (AS 3600, 2009)
(3) Model proposed by Neupane (Neupane et al., 2014)
(4) Model proposed by Diaz Loya (Diaz-Loya et al., 2011)

The development of the flexural tensile strength of fly ash geopolymer concrete is predicted based on the measured compressive strength at 28 days. The long term flexural tensile strength can be predicted using the model proposed by AS 3600, Diaz Loya and Neupane models (AS 3600, 2009, Neupane et al., 2014, Diaz-Loya et al., 2011), **Figure 5.16**. It was found that the long term performance of the actual measured flexural tensile strength is higher than that predicted by all models. This would indicate that the fly ash geopolymer concrete has superior flexural tensile strength compared to OPC concrete, on which the predictions are based. This finding is in agreement with other authors who found that fly ash geopolymer concrete exhibits a higher flexural tensile strength than OPC concrete (Diaz-Loya et al., 2011, Fernandez-Jimenez et al., 2006).

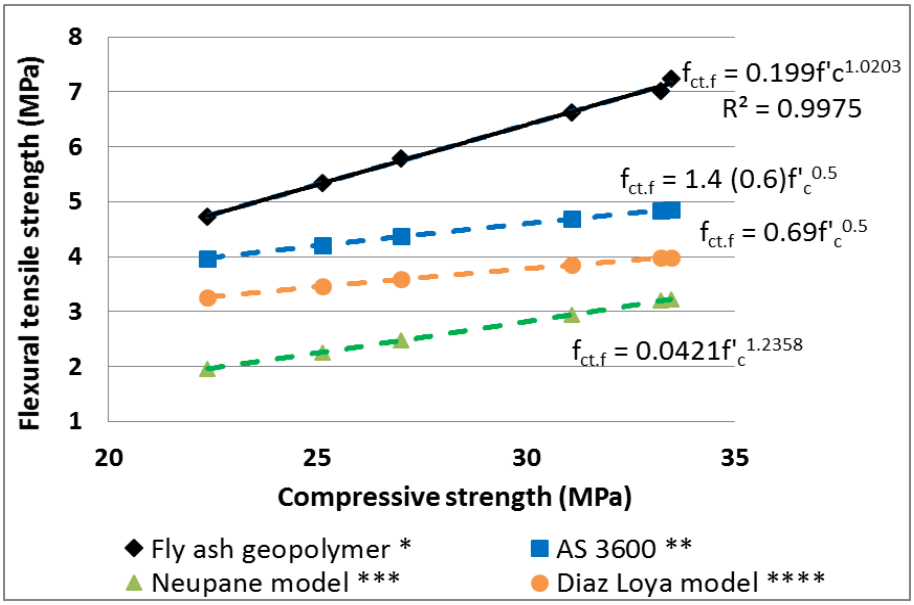

Note : * Actual, based on laboratory results, (AS 1012.11, 2000)
** Predicted 1, Australian Standard, Article 3.1.1.3 (AS 3600, 2009)
*** Predicted 2, model proposed by Neupane (Neupane et al., 2014)
**** Predicted 3, model proposed by Diaz Loya (Diaz-Loya et al., 2011)

Figure 5.16 Correlation between flexural tensile strength and compressive strength of fly ash geopolymer concrete in time

A general regression model for fly ash geopolymer concrete based on the correlation between flexural tensile strength and compressive strength (**Figure 5.16**) can be made as follows:

$$f_{ct.f} = 0.199(fc')^{1.0203} \qquad (5.5)$$

where '$f_{ct.f}$' is the flexural tensile strength and fc' is the compressive strength. The regression model shows that the model fitted the data with the coefficient of determination of 99.75%. Again it should be noted that the model is based on a limited number of data.

Correlation between compressive strength and uniaxial tensile strength

A comparison of the uniaxial tensile strength of fly ash geopolymer concrete against those predicted by AS 3600 and other models (AS 3600, 2009, Neupane et al., 2014, Raphael, 1984, Oluokun et al., 1991) is presented in **Table 5.13.** A scatter plot of the uniaxial tensile strength versus the compressive strength and a regression model representing the relationship between the two variables is shown in **Figure 5.17**.

Table 5.13 Comparison of uniaxial tensile strength of fly ash geopolymer concrete to the existing standards

Age of concrete (days)	Compres-sive strength f'c (MPa)	Actual Measured uniaxial tensile from AS 3600 (1) $f_{ct} = 0.9\sqrt{f'_{ct.sp}}$ (MPa)	Predicted 1 Mean values uniaxial tensile AS 3600 (2) $f_{ct} = 1.4(0.36)\sqrt{f'c}$ (MPa)	Predict 2 Raphael model (3) $f_{ct.f} = (0.9)\ 0.3\ f'^{2/3}_c$ (MPa)	Predict 3 Oluokun model (4) $f_{ct} = (0.9)\ 0.2\ f'^{0.7}_c$ (MPa)	Predict 4 Neupane model (5) $f_{ct} = 0.2605\ f'^{0.7129}_c$ (MPa)
28	22.37	1.91	2.38	2.14	1.59	2.39
56	25.13	2.19	2.53	2.32	1.72	2.59
90	27.01	2.52	2.62	2.43	1.81	2.73
180	31.09	3.03	2.81	2.67	2.00	3.02
360	33.23	3.44	2.91	2.79	2.09	3.17
540	33.47	3.72	2.92	2.80	2.10	3.18

Note: (1) Based on laboratory results, (AS 1012.10, 2000)
(2) Australian Standard, Article 3.1.1.3 (AS 3600, 2009)
(3) Model proposed by Raphael (Raphael, 1984)
(4) Model proposed by Oluokun (Oluokun et al., 1991)
(5) Model proposed by Neupane (Neupane et al., 2014)

The measured compressive strength has been used to predict the long term performance of uniaxial tensile strength based on AS 3600, Raphael, Oluokun

and Neupane models (AS 3600, 2009, Raphael, 1984, Oluokun et al., 1991, Neupane et al., 2014). Similar to the flexural tensile strength, it was found that the long term performance of the actual measured uniaxial tensile strength of fly ash geopolymer concrete is higher than the characteristic uniaxial tensile strength (predicted 1) calculated using the Australian Standard (AS 3600, 2009). The results also show that the actual measured uniaxial tensile strength is slightly higher than that predicted by AS 3600 and the model proposed by Oluokun (an improve model based on the Raphael model) at 28 days, **Figure 5.17**. However, the difference between the actual measured uniaxial tensile strength against AS 3600 and the Oluokun models becomes increasingly larger with time. This result confirms the previous findings on the flexural tensile strength. It also corroborates the finding that the fly ash geopolymer concrete has a higher tensile strength compared to OPC concrete (Neupane et al., 2014, Bernal et al., 2012).

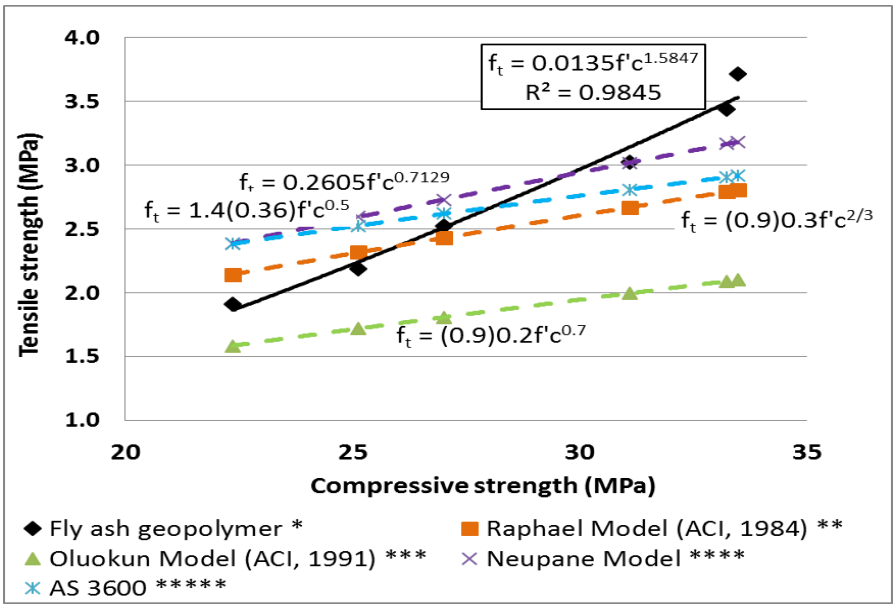

Note : * Actual, based on laboratory results, (AS 1012.10, 2000)
** Predicted 2, model proposed by Raphael (Raphael, 1984)
*** Predicted 3, model proposed by Oluokun (Oluokun et al., 1991)
**** Predicted 4, model proposed by Neupane (Neupane et al., 2014)
***** Predicted 1, Australian Standard, Article 3.1.1.3 (AS 3600, 2009)

Figure 5.17 Correlation between uniaxial tensile strength and compressive strength of fly ash geopolymer concrete in time

The results also indicated that the fly ash geopolymer concrete has slow uniaxial tensile strength development compared to the model proposed by Neupane

(Neupane et al., 2014) in the short term. However, over the long term the fly ash geopolymer concrete exhibits a higher strength compared to the Neupane model. This is attributed to the high silicate content of fly ash precursor in the fly ash geopolymer concrete which is proposed as the cause of the slow geopolymer reaction time (Silva et al., 2007, Sagoe-Crentsil & Weng, 2007) as discussed in **Chapter 4**.

A model, representing the correlation between uniaxial tensile strength and compressive strength, **Figure 5.17,** based on the regression analysis can be made as follows:

$$f_t = 0.0135(fc')^{1.5847} \qquad (5.6)$$

where 'f_t' was the uniaxial tensile strength and fc' was the compressive strength. The coefficient of determination is 98.45% which indicates that the model fits the data well. It also should be noted that this is based on a small sample size of data.

Overall the compressive strength, modulus of elasticity and tensile strength demonstrated a significant increase with time. An increase in compressive strength is accompanied by an increase in modulus of elasticity and tensile strength which indicates that fly ash geopolymer concrete demonstrates a similar behaviour to OPC concrete. However, although fly ash geopolymer concrete demonstrates a lower compressive strength and modulus of elasticity, it has a superior tensile strength compared to OPC concrete. This would indicate that the use of the existing Australian standard (AS 3600, 2009) might not be directly applicable to calculate the modulus of elasticity. However, it might be applied to predict the tensile strength of fly ash geopolymer concrete.

5.8. Durability properties of fly ash geopolymer concrete

This section presents experimental results of the durability properties of fly ash geopolymer concretes. The mix design was based on the preliminary research data in **Chapter 4**.

5.8.1. Porosity and water absorption

The porosity test was carried out to identify the volume of voids and the possible presence of cracks in accordance with ASTM C642-97 (2003). While, the water absorption test was performed to determine the volume of water absorbed in accordance with AS 1012.21 (1999), the test also provides additional information regarding the connectivity of the pore network. The test results are shown in **Table 5.14**, **Figure 5.18** and **Figure 5.19** (calculations in **Appendix H** and **Appendix I**, respectively).

Table 5.14 Porosity and water absorption of fly ash geopolymer concrete

Time (days)	Porosity (%)	Water absorption (%)
28	14.44	7.75
56	14.39	7.33
90	14.35	7.22
180	14.29	6.89
360	14.04	6.82
540	13.97	6.84

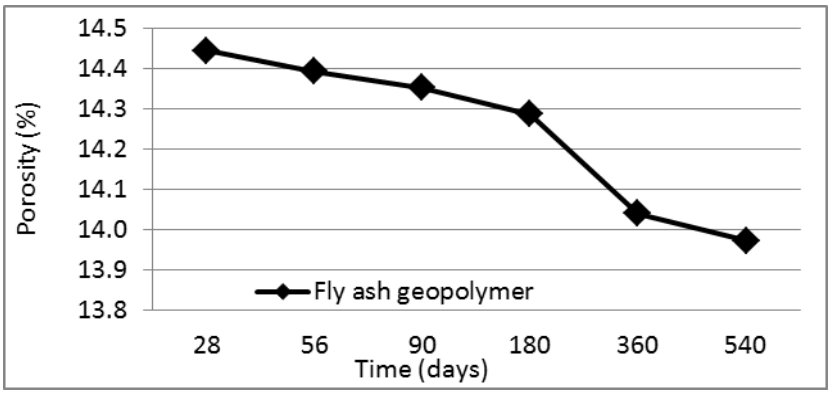

Figure 5.18 Porosity development of fly ash geopolymer concrete

The porosity of concrete is associated with the volume of voids, with a high density suggesting lower porosity and a high porosity indicating a high volume of voids.

The results show that the average porosity measurement of the fly ash geopolymer concrete is 14.24%. The long term data demonstrates a significant decrease in porosity with time (**Figure 5.18**). It is observed that the initial porosity at 28 days was 14.44% decreasing to 14.04% at 360 days and 13.97% at 540 days, with an overall decrease of 3.25% observed from 28 to 540 days.

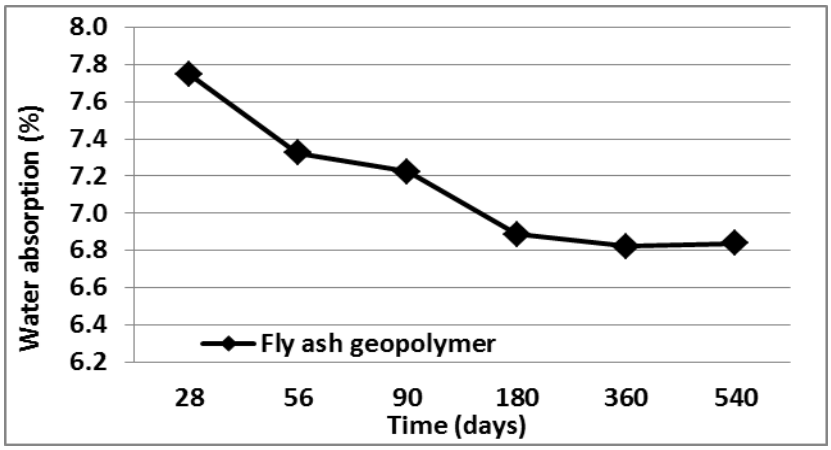

Figure 5.19 Water absorption development of fly ash geopolymer concrete

The change over time of the water absorption demonstrates a similar trend to the development of porosity (**Figure 5.19**). The results show that the average water absorption measurement is 7.14% with an initial absorption of 7.75% observed at 28 days. The long term data displays a significant reduction to 6.82% at 360 days and 6.84% at 540 days with an overall reduction of 11.74% observed from 28 to 540 days.

According to Technical Report No.54 (2000) published by the Concrete Society, the quality of concrete can be determined based on its porosity value (**Table 3.8 Section 3.6.1**). Thus, based on the porosity measurement, the initial and long term porosity of fly ash geopolymer concrete can be classified as “medium porosity” with a concrete quality of “average quality”.

The high porosity and water absorption is significantly influenced by the fineness and the shape of the fly ash precursors. The high porosity is attributed to the low fineness of fly ash precursors (64.78% passing sieve 45 μm, **Appendix A**) compared to OPC concrete (fineness of OPC approximately 75% - 80%) as suggested by Neville (2011). The spherical shape of fly ash precursors with a big diameter of 27.99 μm (**Appendix A**) causes an uneven material distribution reducing the ability to fill the gap or the crack between the aggregates, thus increasing the connectivity of the pore network between the geopolymer pastes and the aggregates. Sinsiri et al. (2010) also found that the porosity of fly ash based geopolymer concrete is affected by the fineness and the shape of fly ash precursors, with a higher fineness of material filling the crack between the aggregates and leading to a lower porosity. This could indicate a high interconnectivity of capillary pores within the specimen as in agreement with Sagoe-Crentsil et al. (2010).

Furthermore, the high porosity and water absorption of fly ash geopolymer concrete can also be attributed to the high Na_2O dosage (Na_2O = 15%) in the solution. According to Xu & Deventer (2000) and Duxson et al. (2007a), a combination of a high Na_2O dosage and the additional soluble silicates results in the reaction occurring at a higher rate. A combination between high Na_2O dosage and the Na_2O from the sodium silicates solution increases the reaction rate of fly ash geopolymer concrete. It is hypothesised that this effect causes a gap between the geopolymer pastes and the aggregate and leads to a high porosity and the connectivity of the pore network in short term periods.

The porosity and water absorption demonstrated a tendency to reduce over time. This is attributed to the development of the geopolymeric gel during the curing process. These gels fill the interface between the geopolymer pastes and the aggregates, and reduce the volume of the pore structures. However, although the porosity shows a marginal reduction, the mechanical properties (i.e. compressive strength, modulus of elasticity and tensile strength (see previous discussion on **Section 5.7**) demonstrate a significant increase with time. It can be inferred that the increase is a continuing effect of the geopolymeric reaction. This ongoing reaction is attributed to the high silicate content in the fly ash precursor which affects the Si/Al ratio and tends to delay the geopolymeric reaction rate as suggested by Silva et al. (2007). This finding is also in an agreement with Olivia

et al. (2008). The authors found that the ability to fill the pore structures of geopolymer concrete mainly depends on the curing process and the increase of strength is only the continuing effect of the geopolymeric reaction without any hydration.

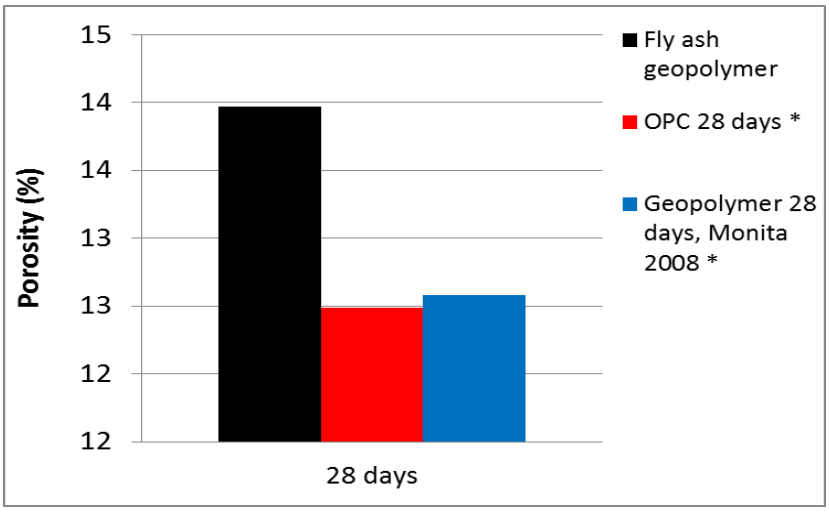

Note: * Geopolymer with w/b = 0.25, NaOH = 14M (Olivia et al., 2008)

Figure 5.20 Comparison of porosity

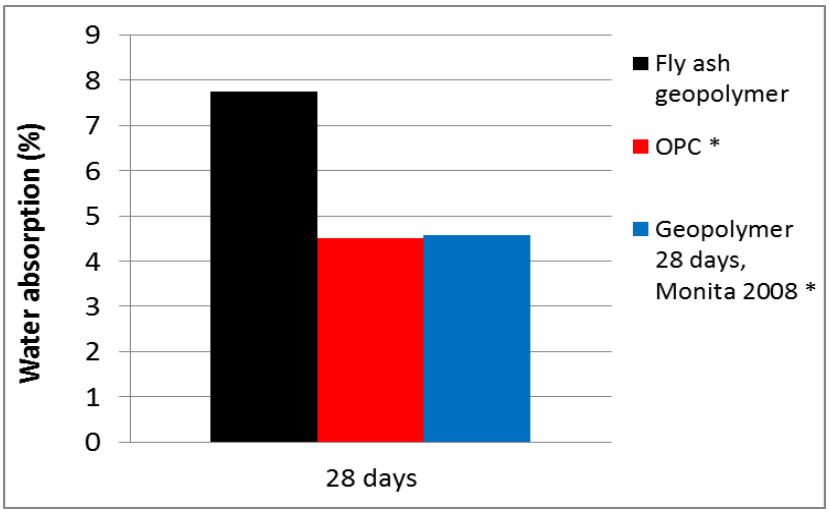

Note: * Geopolymer with w/b = 0.25, NaOH = 14M (Olivia et al., 2008)

Figure 5.21 Comparison of water absorption

Overall, the fly ash geopolymer concrete demonstrates a higher porosity and water absorption compared to OPC concrete and other researcher (Olivia et al.,

2008) as shown in **Figure 5.20** and **Figure 5.21**. This indicates that the fly ash geopolymer concrete shows a low durability performance with respect to aggressive agents such as carbon dioxide and chloride. However, the decrease of porosity and water absorption with time indicates that the behaviour in the long-term is improving.

5.8.2. Ultrasonic Pulse Velocity

The ultrasonic sonic pulse velocity (UPV) test is a technique to determine the bulk property of concrete. This test also identifies the possibility of cavities, cracks or defects within the concrete. The pulse velocity depends on the density and the elastic properties which are related to the quality and strength of the concrete. The velocity test results are shown in **Table 5.15** and **Figure 5.22** (calculation in **Appendix J)**.

Table 5.15 Velocity test of fly ash geopolymer concrete

Time (days)	Velocity (km/s)
28	2.81
56	2.90
90	3.06
180	3.10
360	3.38
540	3.50

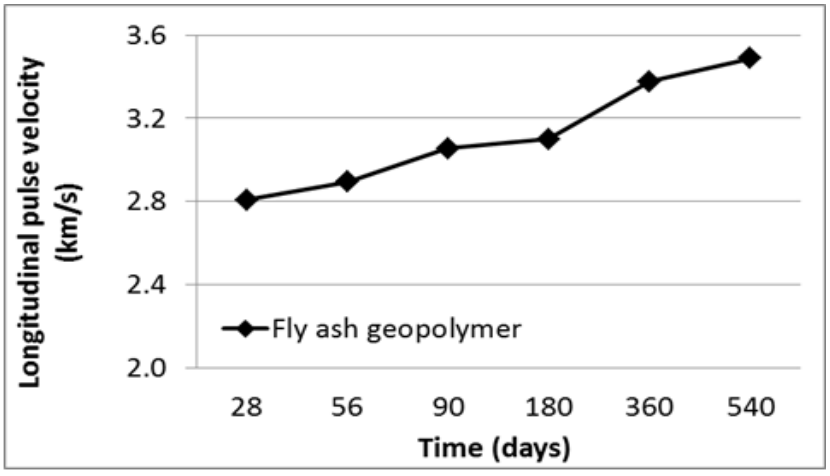

Figure 5.22 Velocity test of fly ash geopolymer concrete

The velocity exhibits a significant increase with concrete age. The velocity is seen to increase from 2.81 km/s at 28 days to 3.49 km/s at 540 days with an overall increase of 24.56%. This indicates that the bulk properties and the quality of the concrete are getting better over time. This finding corroborates the previous findings on the reduction of porosity and water absorption.

According to the International Atomic Energy Agency (IAEA, 2002), the quality of concrete can be determined based on the velocity measurement. Fly ash geopolymer concrete shows an initial velocity of 2.81 km/s at 28 days which is classified as “poor” quality of concrete as shown in **Table 3.9** (**Section 3.6.4 Chapter 3**). However, an increase of velocity to 3.50 km/s at 540 days raises the classification of fly ash geopolymer concrete to “good”.

Compared to OPC concrete, fly ash geopolymer concrete demonstrates a lower performance in terms of velocity measurement. Although the velocity measurement shows the highest value at 540 days with the velocity of 3.50 km/s, the velocity of fly ash geopolymer concrete is still slightly lower than the standard pulse velocity of OPC concrete which is in the range 3.5 – 4.5 km/s as suggested in NISTIR 6975 report (Garbacz & Garboczi, April 2003).

5.8.3. Water permeability

The deterioration of concrete is generally caused by the penetration of aggressive agents, such as chloride, sulphate and CO_2, into the concrete. These agents will first affect the surface layer of concrete by forming a micro-environment of a corrosive substance and then penetrate into the interior of concrete. Therefore, it is important to consider the quality of the concrete surface in resisting the transportation of these agents into the concrete.

The water permeability test was carried out to determine the volume of water that penetrates into the concrete, as well as the surface permeability which is related to the durability of concrete. The water permeability index was measured by plotting the flow of water recorded against the square root of time for the 15 minutes test duration. The data points between 5 and 15 minutes were used for further analysis as the points before 5 minutes were generally found to be unstable. The selected data points were fitted by a line and the slope was referred as the water permeability index of the specimens (Henderson et al., 2004, Basheer et al., 2007).

The water permeability test results, represented by the water permeability index, are shown in **Table 5.16** and **Figure 5.23**. The detailed calculation is presented in **Appendix K**.

Table 5.16 Water permeability of fly ash geopolymer concrete

Time (days)	Water permeability index ($m^3x10^{-7}/\sqrt{min}$)	Water permeability ($m/s\ x10^{-11}$)
28	12.043	2.907
56	11.801	2.859
90	11.668	2.810
180	11.609	2.757
360	11.642	2.770
540	11.588	2.700

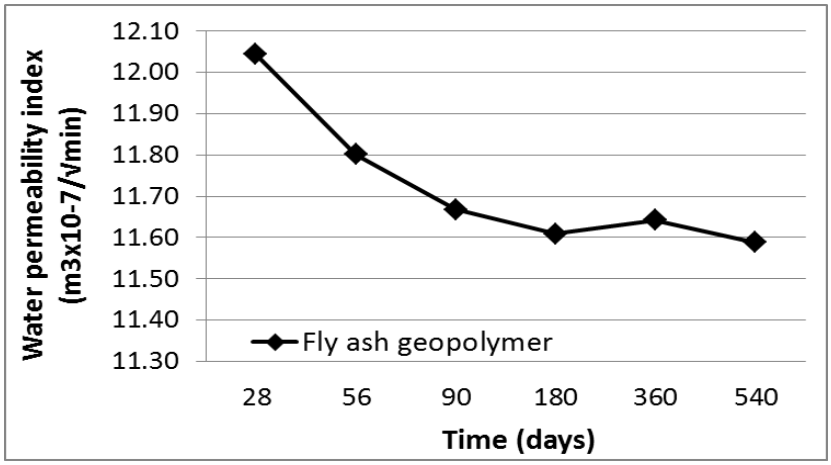

Figure 5.23 Water permeability of fly ash geopolymer concrete

The water permeability of concrete is associated with the ability of the surface layer to resist the penetration of aggressive agents. High water permeability index indicates a low quality of the surface layer which can lead to a low durability for the concrete. It also indicates the ease with which water penetrates into the concrete.

Table 5.16 and **Figure 6.23** show the variation of the water permeability with age of concrete. The initial water permeability index (WPI) demonstrates a high value of 12.043 $m^3x10^{-7}/\sqrt{min}$ at 28 days. However, it shows a significant decrease to 11.642 $m^3x10^{-7}/\sqrt{min}$ at 360 days and 11.588 $m^3x10^{-7}/\sqrt{min}$ at 540 days with an

overall decrease of 3.78%. This indicates that the quality of the surface layer is getting better with time. This finding also corroborates the previous findings on the reduction of porosity and water absorption.

The high water permeability value is attributed to a combination of the low quality surface as shown in **Figure 5.24** and the high porosity of the concrete reported previously. The surface demonstrates a less dense structure, also showing cracking over the whole surface. The low quality of the surface is attributed to the fast initial setting reaction which is caused by the high Na_2O dosage (Na_2O = 15%). According to Ghosh & Ghosh (2012), increasing the Na_2O dosage in the fly ash based geopolymer concrete will increase the initial setting time.

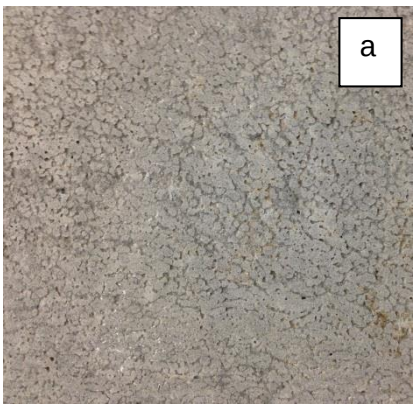

Figure 5.24 External surface of fly ash geopolymer concrete

5.8.4. Correlation between the mechanical to permeation properties

A regression analysis is performed to investigate the relationships between the mechanical properties and the permeation properties. The correlation between the UPV, porosity and water absorption results and the compressive strength, modulus of elasticity, flexural and uniaxial tensile strength results are presented in **Figure 5.25**, **Figure 5.26**, **Figure 5.27** and **Figure 5.28**, respectively.

Figure 5.25 shows that the correlation of the compressive strength of fly ash geopolymer concrete follows a positive linear relationship with UPV. The increase in UPV indicates that the bulk property and the quality of fly ash geopolymer concrete increases with the strength. **Figure 5.25** also demonstrates that the porosity and the water absorption slightly reduce along with the increase of compressive strength. The decrease of porosity and water absorption indicates

that the total cavities, cracks, voids or defects within the concrete specimens are reducing.

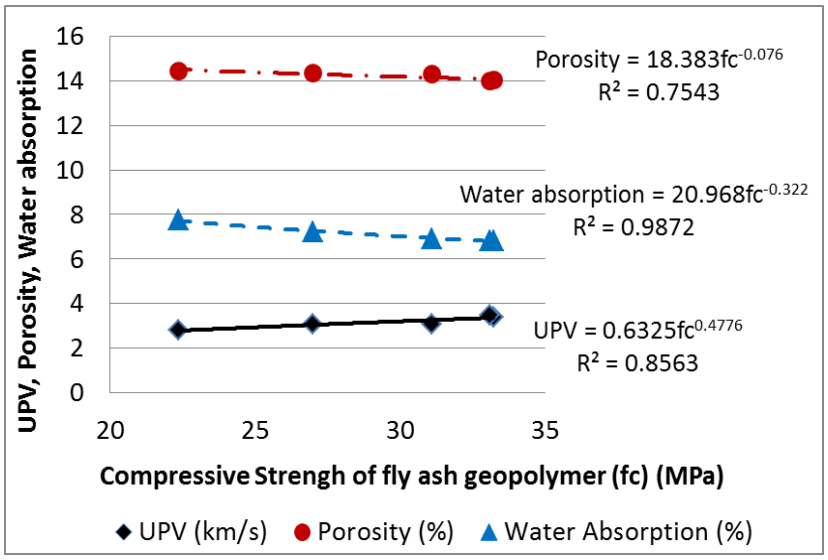

Figure 5.25 Correlation between compressive strength and UPV, porosity and water absorption of fly ash geopolymer concrete

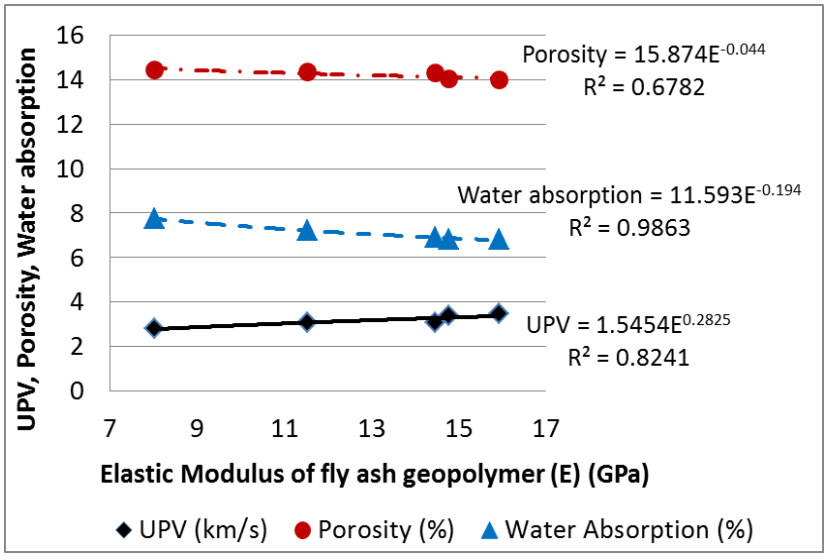

Figure 5.26 Correlation between elastic modulus and UPV, porosity and water absorption of fly ash geopolymer concrete

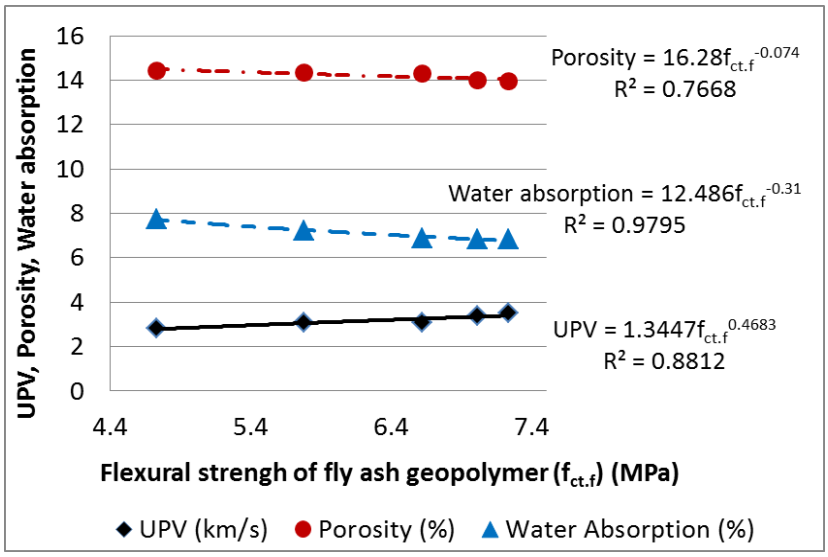

Figure 5.27 Correlation between flexural tensile strength and UPV, porosity and water absorption of fly ash geopolymer concrete

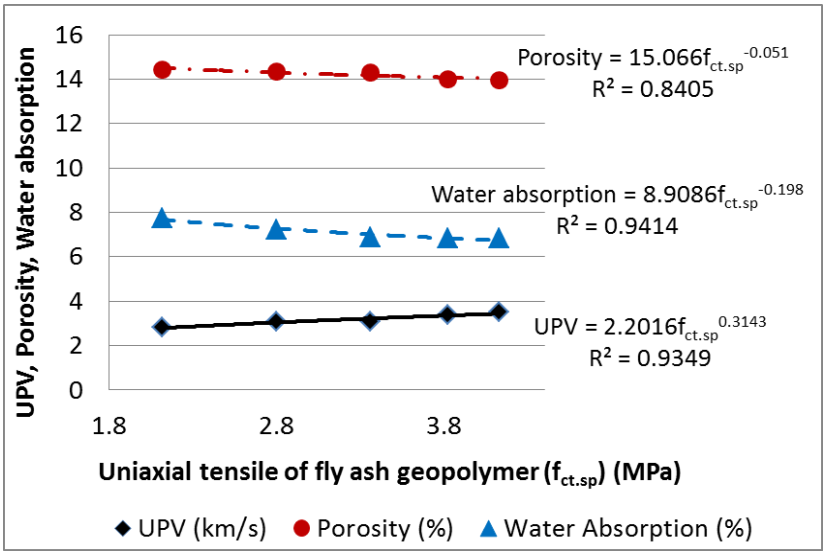

Figure 5.28 Correlation between uniaxial tensile strength and UPV, porosity and water absorption of fly ash geopolymer concrete

The correlation between modulus of elasticity to UPV, porosity and water absorption also demonstrates a similar trend with the compressive strength as shown in **Figure 5.26**. This demonstrates that the stiffness of fly ash geopolymer concrete which is indicated by modulus of elasticity value also improves along with the improvement of concrete quality. Similar findings are also found on the tensile strength which is represented by the flexural tensile strength (**Figure 5.27**)

and uniaxial tensile strength (**Figure 5.28**). These findings corroborate the previous finding on the development of mechanical properties. The development of the mechanical properties of fly ash geopolymer concrete is mirrored by the increase of the bulk properties and quality.

5.8.5. Resistivity

The electrical resistivity of concrete is an important factor concerning the rate of the corrosion of the reinforcing steel once the process has been initiated. According to Morris et al. (2002), the electrical resistivity of concrete is an effective parameter to evaluate the risk of reinforcing steel corrosion particularly when corrosion is induced by chloride attack. A concrete material with high resistivity will show a lower corrosion rate compare to a concrete with a low resistivity. The resistivity test results are shown in **Table 5.17**.

Table 5.17 shows variation of resistivity with age of concrete. It should be noted that the maximum value readable by the test equipment was 99 kΩcm. Thus the actual resistivity of the concrete may be higher, though this value is high enough to predict the corrosion risk in accordance with International Atomic Energy Agency (IAEA, 2002).

Table 5.17 Resistivity of fly ash geopolymer concrete

Time (days)	Resistivity (kΩcm)
28	8.0
56	20.8
90	38.9
180	53.6
360	99.0
540	99.0

The initial resistivity of fly ash geopolymer concrete demonstrates a low resistivity value of 8.0 kΩcm which is classified as a “high” corrosion risk (**Table 3.10 Chapter 3**) in accordance with IAEA (2002). This indicates the potential to have a high corrosion rate if corrosion is initiated, which would adversely affect the durability of geopolymer concretes containing reinforcing steel. However, the

resistivity of the fly ash geopolymer concrete demonstrates a significant increase over time. The classification of corrosion risk reduces from “low” to “negligible” at 56 days.

The low resistivity of fly ash geopolymer concrete is also affected by the high activator modulus (15% Na_2O). A high activator modulus increases NaOH concentration in the activator which leads to the increasing in ionic concentration in the pore fluid of fly ash geopolymer specimens. As the fly ash geopolymer concrete (G15-1.00) was activated by high alkaline solution, it increases the ionic concentration and leads to the high conductivity which causes the low resistivity.

The low resistivity is also attributable to the high porosity (**Figure 5.18**) and water permeability (**Figure 5.23**). High porosity leads to a high ionic concentration within the pore structure and allows the electrical current to pass through the specimen easily. McCarter et al. (2000) also observed that the conductivity of saturated concrete is affected by the extent of connected capillary porosity in the pore structure and the ionic concentration within the pore structure.

5.8.6. Chloride diffusion

Chloride diffusion data for the fly ash geopolymer concrete was obtained from a chloride ponding test. Experimental details are explained on the previous section (**Section 3.6.6 Chapter 3**) and the results are shown in **Table 5.18**.

The chloride diffusion coefficient (D_a) and the surface concentration (C_s) are estimated by plotting the chloride profiles and determining the best fitted curve using Fick’s 2nd Law as suggested by Crank (1975). The best-fit curve obtained using Microsoft Excel (Solver) is shown in **Figure 5.29**.

Table 5.18 Chloride content by weight of sample and mass of cement (%)

Specimen	Depth (mm)	Chloride (Cl^-) content	
		% by mass sample	% by mass cement
Fly ash geopolymer	0-20	0.03716	0.26543
	20-40	0.03348	0.23914
	40-100	0.02074	0.14814

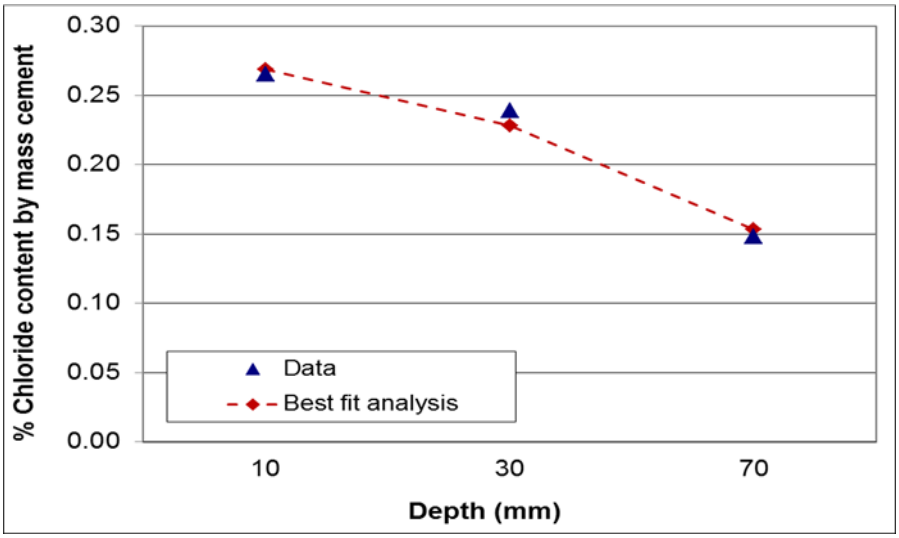

Figure 5.29 Best fitted curve to calculate chloride diffusion using Fick's 2nd law of diffusion, fly ash geopolymer concrete

The chloride diffusion coefficients are shown in **Table 5.19**. The chloride diffusion coefficient is 7.96×10^{-10} m^2/s which demonstrates a higher value compared to OPC concrete. The high value is attributed to the high porosity and high permeability as shown in **Table 5.14** and **Table 5.16**. The high porosity provides a route for the chloride ions to penetrate the concrete through the interconnected pores.

Table 5.19 Chloride diffusion and surface chloride content

Specimen	Chloride diffusion coefficient (D_a) (m^2/s)	Surface chloride content (C_s) (%)
Fly ash geopolymer, G15-1.00	7.96×10^{-10}	0.29
OPC *	11.80×10^{-11}	0.16

Note: * Adam (2009)

The high chloride diffusion of the concrete specimens is affected by the ability of the hydration products to retain the chloride ingress. These retained chloride ions can be referred to as chloride binding (Luping & Nilsson, 1993). In OPC concrete, the chloride diffusion is significantly affected by the C-S-H gel (the result of the hydration). A part of the chloride ion ingress is retained and bound by the C-S-H

gel. The free chloride ions that are not bound by C-S-H gel are able to travel through the pore solution and induce corrosion on the reinforcing bars.

Other authors have discussed the influence of NaOH and CaO. (Chindaprasirt & Chalee, 2014) found that chloride ions are bound by the NaOH and CaO. A higher NaOH concentration bound more chloride ions while a high content of CaO reacted with silicate compounds to form a C-S-H gel (similar to the cement gel in OPC concrete). The NaOH concentration coupled with the CaO content to increase the chloride binding capacity of geopolymer and reduce the chloride diffusion coefficient.

However, the finding in the research reported here shows that fly ash geopolymer concrete exhibits a higher chloride rate of diffusion than that OPC concrete. This is attributed to the high porosity and high permeability value which is affected by the high Na_2O content as explained in the previous section.

Table 5.20 Comparison of chloride diffusion

Components	FA Geopolymer G15-1.00	Adam [1] G7.5-1.00	Adam [1] OPC
CaO (%)	0.18	3.47	64.27
SiO_2 (%)	70.30	49.45	19.90
Si/Al ratio	3.04	1.67	-
Na_2O (%)	15	7.5	-
Chloride diffusion (m/s)	$7.96x10^{-10}$	$3.10x10^{-11}$	$11.8x10^{-11}$

Note: [1] Adam (2009)

Table 5.20 displays a comparison of the chloride diffusion coefficient using the same mix design proportion, but with a lower Si/Al ratio, lower Na_2O dosage and higher CaO content. It shows the effect of CaO content and Na_2O dosage on the chloride resistance is in agreement with other researchers (Adam, 2009, Chindaprasirt & Chalee, 2014).

5.8.7. Depth of carbonation

The results of the accelerated carbonation (20% $\pm$ 1% CO_2 at $20^{O}C \pm 1^{O}C$ and 70% $\pm$ 1% RH) are shown in **Figure 5.30** and **Figure 5.31.** The change of colour between the carbonated and non-carbonated region as displayed by the

phenolphthalein indicator is shown in **Figure 5.30**. The overall colour of the non-carbonated region is bright pink (**Figure 5.30**). From this it can be inferred that the concrete demonstrates a low pH (as in pH 12) in the pore solution.

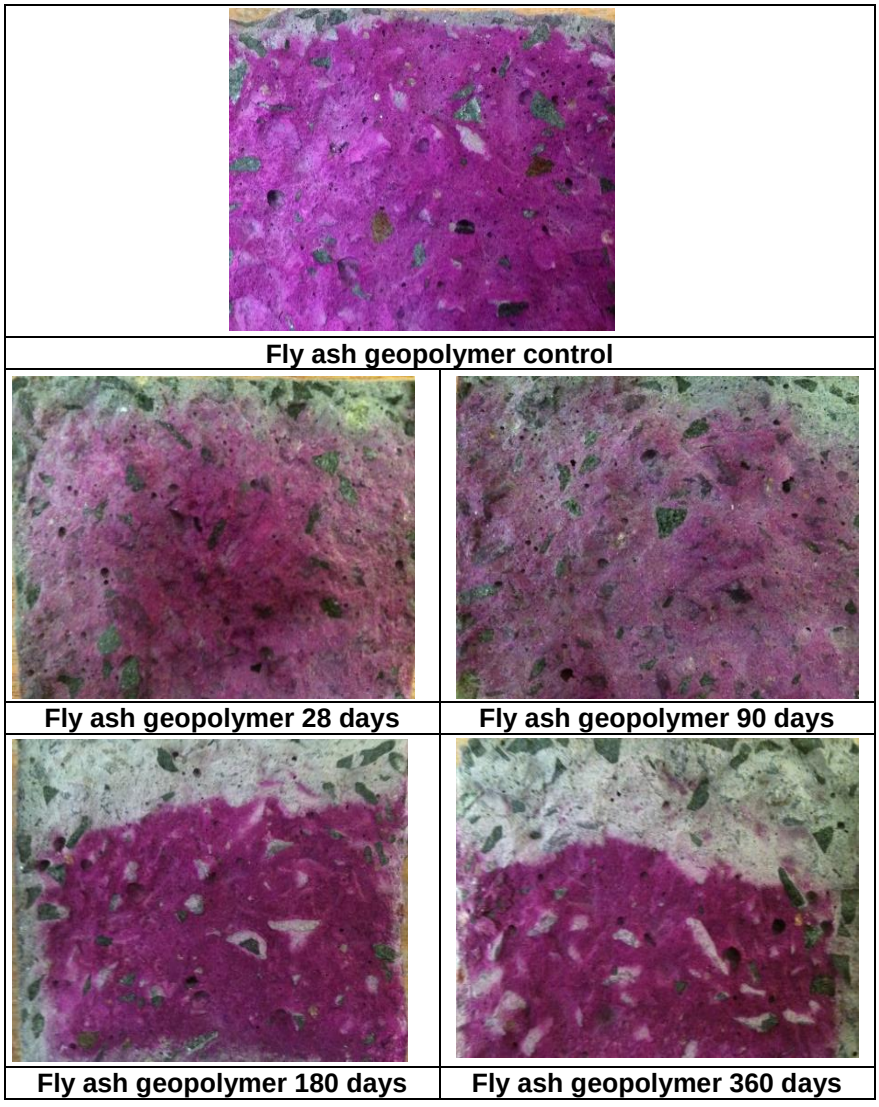

Figure 5.30 Depth of carbonation of fly ash geopolymer concrete using phenolphthalein indicator

Following carbonation there is a clear border between the coloured and colourless area in the geopolymer specimens. The geopolymer specimens displayed a colourless region in the outer layer with a graduation in colour to the inner part of the specimen. It is the NaOH that can be carbonated during the

carbonation process reacting with CO_2 forming Na_2CO_3 and releasing water. It can be presumed that the carbonation of NaOH is a full carbonation which is similar to that of $Ca(OH)_2$ and C-S-H in the OPC.

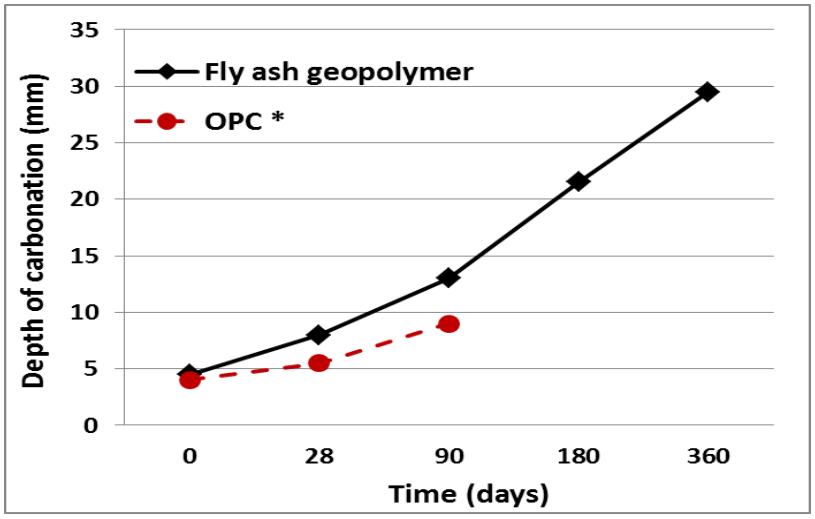

Note: * Adam (2009)

Figure 5.31 Depth of carbonation of fly ash geopolymer concrete

Fly ash geopolymer concrete demonstrates a higher depth of carbonation compared to OPC concrete. This can be attributed to the high porosity (**Figure 5.18**) and high permeability (**Figure 5.23**) (found in the previous section). These lead to the high diffusivity of CO_2 into the concrete. According to Neville (2011), the fundamental factor controlling the carbonation is the diffusivity process which is related to the function of the pore system of the specimen.

The carbonation rate coefficient (C) (**Table 6.11**) fitted to the square root of time by a function as shown in **Figure 5.23**. It was found that the relationship in **Equation 2.26** gives a good correlation coefficient (R) with coefficient of determination of 91.3% suggesting that the model fits the data well.

Table 5.21 Depth of carbonation (X) and carbonation rate coefficient (C)

Carbonation	Age (days)				
	0	28	90	180	360
Depth of carbonation (X) (mm)	4.5	8.0	13.0	21.5	29.5
Carbonation rate coefficient (C) (mm/days$^{1/2}$)	0.00	0.66	0.90	1.27	1.32

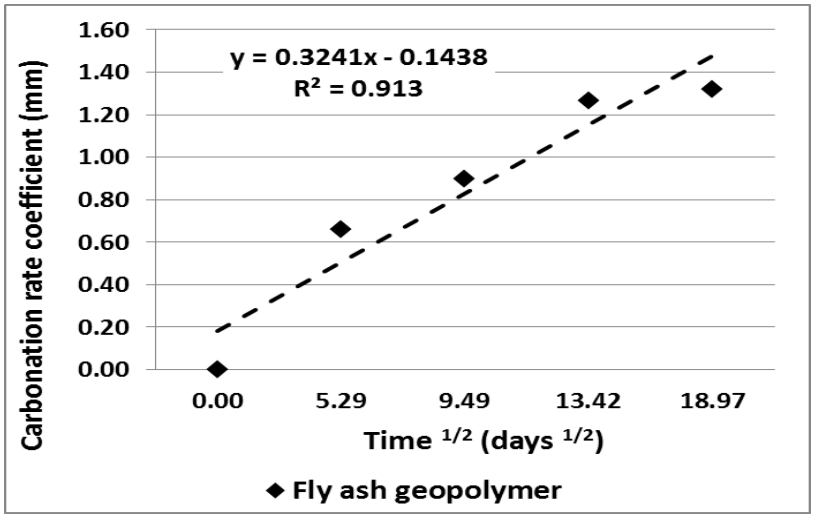

Figure 5.32 Depth of carbonation of fly ash geopolymer concrete versus square root of time

The average carbonation rate coefficient (C) was 1.01 mm/days$^{1/2}$. Comparing this to OPC concrete with C = 0.41 mm/days$^{1/2}$ (Adam, 2009) demonstrates a higher value of carbonation rate than for OPC. This is attributable to the high content of $Ca(OH)_2$ in OPC concrete. As the quantity of $Ca(OH)_2$ is high, more CO_2 is required to convert all the $Ca(OH)_2$ to $CaCO_3$ (**Equation 2.19)**. After all the $Ca(OH)_2$ is converted to $CaCO_3$, the carbonation of C-S-H takes place. In contrast to OPC concrete, the high carbonation rate of fly ash geopolymer concrete might be affected by (1) the low content of CaO to react with CO_2 (**Table 3.1**) and (2) the high porosity (**Table 5.14**) and permeability value (**Table 5.16**). The low quantity of CaO results in there being less material available to react with the CO_2, hence leading to a faster carbonation process. In addition, the high porosity and water permeability value increase the rate of penetration of CO_2. This finding is in agreement with Bier in Neville (2011). The author found that the presence of fly ash results in a more rapid carbonation, attributed to the decrease of available $Ca(OH)_2$ to react with the CO_2.

5.9. Summary of chapter 5

The result of the investigation on the long term mechanical properties of fly ash geopolymer concrete can be summarized as follows:

1. The average density of fly ash geopolymer concrete is 2320 kg/m^3, lower than OPC concrete (characterised by a density of approximately 2400 kg/m^3), due to the low specific gravity of the raw materials. It also demonstrates an increase with time due to the on-going geopolymeric reaction.
2. The fly ash geopolymer concrete strength demonstrates an improvement in strength with age. This attributes to the slow formation of the geopolymeric network due to the high Si/Al ratio in the fly ash precursor.
3. The low strength of fly ash geopolymer concrete compared to OPC concrete is attributable to the low content of CaO in the fly ash precursor.
4. The modulus of elasticity of fly ash geopolymer demonstrates a lower strength compared to traditional OPC concrete over the long term.
5. The relationship between the compressive strength and modulus of elasticity of fly ash geopolymer concrete follows a positive linear relationship with time, similar to that shown by traditional OPC concrete.
6. The flexural tensile strength and uniaxial tensile strength of fly ash geopolymer concrete shows an increase with time. These findings are consistent with a slow geopolymeric reaction due to the high silicate content in the fly ash precursors.
7. For fly ash geopolymer concrete, the relationship between the flexural tensile strength and uniaxial tensile strength with compressive strength is similar to that for OPC concrete.
8. Fly ash geopolymer concrete has a lower modulus of elasticity, higher flexural tensile strength and uniaxial tensile strength compared to OPC concrete.
9. The use of the existing Australian Standard can be applied conservatively to determine flexural tensile strength and uniaxial tensile strength of fly ash geopolymer concrete. However, it might not be used to determine the

modulus of elasticity due to the low modulus of elasticity of fly ash geopolymer concrete compared to that of OPC concrete.

10. The improved performance of fly ash concrete with time suggests that the structural use of fly ash concrete is feasible.

In terms of durability properties, the result of the investigation of fly ash geopolymer concrete can be summarized as follows:

1. The porosity and water absorption of fly ash geopolymer concrete are higher than those of OPC. This attributable to the low fineness and spherical shape of the fly ash precursors. The high Na_2O dosage also affects the porosity of fly ash geopolymer concrete, becoming greater due to the rapid reaction during the mixing process.
2. The porosity and water absorption development shows a decrease over time due to the development of the geopolymeric gel during the curing process which fills the interface between the geopolymer pastes and the aggregates, thus reducing the volume of the pore structures.
3. Fly ash geopolymer concrete demonstrates an increase of UPV with time which indicates that the bulk properties and the quality are improving. Compared to OPC concrete, fly ash geopolymer concretes demonstrates a lesser increase in pulse velocity with age of concrete.
4. Fly ash geopolymer concrete exhibits a high value of water permeability due to the low quality surface (less dense and cracked). This is attributable to the fast initial setting reaction during the mixing process which is a result of the high Na_2O dosage (Na_2O = 15%).
5. The relationship between the mechanical properties (i.e. compressive strength, modulus of elasticity and tensile strength) with UPV follows a positive linear relationship with concrete age, analogous to that shown by traditional OPC concrete. An increase of mechanical properties is followed by an increase of UPV. The increase in mechanical properties of fly ash geopolymer concrete is associated with a decrease of porosity and water absorption. These findings confirm that the quality of fly ash geopolymer concrete is getting better with time.

6. Fly ash geopolymer concrete exhibits a low resistivity in the short term which indicates the potential to support a high corrosion rate if corrosion is initiated. However, the resistivity demonstrates a significant increase over time.
7. The low resistivity of fly ash geopolymer concrete affected by the high activator modulus (15% Na_2O) which leads to the increasing in ionic concentration in the pore fluid. It is also attributable to the high porosity and water permeability which leads to a high ion concentration within the pore structure.
8. Fly ash geopolymer concrete exhibits a high chloride diffusion due to the high porosity and high permeability value which is affected by the high Na_2O content and the fineness and shape of fly ash precursor.
9. Fly ash geopolymer concrete demonstrates a high depth of carbonation due to the high porosity and permeability.
10. The rate of carbonation of fly ash geopolymer concrete shows a higher value compared to that of OPC concrete due to the low CaO content in fly ash to react with the CO_2, and the high porosity and permeability value.

6. MECHANICAL AND DURABILITY PROPERTIES OF AAS CONCRETE

6.1. Overview

The previous investigation on the mortar strength of AAS mortar in **Chapter 4** has confirmed the possibility of producing concrete using 100% slag as cement replacement.

The previous investigation on the mortar strength of AAS specimens found that an activator modulus of 1.00 gives the optimum performance for strength development. The early compressive strength of AAS specimens is higher than that of OPC mortar but tends to reduce to become less than that of the OPC specimens. It was found that increasing the alkali modulus caused a reduction in the strength with time. Based on these findings, an AAS concrete with an Na_2O dosage of 5% and an M_s of 1.00 was selected for the long term tests.

This chapter presents the experimental investigation of the long term performance of the mechanical properties and durability of AAS concrete. The mechanical properties were examined at 28, 56, 90, 180, 360 and 540 days. The testing included assessment of the compressive strength, the modulus of elasticity, the modulus of rupture, the indirect tensile strength and the density. The durability properties of AAS concrete were also determined by assessing the porosity, water absorption, water permeability and ultrasonic pulse velocity tests, as well as resistivity, chloride diffusion and carbonation tests.

6.2. Materials

6.2.1. Slag

The same GGBS as used for the mortar tests was used to prepare the AAS concrete specimens. The properties of the GGBS are described in **Chapter 3 Section 3.2.2**.

6.2.2. Alkaline activators

The same alkaline activators of sodium silicate and sodium hydroxide as used in the AAS mortar were used for the AAS concrete specimens. A low alkaline solution of 10M NaOH concentration was used for AAS concrete (compared to the fly ash geopolymer concrete). The properties of alkaline activators are described in **Chapter 3 Section 3.2.3**.

6.2.3. Aggregates

The same fine and coarse aggregates as used for the fly ash geopolymer concrete were used to prepare the AAS concrete. The properties of the fine and coarse aggregates are described in **Chapter 5 Section 5.2.4**. The typical grading of the combined aggregate is shown in **Table 3.6 Chapter 3 Section 3.2.5**.

6.3. Mix proportions

The same mix design (with the exception of the Na_2O dosage) as used for fly ash geopolymer concrete was used to prepare the AAS concrete. The detail of the mix design is described in **Chapter 5 Section 5.3**. However, an Na_2O dosage of 5% with an M_s of 1.00 for AAS concrete was selected to achieve the target strength (based on the results in **Chapter 4).**

The AAS concrete specimens were prepared using a water binder ratio (w/b) of 0.52. The volume of aggregates to the total volume of mixture was kept to 72%. The quantity of water has been taken as the sum of water contained in the sodium silicate, sodium hydroxide and the added water, while the quantity of solid was determined by the mass of slag and the solid contained in the alkaline activator solution (Adam, 2009).

Table 6.1 summarizes the details. A blend of liquid sodium silicate and sodium hydroxide provides an M_s of 1.00. The Na_2O dosage (the ratio of Na_2O in alkaline solution to the mass of fly ash is 5%.

Table 6.1 Mix design of AAS concrete (kg/m^3)

Mixture	GGBS	Aggregate			Activator		Added water
		Sand	7 mm	10 mm	Na_2SiO_3	NaOH 10M	
AAS5-1.00	415	784	346	693	71	46	136

6.4. Mixing and curing process

The same mixing procedure as used for the fly ash geopolymer concrete was applied to prepare the AAS concrete. The detail of mixing procedures is described in **Figure 5.1** in **Chapter 5 Section 5.4**. The mixing procedure is shown in **Figure 6.1**.

Figure 6.1 Casting process of AAS concrete

The standard curing regime of OPC concrete was applied to the AAS concrete specimens due to the similarity of the hydration products, i.e. C-S-H gel. The specimens were de-moulded after 24 hours followed by water curing at 20^{O}C for 6 days and then left at room temperature until testing.

6.5. Workability

The workability of the concrete was measured using a slump test in accordance with Australian Standard (AS 1012.3.1, 1998) using a truncated cone as described in **Chapter 5 Section 5.5**. The result of the slump test of the AAS concrete is shown in **Figure 6.2**.

Figure 6.2 Slump test of fresh AAS concrete

The workability of the AAS concrete could be obtained using the traditional slump test with a value of 200.0 mm recorded. The value was similar to that of traditional concrete grade C40 (40 N/mm^2) which has the specified slump of 180 $\pm$ 40 mm and maximum slump at site of 220 mm (Stanley, 2011).

6.6. Density development

The density of the AAS concrete was measured using the rapid measurement method in accordance with Australian Standards (AS 10.12.12.1, 1998). The density development is shown in **Table 6.2** (calculations provided in **Appendix C**).

The density tended to increase with time (**Figure 6.3**) with an initial density at 28 days of 2452.6 kg/m^3 increasing to a final density of 2459.5 kg/m^{3}at 540 days Overall an increase in density of 0.28% was observed..

The density shows a comparable density to OPC concrete with a density of 2400 kg/m^3 (AS 3600, 2009). This can be attributed to the specific gravity of the slag of the AAS concrete (2.95) being comparable to that of Portland cement with a specific gravity of 3.0 – 3.2 (Cement Australia, 2013).

Table 6.2 Density development of AAS concrete

Time (days)	Density (kg/m^3)
28	2452.6
56	2454.0
90	2456.9
180	2457.8
360	2457.9
540	2459.5
Average Density	2456.4
	2460

Note: The average density of a group of specimens is rounded to the nearest 20 kg/m^3 (AS 10.12.12.1, 1998).

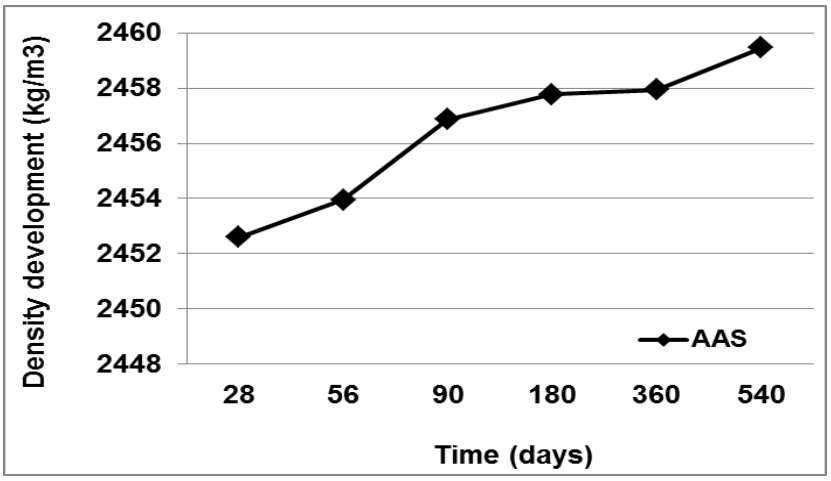

Figure 6.3 Density development of AAS concrete

6.7. Long term mechanical properties of AAS concrete

6.7.1. The development of compressive strength

The strength development of AAS concrete, based on the mix proportion as described in **Section 6.3** is shown in **Table 6.3** and **Figure 6.4**.

Table 6.3 Compressive strength of AAS concretes

Mix	Compressive strength (MPa)					
	28 day	56 day	90 day	180 day	360 day	540 day
Compressive strength (MPa)	39.47	41.59	41.26	40.43	40.35	38.31
Standard deviation	1.11	1.22	1.18	2.06	0.25	1.91

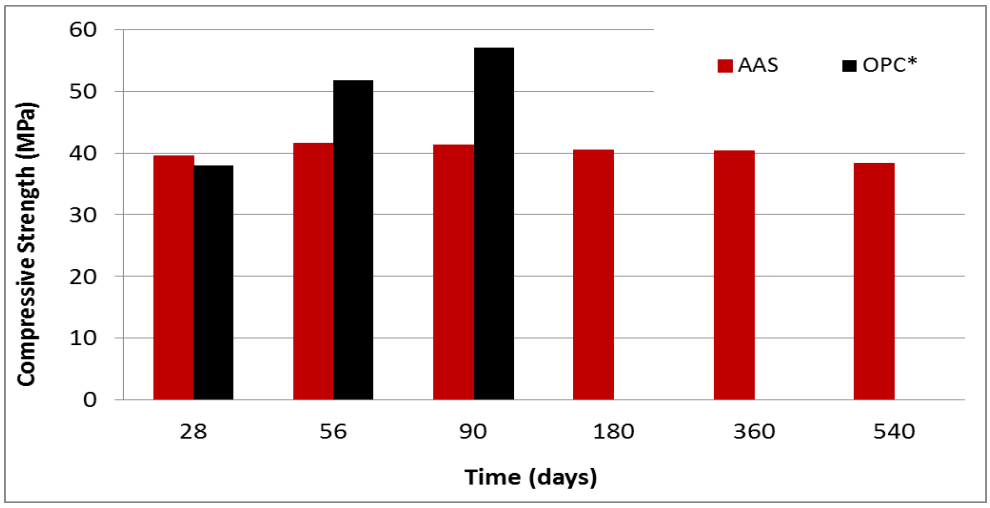

Note: * (Adam, 2009)

Figure 6.4 Strength development of AAS concrete

In contrast with the fly ash geopolymer concrete in **Chapter 5**, the AAS concrete demonstrates a comparable initial strength of 39.47 MPa with the OPC concrete and meets the designed compressive strength of 40 $\pm$ 10 MPa at 28 days. A slight increase in the AAS concrete strength is also observed up to 56 days age. However, beyond that, the compressive strength of the AAS concrete does not display any significant increase with time, but shows a slight reduction in strength. It is observed that the highest strength of AAS concrete of 41.59 MPa is achieved at 56 days. However, this strength reduces to 40.35 MPa and 38.31 MPa at 360 and 540 days, respectively.

Figure 6.5 presents the strength development of the AAS concrete reported for this work compared to previously reported data, while **Table 6.4** gives the silicates and aluminates contents of the respective GGBS's.

Figure 6.5 shows the strength development of the AAS concrete with a Si/Al ratio of 2.59 compared to the previous research conducting by Adam (2009) with a Si/Al ratio of 2.49. The higher Si/Al ratio slightly reduces the early age reaction of the AAS mixes. Increasing the Si/Al ratio reduces the strength from 44.30 MPa to 39.47 MPa at 28 days, while a reduction in strength is also observed at 90 days from 45.30 MPa to 41.26 MPa. This is attributed to the reduction of the alkalinity and the consumption of Na^+ by the alumino-silicate reaction products which lead to the deferment of the early age reaction and causes a lower strength at 28 days. According to Wang & Scrivener (1995), a higher Si/Al ratio tends to reduce the early age reaction. The early age reactions in the AAS system are fundamentally based on an alkali mediated dissolution mechanism. A similar finding was also found by Bernal et al. (2012). Using a sodium hydroxide based-solution, they found that an increase of Si/Al ratio was followed by an increase of compressive strength. However, a higher ratio of Si/Al tended to delay the early age reaction resulting in lower initial strength. Other researchers have also identified that strength development has been affected by the ratio of silicates and aluminates (Bernal et al., 2012, Wang & Scrivener, 1995, Sakulich et al., 2010).

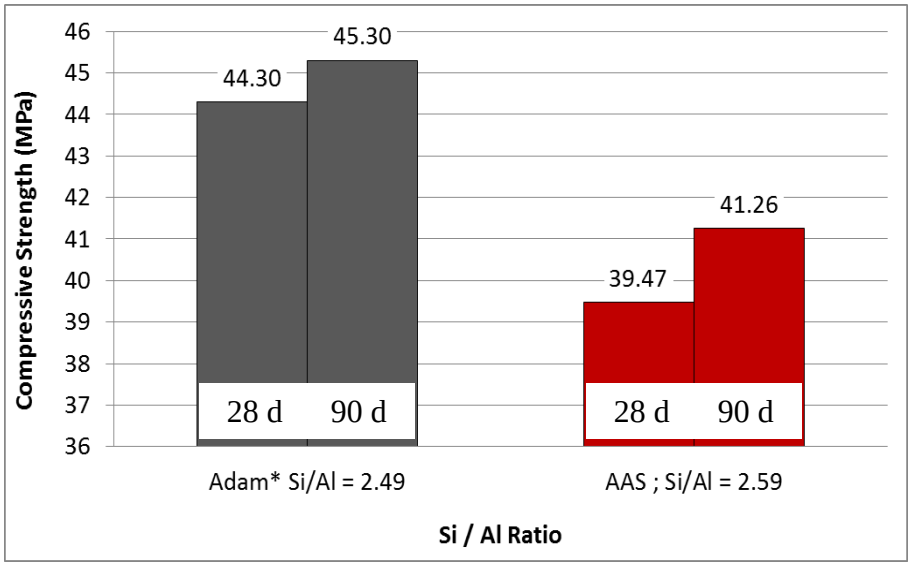

Note: * Adam (2009)

Figure 6.5 Effect of Si/Al ratio on AAS concrete

Table 6.4 Comparison of chemical composition of GGBS precursor

Components	AAS (%)	Adam[1] (%)
SiO_2	36.87	33.45
Al_2O_3	14.23	13.46
Si/Al ratio	2.59	2.49
Compressive Strength at 90 days (MPa)	41.26	45.30

Note: [1] Adam (2009)

6.7.2. The development of modulus of elasticity

The development of the modulus of elasticity of AAS concrete with time is shown in **Table 6.5** and **Figure 6.6**.

Table 6.5 Modulus of elasticity of AAS concrete

Age of concrete (days)	Compressive strength (MPa)	Modulus of elasticity (MPa)
28	39.47	26768
90	41.26	22361
180	40.43	18931
360	40.35	17446
540	38.31	15279

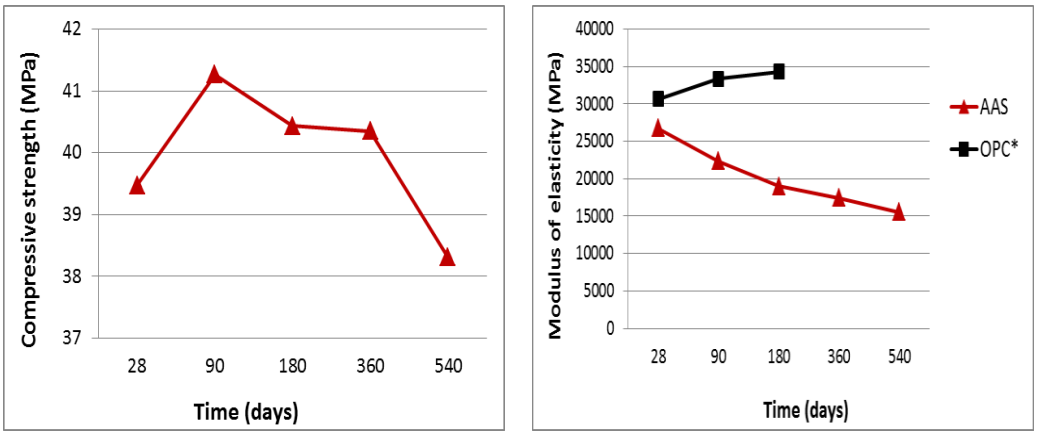

Note: * Adam (2009)

Figure 6.6 Compressive strength vs modulus of elasticity of AAS concrete

The results show that AAS concrete has a comparable modulus of elasticity to that of OPC concrete in the short term. However, the long term results show that the modulus of elasticity of AAS concrete reduces with time and becomes lower than that of OPC concrete (**Figure 6.6**). The AAS concrete achieves a modulus of elasticity of 26768 MPa at 28 days, decreasing to 17446 MPa at 360 days and 15279 MPa at 540 days. This would indicate that the interaction between the AAS paste and the aggregates at the aggregate/paste interface, the principal factor that affecting the modulus of elasticity, becomes brittle. Overall a decrease in modulus of elasticity of 42.92% is observed between 28 and 540 days.

The decreasing of the modulus of elasticity is contrary to the trend exhibited by OPC concrete. This indicates that the existing Australian Standard (AS 3600, 2009) which is based on OPC characteristics should not be used to predict the modulus of elasticity of AAS concrete in the long term.

Overall, the modulus of elasticity of AAS concrete shows comparable values to that of OPC concrete in short term behaviour. However, the use of AAS concrete over the long term needs to be further studied on account of the reduction with age.

6.7.3. The development of flexural tensile strength

The development of the flexural tensile strength of AAS concrete based on the modulus of rupture test results is shown in **Table 6.6** and **Figure 6.7**.

Table 6.6 Flexural tensile strength of AAS concrete

Age of concrete (days)	Compressive strength f'_c (MPa)	Actual Measured flexural tensile strength [1] $f_{ct.f}$ (MPa)	Predicted mean values flexural tensile strength AS 3600 [2] $f_{ct} = 1.4\ (0.6)\ \sqrt{f'_c}$ (MPa)	Flexural tensile strength ratio (measured / calculated)
28	39.47	6.04	5.28	1.14
56	41.59	5.92	5.42	1.09
90	41.26	5.76	5.40	1.07
180	40.43	5.51	5.34	1.03
360	40.35	5.38	5.34	1.01
540	38.31	5.16	5.20	0.99

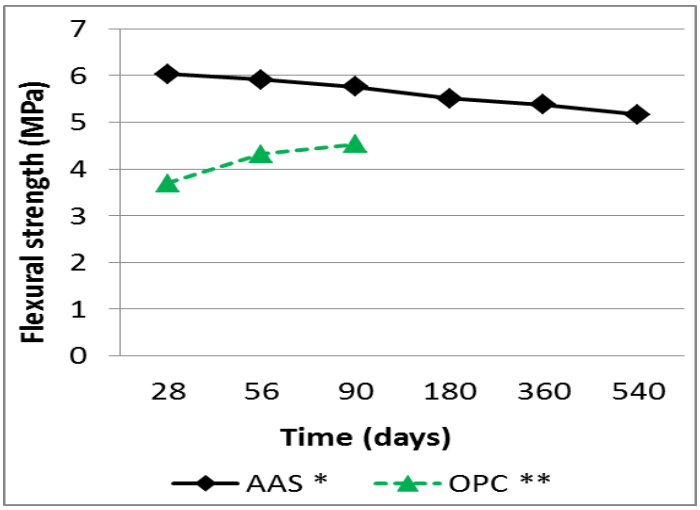

Note : * Actual, based on laboratory results (AS 1012.11, 2000)
** Based on previous research (Adam, 2009, AS 3600, 2009)

Figure 6.7 Actual measured flexural tensile strength of AAS concrete

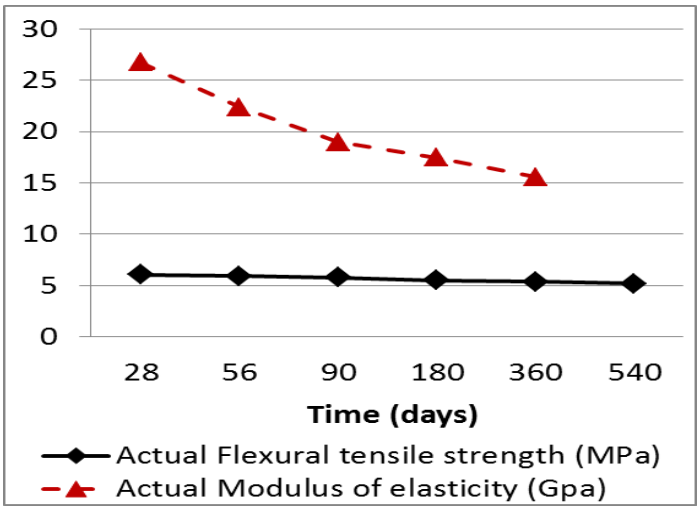

Figure 6.8 Comparison between flexural tensile strength vs modulus of elasticity of AAS concrete

The results show that AAS concrete has a higher flexural tensile strength compared to that of OPC concrete in the short term. However, the long term data demonstrates a significant decrease in flexural tensile strength with time, similar to the decrease in compressive strength observed previously, **Figure 6.7**. The AAS concrete shows a measured flexural tensile strength of 6.04 MPa at 28 days. The long term performance of AAS concrete shows a decrease of 5.38

MPa at 360 days and 5.16 MPa at 540 days, with an overall decrease of 14.57% observed from 28 to 540 days. The decrease in flexural tensile strength is also in agreement with the decrease of modulus of elasticity observed with time **(Figure 6.8**). Similar findings were also reported by Shi et al. (2006) and Sofi et al. (2007). The authors found that the alkali-activated slag concretes demonstrate higher flexural strength than OPC concrete, when the compressive strength is comparable.

Similar to fly ash geopolymer concrete, the actual measured flexural tensile strength of AAS concrete is found to be higher than the characteristic flexural tensile strength predicted by AS 3600 under short term performance, **Figure 6.9**. The decrease with time of the flexural strengths observed for the AAS concrete also indicates that the existing Australian Standard (AS 3600, 2009) should not be used to predict the flexural strength of AAS concrete over the long term. Similar results were also found by Bernal et al. (2012). The authors found that the flexural tensile strength of AAS concrete is higher than that identified in ACI 318-08, as being representative of OPC concrete.

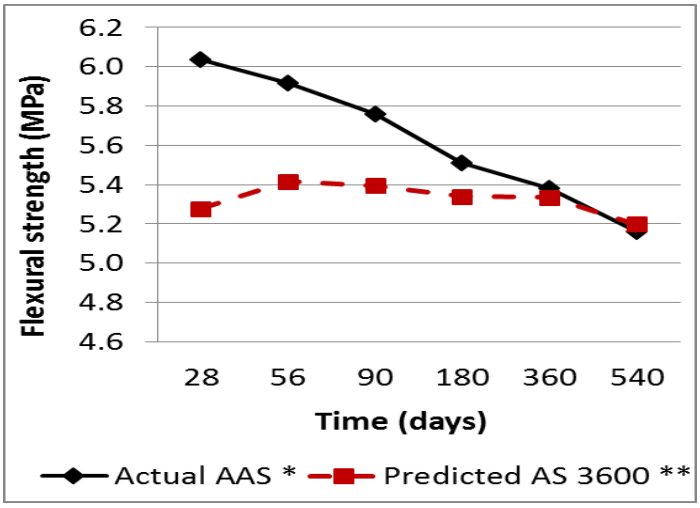

Note : * Actual, based on laboratory results (AS 1012.11, 2000)
** Predicted, calculated based on article 3.1.1.3 (AS 3600, 2009)

Figure 6.9 Flexural tensile strength of AAS concrete compared to AS 3600

6.7.4. The development of uniaxial tensile strength

The results of the uniaxial tensile strength, based on the indirect tensile strength test (splitting test) results, are shown in **Table 6.7** and **Figure 6.10**.

Table 6.7 Uniaxial tensile strength of AAS concrete

Age of concrete (days)	Compressive strength (MPa)	Measured indirect tensile strength $f_{ct.sp}$ (MPa)	Actual Uniaxial tensile strength from AS 3600 $f_{ct} = 0.9\sqrt{f'_{ct.sp}}$ (MPa)	Predicted Mean values uniaxial tensile strength from AS 3600 $f_{ct} = 1.4 (0.36)\sqrt{f'c}$ (MPa)	Uniaxial tensile strength ratio (measured / characteris-tic)
28	39.47	3.33	3.00	3.17	0.95
56	41.59	3.30	2.97	3.25	0.91
90	41.26	3.26	2.94	3.24	0.91
180	40.43	3.26	2.93	3.20	0.92
360	40.35	3.21	2.89	3.20	0.90
540	38.31	3.16	2.85	3.12	0.91

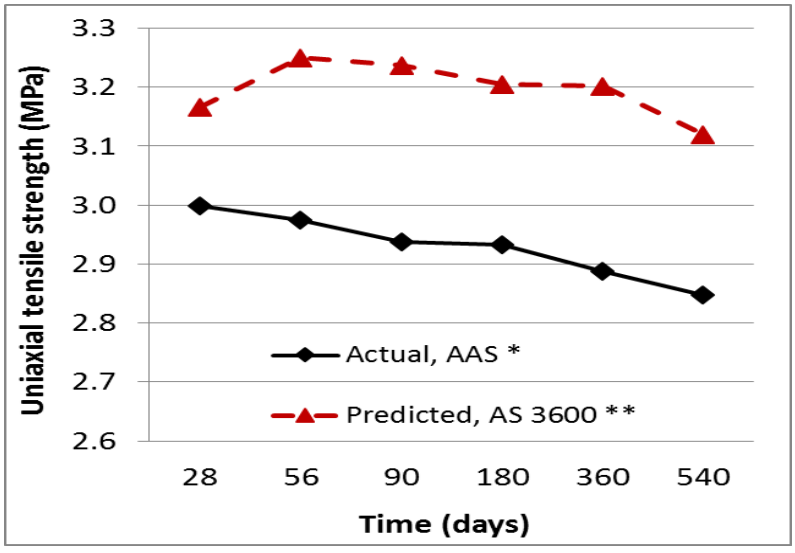

Note: * Actual, based on laboratory results, (AS 1012.10, 2000)
** Predicted, calculated based on article 3.1.1.3 (AS 3600, 2009)

Figure 6.10 Uniaxial tensile strength of AAS concrete

The uniaxial tensile strength of AAS concrete is predicted to be 3.17 MPa at 28 days and 3.25 MPa at 56 days, and decreases to 3.12 MPa after 540 days.

However, the observed uniaxial tensile strength was 3.00 MPa, slightly lower than the mean values uniaxial tensile strength, f_{ct} = 3.17 MPa, predicted by AS 3600, based on the compressive strength at 28 days (**Figure 6.10**). The measurements of the long term performance show a decrease of 2.89 MPa at 360 days and 2.85 MPa at 540 days, with an overall decrease of 5% observed from 28 to 540 days. This finding was lower than that to the flexural tensile strength test results. This is attributed to the loading arrangement of the AAS concrete during the test. The volume of material which is subjected to critical stress in the flexural tensile strength test is much smaller than in the indirect tensile strength test. Thus the likelihood of a critical crack propagating is greater in the indirect test (where the volume of high stressed material is greater) resulting in a higher stress reached in the flexural test).

The long term results for the uniaxial tensile strength tests were found to show the same trends as for the compressive strength, the flexural tensile strength and modulus of elasticity. That is the uniaxial tensile strength had a tendency to reduce with time (**Figure 6.11**).

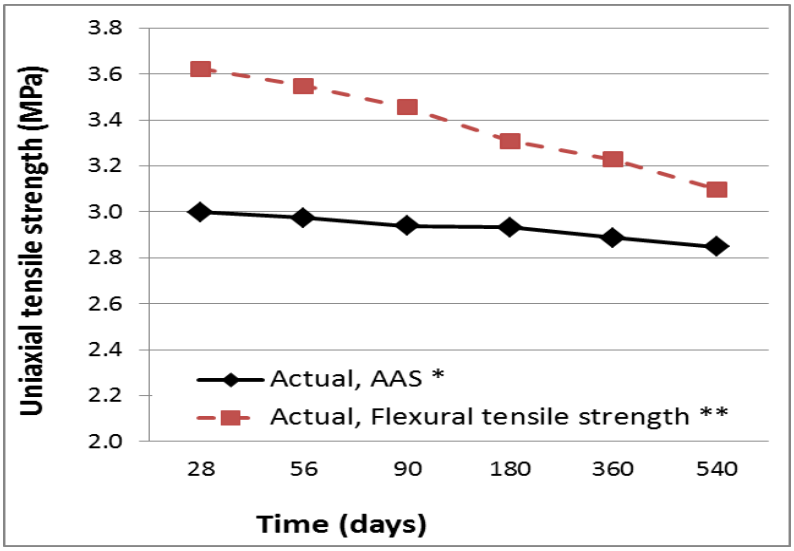

Note: * Actual, based on lab. results (AS 1012.10, 2000)
** Actual, based on lab. results (AS 1012.11, 2000) and (AS 3600, 2009)

Figure 6.11 Uniaxial vs flexural tensile strength of AAS concrete

6.7.5. Correlation between compressive strength and the modulus of elasticity and tensile strength

A regression analysis is performed to investigate the relationships between the compressive strength to the modulus of elasticity, the compressive strength to the flexural tensile strength, and the compressive strength to the uniaxial tensile strength of AAS concrete specimens.

Correlation between compressive strength and modulus of elasticity

The comparison of the modulus of elasticity of AAS concrete to the existing Australian Standard (AS 3600, 2009) and the Ng & Foster model proposed by Concrete Institute of Australia is shown in **Table 6.8** and **Figure 6.12**.

Using the equations from the existing Australian Standard (**Equation 3.3**) (AS 3600, 2009) and the equation proposed by Ng & Foster (**Equation 2.10**) (Concrete Institute of Australia, 2011), based on the 28 days strength performance, the long term behaviour of the modulus of elasticity of AAS concrete can be predict based on its compressive strength as shown in **Figure 6.12**.

Table 6.8 Comparison of modulus of elasticity of AAS concrete to the existing standards

Age of concrete (days)	Compressive strength (MPa)	Actual Modulus of Elasticity (1) AS1012.17 (MPa)	Predicted 1 Modulus of Elasticity (2) AS3600 (MPa)	Predicted 2 Model Ng & Foster (3) (MPa)
28	39.47	26768	32317	22028
90	41.26	22361	32822	22551
180	40.43	18931	32644	22310
360	40.35	17446	32748	22287
540	38.31	15279	31808	21683

Note : (1) Based on laboratory results, Australian Standard (AS 1012.17, 1997)
(2) Australian Standard, Article 3.1.2(a) (AS 3600, 2009)
(3) Model proposed by Ng & Foster (Concrete Institute Australia, 2011)

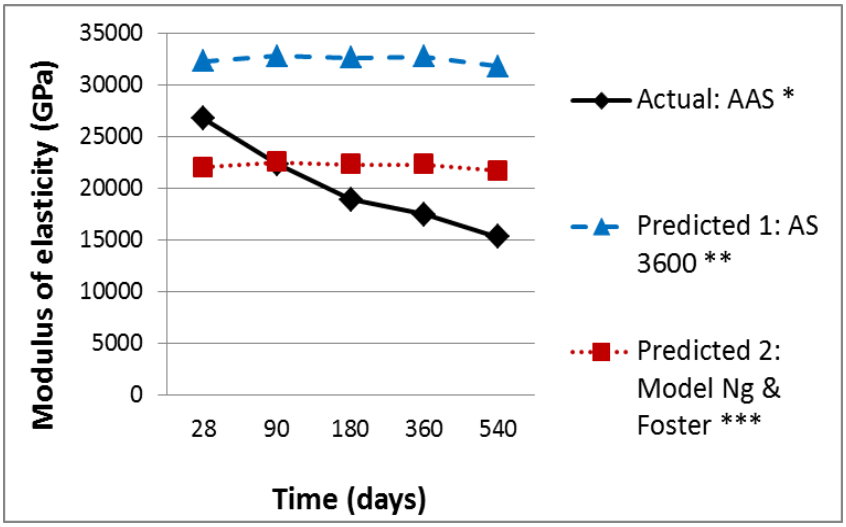

Note: * Actual, based on laboratory results, Australian Standard (AS 1012.17, 1997)
** Predicted 1, Australian Standard, Article 3.1.2(a) (AS 3600, 2009)
*** Predicted 2, proposed by Ng & Foster (Concrete Institute Australia, 2011)

Figure 6.12 Comparison of modulus of elasticity of AAS concrete to existing standards

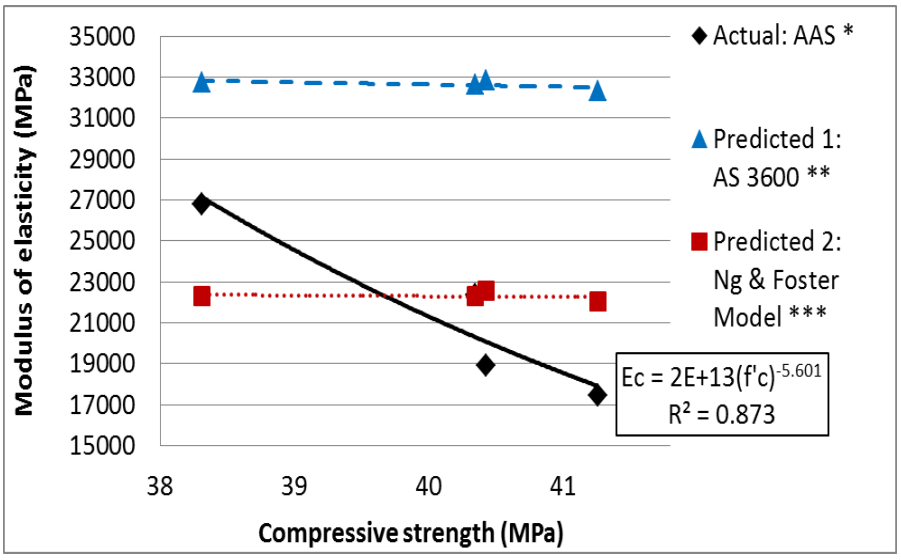

Note * Actual, based on laboratory results, Australian Standard (AS 1012.17, 1997)
** Predicted 1, Australian Standard, Article 3.1.2(a) (AS 3600, 2009)
*** Predicted 2, Proposed by Ng & Foster (Concrete Institute Australia, 2011)

Figure 6.13 Correlation between modulus of elasticity and compressive strength of AAS concrete in time

The test results show that AAS concrete demonstrates a modulus of elasticity similar to that predicted based on AS 3600, over the short term. The Ng & Foster model (Concrete Institute Australia, 2011) shows a similar trend but predicts a lower elastic modulus than that predicted by AS 3600. Hence, applying the formulae, it can be inferred that the predicted elastic modulus for AAS concretes slightly reduce along with a reduction in compressive strength in the long term (AS 3600, 2009, Concrete Institute Australia, 2011). The observations found that the actual modulus of elasticity of AAS concrete exhibits a greater rate of reduction than that predicted by AS 3600 and Ng & Foster model. The short term tests of the AAS concrete at 28 days age show a similar modulus of elasticity with that predicted, which indicates that the equation proposed by Ng & Foster in Concrete Institute Australia (2011) can be applied. However, the test results subsequently show a reduction with time (**Figure 6.13**), indicating the model does not correctly predict the performance in the long term.

The coefficient of determination of the correlation between modulus of elasticity and compressive strength is 87.3% which indicates that the models fit the data well. However, it should be noted that this is based on a small sample size of data. A general regression model representing the correlation between static modulus of elasticity and compressive strength is suggested, **Figure 6.13**, giving the following equation:

$$E_c = 2x10^{13}\left(fc'\right)^{-5.601} \qquad (5.7)$$

where E_c is the static modulus of elasticity and fc' is the compressive strength.

Correlation between compressive strength and flexural tensile strength

The comparison of the flexural tensile strength of AAS concrete to the existing Australian Standard (AS 3600, 2009) and the Ng & Foster model proposed by the Concrete Institute of Australia is shown in **Table 6.9** and **Figure 6.14**.

As with the fly ash geopolymer concrete, the flexural strength of AAS concrete has been predicted based on the 28 days compressive strength as proposed in AS 3600 and the models proposed by Diaz Loya and Neupane (AS 3600, 2009, Diaz-Loya et al., 2011, Neupane et al., 2014). These models were chosen due to their being no specific model for AAS concrete to predict the correlation between

compressive strength and flexural tensile strength. The measured flexural tensile strength results show that AAS concrete exhibits a higher flexural tensile strength compared to the other models, **Table 6.14**.

Table 6.9 Comparison of flexural tensile strength of AAS concrete to the existing standards

Age of concrete (days)	Compressive strength f'c (MPa)	Measured flexural tensile strength (1) $f_{ct.f}$ (MPa)	Mean values flexural tensile strength AS 3600 (2) $f_{ct} = 1.4\ (0.6)\sqrt{f'_c}$ (MPa)	Neupane model (3) $f_{ct.f} = 0.0421\ f'^{1.2358}_c$ (MPa)	Diaz Loya model (4) $f_{ct} = 0.69\ \sqrt{f'_c}$ (MPa)
28	39.47	6.04	5.28	3.95	4.33
56	41.59	5.92	5.42	4.22	4.45
90	41.26	5.76	5.40	4.18	4.43
180	40.43	5.51	5.34	4.07	4.39
360	40.35	5.38	5.34	4.06	4.38
540	38.31	5.16	5.20	3.81	4.27

Note : * Based on laboratory results, (AS 1012.11, 2000)
** Australian Standard, Article 3.1.1.3 (AS 3600, 2009)
*** Model proposed by Neupane (Neupane et al., 2014)
**** Model proposed by Diaz Loya (Diaz-Loya et al., 2011)

The models predict that there would be a reduction in the development of flexural tensile strength with time, based on the reduction of compressive strength, **Figure 6.14**. The measured flexural strength demonstrates a higher value compared to the other predicted models, however, it was found that the decrease in the measured flexural tensile strength is significantly higher than that predicted by the models. This would indicate that the existing models should not be used to predict the flexural strength of AAS concrete.

In addition, a general regression model for AAS concrete based on the correlation between flexural strength and compressive strength with the coefficient of determination of 78.83% (**Figure 6.14**) can be suggested as follows:

$$f_{ct.f} = 777.47\left(fc'\right)^{-1.328} \qquad (5.8)$$

where $f_{ct.f}$ is the flexural tensile strength and fc' is the compressive strength. However, the model is developed based on a limited number of concrete

specimens, thus a further validation is required before adopting this model. These results are in agreement with those observed for the compressive strength and modulus of elasticity in previous sections.

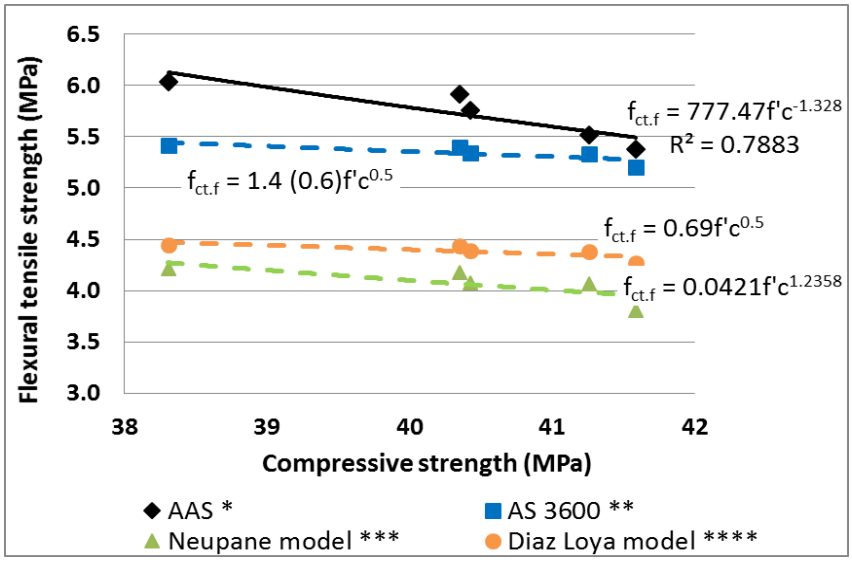

Note : * Based on laboratory results, (AS 1012.11, 2000)
** Australian Standard, Article 3.1.1.3 (AS 3600, 2009)
*** Model proposed by Neupane (Neupane et al., 2014)
**** Model proposed by Diaz Loya (Diaz-Loya et al., 2011)

Figure 6.14 Correlation between flexural tensile strength and compressive strength of AAS concrete in time

Correlation between compressive strength and uniaxial tensile strength

The comparison of the uniaxial tensile strength of AAS concrete to that predicted by AS 3600 and the other models proposed by AS 3600, Raphael and Oluokun (AS 3600, 2009, Raphael, 1984, Oluokun et al., 1991) is presented in **Table 6.10** and **Figure 6.15**.

The predicted correlation between uniaxial tensile strength and compressive strength was based on the measured compressive strength development. From these models, it is predicted that the tensile strength of AAS concrete will increase with an increase in compressive strength. However, it was found that the measured uniaxial tensile strength of AAS concrete tends to reduce with time.

Table 6.10 Comparison of uniaxial tensile strength AAS concrete to the existing standards

Age of concrete (days)	Compressive strength f'c (MPa)	Uniaxial tensile strength from AS 3600 (1) $f_{ct} = 0.9\sqrt{f'_{ct.sp}}$ (MPa)	Mean values uniaxial tensile strength AS 3600 (2) $f_{ct} = 0.36\sqrt{f'c}$ (MPa)	Raphael model (3) $f_{ct.f} = (0.9)\ 0.3\ f'^{2/3}_{c}$ (MPa)	Oluokun model (4) $f_{ct} = (0.9)\ 0.2\ f'^{0.7}_{c}$ (MPa)
28	39.47	3.00	3.17	3.13	2.36
56	41.59	2.97	3.25	3.24	2.45
90	41.26	2.94	3.24	3.22	2.43
180	40.43	2.93	3.20	3.18	2.40
360	40.35	2.89	3.20	3.18	2.40
540	38.31	2.85	3.12	3.07	2.31

Note :(1) Based on laboratory results, (AS 1012.10, 2000)
(2) Australian Standard, Article 3.1.1.3 (AS 3600, 2009)
(3) Model proposed by Raphael (Raphael, 1984)
(4) Model proposed by Oluokun (Oluokun et al., 1991)

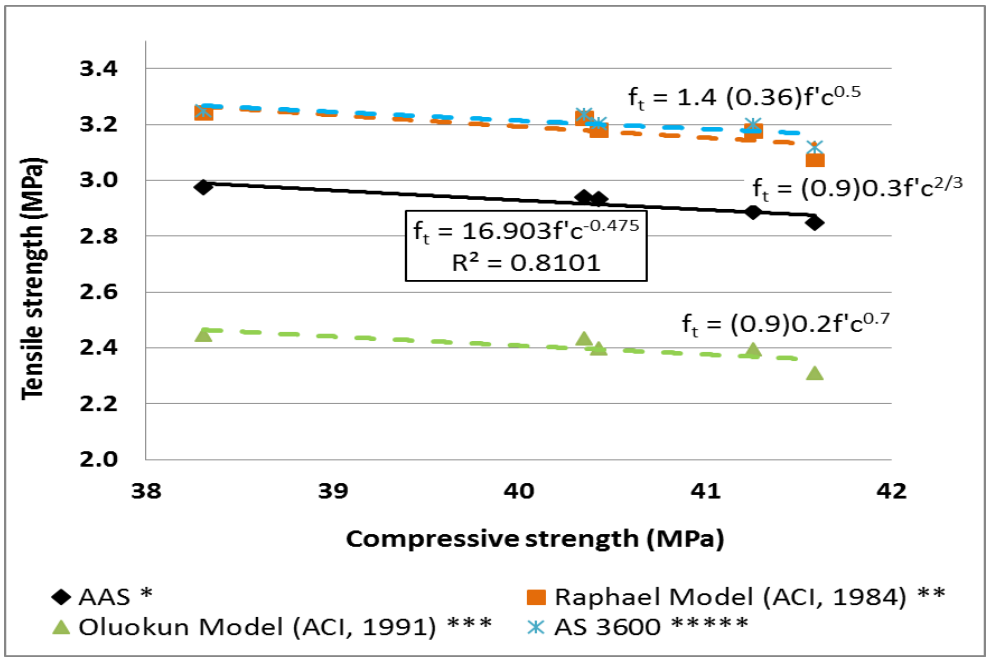

Note : * Based on laboratory results, (AS 1012.10, 2000)
** Model proposed by Raphael (Raphael, 1984)
*** Model proposed by Oluokun (Oluokun et al., 1991)
***** Australian Standard, Article 3.1.1.3 (AS 3600, 2009)

Figure 6.15 Correlation between uniaxial tensile strength and compressive strength of AAS concrete in time

The correlation between the uniaxial tensile strength and compressive strength of AAS concrete can be developed using a general regression with the coefficient determination of 81.01%. However, the regression model was developed based on its strength at 56 days. This was due to the reduction of strength which started at 90 days as shown in **Figure 6.15**. The proposed equation is as follows:

$$f_t = 16.903(fc')^{-0.475} \quad (5.9)$$

where f_t is the uniaxial tensile strength and fc' is the compressive strength.

Overall the development of the compressive strength, modulus of elasticity and tensile strength of AAS concrete shows a significant decrease over time. A decrease in compressive strength is followed by a decrease in modulus of elasticity and tensile strength which represents a different behaviour to that of OPC concrete. Although, AAS concrete shows comparable mechanical properties to OPC concrete in short term performance, the decrease of compressive strength and the associated decrease of modulus of elasticity and tensile strength indicates that the existing Australian standard (AS 3600, 2009) should not be applied for AAS concrete.

6.8. Durability properties of AAS concrete

This section presents the detail of the experimental measurements of the durability properties of AAS concrete. The mix design was based on the preliminary research data in **Chapter 4**.

6.8.1. Porosity and water absorption

The porosity and water absorption test results are shown in **Table 6.11**, **Figure 6.16** and **Figure 6.17** (calculations are presented in **Appendix H** and **Appendix I**, respectively).

The average porosity of the AAS concrete is found to be 9.29% while the long term data demonstrates a significant increase with time (**Figure 6.16**). It is observed that the initial porosity is 8.15% at 28 days is followed by a significant increase to 9.77% at 360 days and to 10.70% at 540 days, with an overall increase of 31.29% observed from 28 to 540 days.

Table 6.11 Porosity and water absorption of AAS concrete

Time (days)	Porosity (%)	Water absorption (%)
28	8.15	4.79
56	8.52	4.97
90	9.05	5.20
180	9.56	5.26
360	9.77	5.30
540	10.70	5.36

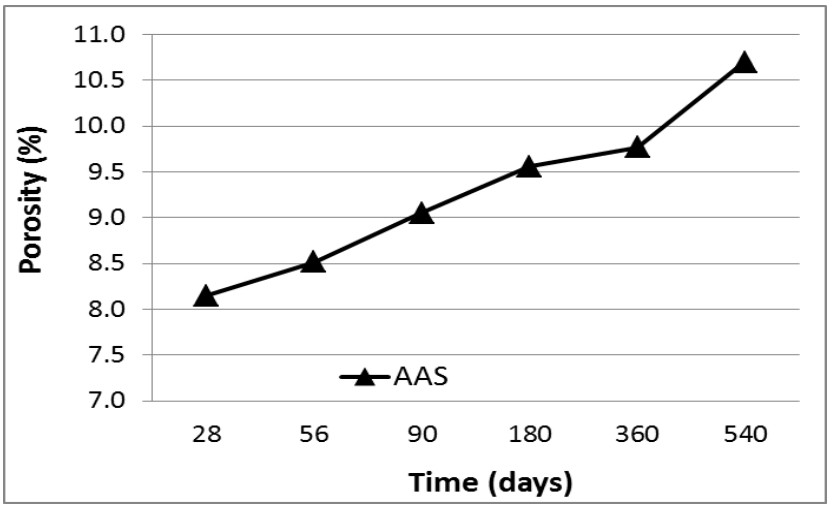

Figure 6.16 Porosity development of AAS concrete

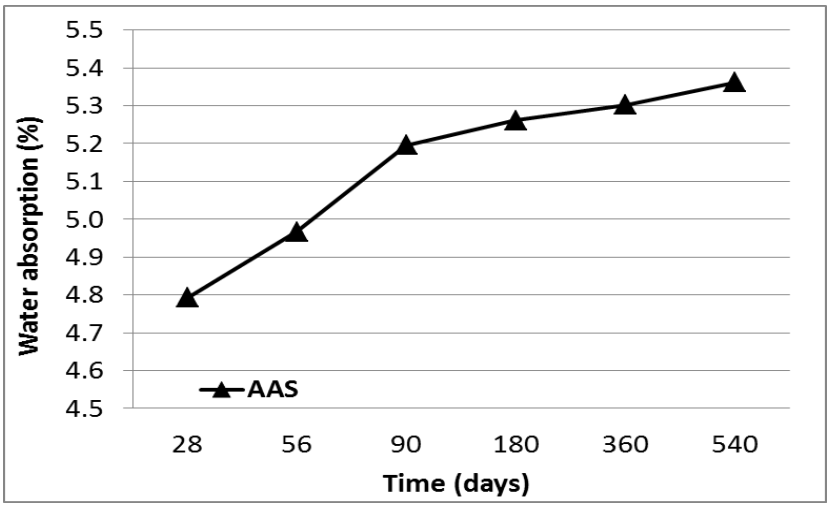

Figure 6.17 Water absorption development of AAS concrete

The development of the water absorption of AAS concrete shows a similar trend to the development of porosity (**Figure 6.17**). It was found that the average water absorption measurement is 5.36% with the initial absorption of 4.79% observed at 28 days. The long term data displays a significant increase to 5.30% at 360 days and to 5.36% at 540 days with an overall increase of 11.88% observed from 28 to 540 days.

Based on these results, the initial porosity of AAS concrete can be classified as "low porosity" with a concrete quality of "good quality" (porosity value < 10%) in accordance with Technical Report No.54 (2000). However, the increase of porosity measurements over time changes the classification to "medium porosity" and reduces the quality to an "average quality" of concrete in long term periods.

The porosity is significantly influenced by the fineness and shape of the slag precursors. The low porosity of the AAS concrete can be attributed to the fineness of the slag precursor (92.02% passing sieve 45 μm, **Appendix A**) compared to the fineness of fly ash precursor (64.78%). The slag precursor also has a higher fineness compared to OPC (with a fineness of approximately 75% - 80%) as suggested by Neville (2011). High fineness affects the distribution of the material within the specimen and fills the cracks between the aggregates, which lead to a lower porosity, thus reducing the connectivity of the pore network between the geopolymer pastes and the aggregates. Furthermore, the irregular shape of the slag precursor also affects its specific surface area. High specific surface area (**Appendix A**) increases the reaction between the slag and the solution and leads to a high density which results in a lower porosity as observed by other researchers (Sinsiri et al., 2010).

Overall, AAS concrete demonstrates a better performance in terms of porosity (**Figure 6.18**) and a comparable in terms of water absorption (**Figure 6.19**) compared to fly ash geopolymer and OPC concrete as also reported by Olivia et al. (2008) and Bernal et al. (2012). This indicates that AAS concrete would exhibit a better durability performance in terms of the penetration of aggressive agents such as carbon dioxide and chloride. However, the increase of porosity and water absorption with time indicates that the behaviour of long-term durability of AAS concrete is questionable.

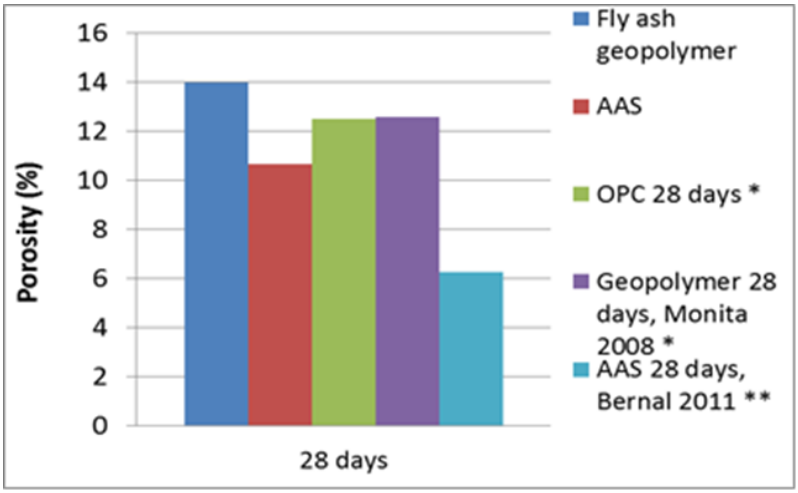

Note : * Geopolymer with w/b = 0.25, NaOH = 14M (Olivia et al., 2008)
** AAS with GBFS/(GBFS+MK) = 1.0, S/A = 3.6 (Bernal et al., 2012)

Figure 6.18 Comparison of porosity

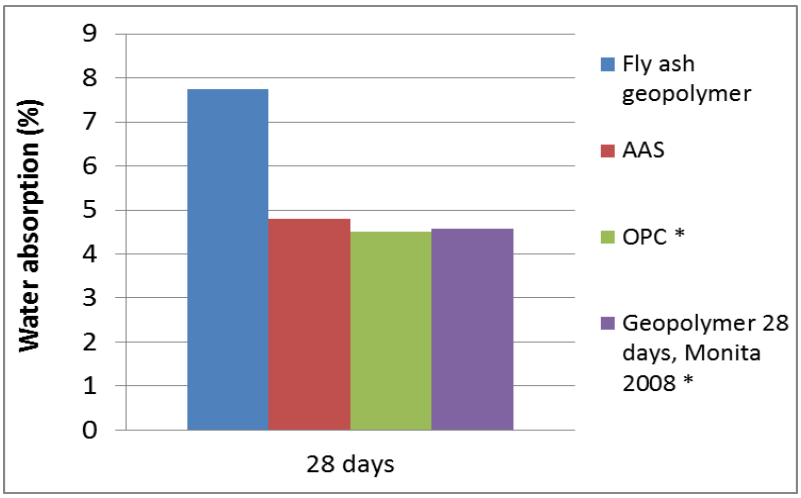

Note : * Geopolymer with w/b = 0.25, NaOH = 14M (Olivia et al., 2008)

Figure 6.19 Comparison of water absorption

6.8.2. Ultrasonic Pulse Velocity

The pulse velocity test results of AAS concrete are shown in **Table 6.12** and **Figure 6.20**. The detail calculation is presented in **Appendix J**.

Table 6.12 Velocity test of AAS concrete

Time (days)	Velocity (km/s)
28	3.91
56	3.87
90	3.75
180	3.71
360	3.69
540	3.62

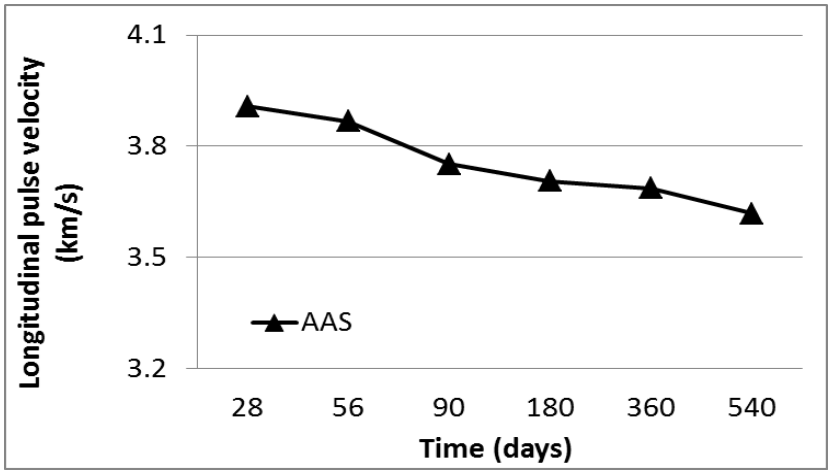

Figure 6.20 Velocity test of AAS concrete

The velocity through AAS concrete significantly decreases with age (**Figure 6.20**). The velocity decreases from 3.91 km/s at 28 days to 3.62 km/s at 540 days with an overall decrease of 7.42%. This indicates that the quality is going down with age and corroborates the previous findings on the increase of porosity and water absorption with age.

This quality of AAS concrete can be determined in accordance with International Atomic Energy Agency (IAEA, 2002) as shown in **Table 3.9** (**Section 3.6.4 Chapter 3**). Based on this, the concrete can be classified as “good” quality with an initial velocity value of 3.91 km/s at 28 days and final velocity value of 3.62 km/s at 540 days.

Compared to fly ash geopolymer concrete which exhibits a lower velocity compared to OPC concrete, the AAS concrete demonstrates a comparable performance with the OPC concrete. According to the NISTIR 6975 report

(Garbacz & Garboczi, April 2003), the standard pulse velocity of OPC concrete is in the range 3.5 – 4.5 km/s.

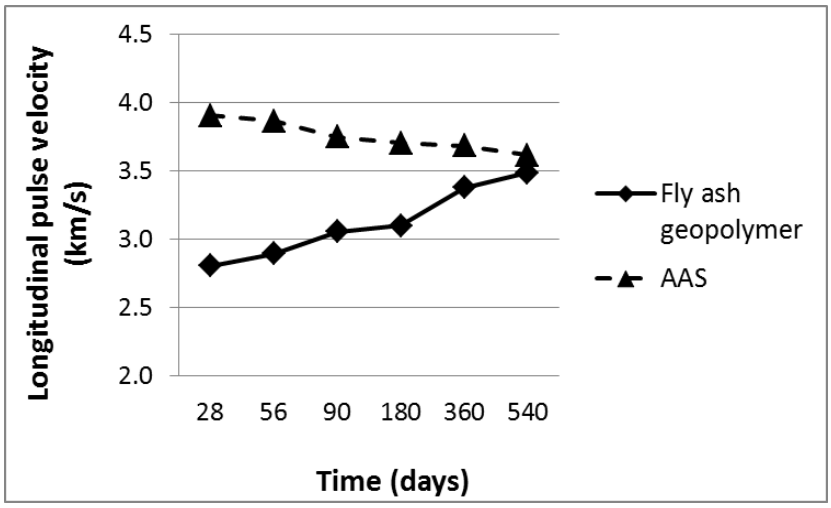

Figure 6.21 Velocity test of fly ash geopolymer and AAS concretes

Figure 6.21 shows that the velocity of AAS concrete is higher than that of fly ash geopolymer concrete in the short term, which suggests that the quality of AAS concrete is better than fly ash geopolymer concrete. This result corroborates the previous finding on the mechanical properties which found that AAS concrete demonstrates higher mechanical properties compared to fly ash geopolymer concrete at 28 days. However, the velocity of AAS concrete decreases significantly with time as observed for the mechanical properties. These findings indicate that AAS concrete might not be appropriate as a structural material to replace cement-based concrete.

6.8.3. Water permeability

The water permeability test results, represented by the water permeability index, are shown in **Table 6.13** and **Figure 6.22** (calculation presented in **Appendix J)**.

The initial water permeability index (WPI) of AAS concrete exhibits a value of 5.295 $m^3x10^{-7}/\sqrt{min}$ at 28 days. However, the WPI demonstrates a significant increase over time (**Figure 6.22**). The final WPI increases to 6.768 $m^3x10^{-7}/\sqrt{min}$ at 360 days and to 7.823 $m^3x10^{-7}/\sqrt{min}$ at 540 days with an overall increase of

47.74% observed from 28 to 540 days. This is indicative of a decrease of the surface quality. This finding also corroborates the previous findings on the increase of porosity and water absorption in previous sections.

Table 6.13 Water permeability of AAS concrete

Time (days)	Water permeability index ($m^3x10^{-7}/\sqrt{min}$)	Water permeability ($m/s\ x10^{-11}$)
28	5.295	1.240
56	5.849	1.369
90	6.114	1.431
180	6.383	1.491
360	6.768	1.578
540	7.823	1.832

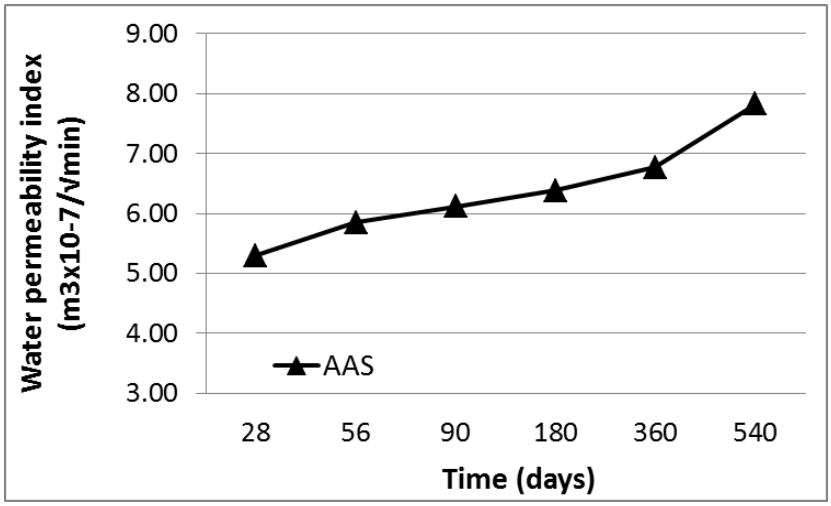

Figure 6.22 Water permeability of AAS concrete

Figure 6.23 shows the comparison of water permeability between AAS and fly ash geopolymer concretes with time. Although the water permeability index (WPI) of the AAS concrete shows an increase over time, however it exhibits a lower WPI compared to that of fly ash geopolymer concrete. This is attributed to the better quality surface of the AAS concrete as shown in **Figure 6.24(b)**. The surface of the AAS concrete demonstrates a denser concrete surface compared to that of the fly ash geopolymer concrete.

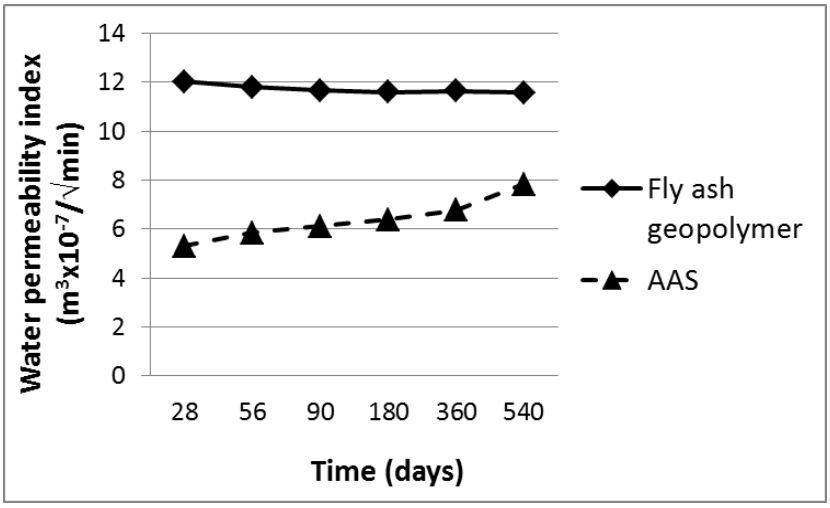

Figure 6.23 Water permeability of fly ash geopolymer and AAS concretes

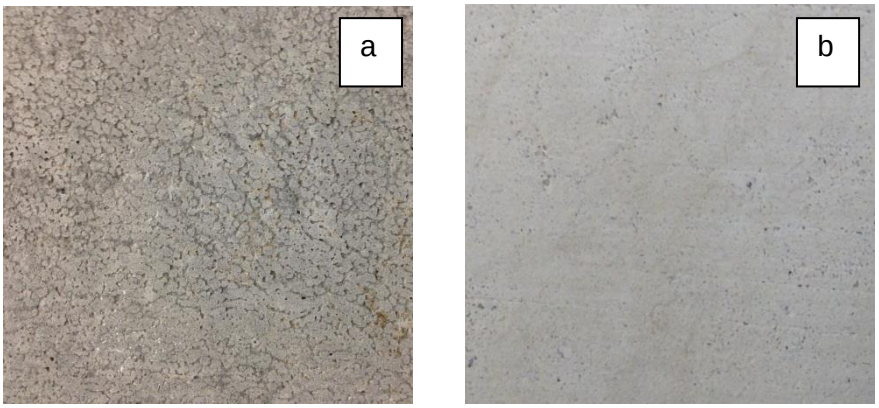

Figure 6.24 External surface: fly ash geopolymer (a) and AAS (b) concretes

Overall the fly ash geopolymer concrete shows a higher value compared to the AAS concrete, though the water permeability shows a slight decrease with time reaching a constant value after 180 days. This behaviour is similar to the water absorption results (**Figure 5.19**) which might be attributed to the development of the geopolymer gel during the geopolymeric reaction which blocks the pores within the specimen as observed also by Olivia et al. (2008).

Although the AAS concrete demonstrates a lower value than the geopolymer concrete, it displays an increase of water permeability with time. This correlates with the porosity, (**Figure 6.16**) and water absorption (**Figure 6.17**) data and raises questions over the long term performance.

6.8.4. Correlation between the mechanical to permeation properties

The regression analysis is performed to investigate the relationships between the mechanical properties and the permeation properties specimens. The correlation between the UPV, porosity and water absorption results with the compressive strength, modulus of elasticity, flexural and uniaxial tensile strength results are presented in **Figure 6.25**, **Figure 6.26**, **Figure 6.27** and **Figure 6.28**, respectively.

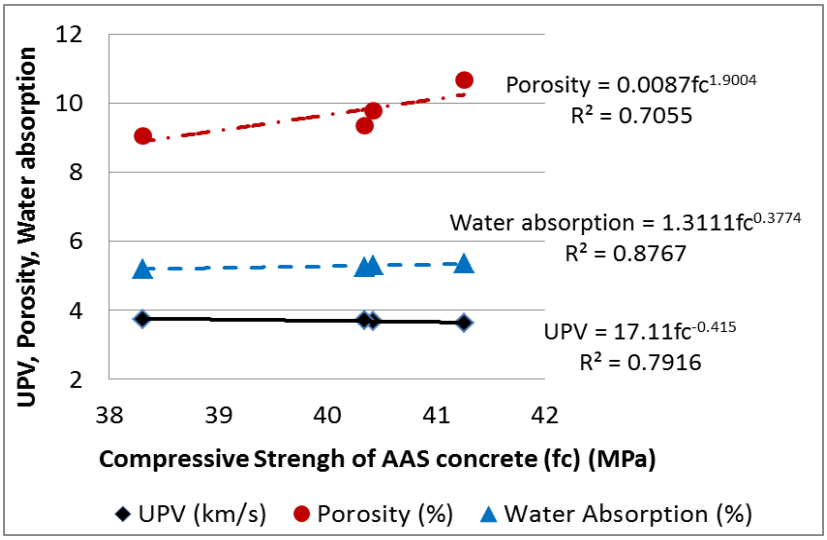

Figure 6.25 Correlation between compressive strength and UPV, porosity and water absorption of AAS concrete

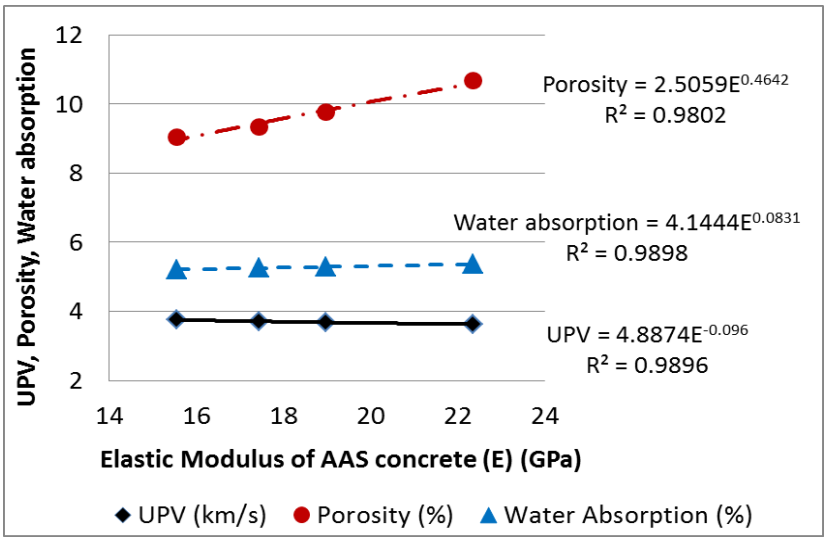

Figure 6.26 Correlation between elastic modulus and UPV, porosity and water absorption of AAS concrete

Figure 6.25 shows that a decrease in compressive strength corresponds with a decrease of UPV which indicates a reduction in the quality with age. This decrease is also associated with an increase of water absorption and porosity. These results indicate that the total cavities, cracks, voids or defects within the concrete has increased and led to the lower quality. The decrease of UPV coupled with the increase of porosity and water absorption corroborate the previous finding in **Section 6.7.**

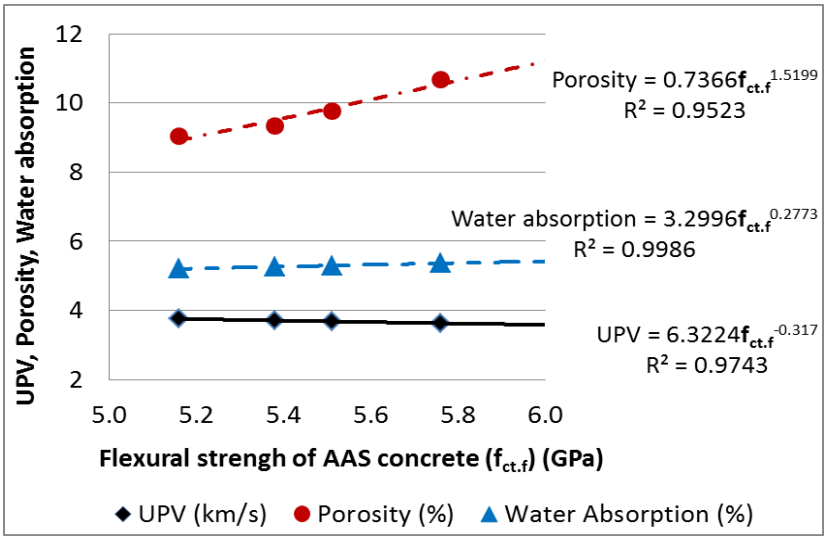

Figure 6.27 Correlation between flexural tensile strength and UPV, porosity and water absorption of AAS concrete

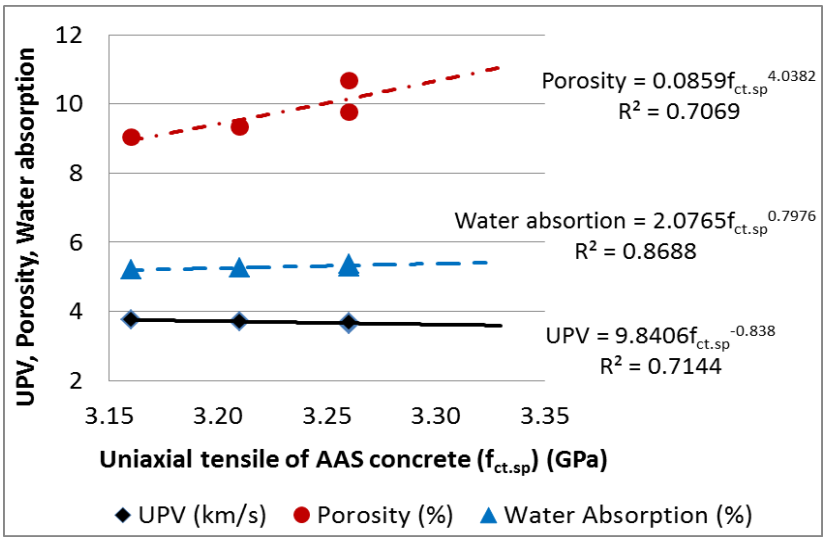

Figure 6.28 Correlation between uniaxial tensile strength and UPV, porosity and water absorption of AAS concrete

The correlation between modulus of elasticity to UPV, porosity and water absorption also shows a similar trend with the compressive strength as shown in **Figure 6.26**. A decrease in modulus of elasticity correlates with a decrease of UPV and an increase of porosity and water absorption. Similar findings are also found for the flexural and uniaxial tensile strength as shown in **Figure 6.27** and **Figure 6.28**, respectively. These findings corroborate the previous finding on the development of mechanical properties (**Section 6.7**).

6.8.5. Resistivity

The resistivity test results are shown in **Table 6.14**. AAS concrete exhibits a high resistivity, over 99 kΩcm, from the outset and maintains this high resistivity over time. This shows that the likelihood to have corrosion was “negligible” for AAS concrete, which would lead to a reduced rate of corrosion of any reinforcement and a better durability for reinforced AAS concrete structures.

As explained on the previous section on fly ash geopolymer concrete (**Section 5.8.4 Chapter 5**), the resistivity of the concrete specimen is affected by the porosity and water permeability. The high resistivity of AAS concrete is attributed to the low porosity (**Figure 6.16**) and low water permeability (**Figure 6.22**). This leads to the low ion concentration within the pore structure and hampers the electrical current that can pass within the specimen (as observed by McCarter et al. (2000).

Table 6.14 Resistivity of AAS concrete

Time (days)	Resistivity (kΩcm)
28	99.0
56	99.0
90	99.0
180	99.0
360	99.0
540	99.0

Figure 6.29 shows the resistivity of AAS concrete and fly ash geopolymer with time. The resistivity is higher than that of fly ash geopolymer concrete. This

indicates that the potential for corrosion is low and leads to better durability for reinforced AAS concrete. Similar findings were also found by Adam (2009) who found that the conductivity and charge passed for fly ash geopolymer is higher than for AAS concrete which indicates that fly ash geopolymer shows a lower resistivity towards the potential of corrosion risk compared to AAS concrete.

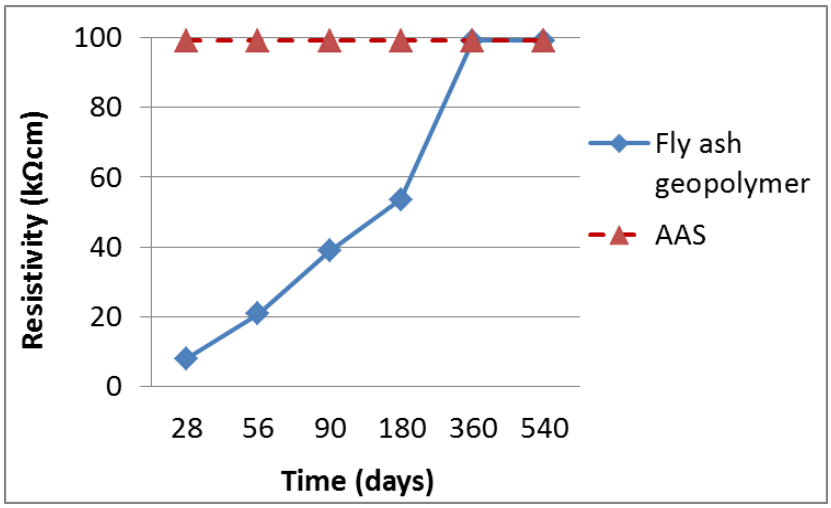

Figure 6.29 Resistivity of fly ash geopolymer and AAS concretes

It should be noted that the resistivity measurement was performed in laboratory conditions and the higher value of resistivity might be attributed to the ambient conditions in the laboratory, 20^{O}C and low relative humidity compared to likely exposure conditions in an external aggressive environment.

6.8.6. Chloride diffusion

The results of the chloride ponding test are shown in **Table 6.15**. While, the best fitted curves of AAS concretes are shown in **Figure 6.30**.

The chloride diffusion coefficients are shown in **Table 6.16**. The chloride diffusion coefficient (D = 8.34x10^{-12} m^2/s) is low (compared to OPC concrete) due to the low porosity (**Table 6.11)** and water permeability (**Table 6.13**).

Similar to OPC concrete, the chloride diffusion of AAS concrete is significantly affected by the C-S-H gel. However, the lower chloride diffusion coefficient of AAS concrete compared to that of OPC concrete is also attributable to the NaOH

concentration and the fineness of slag materials. AAS concrete demonstrates a lower CaO content than OPC concrete, but the NaOH concentration, which is used as the activator solution, increases the binding capacity of AAS concrete. Furthermore, the low fineness reduces the porosity of AAS concrete by filling the gaps between the AAS paste and the aggregates.

Table 6.15 Chloride content by weight of sample and mass of cement (%)

Specimen	Depth (mm)	Chloride (Cl^-) content	
		% by mass sample	% by mass cement
AAS	0-20	0.05139	0.36706
	20-40	< 0.01000	< 0.01000
	40-100	0.03716	0.01013

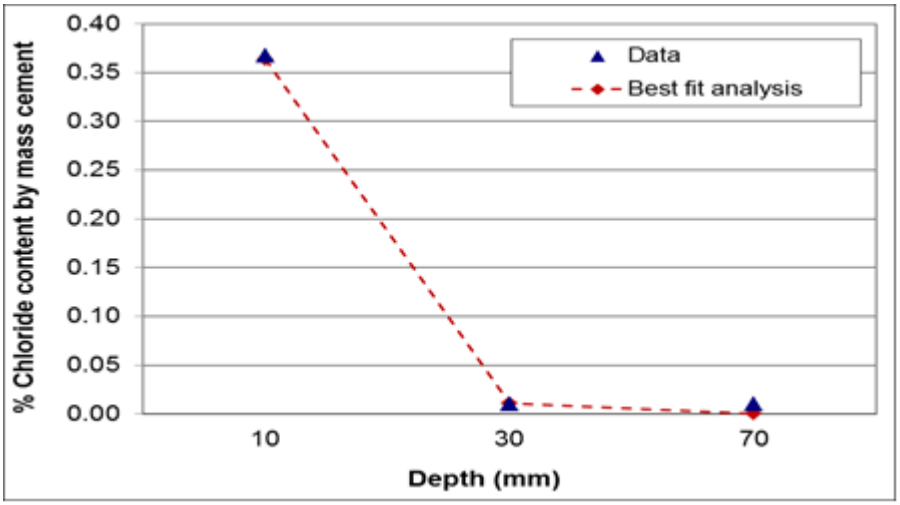

Figure 6.30 Best fitted curve to calculate chloride diffusion using Fick's 2nd law of diffusion, AAS concrete

Table 6.16 Chloride diffusion and surface chloride content

Specimen	Chloride diffusion coefficient (D) (m^2/s)	Surface chloride content (C_s) (%)
AAS	$8.34x10^{-12}$	0.98385
OPC *	$11.8x10^{-11}$	0.16

Note: * Adam (2009)

Table 6.17 Comparison of chloride diffusion and surface chloride content

Specimen	Chloride diffusion coefficient (D) (m^2/s)	Surface chloride content (Cs) (%)
Fly ash geopolymer	$7.96x10^{-10}$	0.28968
AAS	$8.34x10^{-12}$	0.98385
OPC *	$11.8x10^{-11}$	0.16

Note: * (Adam, 2009)

The surface chloride content analysis shows that the AAS concrete exhibits a higher surface chloride content compared to fly ash geopolymer concrete as shown in **Table 6.17** (obtained from best fitted curve, 2nd Fick's Law). The results obtain from accredited laboratory tests also show a high chloride content (by mass cement, **Table 6.16**) at a depth of 0 – 20mm. However, the low value of chloride content at a depth of 40 – 100mm indicates that the chloride is accumulated at the surface layer and showed a very slow diffusion process due to the low porosity and permeability of the bulk concrete.

This finding together with the resistivity results of the previous section show that AAS concrete demonstrates a high level of resistance to chloride ingress. Similar finding were also found by Roa-Rodriguez et al. (2014). According to the authors, AAS concrete demonstrates a low value of chloride permeability and high resistance of electrical resistivity indicating that this material can be considered as a high performance material.

6.8.7. Depth of carbonation

The results of the accelerated carbonation of AAS concrete are shown in **Figure 6.31** and **Figure 6.32.** The change of colour between carbonated and non-carbonated region is shown in **Figure 6.31**.

The overall colour of the non-carbonated region of AAS concrete is dark pink coloured after spraying with the phenolphthalein indicator (darker than for the geopolymer concrete), (**Figure 6.31**). Hence, it can be inferred that AAS concrete demonstrates a higher pH of the pore solution compared to fly ash geopolymer concrete in previous discussions (**Section 5.8.7**).

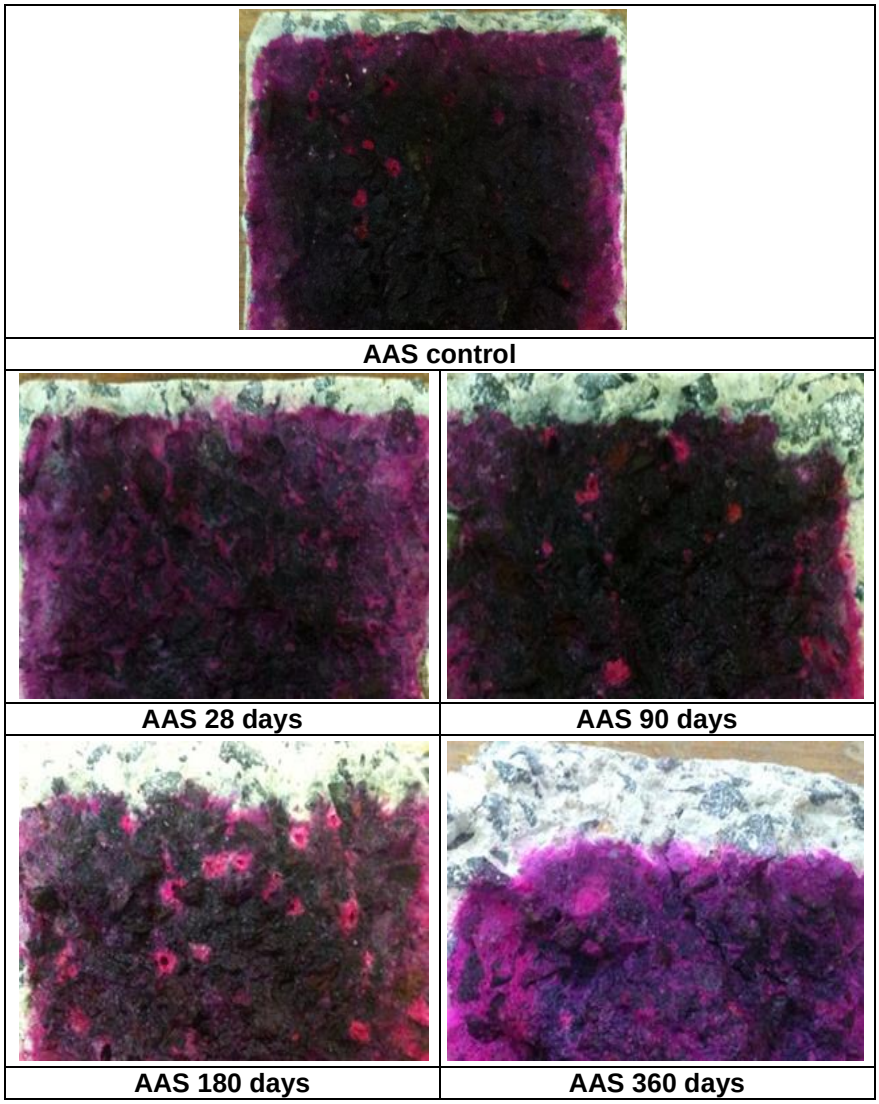

Figure 6.31 Depth of carbonation AAS concrete using phenolphthalein indicator

The AAS specimens show a clear definition between the carbonated and un-carbonated concrete (**Figure 6.31**). The carbonation is similar to that of OPC concrete due to the similarity of the hydration products of $Ca(OH)_2$ and the C-S-H gel. If full carbonation occurs, the border between the carbonated and un-carbonated concrete can be seen clearly due to the availability of $Ca(OH)_2$ and C-S-H in concrete specimens (Neville, 2011).

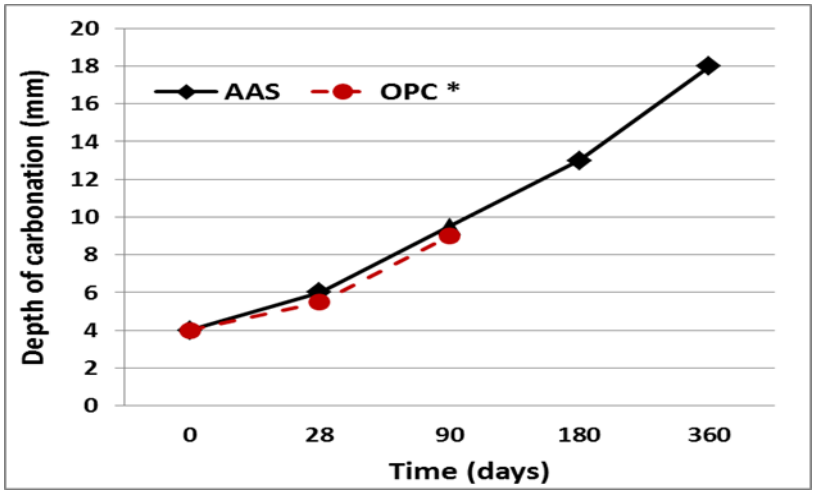

Note: * Adam (2009)

Figure 6.32 Depth of carbonation of AAS concrete

Table 6.18 Depth of carbonation (X) and carbonation rate coefficient (C) of AAS concrete

Carbonation	Age (days)				
	0	28	90	180	360
Depth of carbonation (X) (mm)	4.0	6.0	9.5	13.0	18.0
Carbonation rate coefficient (C) (mm/days$^{1/2}$)	0.00	0.38	0.58	0.67	0.74

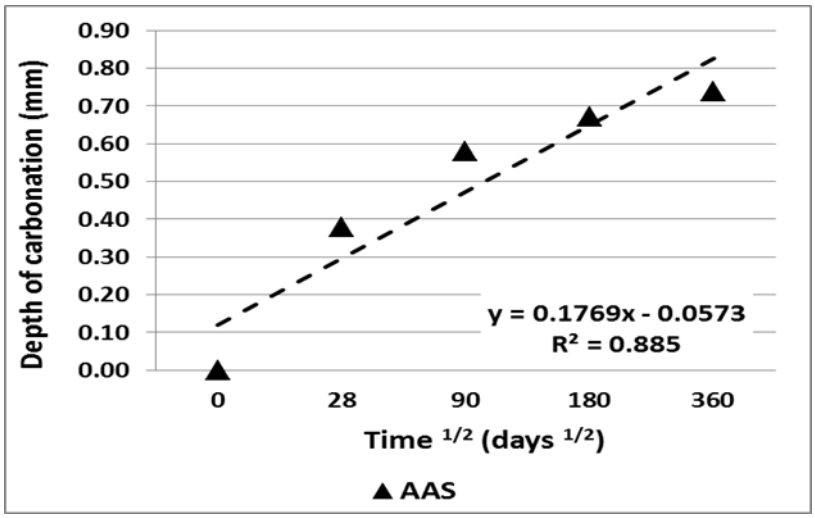

Figure 6.33 Depth of carbonation of AAS concrete versus square root of time

The depth of carbonation (X) (**Table 6.18**) versus time ($t^{1/2}$) data was fitted by a function as shown in **Figure 6.33**. It was found that the relationship in **Equation 2.26** gave a good correlation coefficient (R) with a coefficient of determination of 88.50% and suggested that the model fitted the data well. The values of carbonation rate coefficient (K) are also presented in **Table 6.18**.

The average carbonation rate coefficient (C) of AAS concrete is 0.59 mm/days$^{1/2}$ which is a slightly higher value than for OPC concrete (C = 0.41 mm/days$^{1/2}$) (Adam, 2009). There are two reasons for the higher rate of carbonation. Firstly, the low content of CaO in the slag precursors compared to OPC concrete (**Table 3.1**) which leads to little material being available to react with CO_2. This is similar to fly ash geopolymer concrete, however, the content of CaO in slag is higher than in fly ash. Therefore, the AAS concrete demonstrates a lower rate of carbonation compared to fly ash geopolymer concrete. Secondly, according to Bakharev et al. (2001), when AAS concrete is exposed to an atmosphere rich in CO_2, there is a reduction in pH at the surface and crystallisation of calcite as well as decalcified of the C-S-H gel. This leads to an increase of porosity, thus increasing the penetration rate. Furthermore, due to the low ratio of Ca/Si in the C-S-H gel of AAS concrete, the decalcification of the C-S-H gel as a result of carbonation is faster compared to the carbonation rate of $Ca(OH)_2$ in OPC concrete.

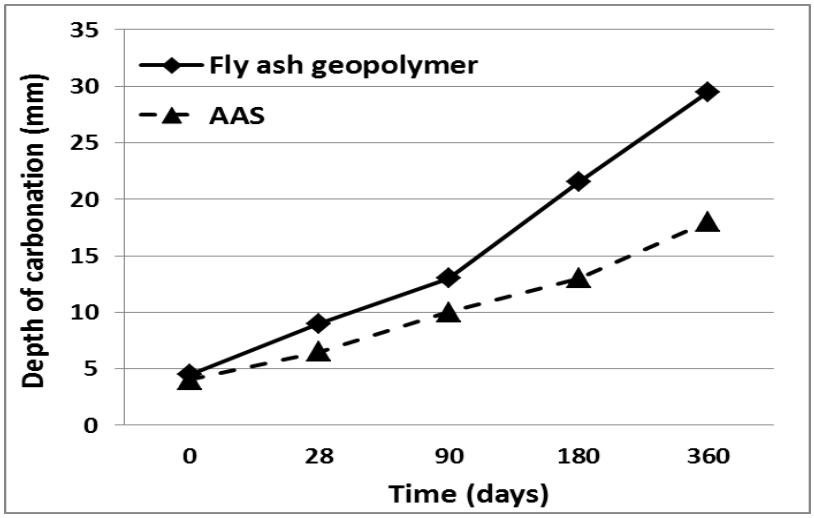

Figure 6.34 Carbonation of AAS and fly ash geopolymer concretes

Compared to fly ash geopolymer concrete, the products of AAS concrete are $Ca(OH)_2$ and C-S-H which are the main reactants for the carbonation reaction, However, the carbonation of AAS concrete is slower (**Figure 6.34**). This is attributed to the lower permeation properties of AAS concrete compared to fly ash geopolymer concrete which leads to a less porous material, thereby decreasing the rate of penetration of CO_2.

6.9. Summary of chapter 6

The result of the investigation on the long term mechanical properties of AAS concrete can be summarized as follows:

1. The average density of AAS concrete is 2460 kg/m^3 and shows a comparable value to that of OPC concrete (density of approximately 2400 kg/m^3). The density of AAS concrete increases with time.
2. AAS concrete demonstrates a comparable compressive strength to OPC concrete in the short term. However, it shows a decrease in strength with age.
3. The strength development of AAS concrete is affected by the Si/Al ratio. A higher Si/Al ratio tends to delay the early age reaction and results in a low initial strength.
4. The AAS concrete exhibits a comparable modulus of elasticity to that of OPC concrete in short term behaviour. However, it shows a reduction in with time.
5. The flexural tensile strength and uniaxial tensile strength of AAS concrete decrease with time. These findings are consistent with the decrease of compressive strength and modulus of elasticity in long term performance.
6. Similar to that of fly ash geopolymer concrete, AAS concrete also shows a higher flexural tensile strength compared to uniaxial tensile strength due to the stress distribution during testing.
7. AAS concrete has a comparable modulus of elasticity, higher flexural tensile strength and uniaxial tensile strength compared to OPC concrete in short term periods. However, the use of AAS concrete over the long

term needs to be further studied on account of the reduction of these properties.

8. For AAS concrete, the relationship between the modulus of elasticity, flexural tensile strength and uniaxial tensile strength with compressive strength shows an opposite trend to that of OPC concrete.
9. Although AAS concrete exhibits comparable mechanical properties with OPC concrete in short term performance, the decrease of compressive strength, decrease of modulus of elasticity and decrease of tensile strength indicates that the existing Australian standard (AS 3600, 2009) might not be applied to AAS concrete.
10. In general, AAS concrete demonstrates a better performance than fly ash geopolymer concrete. However, due to reduction in performance with time it is suggested that the use of AAS concrete is not recommended for long term use at present.

In terms of durability properties, the result of the investigation of AAS concrete can be summarized as follows:

1. The porosity and water absorption of AAS concrete shows a low value. This is attributable to the high fineness and the irregular shape of the slag precursors. The irregular shape correlates to a high specific surface area, thus increasing the reaction between the slag and the solution which leads to a high density and results in lower porosity.
2. Although AAS concrete demonstrates a low value of porosity and water absorption, the increase of porosity and water absorption with time indicates that the behaviour in long-term durability is questionable.
3. AAS concrete exhibits a decrease of UPV with time which indicates that the quality of AAS concrete is reducing over time. Compared to OPC concrete, AAS concrete demonstrates a comparable performance in velocity.
4. AAS concrete shows a low value of water permeability due to the high quality dense surface. This is attributable to the high fineness of the slag precursors which fill the gaps in the pore structure.

5. AAS concrete demonstrates a negative linear relationship between compressive strength, modulus of elasticity and tensile strength and UPV with time. This shows a different behaviour to that shown by OPC concrete. A decrease of mechanical properties is associated with a decrease of UPV. A decrease in mechanical properties of AAS concrete is associated with an increase of porosity and water absorption.
6. AAS concrete exhibits a high resistivity in short term performance which indicates a low likelihood of corrosion. This attributable to the low porosity and water permeability, leading to the low ion concentration within the pore structure.
7. AAS concrete demonstrates low chloride diffusion due to the low porosity and low permeability value. This is also attributable to the NaOH concentration which increases the chloride binding capacity of the concrete.
8. The depth of carbonation of AAS concrete is slightly higher than that of OPC concrete. This attributable to the slightly lower CaO content in the slag precursors which leads to less material available to react with the CO_2.
9. The rate of carbonation of AAS concrete demonstrates a lower value compared to fly ash geopolymer concrete due to the higher content of CaO in the slag precursors to react with CO_2. This also attributable to the lower porosity and permeability of AAS concrete.
10. In general, AAS concrete demonstrates a good durability performance in resisting chloride diffusion and carbonation. However, an increase in porosity and permeation properties coupled with a reduced UPV with age raises a question regarding the long term performance of AAS concrete.

7. MICROSTRUCTURE STUDIES OF FLY ASH GEOPOLYMER AND AAS CONCRETES

7.1. Overview

A microstructure study was performed to investigate the structure of the fly ash geopolymer and AAS concrete, particularly the pore structure and the potential presence of micro-cracks. Scanning Electron Microscopy (SEM) was used to obtain surface images and to record micrographs. Energy Dispersive X-Ray Spectroscopy (EDX) was used as an additional tool for semi-quantitative analysis to identify the percentage of each element within the specimens. Only the major elements are shown together with the calculation of the Si/Al ratio and Ca/Si ratio for the fly ash geopolymer and AAS concretes, respectively.

The SEM analysis was undertaken on a Philips XL30 SEM using high vacuum mode as well as backscatter electron detectors. The microscope was coupled with an Oxford X-MaxN 20 EDXS Detector for elemental analysis. The working voltage was between 10 – 30 kV, dependant on the magnification requirement of the specimen. The spot size was set to 5. The analysis of the EDX spectra was performed using Moran Scientific Analysis software.

The process of sample preparation for the SEM investigation was as follows: the samples were cut using a diamond saw to a size of 3 to 6 mm in height and approximately 10 mm in diameter. The samples were then left to dry in the oven for 24 hours to remove any moisture before they were gold coated for imaging. The samples for EDX analysis were left un-coated. Samples were mounted on the SEM sample stage with conducting double-sided carbon tape. The SEM and EDX analysis was performed using two samples for each data point of fly ash geopolymer and AAS concrete.

7.2. Microstructure study of fly ash geopolymer specimens

7.2.1. Fly ash geopolymer mortars

Images of the concrete matrix of the fly ash geopolymer mortars FG-A and FG-B are presented in **Figure 7.2**, **Figure 7.3**, **Figure 7.4**, and **Figure 7.5**.

Based on the SEM image analysis of the fly ash geopolymer mortar at an alkali modulus (M_s) = 1.00, the microstructure of FG-A (GA15-100) (**Figure 7.2**) shows a less dense microstructure with a more porous surface compared to FG-B (GB15-1.00). This is attributed to the Si/Al ratio in the FG-A. The Si/Al ratio of FG-A (Si/Al ratio = 6.5) (**Figure 7.3**) is higher than that of FG-B (with a Si/Al ratio of 3.6). The high Si/Al ratio found in FG-A would delay the geopolymer reaction time and is hypothesised as the reason for the low strength development of the FG-A mortar as shown in **Figure 7.1(a)**.

The microstructure of fly ash geopolymer mortar specimens at the higher alkali modulus, (M_s) = 1.25, were found to have a more porous surface than for the corresponding mortars at (M_s) = 1.00. The Si/Al ratio of FG-A (GA15-100) is 6.5 (**Figure 7.2**) and increases to 9.1 at M_s = 1.25 (**Figure 7.7**), while FG-B (GB15-1.00) has a Si/Al ratio of 3.6 (**Figure 7.3**) which increases to 4.5 at the higher alkali modulus (**Figure 7.4**). The higher Si/Al ratio is again hypothesised as the cause of the reduction of strength, **Figure 7.1(b)**.

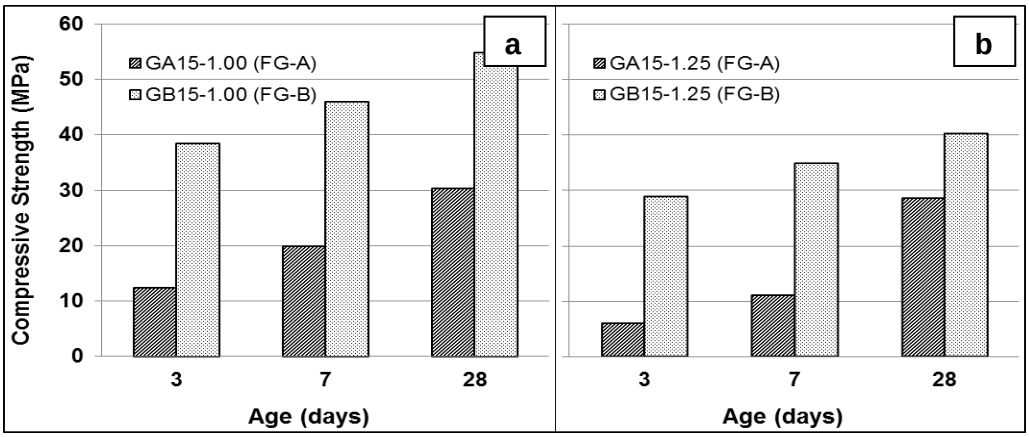

Figure 7.1 Comparison of strength due to the effect of alkali modulus; Fly ash geopolymer mortars FG-A and FG-B

The higher amount of crystalline form in PFA 1 (as described in **Section 3.2.1 Chapter 3**) also affects the strength development of FG-A. The crystalline compounds are more difficult to dissolve than the amorphous compounds during the first step of geopolymerisation (dissolution mechanism) and yield lower amounts of reactive SiO_2 and Al_2O_3 to combine during the transportation

(coagulation phase) of geopolymeric reaction, thus resulting in a lower mechanical strength (Diaz-Loya et al., 2010).

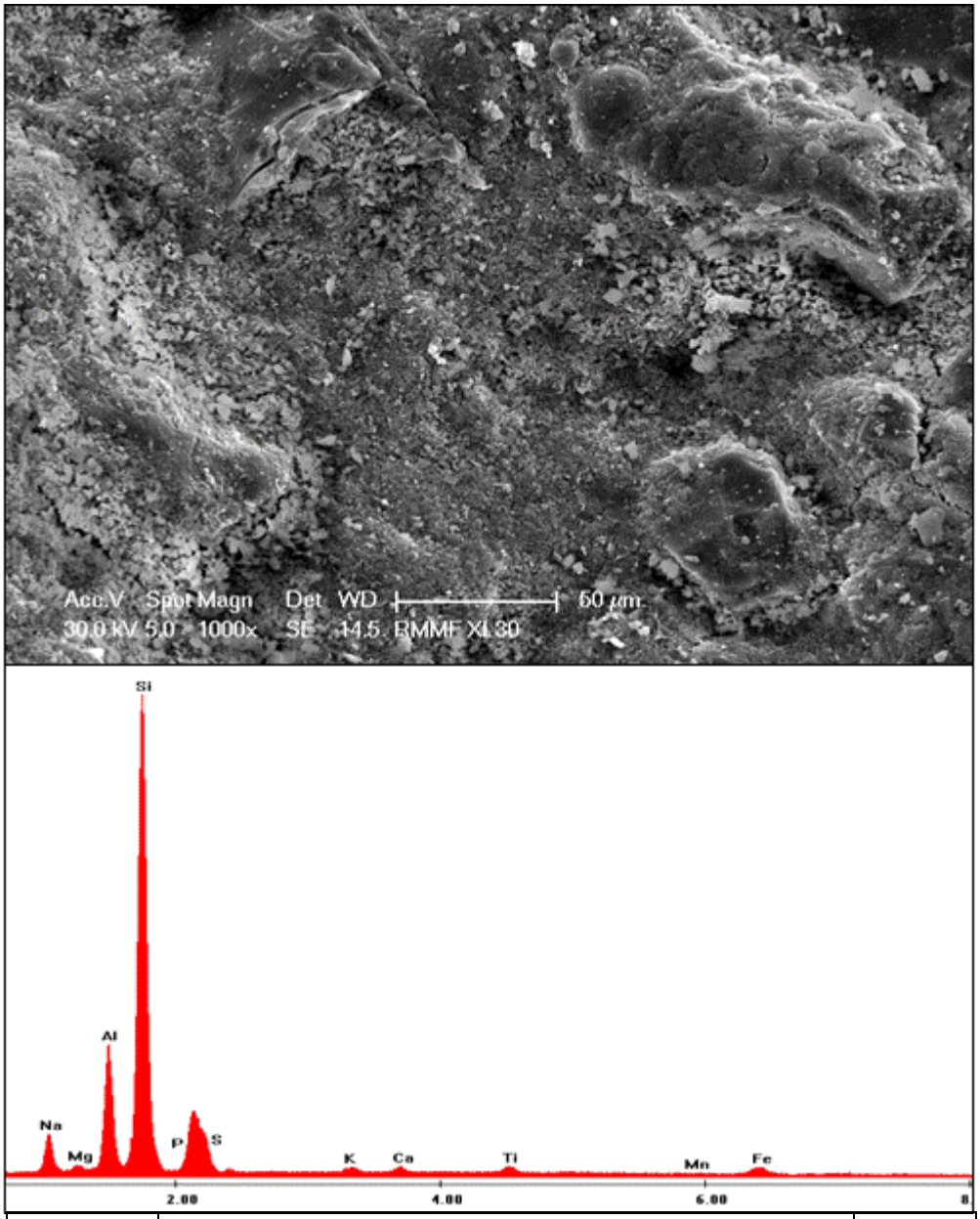

Spot/Area	Element (%)						Si/Al ratio
	Na	Mg	Al	Si	Ca	Fe	
Surface	6.3	0.7	10.8	70.4	1.2	2.5	6.5

Figure 7.2 Fly ash geopolymer mortar, FG-A ; GA15-1.00

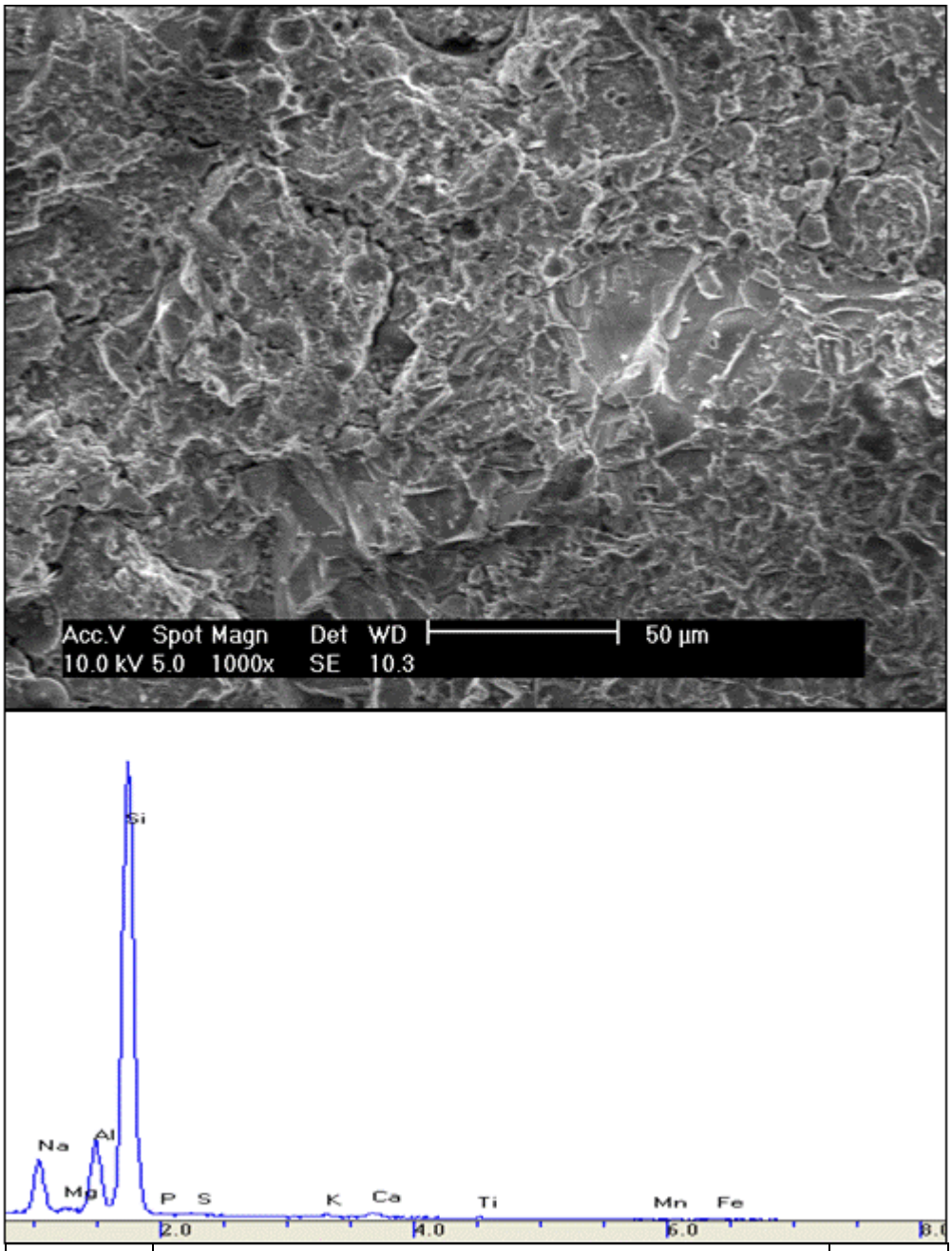

Spot/Area	Element (%)						Si/Al ratio
	Na	Mg	Al	Si	Ca	Fe	
Surface	19.2	0.8	17.2	61.5	1.0	0.2	3.6

Figure 7.3 Fly ash geopolymer mortar, FG-B ; GB15-1.00

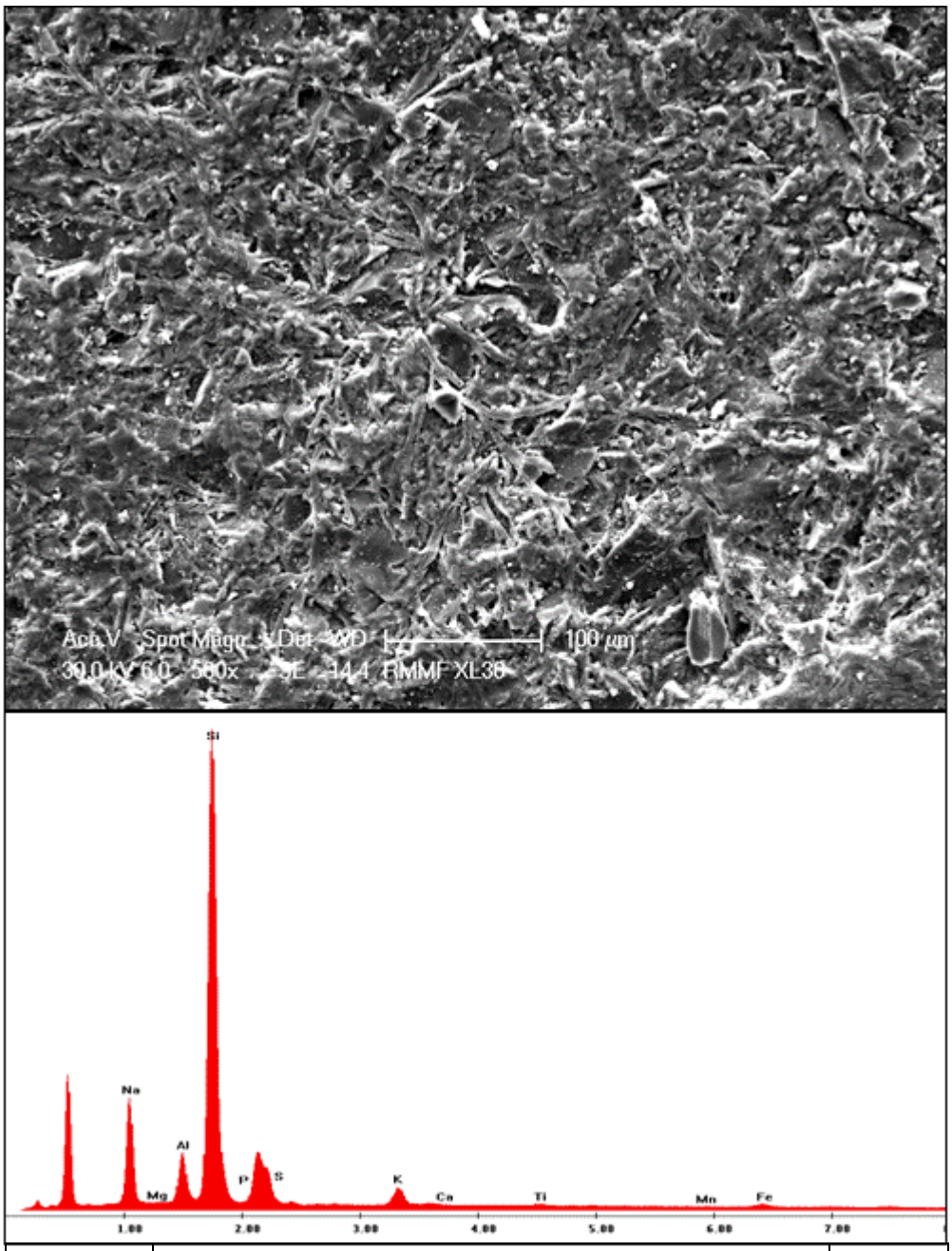

Spot/Area	Element (%)						Si/Al ratio
	Na	Mg	Al	Si	Ca	Fe	
Surface	19.9	0.1	7.4	67.1	0.2	0.7	9.1

Figure 7.4 Fly ash geopolymer mortar, FG-A ; GA15-1.25

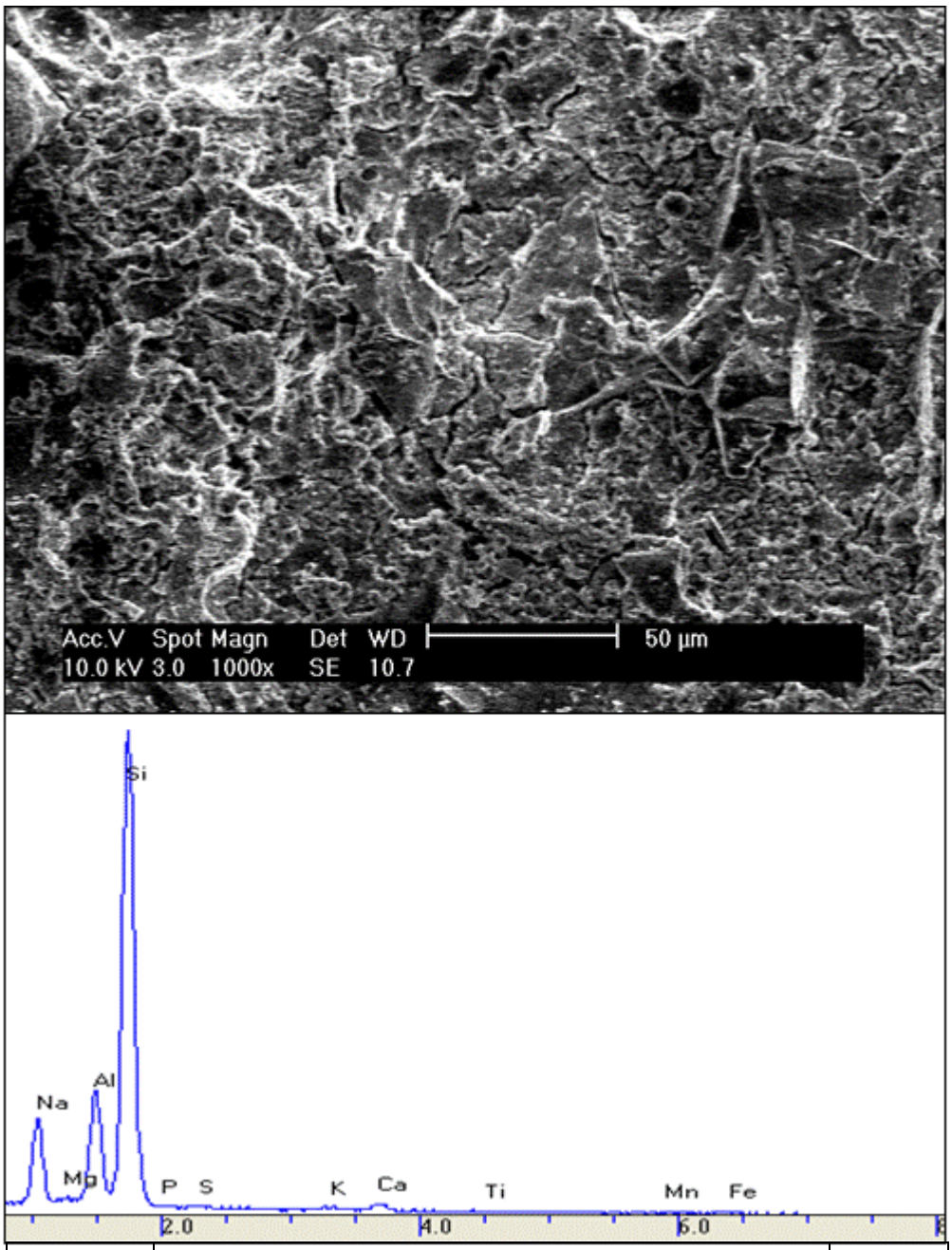

Spot/Area	Element (%)						Si/Al ratio
	Na	Mg	Al	Si	Ca	Fe	
Surface	12.6	0.4	14.9	66.4	2.7	2.4	4.5

Figure 7.5 Fly ash geopolymer mortar, FG-B ; GB15-1.25

7.2.2. Fly ash geopolymer concrete

The concrete matrix of the fly ash geopolymer concrete is shown in **Figure 7.8** and **Figure 7.9**. Based on the SEM image analysis, the microstructure is identified as being porous and leads to the high permeation properties as shown in **Figure 7.7**. These explain the high carbonation and chloride diffusion rate on the previous findings (**Section 5.8**). The porous microstructure is also responsible for the low strength of fly ash geopolymer concrete as shown in **Figure 7.6**.

The major components found in fly ash geopolymer concrete are Si and Al, with other elements such as Na, Mg, Ti and Fe being found in significantly lower quantities. According to Davidovits (2002), the structure of a geopolymer matrix is determined by the atomic ratio of Si/Al during the geopolymerisation process. Based on the EDX analysis in **Figure 7.8** and **Figure 7.9**, it is apparent that the matrix of the fly ash geopolymer concrete mainly comprises Si-Al-O. The geopolymer matrix is identified as a (Si)-polysialate-disiloxo, which forms a -Si-O-Al-O-Si-O-Si-O- geopolymer matrix with a Si/Al ratio of 3.38.

The high Si/Al ratio of fly ash geopolymer concrete at 3.38 (Si/Al ratio > 1) is hypothesised as the cause of the slow development of the mechanical properties of fly ash geopolymer concrete. These properties being related to the slow strength development observed in the material. **Figure 7.6** exhibits the mechanical properties development of fly ash geopolymer concrete over time. The initial mechanical properties exhibit a low strength, however they show a significant increase over time. The increase of mechanical properties follows by the decrease of the permeation properties as shown in **Figure 7.7**.

According to (Silva et al., 2007), a high Si/Al ratio affects the setting time of the geopolymeric reaction during the condensation stage. A condensation reaction between aluminates and silicates predominantly occurs in a mixture with a low Si/Al ratio (Si/Al ratio ~ 1). This results, primarily, in the formation of (Si)-polysialate geopolymer structures. An increase of the Si/Al ratio (Si/Al > 1), however, leads to the formation of oligomeric silicates, a condensation reaction among the silicates themselves, and creates a geopolymeric network of (Si)-polysialate-siloxo and (Si)-polysialate-disiloxo. Other authors have assumed that the rate of condensation between aluminates and silicates is faster than among silicates (Weng & Sagoe-Crentsil, 2007, Sagoe-Crentsil & Weng, 2007).

The SEM analysis also shows un-reacted fly ash microspheres (**Figure 7.10**, **Figure 7.12** and **Figure 7.14**) and partially dissolved fly ash (**Figure 7.11**, **Figure 7.13**). These un-reacted particles are due to the high silicate content in the fly ash precursors. The presence of the unreacted particles is summarised as being the cause of the slow strength development with time as shown in **Figure 7.6**.

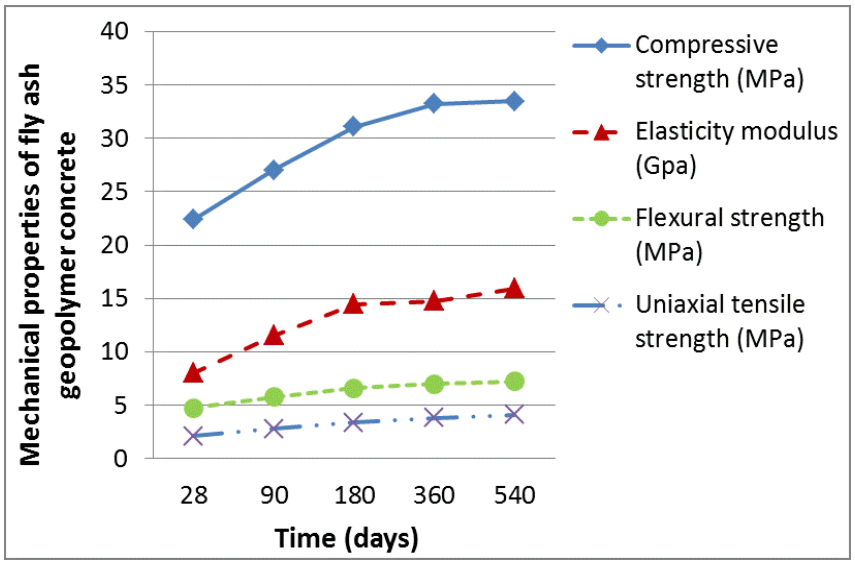

Figure 7.6 Mechanical properties of fly ash geopolymer concrete

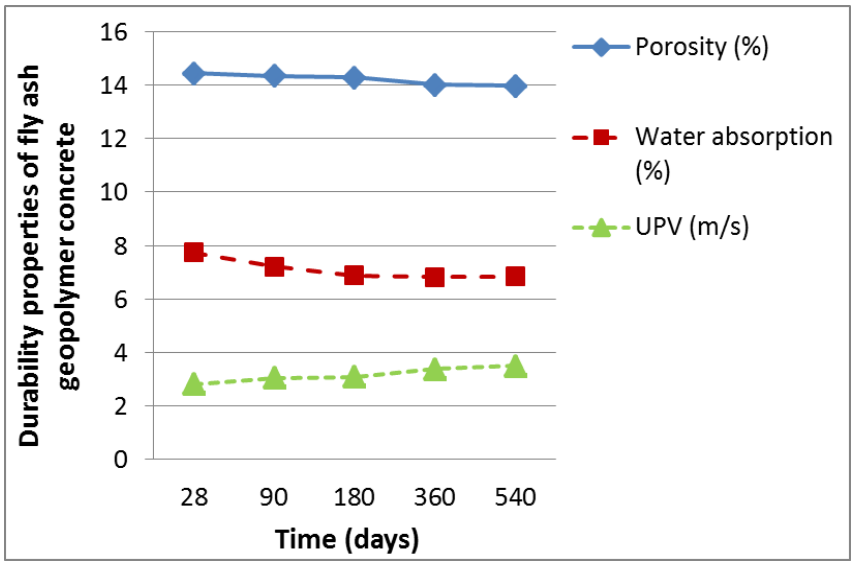

Figure 7.7 Durability properties of fly ash geopolymer concrete

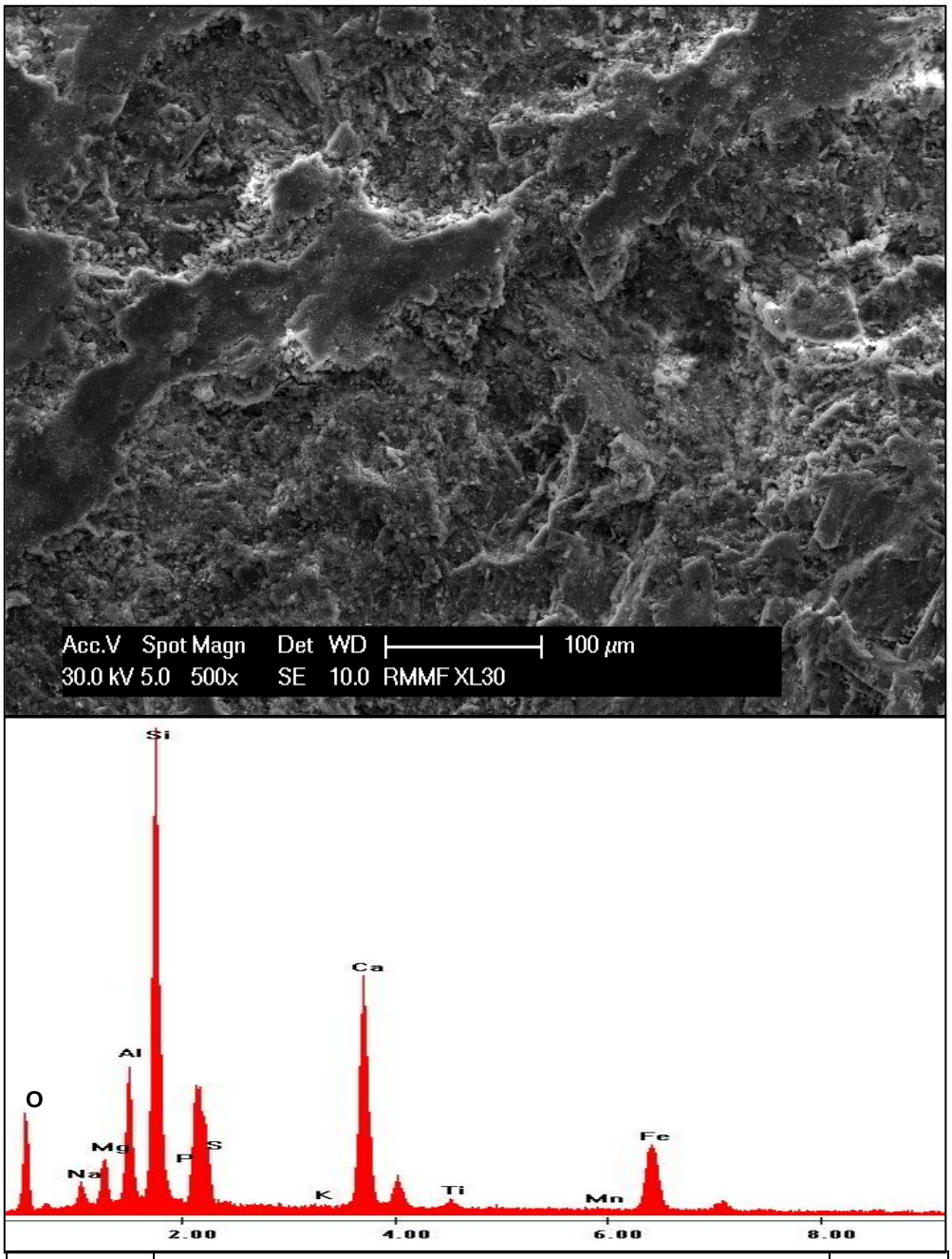

Spot/Area	Element (%)						Si/Al ratio
	Na	Mg	Al	Si	Ca	Fe	
Surface	3.9	5.1	12.4	42.7	18.9	10.8	3.44

Figure 7.8 Fly ash geopolymer concrete, area 1, at 360 days

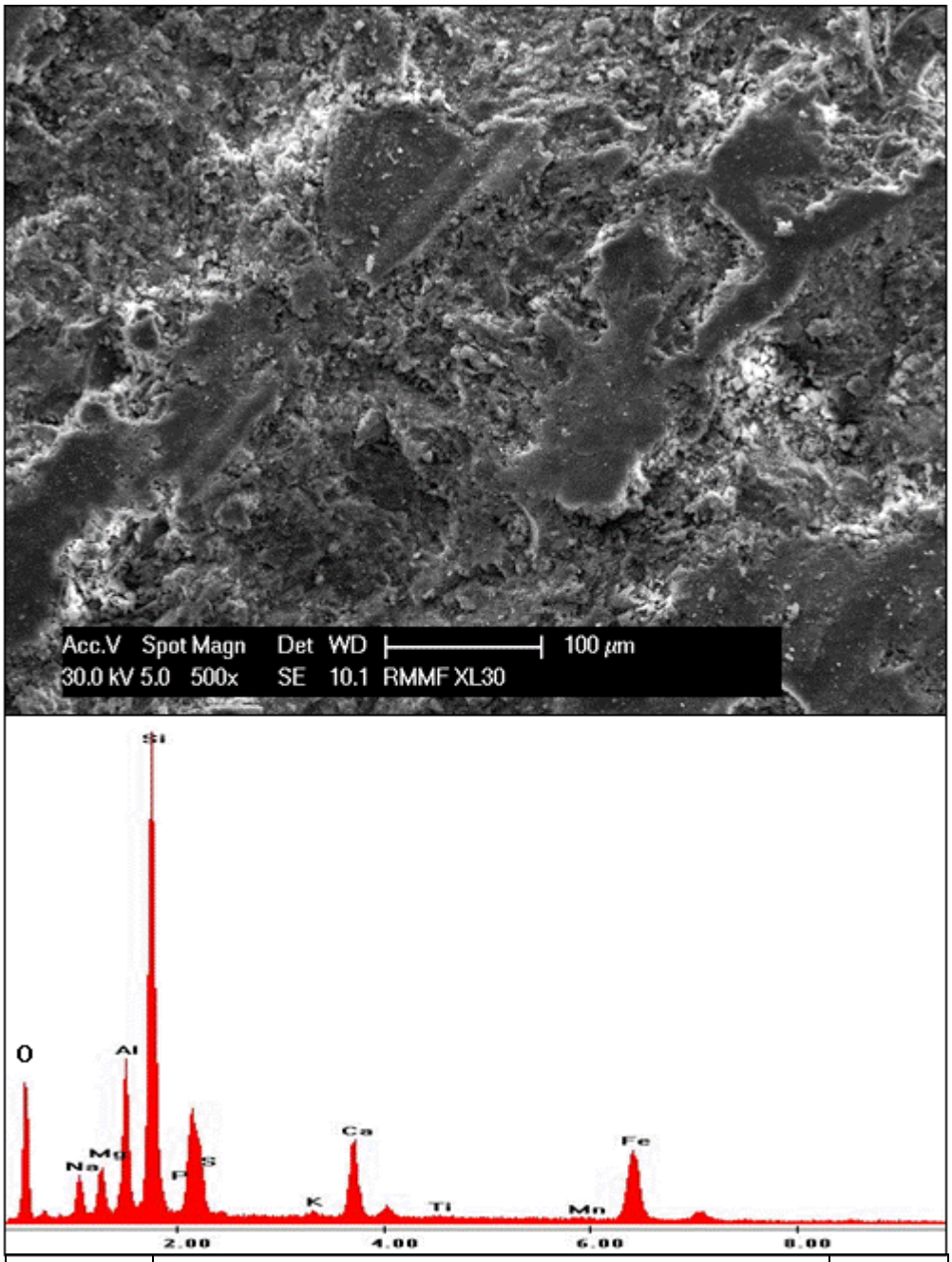

Spot/Area	Element (%)						Si/Al ratio
	Na	Mg	Al	Si	Ca	Fe	
Surface	4.9	5.4	14.7	48.7	8.0	7.3	3.32

Figure 7.9 Fly ash geopolymer concrete, area 2, at 360 days

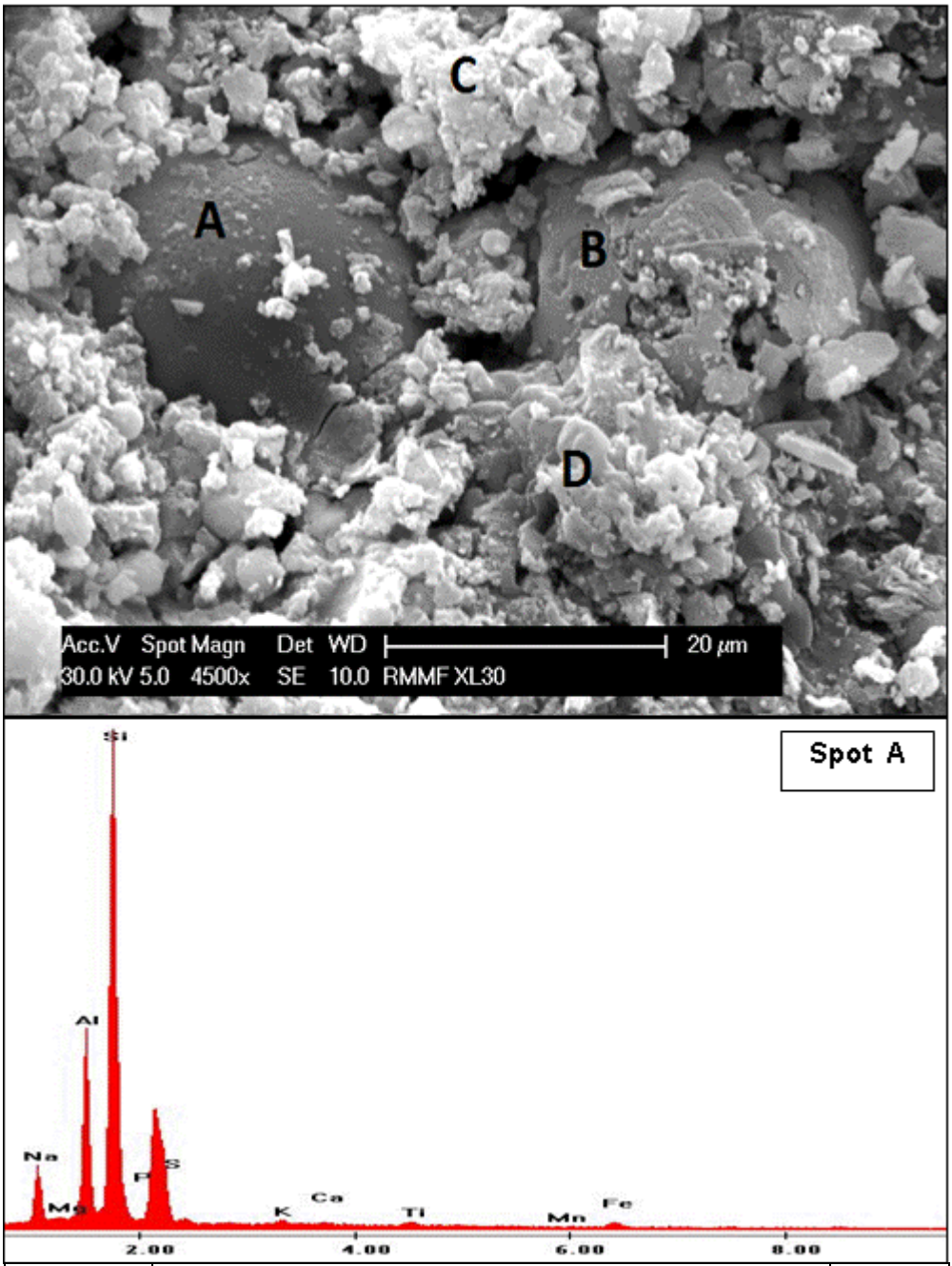

Spot/Area	Element (%)						Si/Al ratio
	Na	Mg	Al	Si	Ca	Fe	
A	7.7	0.3	19.5	66.5	0.5	1.5	3.41
B	1.1	0.3	25.4	67.4	0.3	1.4	2.65
C	7.6	0.2	21.1	64.9	0.4	1.7	3.08
D	5.2	0.3	19.9	69.8	0.3	1.6	3.51

Figure 7.10 Fly ash particles in geopolymeric gel

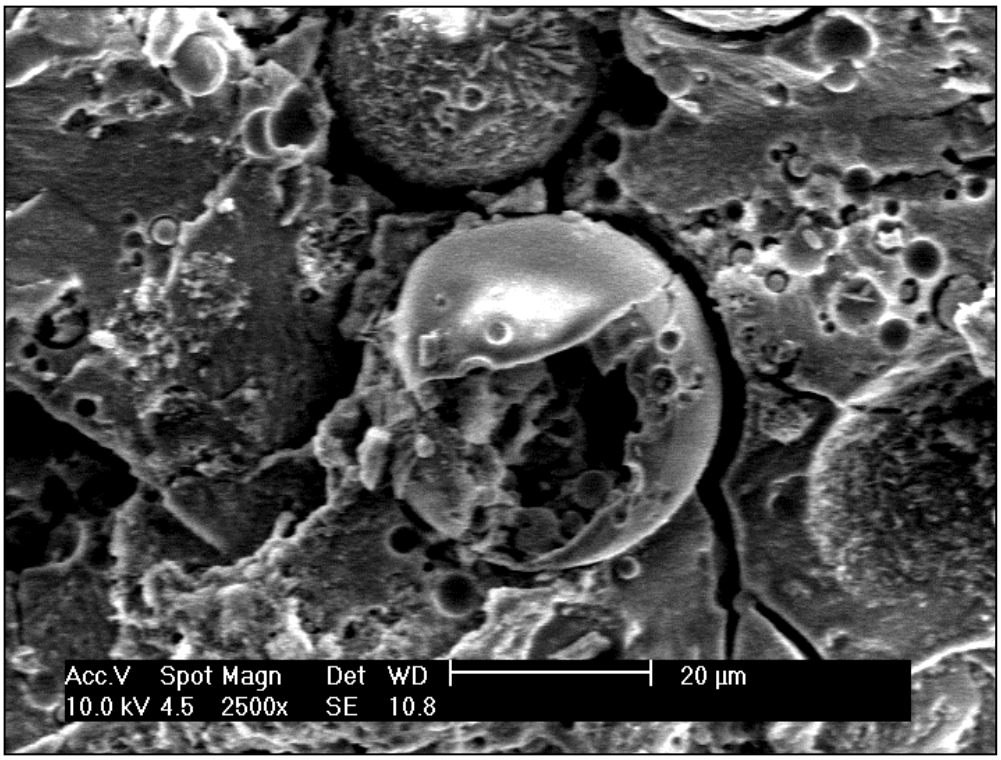

Figure 7.11 Partially dissolved fly ash 1

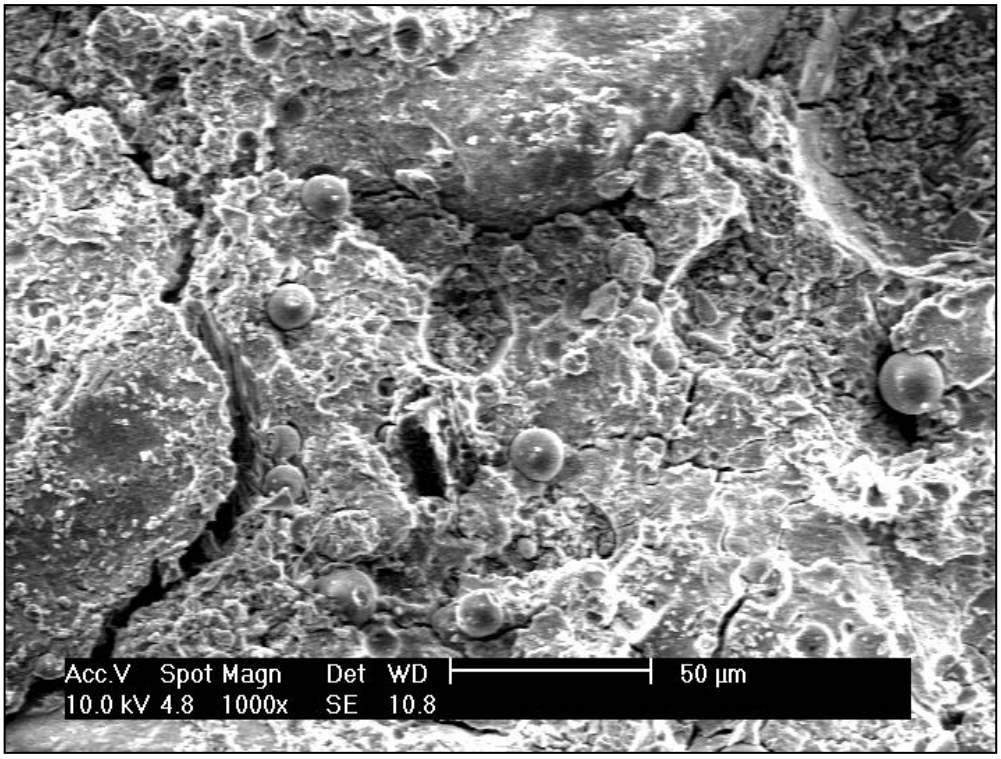

Figure 7.12 Un-reacted fly ash 1

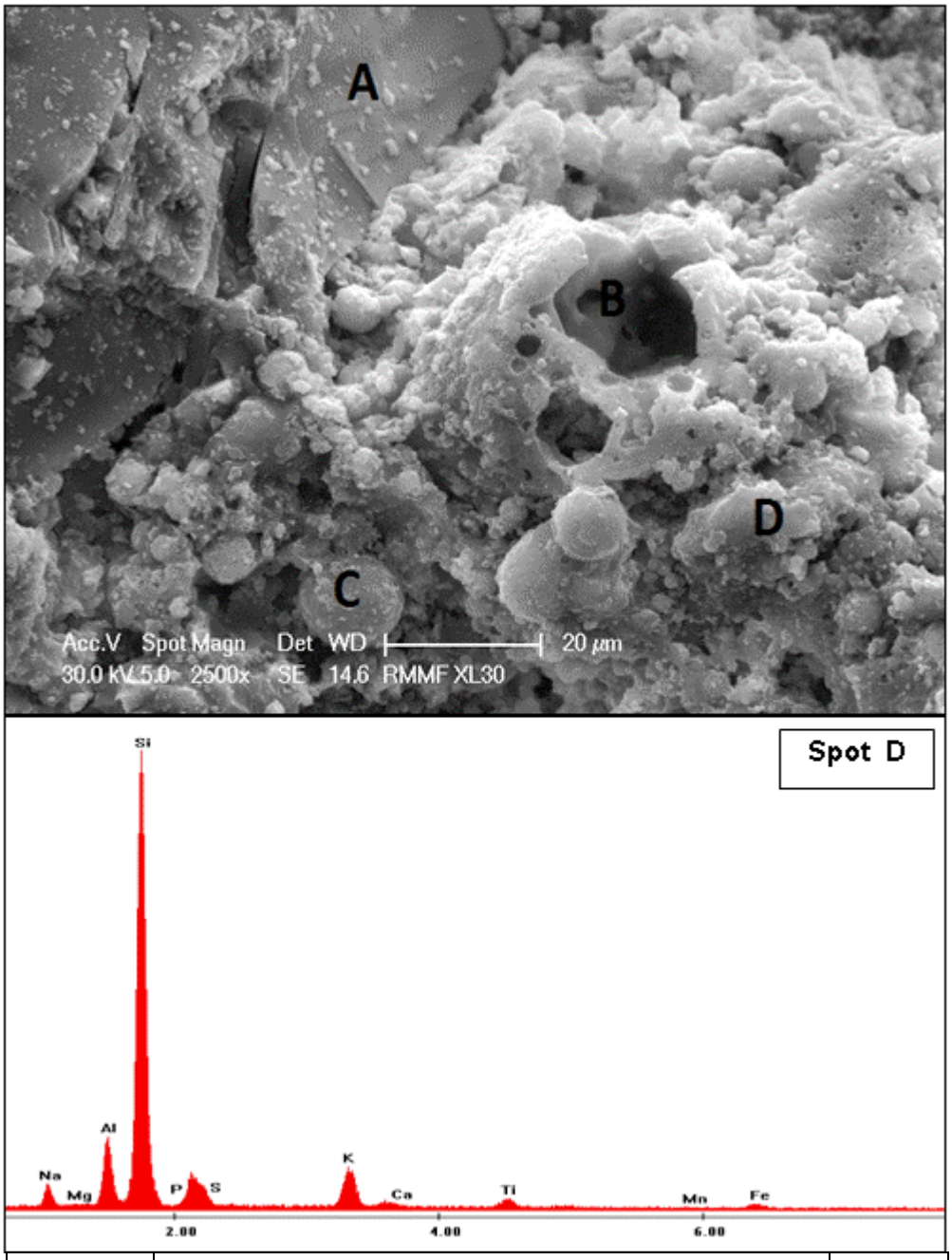

Spot/Area	Element (%)						Si/Al ratio
	Na	Mg	Al	Si	Ca	Fe	
A	1.2	0.1	2.1	91.6	0.1	1.2	43.6
B	1.3	0.3	12.1	51.1	1.6	4.1	4.23
C	1.7	0.1	16.8	64.2	0.2	1.3	3.82
D	4.4	0.2	8.9	70.0	0.5	1.8	7.87

Figure 7.13 Partially dissolved fly ash 2

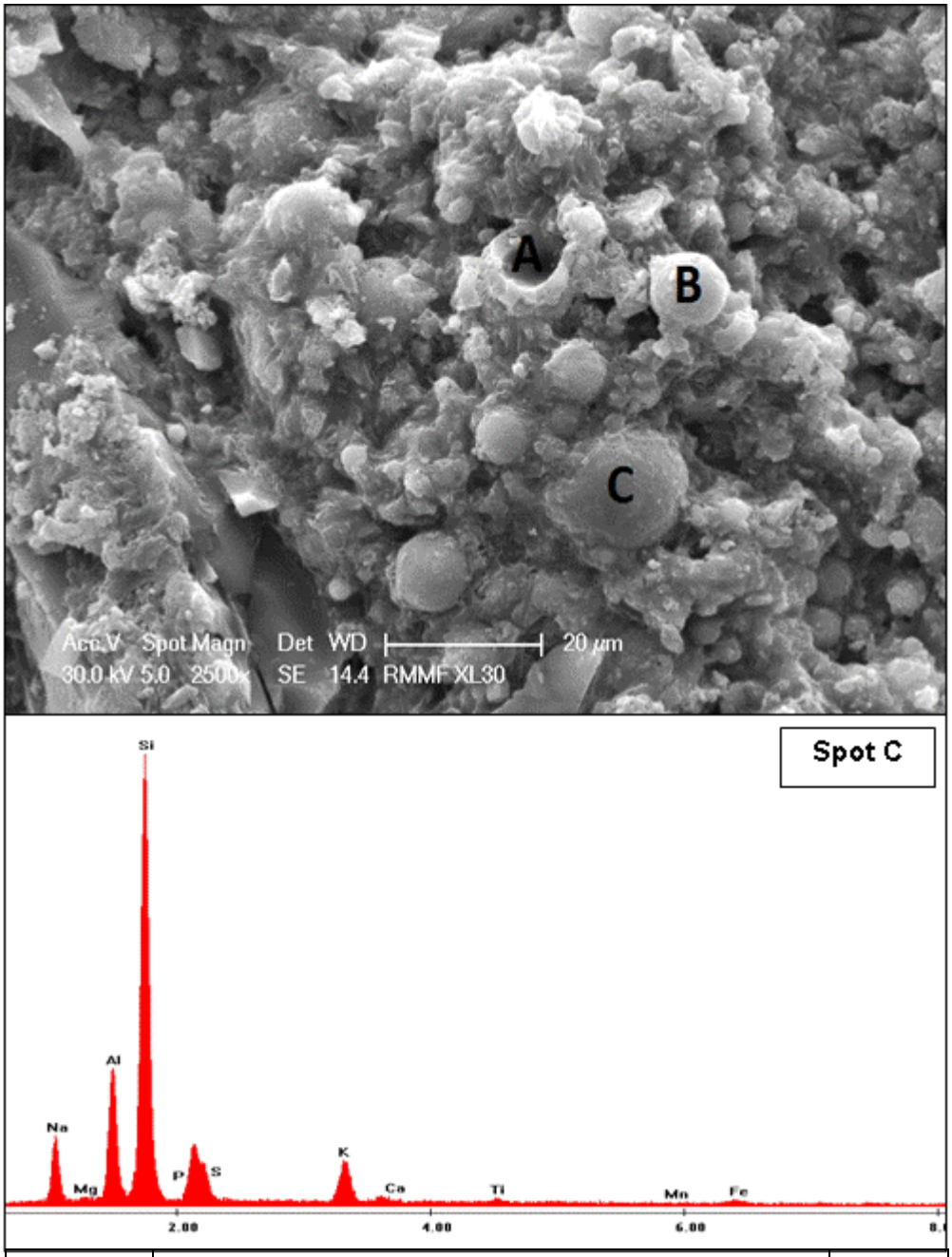

Spot/Area	Element (%)						Si/Al ratio
	Na	Mg	Al	Si	Ca	Fe	
A	9.5	0.3	14.9	63.6	0.4	1.3	4.27
B	15.2	0.1	20.1	52.6	0.2	0.9	2.62
C	15.1	0.2	20.5	54.3	0.1	1.2	2.65

Figure 7.14 Un-reacted fly ash 2

Fly ash geopolymer concrete also exhibits a porous microstructure with cracks/gaps between the fly ash particles and the geopolymer matrix as shown in **Figure 7.13**. This explains the high porosity, high water absorption and high permeability, **Section 5.8**. The porous microstructure is also inferred as the cause of the high rate of carbonation and rate of chloride diffusion, **Section 5.8.6** and **Section 5.8.7**. This can also explain the low strength development over periods of time, in agreement with Steveson & Sagoe-Crentsil (2005), who found that the interface between these particles and the geopolymer matrix significantly affects the overall strength.

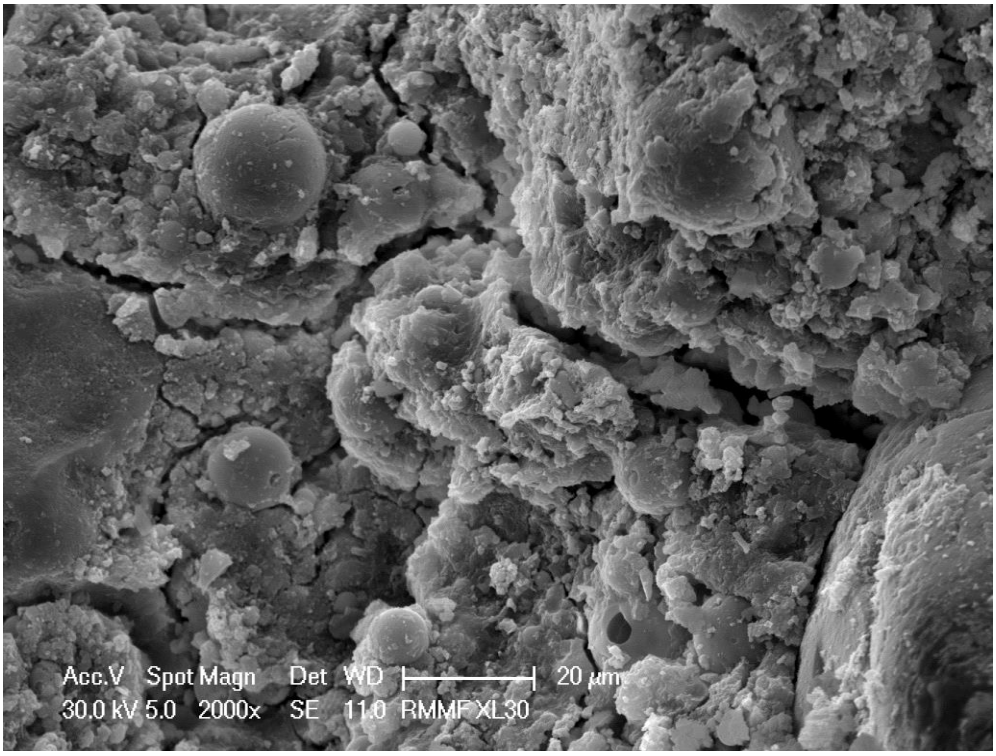

Figure 7.15 Porous microstructure of fly ash geopolymer concrete

7.3. Microstructure study of AAS specimens

7.3.1. AAS mortars

Images of the microstructure of the AAS mortars are presented in **Figure 7.16**, **Figure 7.17** and **Figure 7.18**, respectively. Based on the SEM analysis, the matrix of the AAS5-1.00 and AAS5-1.125 mortars are fairly uniform with the two showing similar appearance (**Figure 7.16** and **Figure 7.17)**. Most of the slag grains have been dissolved by the alkali solution, forming a C-S-H gel with the silica from the solution, as evidenced by the low Ca/Si ratio (**Figure 7.16**, **Figure 7.17**). The microstructure of both AAS mortars appears to be dense, however a few micro-cracks can be observed. The distribution of micro-cracks appears uniform in the surface of the specimens.

The microstructure of the AAS5-1.25 (**Figure 7.18**) is less dense with fewer micro-cracks compared to the AAS5-1.00. However, the size of the micro-cracks at the interface of the C-S-H gel and un-reacted slag particles is wider than for the AAS5-1.00 mix, as shown in **Figure 7.16** and **Figure 7.18**.

The EDX analysis, **Table 7.18,** shows silicate (Si) and calcium (Ca) as the main elements of the AAS mortars. The major hydration products found in all the AAS mixes (AAS5-1.00, AAS5-1.125 and AAS5-1.25) were an amorphous to poorly crystalline C-S-H gel (with a Ca/Si ratio of 0.204, 0.217 and 0.378, respectively). This suggests that the types of C-S-H gel in all the AAS mortars exhibit a Ca/Si ratio lower than that of the C-S-H gel in an OPC based mortar. This is in agreement with other researchers (Chen & Brouwers, 2007, Wang & Scrivener, 1995).

Table 7.18 The Ca/Si ratio of AAS mortars

Mix	M_s	Na	Mg	Al	Si	Ca	Ca/Si Ratio
AAS5-1.00	1.00	5.7	3.4	6.6	69.9	14.2	0.204
AAS5-1.125	1.125	5.6	3.4	6.1	69.5	15.1	0.217
AAS5-1.25	1.25	5.7	2.6	5.8	61.7	23.3	0.378

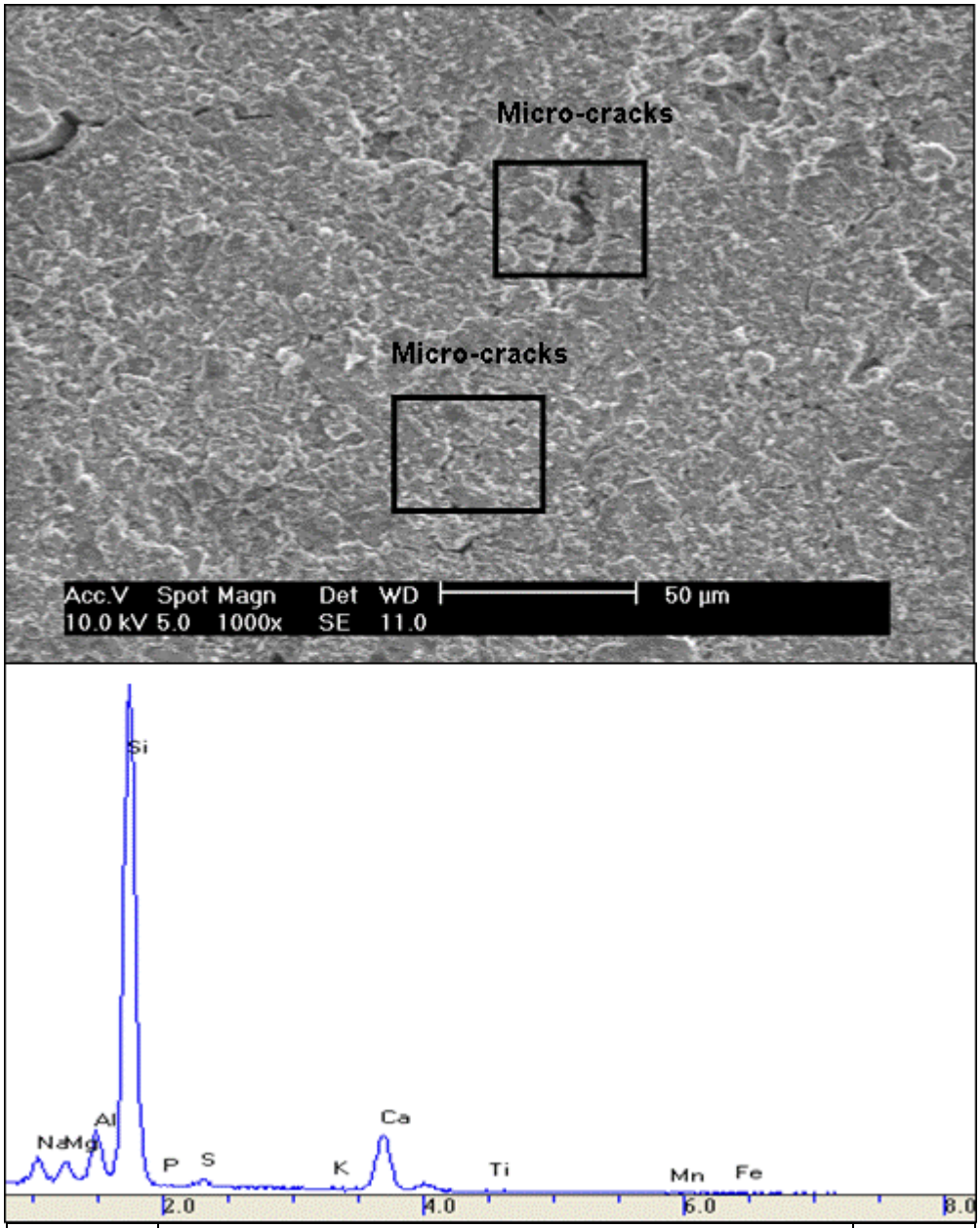

Spot/Area	Element (%)						Ca/Si ratio
	Na	Mg	Al	Si	Ca	Fe	
Surface	5.7	3.4	6.6	69.9	14.2	0.1	0.204

Figure 7.16 SEM image of AAS mortar ; AAS5-1.00

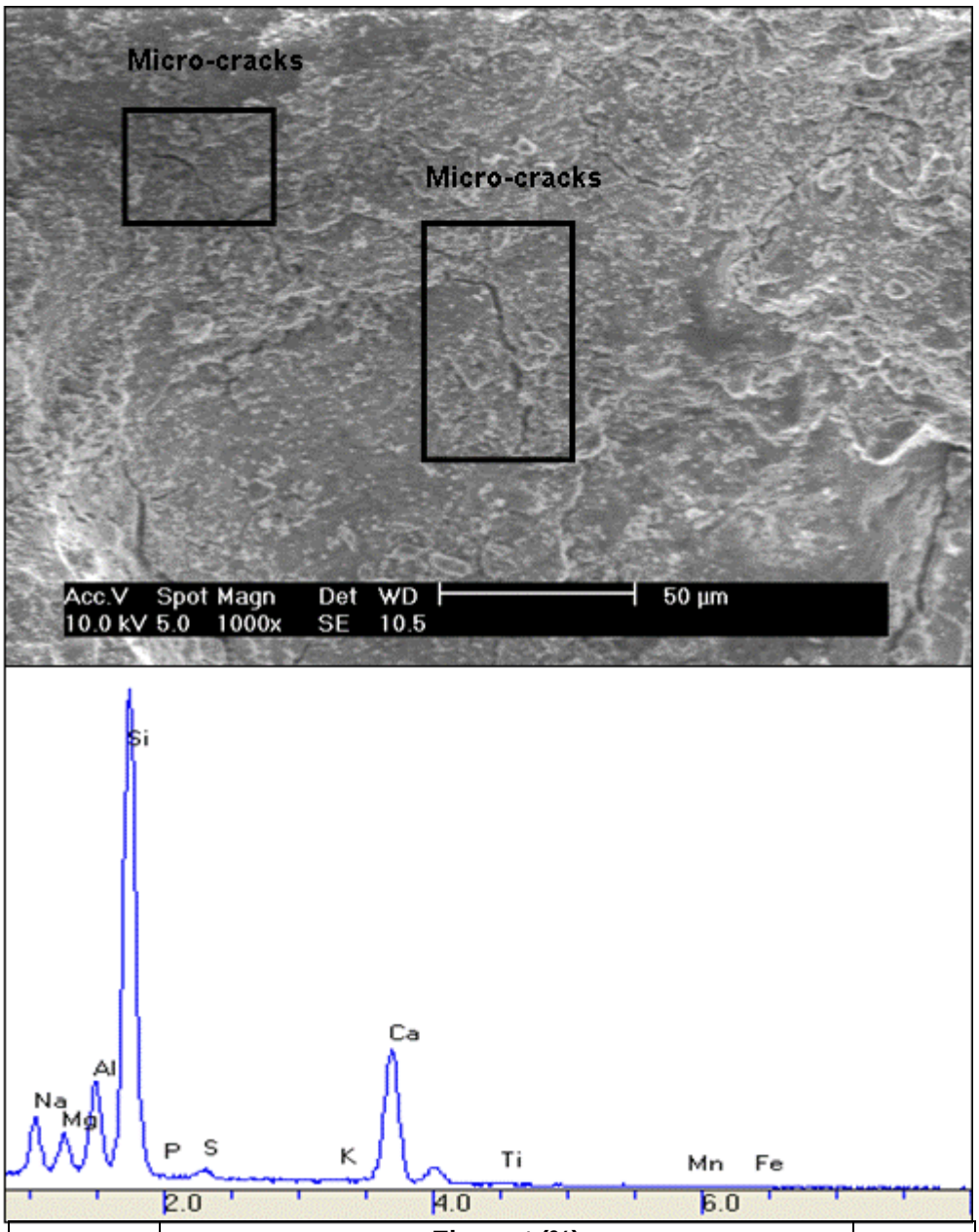

Spot/Area	Element (%)						Ca/Si ratio
	Na	Mg	Al	Si	Ca	Fe	
Surface	5.6	3.4	6.1	69.5	15.1	0.1	0.217

Figure 7.17 SEM image of AAS mortar ; AAS5-1.125

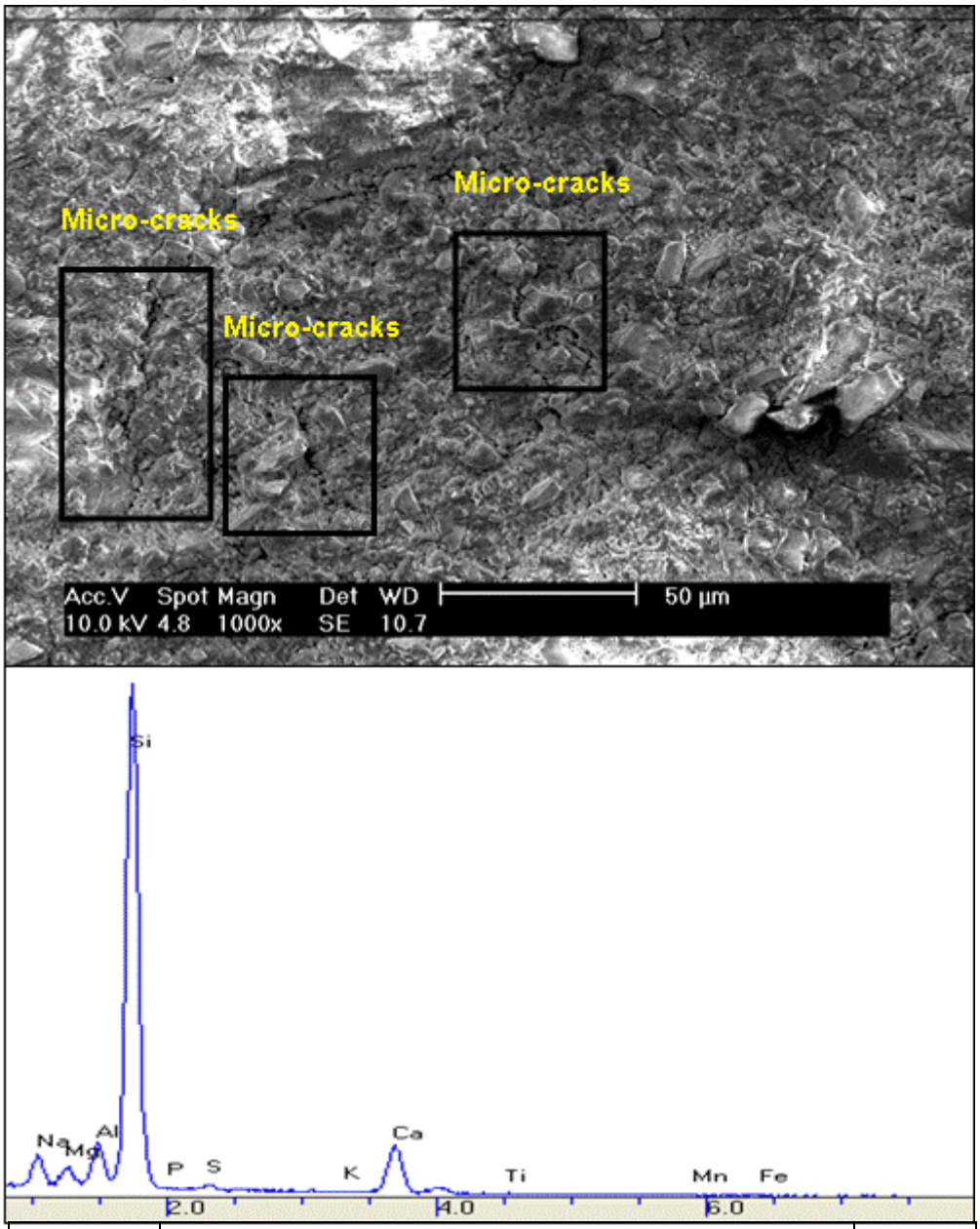

Spot/Area	Element (%)						Ca/Si ratio
	Na	Mg	Al	Si	Ca	Fe	
Surface	5.7	2.6	5.8	61.7	23.3	0.8	0.378

Figure 7.18 SEM image of AAS mortar ; AAS5-1.25

7.3.2. AAS concrete

The microstructure of the AAS concrete is shown in **Figure 7.21** and **Figure 7.22**. Based on the SEM image analysis, the microstructure shows a dense nature, caused by the dissolution of most of the slag grain particles by the alkaline solution forming a C-S-H gel (**Figure 7.21**, **Figure 7.22**). This dense microstructure leads to the low porosity and water permeability of this material, **Section 6.8 Chapter 6**.

Although the general microstructure of the AAS concrete is dense, the SEM image analysis shows a number of micro-cracks on the surface of the specimens as shown in **Figure 7.23** and **Figure 7.24**. The micro-cracks are found at the intersection between the slag grain and the gel as shown in **Figure 7.25**, with the width of micro-cracks being approximately 3 μm.

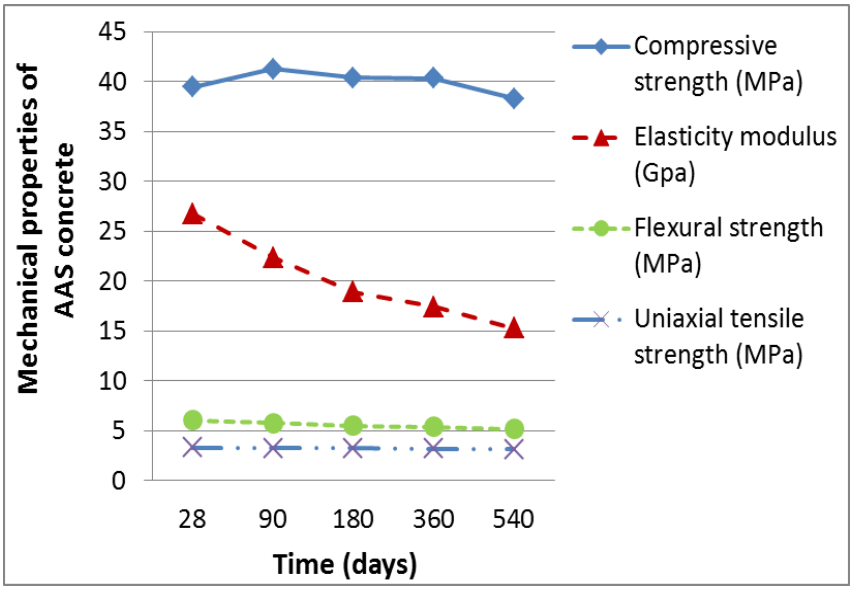

Figure 7.19 Mechanical properties of AAS concrete

Figure 7.19 shows the reduction of mechanical properties (i.e. compressive strength, modulus of elasticity, flexural strength and tensile strength) of AAS concrete over periods of time. This is attributed to the possible growth of the micro-cracks observed at the interface between the AAS pastes and the aggregates (**Figure 7.25**). The interaction of the paste and the aggregates is the primary factor governing the mechanical properties of the material. The

investigation reported in **Section 6.8** demonstrates an increase of porosity, water absorption and water permeability with time (**Figure 7.20**). This can also be explained by the growth of the micro-cracks between the AAS pastes and the aggregates. The observation that the UPV value decreases with time again points to the growth of the cavities, cracks or defects within the AAS concrete. A similar finding was also found by Collins & Sanjayan (2001) who proposed the growth of micro-cracks as an explanation for increasing sorptivity and decreasing strength of specimens.

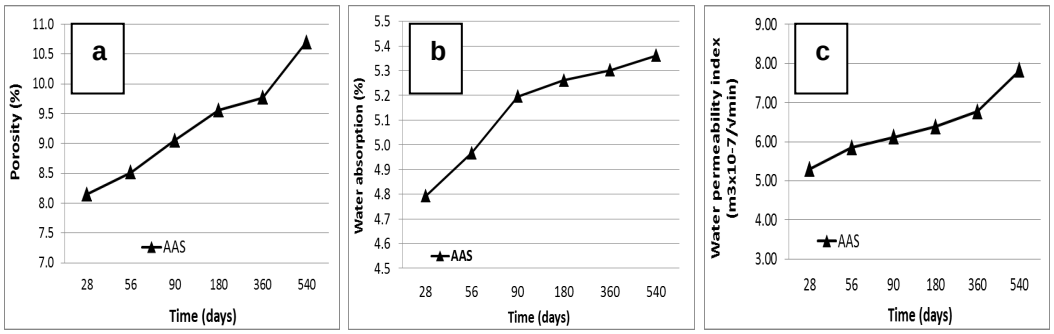

Figure 7.20 The increase of permeation properties of AAS concrete with time; a) Porosity, b) Water absorption, c) Water permeability

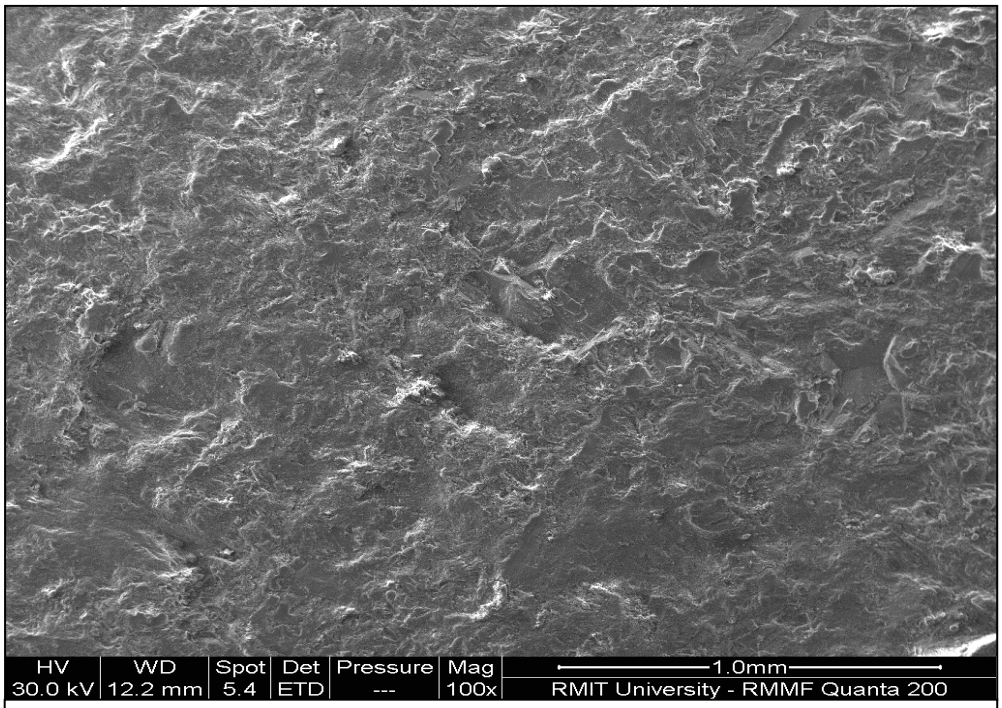

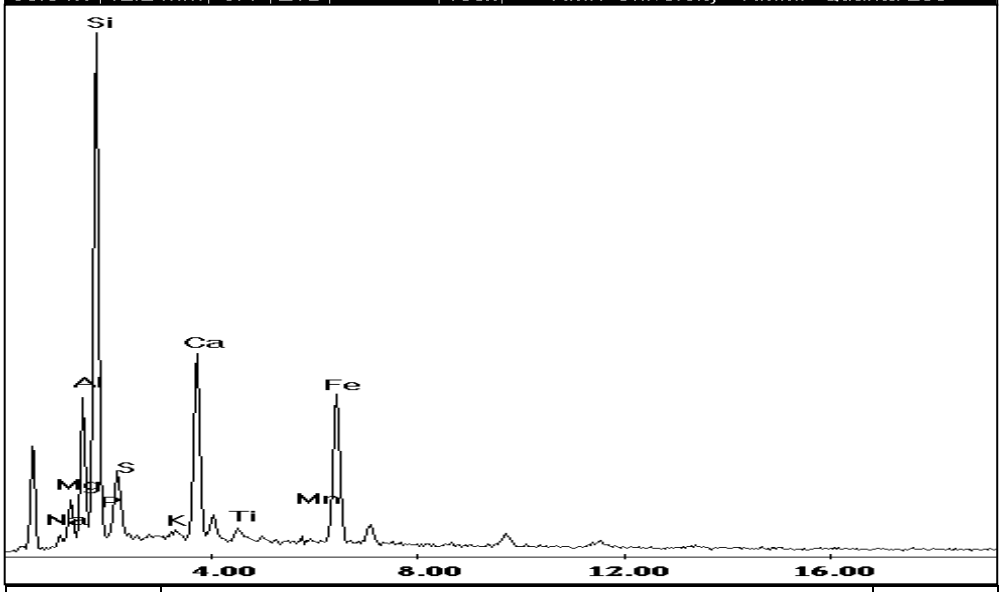

Spot/Area	Element (%)						Ca/Si ratio
	Na	Mg	Al	Si	Ca	Fe	
Surface	2.2	5.1	11.7	44.9	13.5	17.4	0.301

Figure 7.21 AAS concrete, area 1

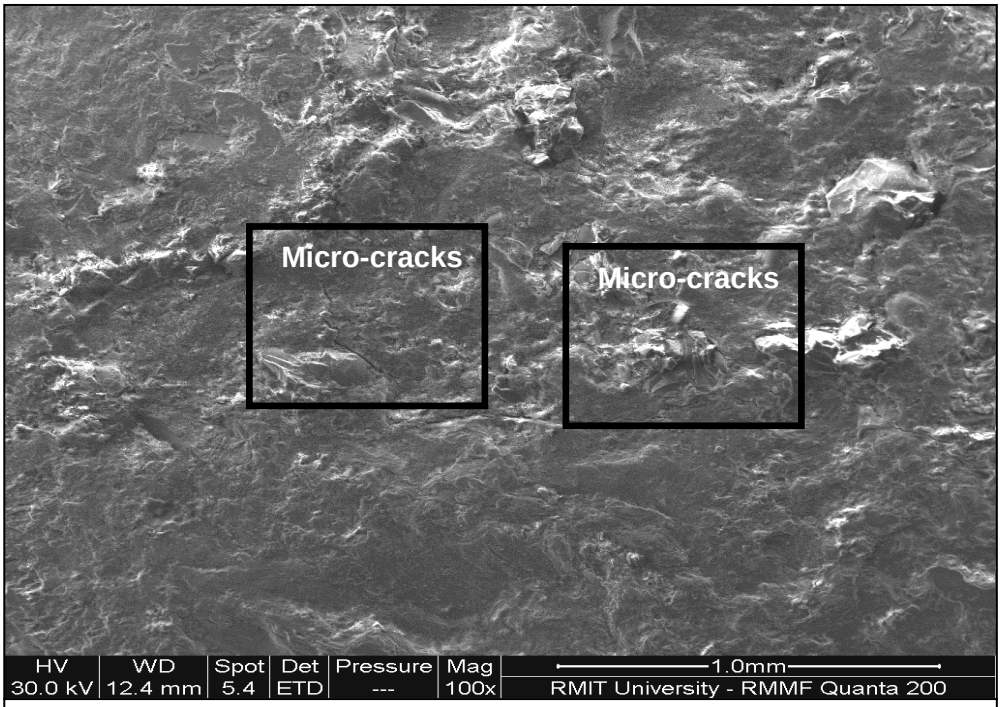

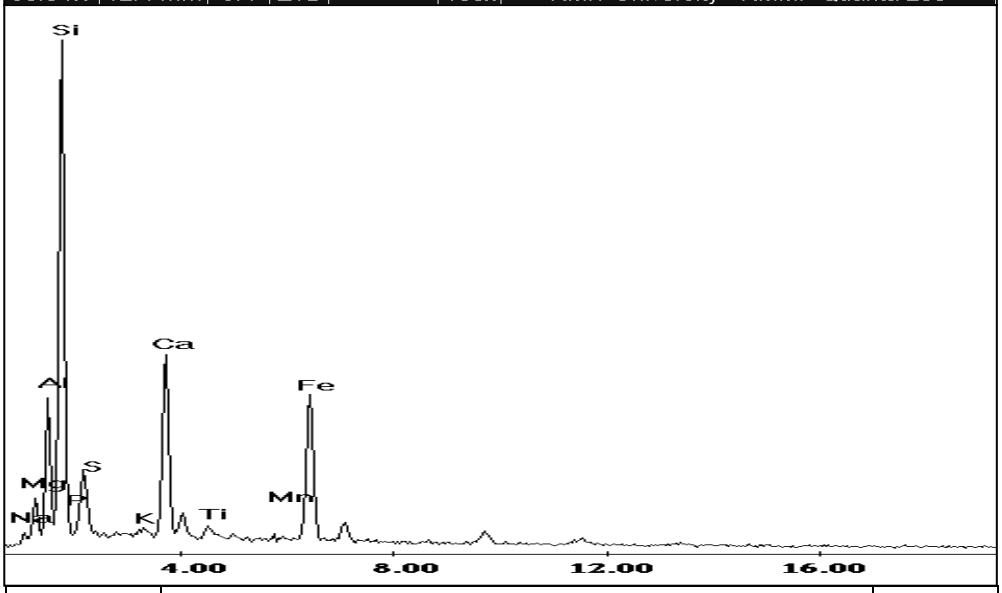

Spot/Area	Element (%)						Ca/Si ratio
	Na	Mg	Al	Si	Ca	Fe	
Surface	2.7	5.0	12.2	44.9	12.9	17.1	0.287

Figure 7.22 AAS concrete, area 2

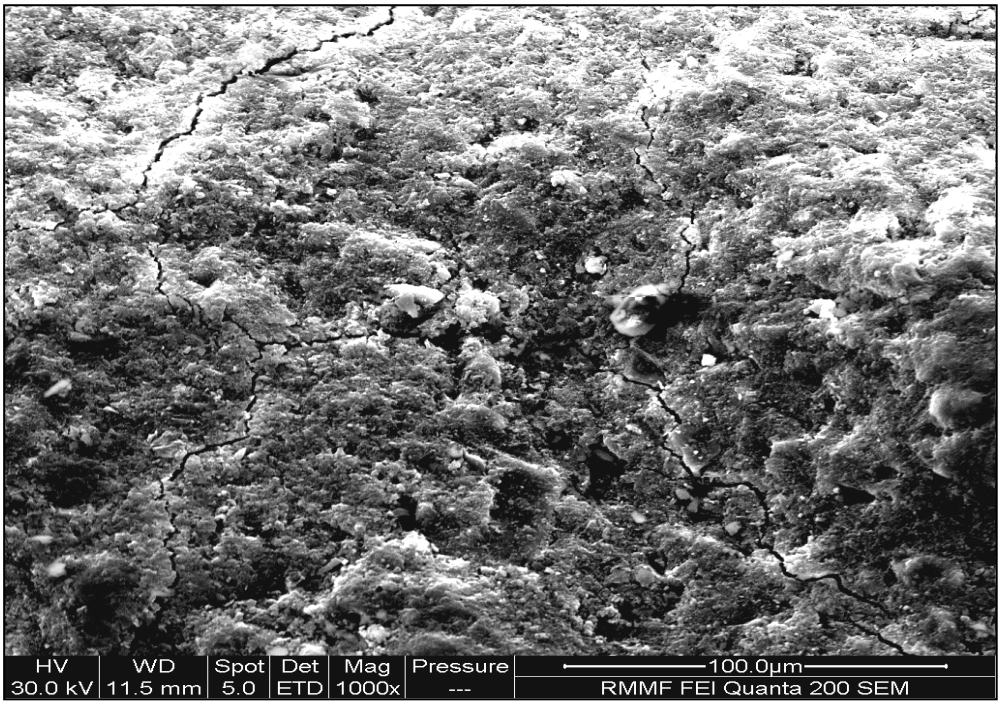

Figure 7.23 Surface micro-cracks of AAS matrix 1

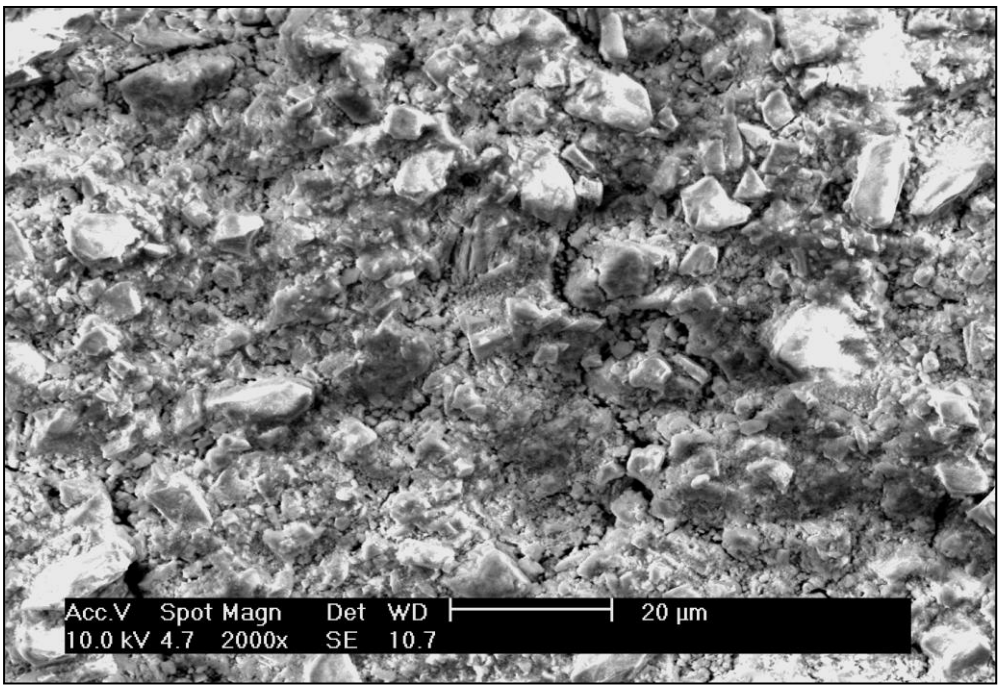

Figure 7.24 Surface micro-cracks of AAS matrix 2

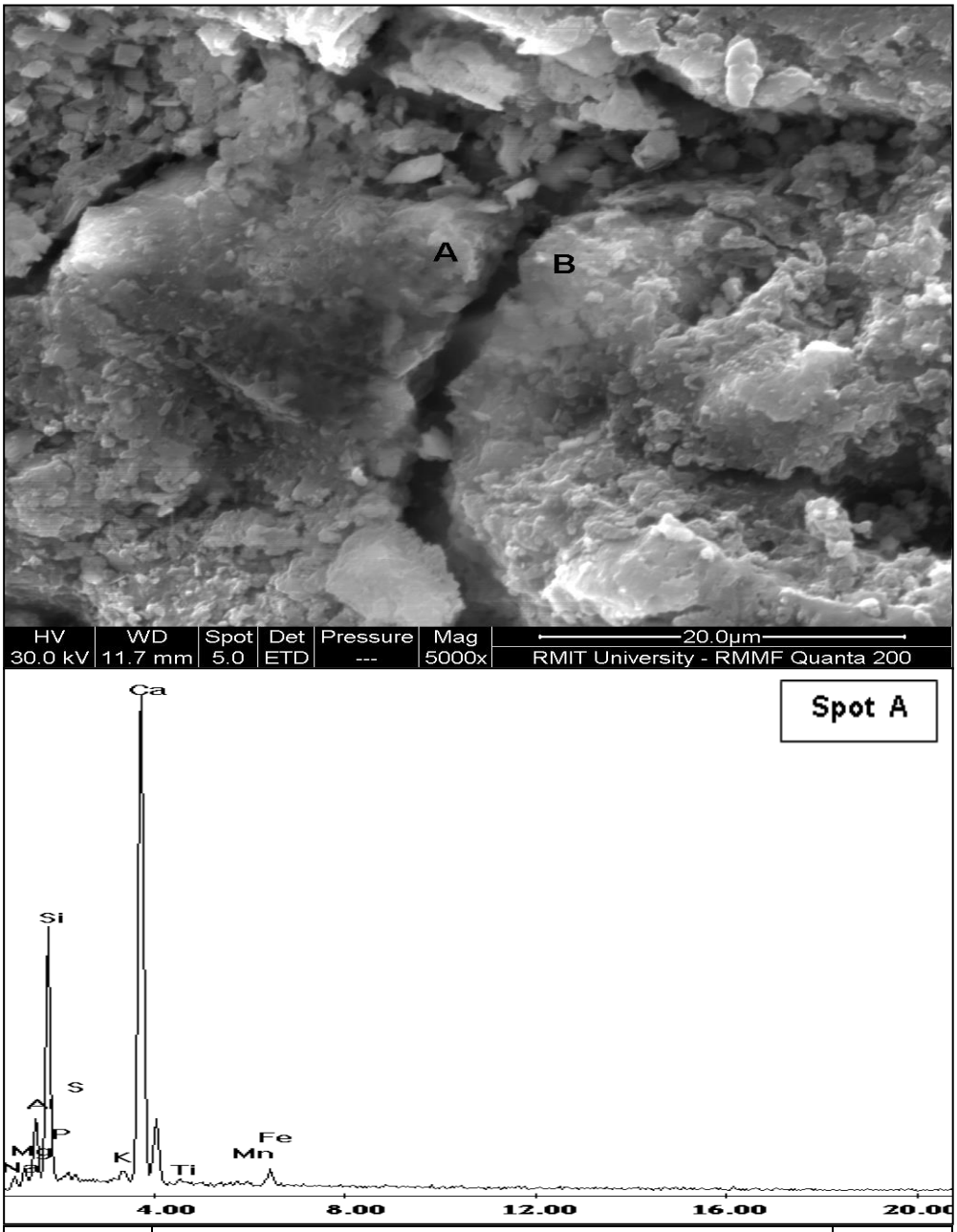

Spot/Area	Element (%)						Ca/Si ratio
	Na	Mg	Al	Si	Ca	Fe	
Surface	3.2	3.1	8.6	29.1	44.9	3.0	0.648

Figure 7.25 Interaction between AAS matrix

7.4. Strength development of fly ash geopolymer and AAS concretes based on its microstructure

In terms of mechanical properties, AAS concrete demonstrates better short term performance compared to that of fly ash geopolymer concrete **(Chapter 5** and **Chapter 6)**. However, over the long term, the AAS concrete shows a reduction in strength (**Figure 7.26**).

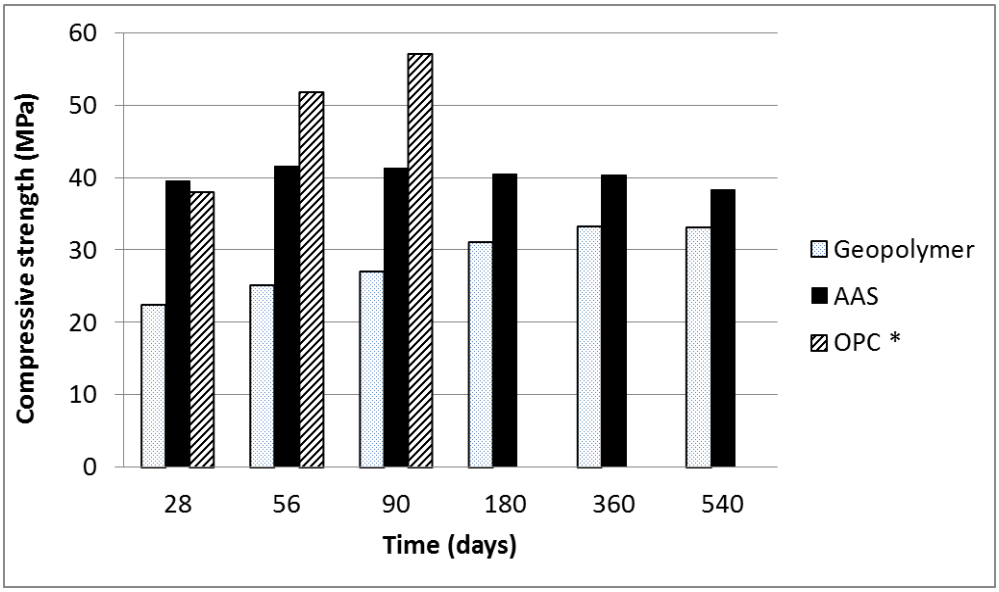

Note: * Adam (2009)

Figure 7.26 Compressive strength of fly ash geopolymer and AAS concretes

The reduction of modulus of elasticity with time (**Section 6.7.2 and Figure 7.27**) further supports the hypothesised growth of the micro-cracks between the AAS pastes and the aggregates, **Figure 7.28** and **Figure 7.29**. As with OPC concrete, the modulus of elasticity is influenced by the interaction between the pastes and the aggregates, and the reduction of modulus of elasticity is hypothesised as being due to the interaction between the AAS paste and the aggregates becoming progressively smaller with time as the micro-cracks observed increase over time.

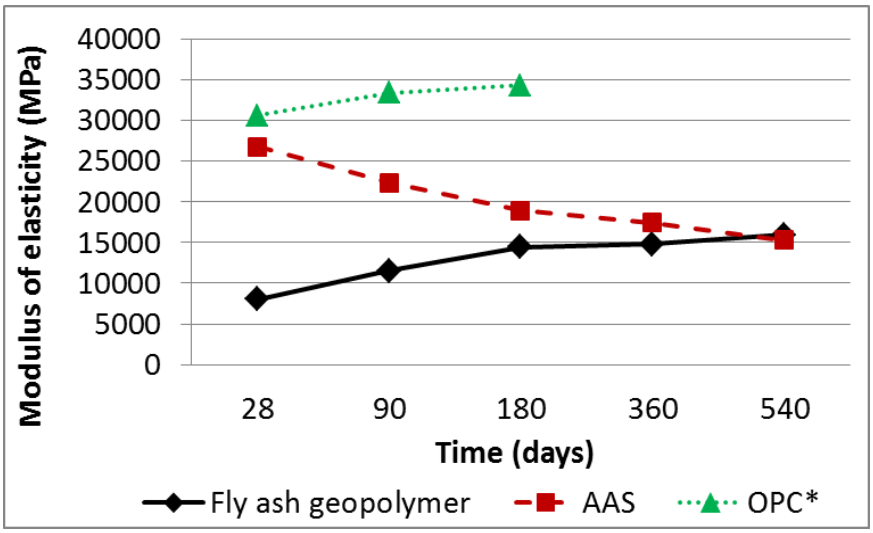

Note: * Adam (2009)

Figure 7.27 Modulus of elasticity of fly ash geopolymer and AAS concretes

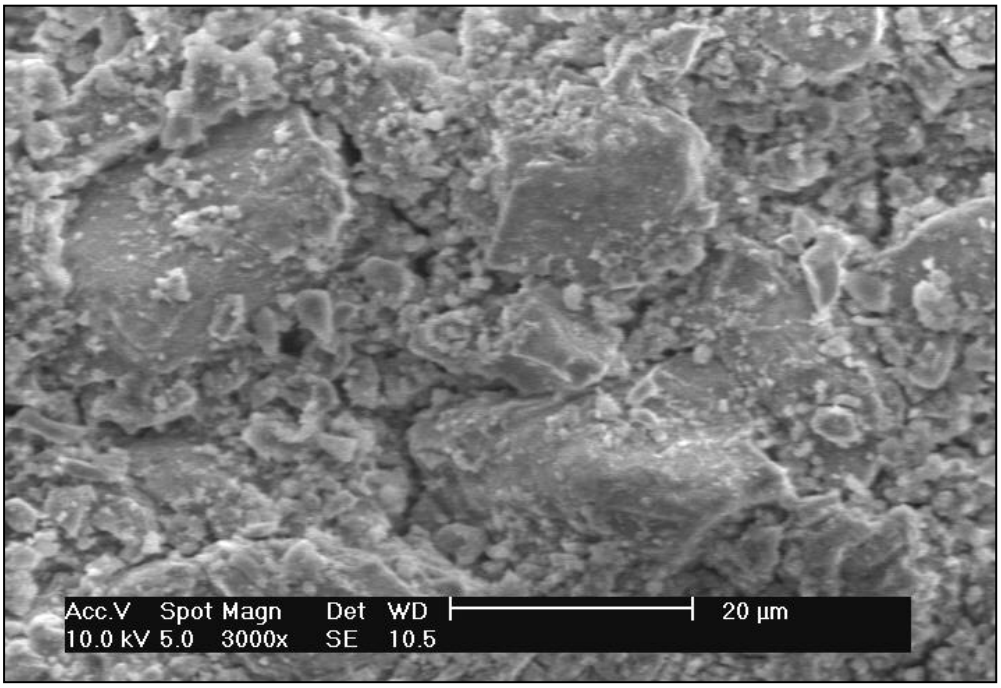

Figure 7.28 SEM image of cracks around un-reacted slag

Figure 7.29 Cracks along the slag grain

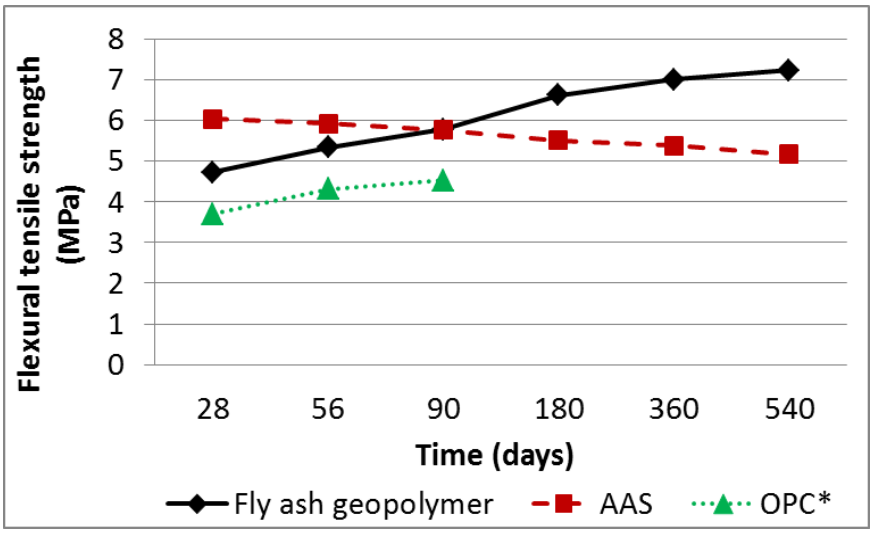

Note: * Adam (2009)

Figure 7.30 Flexural tensile strength of fly ash geopolymer and AAS concretes

This finding is also corroborated by the results of the flexural tensile strength (**Figure 7.30**) and uniaxial tensile strength (**Figure 7.31**) which demonstrate a

reduction over time. According to (Neville (2011)), the tensile strength of concrete is affected by the mechanical interlocking of the coarse aggregate. This aggregates particles act as “cracks arresters” during imposed load. With the growth of cracks between AAS pastes and the aggregates, the ability of the aggregates particles to act as “crack arresters” is compromised, resulting in a reduction of tensile strength.

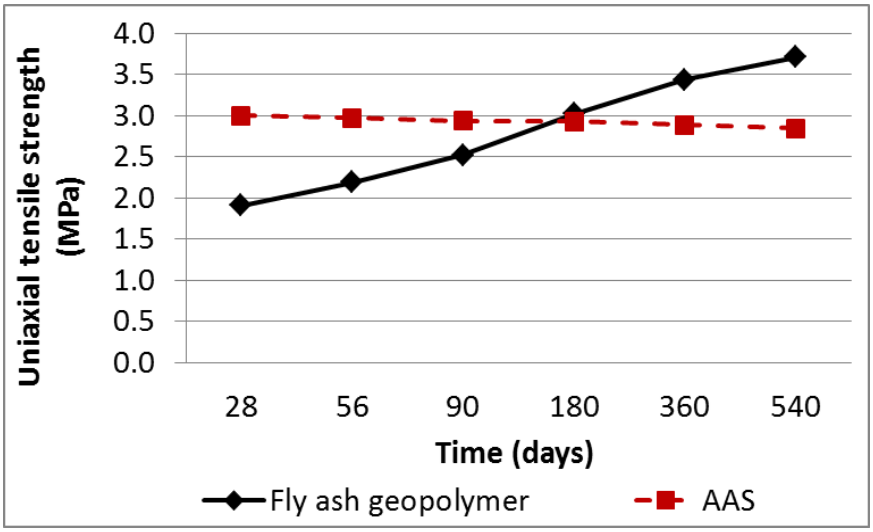

Figure 7.31 Uniaxial tensile strength of fly ash geopolymer and AAS concretes

Relative to AAS concrete, fly ash geopolymer concrete exhibits lower compressive strength (**Figure 7.26**), modulus of elasticity (**Figure 7.27**), flexural tensile strength (**Figure 7.30**) and uniaxial tensile strength (**Figure 7.31**) in the short term. However the fly ash geopolymer concrete exhibits higher values than AAS concrete in the long term, as the mechanical properties demonstrate a slow development over time. This is attributed to the slow formation of the geopolymeric matrix which is caused by the high silicates content in the fly ash precursors which affects the Si/Al ratio (**Figure 7.8** and **Figure 7.9**).

Overall, although the mechanical strength of the AAS concrete is greater in both the short and long term compared to that of fly ash geopolymer concrete, the AAS concrete demonstrates a negative trend which suggests that it may have issues with long term performance as opposed to the fly ash geopolymer concrete which appears to be stable or even increasing in mechanical strength.

7.5. Summary of chapter 7

The result of the investigation on the microstructure studies of fly ash geopolymer and AAS concretes may be summarized as follows:

1. The major components found in fly ash geopolymer specimens are Si and Al, while other elements such as Na, Mg, Ca, Ti and Fe are also found in much lower quantities. This confirms that the matrix of fly ash geopolymer concrete mainly comprises of Si-Al-O with a Si/Al ratio of 3.38 and may be considered as (Si)-poly sialate disiloxo.
2. Un-reacted fly ash is found in higher alkali modulus mixes in fly ash geopolymer due to the high silicate content in the fly ash precursor. These un-reacted particles together with the gap between un-reacted particles and the geopolymer matrix can be inferred as the cause of the low initial strength.
3. The high silicate content of the fly ash precursors results in a high Si/Al ratio which affects the rate of the geopolymeric reaction (setting time). The high Si/Al ratio causes the slow strength development of fly ash geopolymer concrete.
4. Fly ash geopolymer concrete also exhibits a porous microstructure which explains the high permeation properties and hence high chloride diffusion coefficient and high rate of carbonation.
5. The major components found in AAS specimens were Si and Ca with a low Ca/Si ratio in the range of 0.287 – 0.301, this ratio is lower than that of the C-S-H gel found in OPC based concrete.
6. The results suggest that the micro cracks observed at the interface between the AAS pastes and the aggregates in the early age specimens become larger over time. This leads to the increase of porosity, water absorption and water permeability with time. It is also hypothesised as the cause of the reduction of the mechanical properties over time.
7. AAS concrete exhibits better mechanical properties compared to fly ash geopolymer concrete in the short term, however, due to possibility of the development of the interaction between the AAS pastes and the aggregates, the long term performance of AAS concrete is questionable

8. CONCLUSIONS AND RECOMMENDATIONS

8.1. Conclusions

This chapter presents the main conclusion which can be drawn for the investigation of the development of mechanical properties of fly ash geopolymer and AAS concrete in long term performance, the investigation of the durability of fly ash geopolymer and AAS concrete, and the possibility of the application of existing standard to the use of fly ash geopolymer and AAS concretes.

Based on the results of the analysis, the research has drawn the following conclusions:

1. In terms of mechanical properties, the short term behaviour of AAS concrete is better than that of fly ash geopolymer concrete, however fly ash geopolymer concrete shows a better performance in the longer term compared to the AAS concrete.
2. The AAS concrete exhibits a reduction in strength with age hypothesised as being due to the development of existing micro-cracks, while fly ash geopolymer concrete strength demonstrates an improvement with age due to the continuing formation of the geopolymeric network.
3. The low strength of fly ash geopolymer concrete is attributed to the low CaO content, the low fineness and the spherical shape of the fly ash precursors. The slow development of the fly ash geopolymer matrix is attributed to the high Si/Al ratio which leads to the reaction between the silicates which is assumed to be slower than the reaction between aluminates and silicates at lower Si/Al ratios.
4. For AAS concrete, the strength development is affected by the Si/Al ratio. A higher Si/Al ratio tends to reduce the strength of the concrete. The strength is also affected by the classification of the slag which is classified as acid slag (with a basicity coefficient (K_b) < 1).
5. The modulus of elasticity and tensile strength of fly ash geopolymer concrete follow a positive relationship with the compressive strength and demonstrate an increase with age. These findings confirm the existence of a slow

geopolymeric reaction due to the high silicate content in the fly ash precursors. In contrast, AAS concrete demonstrates a negative relationship between the modulus of elasticity and tensile strength to its compressive strength and exhibits a decrease with age.

6. The relationship between the modulus of elasticity and tensile strength of fly ash geopolymer concrete to compressive strength can be predicted based on similar behaviour with OPC concrete which demonstrates a positive relationship and an increase with time. However, it is not possible to predict the relationship for AAS due to the negative relationship with time.

7. Both fly ash geopolymer concrete and AAS concretes show that the flexural tensile strength demonstrates a higher value compared to uniaxial tensile strength in long term performance. This is attributed to the loading arrangement of the concrete specimens during the test. The volume of material which is subjected to critical stress in the flexural tensile strength test is much smaller than in the indirect tensile strength test. Thus the likelihood of a critical crack propagating is greater in the indirect test (where the volume of high stressed material is greater) resulting in a higher stress reached in the flexural test.

8. Compared to OPC, the short and long term performance of fly ash geopolymer concrete exhibits a lower compressive strength and modulus of elasticity, and a higher flexural and uniaxial tensile strength.

9. AAS concrete has a comparable compressive strength and modulus of elasticity, and higher flexural tensile strength and uniaxial tensile compare to OPC concrete in short term performance. In the longer term the values reduce to fall below that of OPC concrete.

10. In terms of durability properties, AAS concrete demonstrates a better performance compared to fly ash geopolymer concrete, i.e. better permeation properties, resistance to corrosion and carbonation.

11. Fly ash geopolymer concrete exhibits higher porosity, water absorption and water permeability compared to AAS concrete. This is attributed to the low fineness and spherical shape of the fly ash precursors which affects the pores structure and compromises the connection between the geopolymer pastes and the aggregate leading to low strength development. Fly ash

geopolymer concrete is also affected by the high Na_2O dosage which causes a rapid reaction during the mixing process. The high permeation properties of fly ash geopolymer concrete are confirmed by the low value of the UPV which indicates a low quality. Moreover, the porosity, water absorption and water permeability of fly ash geopolymer concrete decrease with time which indicates that the on-going geopolymeric reaction continues. This finding is also confirmed by the increasing UPV over time.

12. In contrast, despite the AAS concrete exhibiting a lower value of porosity, water permeability and water absorption compared to fly ash geopolymer concrete, the values show an increase with time which is also confirmed by the decrease of the UPV.

13. Both fly ash geopolymer and AAS concrete demonstrate a high resistivity which indicates a high resistance to the potential to sustain corrosion. The resistivity of fly ash geopolymer concrete increases with time due to the on-going geopolymeric reaction which produces the geopolymer gel. This gel fills the gap within the pore structure and reduces ionic concentration leading to an improvement of resistivity measurement.

14. AAS concrete demonstrates a better resistance to chloride diffusion and carbonation compared to fly ash geopolymer concrete. This attributable to lower porosity and water permeability properties.

15. The major hydration product of fly ash geopolymer concrete is a composite geopolymer matrix and mainly comprised of Si-Al-O with an Si/Al ratio of 3.38 and may be considered to be (Si)-poly sialate disiloxo. While, the major hydration product of AAS concrete is an amorphous to poorly crystalline C-S-H gel with the Ca/Si ratio in the range of 0.287 – 0.301.

16. The microstructures of fly ash geopolymer concrete exhibits un-reacted fly ash particles and an interface between the un-reacted particles and the geopolymer matrix, which can be inferred as the cause of the low strength development. However, despite AAS concrete displaying a denser microstructure compared to fly ash geopolymer concrete, the micro-cracks found between the un-reacted slag particles and the border of the C-S-H gel is postulated as the cause of the strength reduction as these cracks increase in size with time.

17. In general, AAS concrete demonstrates better mechanical properties and durability properties than fly ash geopolymer, as well as comparable mechanical properties to OPC concrete in the short term. However, the reduction in performance with time suggests that the use of AAS concrete as a replacement of OPC based concrete is not recommended for long term use at present. In contrast, the improved performance of fly ash geopolymer concrete with time suggests that the use of fly ash geopolymer concrete as an OPC based concrete replacement is feasible.
18. The use of the existing Australian Standard, i.e. AS 3600-2009, may be conservatively applied to predict the flexural tensile strength and uniaxial tensile strength of fly ash geopolymer concrete due to the higher tensile strength values compared to the existing Australian Standard. However, it might not appropriate to determine the modulus of elasticity of fly ash geopolymer concrete due to the over-estimated value using the existing AS 3600-2009.
19. The existing Australian Standard cannot be applied to calculate the modulus of elasticity, flexural tensile strength and uniaxial tensile strength of AAS concrete. This is because of the greater rate of decline of these properties compared to that predicted (based on the existing Australian Standard).

8.2. Recommendations for further research

This thesis has dealt with the development of the mechanical properties of fly ash geopolymer and AAS concretes in long term performance and the investigation of their durability properties. While much information regarding to the performance of the two new concrete materials related to the behaviour of these concretes in long term performance, a number of issues could not be addressed due to time constraints. Therefore, future work should be undertaken to gain a better understanding of the different behaviour between fly ash geopolymer and AAS concretes in long term periods and their application in structural engineering components. This is essential before the two concretes can be widely adopted in commercial applications as structural components. The following recommendations are made for future work:

1. This research shows that the development of fly ash geopolymer concrete requires a heat curing to achieve structural integrity due to the slow setting at room temperature. However, the implementation of heat curing regime on-site is found to be difficult and expensive. Thus, further research on the addition of slag in fly ash geopolymer concrete mix design in order to be able to be cured in normal curing temperature could be explored.
2. This research finds that the chemical composition and the fineness of fly ash raw materials affect the strength development of fly ash geopolymer specimen. Optimising the mix design using different of fly ash sources and different fineness could be investigated to obtain the optimum strength of fly ash geopolymer specimens.
3. This research demonstrates that the micro-structure of fly ash geopolymer concrete is found to be less dense compared to AAS concrete due to the high permeation and high porosity. This leads to the low durability to the ingression of chloride and carbonation. Further, the addition of a material with a better fineness than fly ash (i.e. slag, silica fume or rice husk ash) in fly ash geopolymer concrete mix design in order to improve the permeation properties and reduce the porosity could be investigated.
4. This research shows that of AAS concrete demonstrates a decrease on mechanical properties (i.e. compressive strength, modulus of elasticity and tensile strength) over periods of time. It was found that this is may be caused by the growing of the existing micro-cracks with time. Thus, the investigation of the shrinkage behaviour of AAS concrete over the long term should be undertaken to confirm the previous finding. In addition investigation of the long term development of the micro-cracks is also recommended.
5. Other researches have shown that the use of basalt fibre increases the mechanical properties of high volume of fly ash concrete. Hence, the addition of fibre reinforced or basalt fibre in AAS concrete mix design in order to prevent the decrease of mechanical properties in long term performance could be investigated.

REFERENCES

AASHTO T-259 (1997) Standard Method of Test for Resistance of Concrete to Chloride Ion Penetration. USA: AASHTO.

AASHTO T-260 (1997) Standard Method of Test fo Sampling and Testing for Chloride Ion in Concrete and Concrete Raw Materials. USA: AASHTO.

ACI 116R-00 (2005) Cement and Concrete Terminology : Reported by ACI Comittee 116. Michigan, U.S.A., American Concrete Institute.

ACI 201.2R-08 (2008) Guide to Durable Concrete : Reported by ACI Comittee 201. Michigan, U.S.A.: American Concrete Institute.

Adam, A. A. (2009) Strength and Durability Properties of Alkali-Activated Slag and Fly Ash-based Geopolymer Concrete. School of Civil, Environmental and Chemical Engineering, RMIT University, Melbourne, Australia.

Adam, A. A., Patnaikuni, I., Law, D. W. & Molyneaux, T. C. K. (2007) Strength of mortar containing activated slag and fly ash: Design materials and construction. In proceedings of The 23rd Biennial Conference of the Concrete Institute of Australia : Concrete for future, Adelaide, Australia.

Aitcin, P. C. (2004) High-Performance Concrete. New York, Taylor & Francis e-Library.

Al-Otaibi, S. (2008) Durability of concrete incorporating GGBS activated by water-glass. *Construction & Building Materials,* 22**,** 2059-2067.

Alonso, S. & Palomo, A. (2001) Alkaline activation of metakaolin and calcium hydroxide mixtures: influence of temperature, activator concentration and solids ratio. *Materials Letters,* 47**,** 55-62.

AS 10.12.12.1 (1998) Methods of testing concrete. Method 12.1: Determination of mass per unit volume of hardened concrete - Rapid measuring method. *Australia.* Australian Standard Association.

AS 1012.3.1 (1998) Methods of testing concrete. Method 3.1: Determination of properties related to the consistency of concrete—Slump test. Australia: Australian Standard Association.

AS 1012.9 (1999) Methods of testing concrete. Method 9: Determination of the compressive strength of concrete specimens. Australia: Australian Standard Association.

AS 1012.10 (2000) Methods of testing concrete. Method 10: Determination of indirect tensile strength of conrete cylinders ('Brazil' or splitting test). Australia: Australian Standard Association.

AS 1012.11 (2000) Methods of Testing Concrete. Method 11: Determination of The Modulus of Rupture. Australia: Australian Standard Association.

AS 1012.17 (1997) Methods of testing concrete. Method 17: Determination of the static chord modulus of elasticity and Poisson's ratio of concrete specimens. Australia: Australian Standard Association.

AS 1012.21 (1999) Methods of testing concrete. Method 21: Determination of water absorption and apparent volume of permeable voids in hardened concrete. Australia: Australian Standard Association.

AS 1141.5 (2000) Methods for Sampling and Testing Aggregates. Method 5: Particle Density and Water Absorption of Fine Aggregate. Australia: Australian Standard Association.

AS 1141.6.1 (2000) Methods for Sampling and Testing Aggregates. Method 6.1: Particle Density and Water Absorption of Coarse Aggregate - Weighing-in-Water Method. Australia: Australian Standard Association.

AS 3582.1 (1998) Supplementary Cementitious Materials for Use with Portland and Blended Cement. Part 1: Fly ash. Australia: Australian Standard Association.

AS 3582.2 (2001) Supplementary Cementitious Materials for Use with Portland and Blended Cement. Part 1: Slag - Ground Granulated Iron Blast-furnace. Australia: Australian Standard Association.

AS 3600 (2009) Concrete structures. Australia: Australian Standard Association.

ASTM C109/C109M-07 (2008) Standard Test Method for Compressive Strength of Hydraulic Cement Mortars. *ASTM Annual Books.* USA: ASTM International.

ASTM C597-02 (2003) Standard Test Method for Pulse Velocity Through Concrete. *ASTM Annual Books.* USA: ASTM International.

ASTM C618-03 (2003) Standard Specification for Coal Fly Ash and Raw or Calcined Natural Pozzolan for Use in Concrete. *ASTM Annual Books.* USA: ASTM International.

ASTM C642-97 (2003) Standard Test Method for Density, Absorption, and Voids in Hardened Concrete. *ASTM Annual Books.* USA: ASTM International.

ASTM C989-99 (2003) Ground Granulated Blast-Furnace Slag for Use in Concrete and Mortars. *ASTM Annual Books.* USA: ASTM International.

ASTM C1543-02 (2003) Standard Test Method for Determining the Penetration of Chloride Ion into Concrete by Ponding. *ASTM Annual Books.* USA: ASTM International.

Atis, C. D. & Karahan, O. (2009) Properties of steel fiber reinforced fly ash concrete. *Construction and Building Materials,* 23**,** 392-399.

Australian Greenhouse Office (2007) Analysis of Recent Trends and Greenhouse Indicators 1990 to 2005. Australia, Australian Greenhouse Office.

Autoclam (2010) Autoclam Permeability System Operating Manual. Belfast. Northern Ireland, The Queen University of Belfast.

Bakharev, T. (2000) Alkali Activated Slag Concrete : Chemistry, Microstructure and Durability. Department of Civil Engineering, Monash University, Melbourne, Australia.

Bakharev, T. (2005a) Geopolymeric materials prepared using Class F fly ash and elevated temperature curing. *Cement and Concrete Research,* 35**,** 1224-1232.

Bakharev, T., Sanjayan, J. G. & Cheng, Y. B. (1999a) Alkali Activation of Australian Slag Cements. *Cement and Concrete Research,* 29**,** 113-120.

Bakharev, T., Sanjayan, J. G. & Y.B.Cheng (2001) Resistance of alkali-activated slag concrete to carbonation. *Cement and Concrete Research,* 31**,** 1277-1283.

Barbosa, V. F. F. & MacKenzie, K. J. D. (2003) Thermal behaviour of inorganic geopolymers and composites derived from sodium polysialate. 38**,** 319-331.

Barbosa, V. F. F., MacKenzie, K. J. D. & Thaumaturgo, C. (2000) Synthesis and characterisation of materials based on inorganic polymers of alumina and silica: sodium polysialate polymers. *International Journal of Inorganic Materials,* 2**,** 309-317.

Basheer, L., Kropp, J. & Cleland, D. J. (2001) Assessment of the durability of concrete from its permeation properties: A review. *Construction & Building Materials,* 15**,** 93-103.

Basheer, M., Goncalves, A. F. & Torrent, R. (2007) Chapter 4. Non-Destructive Methods to Measure Water Transport. RILEM.

Basheer, P. A. M., Chidiact, S. E. & Long, A. E. (1996) Predictive models for deterioration of concrete structures. *Construction and Building Materials,* 10**,** 27-37.

Bernal, S. A., Gutierrez, R. M. & Provis, J. L. (2012) Engineering & Durability Properties of Concretes Based on Alkali-activated Granulated Blast Furnace Slag / Metakaolin Blends. *Construction & Building Materials,* 33.

Berry, M., Cross, D. & Stephens, J. (2009) Changing the environment: An alternative "Green" concrete produced without Portland cement. In World of Coal Ash (WOCA) Conference, 4-7 May 2009, Lexington, KY, USA.

Bouzoubaa, N., Zhang, M.-H., Malhotra, V. M. & Golden, D. M. (1999) Blended Fly Ash Cements - A Review. *ACI Materials,* 96**,** 641-650.

Brough, A. R. & Atkinson, A. (2002) Sodium silicate-based, alkali-activated slag mortars. Part I. Strength, hydration and microstructure. *Cement and Concrete Research,* 32**,** 865-879.

Cement Australia (2011) Material Safety Data Sheet. MSDS No. CA08: Fly Ash - Tarong. Australia: Cement Australia.

Cement Australia (2013) Material Safety Data Sheet. MSDS No. CA001: Portland Cement. Australia: Cement Australia.

Cement Concrete & Aggregates Australia (2009) Chloride Resistance of Concrete. Australia, Cement Concrete & Aggregates Australia.

Chang, J. J. (2003) A Study on the Setting Characteristics of Sodium Silicate-activated Slag Pastes. *Cement and Conrete Research,* 33**,** 1005-1011.

Chang, J. J., Yeih, W., Huang, R. & Chen, C. T. (2004) Suitability of several current used concrete durability indices on evaluating the corrosion hazard for carbonated concrete. *Materials Chemistry and Physics,* 84**,** 71-78.

Chen, W. & Brouwers, H. J. H. (2007) The hydration of slag. Part 1: Reaction models for alkali-activated slag. *Journal of Material Science,* 42**,** 428-443.

Chindaprasirt, P. & Chalee, W. (2014) Effect of sodium hydroxide concentration on chloride penetration and steel corrosion of fly ash-based geopolymer concrete under marine site. *Construction and Building Materials,* 63**,** 303-310.

Claisse, P. A., Ganjian, E. & Adham, T. A. (2003) In Situ Measurement of The Intrinsic Permeability of Concrete. *Magazine of Concrete Research,* 55**,** 125-132.

Collins, F. & Sanjayan, J. G. (1999) Workability and Mechanical Properties of Alkali-Activated Slag Concrete. *Cement and Concrete Research,* 29**,** 455-458.

Collins, F. & Sanjayan, J. G. (2000) Effect of pore size distribution on drying shrinkage of alkali-activated slag concrete. *Cement and Concrete Research,* 30**,** 1401-1406.

Collins, F. & Sanjayan, J. G. (2001) Microcracking and strength development of alkali-activated slag concrete. *Cement and Concrete Composites,* 23**,** 345-352.

Concrete Institute Australia (2011) Recommended Practice Geopolymer Concrete. *4.2. Properties of hardened concrete.* Melbourne, Australia.

Crank, J., *The Mathematics of Diffusion*, ed. 2nd. 1975, Oxford (England): Clarendon Press.

Davidovits, J. (1991) Geopolymers: Inorganic polymeric new materials. *Journal of Thermal Analysis,* 37**,** 1633-1656.

Davidovits, J. (1994) Global warming impact on the cement and aggregates industries. *World Resource Review,* 6**,** 263-278.

Davidovits, J. (1994b) Properties of geopolymer cements. In proceedings of 1st International Conference on Alkaline Cements and Concretes Conference, Kiev, Ukraina.

Davidovits, J. (2002) 30 years of successes and failures in geopolymer applications. Market trends and potential breakthroughs. In proceedings of Geopolymer 2002 Conference, October 28-29, Melbourne, Australia.

Deb, P. S., Nath, P. & Sarker, P. K. (2014) The effects of ground granulated blast-furnace slag bending with fly ash and activator content on the workability and strength properties of gepolymer concrete cured at ambient temperature. *Materials and Design,* 62**,** 32-39.

Diaz-Loya, E. I., Allouche, E. N. & Eklund, S. (2010) Factors affecting the suitability of fly ash as source material for geopolymers. *Fuel,* 89**,** 992-996.

Diaz-Loya, E. I., Allouche, E. N. & Vaidya, S. (2011) Mechanical properties of fly-ash-based geopolymer concrete. *ACI Materials Journal,* May - June**,** 300-306.

Douglas, E., Bilodeau, A., Brandstetr, J. & Malhotra, V. M. (1991) Alkali activated ground granulated blast-furnace slag concrete: Preliminary investigation. *Cement and Concrete Research,* 21**,** 101-108.

Douglas, E. & Brandstetr, J. (1990) A preliminary study on the alkali activation of ground granulated blast-furnace slag. *Cement and Concrete Research,* 20**,** 746-756.

Duxson, P., Fernandez-Jimenez, A., Provis, J. L., Lukey, G. C., Palomo, A. & Deventer, J. S. J. v. (2007a) Geopolymer technology: the current state of the art. *Journal of Material Science,* 42**,** 2917-2933.

Duxson, P., Lukey, G. C. & Deventer, J. S. J. v. (2006) Thermal evolution of metakaolin geopolymers: Part 1 – Physical evolution. *Journal of Non-Crystalline Solids,* 352**,** 5541-5555.

Duxson, P., Lukey, G. C. & Deventer, J. S. J. v. (2007b) Physical evolution of Na-geopolymer derived from metakaolin up to 1000 C. *Journal of Materials Science,* 42**,** 3044-3054.

Duxson, P., Provis, J. L., Lukey, G. C., Mallicoat, S. W., Kriven, W. M. & Deventer, J. S. J. v. (2005) Understanding the relationship between geopolymer composition, microstructure and mechanical properties. *Colloids and Surfaces A: Physicochem. Eng. Aspects,* 269**,** 47-58.

Elakneswaran, Y., Nawa, T. & Kurumisawa, K. (2009) Influence of surface charge on ingress of chloride ion in hardened pastes. *Materials and Structures,* 42**,** 83-93.

Escalante-Garcia, J. I., Espinoza-Perez, L. J., Gorokhovsky, A. & Gomez-Zamorano, L. Y. (2009) Coarse blast furnace slag as a cementitious material, comparative study as a partial replacement of Portland cement and as an alkali activated cement. *Construction & Building Materials,* 23**,** 2511-2517.

Escalante-Garcia, J. I., Fuentes, A. F., Gorokhovsky, A., Fraire-Luna, P. E. & Mendoza-Suarez, G. (2003) Hydration Products and Reactivity of Blast-Furnace Slag Activated by Various Alkalis. *Journal of American Ceramic Society,* 86 (12)**,** 2148-2153.

Fernandez-Jimenez, A. & Palomo, A. (2005b) Composition and microstructure of alkali activated fly ash binder: Effect of the activator. *Cement and Concrete Research,* 35**,** 1984-1992.

Fernandez-Jimenez, A., Palomo, A. & Criado, M. (2005a) Microstructure development of alkali-activated fly ash cement: a descriptive model. *Cement and Concrete Research,* 35**,** 1204-1209.

Fernandez-Jimenez, A., Palomo, J. G. & Puertas, F. (1999) Alkali-Activated Slag Mortars : Mechanical Strength Behaviour. *Cement and Concrete Research,* 29**,** 1313-1321.

Fernandez-Jimenez, A. & Puertas, F. (1997) Alkali-Activated Slag Cements: Kinetic Studies. *Cement and Concrete Research,* 27**,** 359-368.

Fernandez-Jimenez, A., Puertas, F., Sobrados, I. & Sanz, J. (2003) Structure of Calcium Silicate Hydrates Formed in Alkaline-Activated Slag : Influence of the Type of Alkaline Activator. *American Ceramic Society,* 86 (8)**,** 1389-1394.

Fernandez-Jimenez, A. M., Palomo, A. & Lopez-Hombrados, C. (2006) Engineering properites of alkali-activated fly ash concrete. *ACI Materials,* Technical paper, Title no. 103-M12**,** 106-112.

Fletcher, R. A., MacKenzie, K. J. D., Nicholson, C. L. & Shimada, S. (2005) The composition range of aluminosilicate geopolymers. *Journal of the European Ceramic Society,* 25**,** 1471-1477.

Flower, D. J. M. & Sanjayan, J. G. (2007) Green house gas emissions due to concrete manufacture. *International Journal of Life Cycle Assessment,* 12**,** 282-288.

Freedonia Group (2010) World Cement. Study # 2591. Industry Study with Forecast for 2013 & 2018. *World Cement.* Cleveland, US: Freedonia Group, Inc.

Garbacz, A. & Garboczi, E. J. (April 2003) NISTIR 6975. Ultrasonic evaluation methods applicable to polymer concrete composites. United States, National Institute of Standards and Technology. Technology Administration. U.S. Department of Commerce.

Gartner, E. (2004) Industrially interesting approaches to "low-CO_2" cements. *Cement and Concrete Research,* 34**,** 1489-1498.

Ghosh, K. & Ghosh, P. (2012) Effect Of Na2O/Al2O3, SiO2/Al2O3 and w/b ratio on setting time and workability of fly ash based geopolymer. *International Journal of Engineering Research and Applications,* 2**,** 2142-2147.

Glukhovsky, V. D., Rostovkaya, G. S. & Rumyna, G. V. (1980) High Strength Slag-Alkali Cement. In 7th International Congress on the Chemistry of Cements, Paris, France.

Hardjito, D. (2005) Studies on Fly Ash-Based Geopolymer Concrete. Department of Civil Engineering, Curtin University of Technology, Melbourne, Australia.

Hardjito, D. & Rangan, B. V. (2005) Development and properties of low-calcium fly ash-based geopolymer concrete. Research Report GC 1. Perth, Australia, Curtin University of Technology.

Hardjito, D., Wallah, S. E., Sumajouw, D. M. J. & Rangan, B. V. (2004) On the Development of Fly Ash-Based Geopolymer Concrete. *ACI Materials Journal,* Technical paper, Title no. 101-M52.

Henderson, G. D., Basheer, P. A. M. & Long, A. E. (2004) Pull-Off Test and Permeation Tests. *In:* Malhotra, V. M. & Carino, N. J. (eds.) *Handbook on Non Destructive Testing of Concrete.* 2nd ed. United States of America: ASTM International and CRC Press.

Ho, D. W. S. (2003) Durability of Concrete. *In:* Chen, W. F. & Liew, J. Y. R. (eds.) *The Civil Engineering Handbook.* 2nd ed. Boca Raton, London, New York, Washington D.C.: CRC Press.

Houst, Y. F. & Wittmann, F. H. (2002) Depth profiles of carbonates formed during natural carbonation. *Cement and Concrete Research,* 32**,** 1923-1930.

Humphreys, K. & Mahasenan, M. (2002) Toward a Sustainable Cement Industry. *Substudy 8: Climate Change.* Battelle. The Business of Innovation.

I.G.Richardson, A.R.Brough, G.W.Groves & C.M.Dobson (1994) The characterization of hardened alkali-activated blast-furnace slag pastes and the nature of the calcium silicate hydrate (C-S-H) phase *Cement and Concrete Research,* 24**,** 813-829.

IAEA (2002) Guide book on Non-Destructive Testing of concrete structures. *Training Courses Series no. 17.* Vienna, Austria: International Atomic Energy Agency.

Isgor, O. B. (2001) A Durability Model for Chloride and Carbonation Induced Steel Corrosion in Reinforced Concrete Members. Department of Civil and Environmental Engineering, Carleton University, Ottawa, Ontario, Canada.

Jaarsveld, J. G. S. v. & Deventer, J. S. J. v. (1996) The potential use of geopolymeric materials to immobilise toxic metals. Part I. Theory and applications. *Minerals Engineering,* 10**,** 659-669.

Jiang, W. (1997) Alkali Activated Cementitious Materials : Mechanisms, Microstructure and Properties. Ph.D Thesis

The Pennsylvania State University, Pennsylvania, U.S.A.

Kett, I., *Engineered concrete mix design and test methods*. 2nd ed. 2010, United States of America: Taylor and Francis Group, LLC.

Kong, D. L. Y., Sanjayan, J. G. & Sagoe-Crentsil, K. (2007) Comparative performance of geopolymer made with metakaolin and fly ash after exposure to elevated temperatures. *Cement and Concrete Research,* 37**,** 1583-1589.

Krivenko, P. V. (1994) Alkaline cements. In The 1st International Conference on Alkaline Cements and Concretes, Kiev, Ukraine.

Krizan, D. & Zivanovic, B. (2002) Effects of dossage and modulus of water glass on early hydration of alkali-slag cements. *Cement and Concrete Research,* 32**,** 1181-1188.

Law, D. W., Adam, A. A., Molyneaux, T. K. & Patnaikuni, I. (2012) Durability Assessment of Alkali Activated Slag (AAS) Concrete. *Materials and Structures,* 45**,** 1425-1437.

Lees, T. P. (1992) Deterioration Mechanism. *In:* Mays, G. (ed.) *Durability of Concrete Structures: Investigation, Repair, Protection.* London, New York, Tokyo, Melbourne, Madras: E & FN Spon. An imprint of Chapman and Hall.

Li, C., Sun, H. & Li, L. (2010) A review: The comparison between alkali-activated slag (Si+Ca) and metakaolin (Si+Al) cements. *Cement and Concrete Research,* 40**,** 1341-1349.

Luping, T. & Nilsson, L.-O. (1993) Chloride binding capacity and binding isotherms of opc pastes and mortars. *Cement and Concrete Research,* 23**,** 247-253.

Markeset, G. & Myrdal, R. (2008) COIN Project Report 7 - Modelling of Reinforcement Corrosion in Concrete - State of The Art. SP 4.1F Service Life Modelling and Prediction. Oslo, Norway, SINTEF Building and Infrastructure.

McCaffrey, R. (2001) Climate change and the cement industry. *Global Cement and Lime Magazine (Environmental Special Issue).*

McCarter, W. J., Starrs, G. & Chrisp, T. M. (2000) Electrical conductivity, diffusion, and permeability of Portland cement-based mortars. *Cement and Concrete Research,* 30**,** 1395-1400.

McGannon, H. E., *The Making, Shaping and Treating of Steel*. 9th ed. 1971, Pittsburgh, USA: United States Steel.

Mehta, P. K. (2001) Reducing the environmental impact of concrete. *Concrete International,* 23**,** 61-66.

Mehta, P. K. (2002) Greening of the concrete industry for sustainable development. *Concrete International,* 24**,** 23-28.

Mehta, P. K. & Monteiro, P. J. M., *Concrete : Microstructure, Properties, and Materials*. 3rd ed. 2006, United States of America: The McGraw-Hill Companies, Inc.

Meyer, C. (2009) The greening of the concrete industry. *Cement and Concrete Composites,* 31**,** 601-605.

Miranda, J. M., Fernandez-Jimenez, A., Gonzalez, J. A. & Palomo, A. (2005) Corrosion Resistance in Activated Fly Ash Mortars. *Cement and Concrete Research,* 35**,** 1210-1217.

Montgomery, F. R., Basheer, P. A. M. & Long, A. E. (1993) A Comparison Between the Autoclam Permeability System and the Initial Surface Absorption Test. In International Conference on Structural Faults and Repair, Edinburgh.

Morris, W., Vico, A., Vazquez, M. & Sanchez, S. R. d. (2002) Corrosion of reinforcing steel evaluated by means of concrete resistivity measurements. *Corrosion Science,* 44**,** 81-99.

Motorwala, A., Shah, V., Kammula, R., Nannapaneni, P. & Raijiwala, D. B. (2013) Alkali activated fly ash-based geopolymer concrete. *International Journal of Emerging Technology and Advanced Engineering,* 3**,** 159-166.

Nath, P. & Sarker, P. K. (2012) Geopolymer concrete for ambient curing condition. In proceedings of The Australasian Structural Engineering Conference 2012 (ASEC 2012), Perth, Western Australia. Engineers Australia.

Neupane, K., Baweja, D., Shrestha, R., Chalmers, D. & Sleep, P. (2014) Mechanical properties of geopolymer concrete: Applicability of relationships defined by AS 3600. *Concrete in Australia.* Australia: Concrete Institute of Australia.

Neville, A. M., *Properties of Concrete*. 5th ed. 2011, England: Pearson Education Limited.

Olivia, M. & Nikraz, H. (2012) Properties of fly ash geopolymer concrete designed by Taguchi method. *Materials and Design,* 36**,** 191-198.

Olivia, M., Sarker, P. & Nikraz, H. (2008) Water penetrability of low calcium fly ash geopolymer concrete In The International Conference On Construction And Building Technology 2008 (ICCBT 2008), 16-20 June 2008, Kuala Lumpur, Malaysia.

Oluokun, F. A., Burdette, E. G. & Deatherage, J. H. (1991) Splitting tensile strength and compressive strength relationship at early ages. *ACI Journal. Technical Paper,* March - April. Title no. 88-M14**,** 115-121.

Onera, A., T, S. A. & Yildiza, R. (2005) An experimental study on strength development of concrete containing fly ash and optimum usage of fly ash in concrete. *Cement and Concrete Research,* 35**,** 1165-1171.

Pacheco-Torgal, F., Castro-Gomes, J. & Jalali, S. (2008) Alkali-activated binders: A review. Part 1. Historical background, terminology, reaction mechanism and hydration products. *Construction & Building Materials,* 22**,** 1308-1314.

Page, C. L. (2007) Corrosion and Protection of Reinforcing Steel in Concrete. *In:* Page, C. L. & Page, M. M. (eds.) *Durability of Concrete and Cement Composites.* Florida, U.S.A: Woodhead Publishing Limited.

Palomo, A., Grutzeck, M. W. & Blanco, M. T. (1999) Alkali-activated fly ashes: A cement for the future. *Cement and Concrete Research,* 29**,** 1323-1329.

Papadakis, V. G., Vayenas, C. G. & Fardis, M. N. (1989) A Reaction problem of engineering approach to the concrete carbonation. *The American Institute of Chemical Engineers,* 35**,** 1639-1650.

Park, S.-S. & Kang, H.-Y. (2006) Strength and microscopic characteristics of alkali-activated fly ash-cement. *Korean Journal Chemical Engineering,* 23**,** 367-373.

Plenge, W. H. (2001) Introducing Vision 2030: Our Industry's 30-Year Map to the Future. *Concrete International,* 23.

Provis, J. L. (2006) Modelling The Formation of Geopolymers. Department of Chemical and Biomolecular Engineering, The University of Melbourne, Melbourne, Australia.

Puertas, F., Fernandez-Jimenez, A. & Blanco-Varela, M. T. (2004) Pore solution in alkali-activated slag cement pastes. Relation to the composition and structure of calcium silicate hydrate. *Cement and Concrete Research,* 34**,** 139-148.

Quan, H. (2011) The effects of change in fineness of fly ash on air-entraining concrete. *The Open Civil Engineering Journal,* 5**,** 124-131.

Ramachandran, V. S. (1995) Concrete Admixtures Handbook - Properties, Science, and Technology. 2 ed.: William Andrew Publishing/Noyes.

Rangan, B. V. (2010) Fly ash-based geopolymer concrete. In proceedings of Proceedings of the International Workshop on Geopolymer Cement and Concrete, Mumbai, India. Allied Publishers Private Limited.

Rangan, B. V., Hardjito, D., Wallah, S. E. & Sumajouw, D. M. J. (2006) Properties and applications of fly ash-based concrete. *Materials Forum,* 30**,** 170-175.

Raphael, J. M. (1984) Tensile strength of concrete. *ACI Journal. Technical Paper,* March - April. Title no. 81-17**,** 158-165.

RILEM Recommendations (1988) CPC-18 Measurement of hardened concrete carbonation depth. RILEM.

RILEM Recommendations (1994) RILEM Recommendations for the Testing and Use of Constructions Materials. CPC-18 Measurement of hardened concrete carbonation depth. RILEM.

Roa-Rodriguez, G., Aperador, W. & Delgado, A. (2014) Resistance to chlorides of the alkali-activated slag concrete. *Int. J. Electrochem. Sci,* 9**,** 282-291.

Rowles, M. & O'Connor, B. (2003) Chemical optimisation of the compressive strength of aluminosilicate geopolymers synthesised by sodium silicate activation of metakaolinite. *Journal of Material Chemistry,* 13**,** 1161-1165.

Roy, D. M. (1999) Alkali-activated Cements Opportunities and Challenges. *Cement and Concrete Research,* 29**,** 249-254.

Sagoe-Crentsil, K., Brown, T. & Yan, S. (2010) Medium to long term engineering properties and performance of high-strength geopolymers for structural applications. *Advances in Science and Technology,* 69**,** 135-142.

Sagoe-Crentsil, K. & Weng, L. (2007) Dissolution processes, hydrolysis and condensation reactions during geopolymer synthesis: Part II—High Si/Al ratio systems. *Journal of Material Science,* 42**,** 3007-3014.

Sakulich, A. R. (2009) Characterization of Environmentally-friendly Alkali Activated Slag Cements and Ancient Building Materials. Drexel University, Philadelphia, Pennsylvania, USA.

Sakulich, A. R., Anderson, E., Schauer, C. L. & Barsoum, M. W. (2010) Influence of Si:Al Ratio on The Microstructural and Mechanical Properties of a Fine-Limestone Agreggate Alkali-activated Slag Concrete. *Materials and Structures,* 43.

Shi, C. (1996) Strength, Pore Structure and Permeability of Alkali-Activated Slag Mortars. *Cement and Concrete Research,* 26 (12)**,** 1789-1799.

Shi, C., Krivenko, P. V. & Roy, D., *Alkali-Activated Cements and Concretes*. 2006, USA: Taylor & Francis.

Shi, C. & Li, Y. (1989) Investigation on Some Factors Affecting The Characteristics of Alkali-Phosphorus Slag Cement. *Cement and Concrete Research,* 19**,** 527-533.

Siddique, R. (2008) Waste Materials and By-Products in Concrete. Springer-Verlag Berlin Heidelberg.

Silva, P. D., Sagoe-Crentsil, K. & Sirivivatnanon, V. (2007) Kinetics of geopolymerization: Role of Al_2O_3 and SiO_2. *Cement and Concrete Research,* 37**,** 512-518.

Sindhunata (2006) A Conceptual Model of Geopolymerisation. Department of Chemical and Biomolecular Engineering, The University of Melbourne, Melbourne, Australia.

Sinsiri, T., Chindaprasirt, P. & Jaturapitakkul, C. (2010) Influence of fly ash fineness and shape on the porosity and permeability of blended cement

pastes. *International Journal of Minerals, Metallurgy and Materials,* 17**,** 683-690.

Sisomphon, K. & Franke, L. (2007) Carbonation rates of concretes containing high volume of pozzolanic materials. *Cement and Concrete Research,* 37**,** 1647-1653.

Slavik, R., Bednarik, V., Vondruska, M. & Nemec, A. (2008) Preparation of geopolymer from fluidized bed combustion bottom ash. *Journal of Materials Processing Technology,* 200**,** 265-270.

Sofi, M., Deventer, J. S. J. v., Mendis, P. A. & Lukey, G. C. (2007) Engineering properties of inorganic polymer concretes (IPCs). *Cement and Concrete Research,* 37.

Song, H.-W. & Saraswathy, V. (2007) Corrosion monitoring of reinforced concrete structures - A review. *Journal of Electrochemical Science,* 2**,** 1-28.

Song, S., Sohn, D., Jennings, H. M. & Mason, T. O. (2000) Hydration of alkali-activated ground granulated blast furnace slag. *Journal of Material Science,* 35**,** 249-257.

Song, X. (2007) Development and Performance of Class F Fly Ash Based Geopolymer Concretes against Sulphuric Acid Attack. School of Civil and Environmental Engineering, The University of New South Wales, Sydney, Australia.

Stanish, K. D., Hooton, R. D. & Thomas, M. D. A. (1997) Testing the Chloride Penetration Resistance of Concrete: A Literature Review. FHWA Contract DTFH61-97-R-00022 “Prediction of Chloride Penetration in Concrete”. Toronto, Ontario, Canada, Department of Civil Engineering University of Toronto.

Stanley, C. (2011) The Use and Abuse of The Slump Test For Measuring The Workability of Concrete. In 36th Conference on "Our World in Concrete & Structures", 14 - 16 August 2011, Singapore.

Steveson, M. & Sagoe-Crentsil, K. (2005) Relationships Between Composition, Structure and Strength of Inorganic Polymers. *Journal of Material Science,* 40.

Sulapha, P., Wong, S. F., Wee, T. H. & Swaddiwudhipong, S. (2003) Carbonation of concrete containing mineral admixtures. *Journal of Materials in Civil Engineering,* 15**,** 134-143.

Sumajouw, M. D. J. & Rangan, B. V. (2006) Low-calcium fly ash-based geopolymer concrete: Reinforced beams and columns. Research Report GC 3. Perth, Australia, Curtin University of Technology.

Sun, P. (2005) Fly Ash Based Inorganic Polymeric Building Material. Wayne State University, Detroit, Michigan, U.S.A.

Swamy, R. N., *Cement Replacement Materials*. Vol. 3. 1986, Glasgow: Surrey University Press.

Swanepoel, J. C. & Strydom, C. A. (2002) Utilisation of Fly Ash is a Geopolymeric Material. *Applied Geochemistry,* 17**,** 1143-1148.

Sykes, A. O., *An Introduction to Regression Analysis*. 1993.

Talling, B. (1989) Effect of curing conditions on alkali-activated slags. In Third International Conference Proceedings. Fly Ash, Silica Fume, Slag, and Natural Pozzolans in Concrete, Trondheim , Norway.

Talling, B. & Brandstetr, J. (1989) Present State and Future of Alkali Activated Slag Concretes. *American Concrete Institute,* 114**,** 1519-1546.

Taylor, H. F. W., *Cement chemistry*. 2nd ed. 1997, London: T. Telford.

Technical Report No.54, *Diagnosis of Deterioration in Concrete Structures: Identification of defects, evaluation and development of remedial action*. 2000: The Concrete Society.

Temuujin, J., Riessen, A. v. & R.Williams (2009) Influence of calcium compounds on the mechanical properties of fly ash geopolymer pastes. *Journal of Hazardous Materials,* 167**,** 82-88.

U.S. Geological Survey (2012) Mineral Commodity Summaries 2012. U.S.A., U.S. Geological Survey.

Wallah, S. E. & Rangan, B. V. (2006) Low-calcium fly ash-based geopolymer concrete: Long-term properties. Research Report GC 2. Perth, Australia, Curtin University of Technology.

Wang, H., Li, H. & Yan, F. (2005) Synthesis and mechanical properties of metakaolinite-based geopolymer. *Colloids and Surfaces A: Physicochem. Eng. Aspects,* 268**,** 1-6.

Wang, S.-D. & Scrivener, K. L. (1995) Hydration Products of Alkali Activated Slag Cement. *Cement and Concrete Research,* 25 (3)**,** 561-571.

Wang, S.-D. & Scrivener, K. L. (2003) ^{29}Si and ^{27}Al NMR study of alkali-activated slag. *Cement and Concrete Research,* 33**,** 769-774.

Wang, S.-D., Scrivener, K. L. & Platt, P. L. (1994) Factors Affecting the Strength of Alkali-Activated Slag. *Cement and Concrete Research,* 24 (6)**,** 1033-1043.

Wardhono, A., Law, D. W. & Molyneaux, T. C. K. (2012) Strength of Alkali Activated Slag and Fly Ash-based Geopolymer Mortar. In proceedings of Procceedings of Microstructural-related Durability of Cementitious Composites, 11-13 April 2012, Amsterdam, The Netherlands. RILEM Publications.

Weng, L. & Sagoe-Crentsil, K. (2007) Dissolution processes, hydrolysis and condensation reactions during geopolymer synthesis: Part I—Low Si /Al ratio systems. *Journal of Material Science,* 42**,** 2997-3006.

Winnefeld, F., Leemann, A., Lucuk, M., Svoboda, P. & Neuroth, M. (2010) Assessment of phase formation in alkali activated low and high calcium fly ashes in building materials. *Construction & Building Materials,* 24**,** 1086-1093.

Xu, H. (2002) Geopolymerisation of Aluminosilicate Materials. Master Thesis. Department of Chemical Engineering, The University of Melbourne, Melbourne, Australia.

Xu, H. & Deventer, J. S. J. v. (2000) The geopolymerisation of alumino-silicate minerals. *International Journal of Mineral Processing,* 59**,** 247-266.

Yang, K.-H., Song, J.-K., Lee, K.-S. & Ashour, A. F. (2009) Flow and compressive strength of alkali-activated mortars. *ACI Materials Journal,* Technical paper, Title no. 106-M07**,** 50-58.

Yip, C. K., Provis, J. L., Lukey, G. C. & Deventer, J. S. J. v. (2008) Carbonate mineral addition to metakaolin-based geopolymers. *Cement and Concrete Composites,* 30**,** 979-985.

Yongde, L. & Yao, S. (2000) Preliminary study on combined-alkali-slag paste materials. *Cement and Concrete Research,* 30**,** 963-966.

Zivica, V. (2007) Effects of type and dosage of alkaline activator and temperature on the properties of alkali-activated slag mixtures. *Construction and Building Materials,* 21**,** 1463-1469.

APPENDICES

Appendix A : Particle size distribution analysis

Appendix B : Compressive strength test results of mortar

Appendix C : Density test results of concrete

Appendix D : Compressive strength test results of concrete

Appendix E : Modulus of elasticity test results of concrete

Appendix F : Flexural strength test results of concrete

Appendix G : Indirect tensile strength test results of concrete

Appendix H : Porosity test results of concrete

Appendix I : Water absorption test results of concrete

Appendix J : Ultrasonic Pulse Velocity (UPV) test results of concrete

Appendix K : Water permeability test results of concrete

Appendix A Particle size distribution analysis

Appendix A : Particle size distribution analysis

Instruments : Malvern Particle Size Analyser Instruments Mastersizer X
Test location : Rheology and Material Processing Centre (RMCP) facility, School of Civil, Environmental and Chemical Engineering, RMIT University, Melbourne, Australia.
Standard : BS 410:1986 – Specification for test sieves

Specimen : Class F Fly ash PFA1

Sample No.	Specific Surface Area (S.S.A) (m^2/g)	Volume Mean D(v, 0.5) (μm)	Passing sieve 45 μm (%)
1	0.4752	27.72	64.08
2	0.4878	27.47	64.86
3	0.5091	26.54	67.22
4	0.4669	30.26	62.94
Average	**0.4848 $\pm$ 0.018**	**27.99 $\pm$ 1.59**	**64.78 $\pm$ 1.81**

Specimen : Class F Fly ash PFA2

Sample No.	Specific Surface Area (S.S.A) (m^2/g)	Volume Mean D(v, 0.5) (μm)	Passing sieve 45μm (%)
1	0.5343	25.40	71.72
2	0.5772	21.81	72.76
3	0.4967	28.28	72.03
4	0.5111	26.87	74.89
Average	**0.5298 $\pm$ 0.035**	**25.59 $\pm$ 2.78**	**72.85 $\pm$ 1.42**

Specimen : GGBS

Sample No.	Specific Surface Area (S.S.A) (m^2/g)	Volume Mean D(v, 0.5) (μm)	Passing sieve 45μm (%)
1	0.6528	17.71	90.04
2	0.6442	19.45	90.90
3	0.6917	17.26	93.90
4	0.6802	18.11	93.23
Average	**0.6672 $\pm$ 0.022**	**18.13 $\pm$ 0.94**	**92.02 $\pm$ 1.84**

Appendix B Compressive strength test results of mortar

Appendix B.1 : Compressive strength test results of mortar, PFA1

Specimen : Fly ash geopolymer mortar
Source : Fly ash type 1 (PFA1)
Alkali modulus : Ms = 1.00

Compressive strength at 3 days					
Specimen ID	Max Load (N)	Width (mm)	Length (mm)	Height (mm)	Compressive strength (MPa)
GA15-1.00-01	32146.9	50.2	50.1	50.2	12.78
GA15-1.00-02	30382.8	50.3	50.2	50.3	12.03
GA15-1.00-03	30539.1	50.1	50.1	50.2	12.17
				Average	12.33
				Standard deviation	0.40

Compressive strength at 7 days					
Specimen ID	Max Load (N)	Width (mm)	Length (mm)	Height (mm)	Compressive strength (MPa)
GA15-1.00-04	49562.5	50.2	50.2	50.3	19.67
GA15-1.00-05	50890.6	50.3	50.2	50.3	20.15
GA15-1.00-06	49889.1	50.1	50.2	50.0	19.84
				Average	19.89
				Standard deviation	0.25

Compressive strength at 14 days					
Specimen ID	Max Load (N)	Width (mm)	Length (mm)	Height (mm)	Compressive strength (MPa)
GA15-1.00-07	62751.6	50.2	50.1	50.2	24.95
GA15-1.00-08	58317.2	50.2	50.1	50.3	23.19
GA15-1.00-09	57500.7	50.0	50.2	50.2	22.91
				Average	23.68
				Standard deviation	1.11

Compressive strength at 28 days					
Specimen ID	Max Load (N)	Width (mm)	Length (mm)	Height (mm)	Compressive strength (MPa)
GA15-1.00-10	76211.0	50.1	50.0	50.1	30.42
GA15-1.00-11	77634.4	49.8	50.0	50.0	31.18
GA15-1.00-12	72992.9	50.2	50.1	50.2	29.02
				Average	30.21
				Standard deviation	1.09

Appendix B.1 : Compressive strength test results of mortar, PFA1

Specimen : Fly ash geopolymer mortar
Source : Fly ash type 1 (PFA1)
Alkali modulus : Ms = 1.125

Compressive strength at 3 days					
Specimen ID	Max Load (N)	Width (mm)	Length (mm)	Height (mm)	Compressive strength (MPa)
GA15-1.125-01	23210.9	50.1	50.2	50.2	9.23
GA15-1.125-02	22875.0	50.2	50.1	50.3	9.10
GA15-1.125-03	23285.1	50.2	50.2	50.2	9.24
				Average	9.19
				Standard deviation	0.08

Compressive strength at 7 days					
Specimen ID	Max Load (N)	Width (mm)	Length (mm)	Height (mm)	Compressive strength (MPa)
GA15-1.125-04	29586.7	50.2	50.2	50.3	11.74
GA15-1.125-05	30828.1	50.2	50.1	50.2	12.26
GA15-1.125-06	29153.9	50.3	50.2	50.3	11.55
				Average	11.85
				Standard deviation	0.37

Compressive strength at 14 days					
Specimen ID	Max Load (N)	Width (mm)	Length (mm)	Height (mm)	Compressive strength (MPa)
GA15-1.125-07	45178.1	50.1	50.0	50.1	18.04
GA15-1.125-08	41085.9	49.9	50.1	50.1	16.43
GA15-1.125-09	42255.5	50.0	50.1	50.1	16.87
				Average	17.11
				Standard deviation	0.83

Compressive strength at 28 days					
Specimen ID	Max Load (N)	Width (mm)	Length (mm)	Height (mm)	Compressive strength (MPa)
GA15-1.125-10	71524.7	50.2	50.2	50.1	28.38
GA15-1.125-11	74283.1	50.1	50.0	50.0	29.65
GA15-1.125-12	71109.4	49.7	50.0	49.9	28.62
				Average	28.88
				Standard deviation	0.68

Appendix B.1 : Compressive strength test results of mortar, PFA1

Specimen : Fly ash geopolymer mortar
Source : Fly ash type 1 (PFA1)
Alkali modulus : Ms = 1.25

Compressive strength at 3 days					
Specimen ID	Max Load (N)	Width (mm)	Length (mm)	Height (mm)	Compressive strength (MPa)
GA15-1.25-01	15093.8	50.1	50.1	50.0	6.01
GA15-1.25-02	14726.6	49.8	50.1	50.0	5.90
GA15-1.25-03	15156.3	50.2	50.1	50.1	6.03
				Average	5.98
				Standard deviation	0.07

Compressive strength at 7 days					
Specimen ID	Max Load (N)	Width (mm)	Length (mm)	Height (mm)	Compressive strength (MPa)
GA15-1.25-04	27070.3	50.2	50.2	50.1	10.74
GA15-1.25-05	27906.3	50.0	50.1	50.1	11.14
GA15-1.25-06	27953.1	50.1	50.2	50.1	11.11
				Average	11.00
				Standard deviation	0.22

Compressive strength at 14 days					
Specimen ID	Max Load (N)	Width (mm)	Length (mm)	Height (mm)	Compressive strength (MPa)
GA15-1.25-07	36420.3	50.0	50.1	50.1	14.54
GA15-1.25-08	36207.1	49.8	50.1	49.9	14.51
GA15-1.25-09	38343.8	50.1	50.2	50.1	15.25
				Average	14.77
				Standard deviation	0.42

Compressive strength at 28 days					
Specimen ID	Max Load (N)	Width (mm)	Length (mm)	Height (mm)	Compressive strength (MPa)
GA15-1.25-10	69937.5	50.2	50.1	50.1	27.81
GA15-1.25-11	72937.5	49.9	50.2	50.0	29.12
GA15-1.25-12	72679.7	50.2	50.1	50.2	28.90
				Average	28.61
				Standard deviation	0.70

Appendix B.2 : Compressive strength test results of mortar, PFA2

Specimen : Fly ash geopolymer mortar
Source : Fly ash type 2 (PFA2)
Alkali modulus : Ms = 1.00

Compressive strength at 3 days					
Specimen ID	Max Load (N)	Width (mm)	Length (mm)	Height (mm)	Compressive strength (MPa)
GB15-1.00-01	97203.1	50.1	50.2	50.1	38.65
GB15-1.00-02	98062.5	50.2	50.2	50.1	38.91
GB15-1.00-03	93945.3	49.8	50.0	50.0	37.73
				Average	38.43
				Standard deviation	0.62

Compressive strength at 7 days					
Specimen ID	Max Load (N)	Width (mm)	Length (mm)	Height (mm)	Compressive strength (MPa)
GB15-1.00-04	112398.0	50.0	50.2	50.1	44.78
GB15-1.00-05	115713.2	49.9	50.0	49.8	46.38
GB15-1.00-06	117703.0	50.2	50.3	50.1	46.61
				Average	45.92
				Standard deviation	1.00

Compressive strength at 14 days					
Specimen ID	Max Load (N)	Width (mm)	Length (mm)	Height (mm)	Compressive strength (MPa)
GB15-1.00-07	128336.0	50.3	50.1	50.2	50.93
GB15-1.00-08	122091.2	50.1	50.2	50.1	48.54
GB15-1.00-09	127119.3	50.2	50.2	50.1	50.44
				Average	49.97
				Standard deviation	1.26

Compressive strength at 28 days					
Specimen ID	Max Load (N)	Width (mm)	Length (mm)	Height (mm)	Compressive strength (MPa)
GB15-1.00-10	138234.0	50.1	50.2	50.2	54.96
GB15-1.00-11	143984.0	50.3	50.2	50.2	57.02
GB15-1.00-12	130891.2	50.0	49.8	49.9	52.57
				Average	54.85
				Standard deviation	2.23

Appendix B.2 : Compressive strength test results of mortar, PFA2

Specimen : Fly ash geopolymer mortar
Source : Fly ash type 2 (PFA2)
Alkali modulus : Ms = 1.125

Compressive strength at 3 days					
Specimen ID	Max Load (N)	Width (mm)	Length (mm)	Height (mm)	Compressive strength (MPa)
GB15-1.125-01	80135.0	50.2	50.1	50.1	31.86
GB15-1.125-02	84519.5	50.0	50.1	50.1	33.67
GB15-1.125-03	76812.8	49.9	49.8	50.0	30.91
				Average	32.15
				Standard deviation	1.40

Compressive strength at 7 days					
Specimen ID	Max Load (N)	Width (mm)	Length (mm)	Height (mm)	Compressive strength (MPa)
GB15-1.125-04	98512.6	50.1	50.2	50.1	39.17
GB15-1.125-05	96450.0	50.3	50.2	50.2	38.20
GB15-1.125-06	91153.1	50.1	50.1	50.0	36.32
				Average	37.89
				Standard deviation	1.45

Compressive strength at 14 days					
Specimen ID	Max Load (N)	Width (mm)	Length (mm)	Height (mm)	Compressive strength (MPa)
GB15-1.125-07	118369.9	50.3	50.2	50.2	46.88
GB15-1.125-08	105896.6	50.1	50.1	50.0	42.19
GB15-1.125-09	106200.0	50.0	50.1	50.0	42.40
				Average	43.82
				Standard deviation	2.65

Compressive strength at 28 days					
Specimen ID	Max Load (N)	Width (mm)	Length (mm)	Height (mm)	Compressive strength (MPa)
GB15-1.125-10	119531.0	49.8	50.1	50.0	47.91
GB15-1.125-11	113203.0	50.2	50.3	50.0	44.83
GB15-1.125-12	112329.4	50.0	50.2	50.1	44.75
				Average	45.83
				Standard deviation	1.80

Appendix B.2 : Compressive strength test results of mortar, PFA2

Specimen : Fly ash geopolymer mortar
Source : Fly ash type 2 (PFA2)
Alkali modulus : Ms = 1.25

Compressive strength at 3 days					
Specimen ID	Max Load (N)	Width (mm)	Length (mm)	Height (mm)	Compressive strength (MPa)
GB15-1.25-01	70750.0	50.1	50.2	50.1	28.13
GB15-1.25-02	76734.4	50.2	50.2	50.1	30.45
GB15-1.25-03	70015.6	49.8	50.0	49.9	28.12
				Average	28.90
				Standard deviation	1.34

Compressive strength at 7 days					
Specimen ID	Max Load (N)	Width (mm)	Length (mm)	Height (mm)	Compressive strength (MPa)
GB15-1.25-04	96954.7	50.2	50.2	50.1	38.47
GB15-1.25-05	82200.0	49.7	50.0	49.9	33.08
GB15-1.25-06	83307.0	50.1	50.2	50.1	33.12
				Average	34.89
				Standard deviation	3.10

Compressive strength at 14 days					
Specimen ID	Max Load (N)	Width (mm)	Length (mm)	Height (mm)	Compressive strength (MPa)
GB15-1.25-07	93315.7	50.1	50.1	50.2	37.18
GB15-1.25-08	94140.2	50.2	50.1	50.1	37.43
GB15-1.25-09	97475.0	50.1	50.0	50.0	38.91
				Average	37.84
				Standard deviation	0.94

Compressive strength at 28 days					
Specimen ID	Max Load (N)	Width (mm)	Length (mm)	Height (mm)	Compressive strength (MPa)
GB15-1.25-10	100906.0	50.2	50.1	50.1	40.12
GB15-1.25-11	101336.0	49.8	49.9	49.9	40.78
GB15-1.25-12	100117.0	50.1	50.2	50.1	39.81
				Average	40.24
				Standard deviation	0.50

Appendix B.3 : Compressive strength test results of mortar, AAS

Specimen : Alkali activated slag mortar
Source : GGBS
Alkali modulus : Ms = 1.00

Compressive strength at 3 days					
Specimen ID	Max Load (N)	Width (mm)	Length (mm)	Height (mm)	Compressive strength (MPa)
AAS5-1.00-01	77575.0	50.1	50.1	50.2	30.91
AAS5-1.00-02	78209.4	50.1	50.0	50.0	31.22
AAS5-1.00-03	80934.4	50.2	50.1	50.1	32.18
				Average	31.44
				Standard deviation	0.66

Compressive strength at 7 days					
Specimen ID	Max Load (N)	Width (mm)	Length (mm)	Height (mm)	Compressive strength (MPa)
AAS5-1.00-04	102680.0	50.1	50.2	50.1	40.83
AAS5-1.00-05	100852.0	49.8	50.0	49.9	40.50
AAS5-1.00-06	92742.2	50.2	50.2	50.1	36.80
				Average	39.39
				Standard deviation	2.24

Compressive strength at 14 days					
Specimen ID	Max Load (N)	Width (mm)	Length (mm)	Height (mm)	Compressive strength (MPa)
AAS5-1.00-07	113162.6	50.3	50.2	50.2	44.82
AAS5-1.00-08	128102.0	50.1	50.2	50.2	50.93
AAS5-1.00-09	114555.0	50.2	50.2	50.0	45.46
				Average	47.07
				Standard deviation	3.36

Compressive strength at 28 days					
Specimen ID	Max Load (N)	Width (mm)	Length (mm)	Height (mm)	Compressive strength (MPa)
AAS5-1.00-10	116766.0	50.2	50.2	50.1	46.33
AAS5-1.00-11	119727.0	49.8	50.0	49.9	48.08
AAS5-1.00-12	124383.0	50.2	50.2	50.3	49.36
				Average	47.93
				Standard deviation	1.52

Appendix B.3 : Compressive strength test results of mortar, AAS

Specimen : Alkali activated slag mortar
Source : GGBS
Alkali modulus : Ms = 1.125

Compressive strength at 3 days					
Specimen ID	Max Load (N)	Width (mm)	Length (mm)	Height (mm)	Compressive strength (MPa)
AAS5-1.125-01	84914.3	50.0	50.1	50.1	33.90
AAS5-1.125-02	77715.7	50.1	50.2	50.1	30.90
AAS5-1.125-03	76309.9	50.3	50.2	50.3	30.22
				Average	31.67
				Standard deviation	1.96

Compressive strength at 7 days					
Specimen ID	Max Load (N)	Width (mm)	Length (mm)	Height (mm)	Compressive strength (MPa)
AAS5-1.125-04	103884.4	50.1	50.0	50.0	41.47
AAS5-1.125-05	102481.7	49.7	50.0	49.9	41.24
AAS5-1.125-06	100762.8	49.8	50.1	50.0	40.39
				Average	41.03
				Standard deviation	0.57

Compressive strength at 14 days					
Specimen ID	Max Load (N)	Width (mm)	Length (mm)	Height (mm)	Compressive strength (MPa)
AAS5-1.125-07	112970.4	50.2	50.1	50.2	44.92
AAS5-1.125-08	108590.6	50.3	50.2	50.3	43.01
AAS5-1.125-09	113821.9	50.1	50.1	50.2	45.35
				Average	44.42
				Standard deviation	1.25

Compressive strength at 28 days					
Specimen ID	Max Load (N)	Width (mm)	Length (mm)	Height (mm)	Compressive strength (MPa)
AAS5-1.125-10	115703.0	50.2	50.1	50.3	46.00
AAS5-1.125-11	113962.5	50.0	50.2	50.2	45.40
AAS5-1.125-12	110554.5	50.1	50.0	50.0	44.13
				Average	45.18
				Standard deviation	0.96

Appendix B.3 : Compressive strength test results of mortar, AAS

Specimen : Alkali activated slag mortar
Source : GGBS
Alkali modulus : Ms = 1.25

Compressive strength at 3 days					
Specimen ID	Max Load (N)	Width (mm)	Length (mm)	Height (mm)	Compressive strength (MPa)
AAS5-1.25-01	91012.6	50.1	50.0	50.0	36.33
AAS5-1.25-02	85531.3	50.0	50.1	50.1	34.14
AAS5-1.25-03	92921.9	49.8	50.1	49.9	37.24
				Average	35.91
				Standard deviation	1.59

Compressive strength at 7 days					
Specimen ID	Max Load (N)	Width (mm)	Length (mm)	Height (mm)	Compressive strength (MPa)
AAS5-1.25-04	114797.0	50.1	50.1	50.2	45.74
AAS5-1.25-05	127938.0	50.2	50.2	50.3	50.77
AAS5-1.25-06	117632.9	50.2	50.1	50.2	46.77
				Average	47.76
				Standard deviation	2.66

Compressive strength at 14 days					
Specimen ID	Max Load (N)	Width (mm)	Length (mm)	Height (mm)	Compressive strength (MPa)
AAS5-1.25-07	116062.6	49.9	50.2	50.0	46.33
AAS5-1.25-08	108671.9	50.2	50.1	50.2	43.21
AAS5-1.25-09	109748.7	50.3	50.1	50.2	43.55
				Average	44.36
				Standard deviation	1.71

Compressive strength at 28 days					
Specimen ID	Max Load (N)	Width (mm)	Length (mm)	Height (mm)	Compressive strength (MPa)
AAS5-1.25-10	109919.7	50.2	50.2	50.1	43.62
AAS5-1.25-11	107465.6	50.0	50.1	50.1	42.90
AAS5-1.25-12	101620.3	50.1	50.1	50.0	40.49
				Average	42.33
				Standard deviation	1.64

Appendix C Density test results of concrete

Appendix C.1 : Density test results of fly ash geopolymer concrete

Standard : AS 1012.12.1 – 1998
Method : Rapid measurement method
Specimen : Fly ash geopolymer concrete
Note : Use the same specimens (total 3 specimens) from 28 to 540 days

Fly ash geopolymer ; density at 28 days							
Specimen ID	Weight SSD (gram)	h_1 (mm)	d_1 (mm)	d_2 (mm)	d_{avg} (mm)	Area (mm^2)	Density (kg/m^3)
G15-1-28-E01	3747.9	193.0	103.1	104.0	103.6	8424.5	2305.1
G15-1-28-E02	3746.7	192.3	103.5	103.3	103.4	8394.7	2320.5
G15-1-28-E03	3755.4	193.5	103.8	104.4	104.1	8506.1	2281.6
						Average	2302.4
						Standard deviation	19.58

Fly ash geopolymer ; density at 56 days							
Specimen ID	Weight SSD (gram)	h_1 (mm)	d_1 (mm)	d_2 (mm)	d_{avg} (mm)	Area (mm^2)	Density (kg/m^3)
G15-1-28-E01	3758.6	193.0	103.1	104.0	103.6	8424.5	2311.7
G15-1-28-E02	3757.5	192.3	103.5	103.3	104.4	8394.7	2327.2
G15-1-28-E03	3759.3	193.5	103.8	104.4	104.1	8506.1	2284.0
						Average	2307.6
						Standard deviation	21.89

Fly ash geopolymer ; density at 90 days							
Specimen ID	Weight SSD (gram)	h_1 (mm)	d_1 (mm)	d_2 (mm)	d_{avg} (mm)	Area (mm^2)	Density (kg/m^3)
G15-1-28-E01	3761.1	193.0	103.1	104.0	103.6	8424.5	2313.2
G15-1-28-E02	3767.0	192.3	103.5	103.3	104.4	8394.7	2333.1
G15-1-28-E03	3763.4	193.5	103.8	104.4	104.1	8506.1	2286.5
						Average	2310.9
						Standard deviation	23.39

Appendix C.1 : Density test results of fly ash geopolymer concrete

Standard : AS 1012.12.1 – 1998
Method : Rapid measurement method
Specimen : Fly ash geopolymer concrete
Note : Use the same specimens (total 3 specimens) from 28 to 540 days

Fly ash geopolymer ; density at 180 days							
Specimen ID	Weight SSD (gram)	h_1 (mm)	d_1 (mm)	d_2 (mm)	d_{avg} (mm)	Area (mm^2)	Density (kg/m^3)
G15-1-28-E01	3782.4	193.0	103.1	104.0	103.6	8424.5	2326.3
G15-1-28-E02	3782.8	192.3	103.5	103.3	104.4	8394.7	2342.9
G15-1-28-E03	3777.2	193.5	103.8	104.4	104.1	8506.1	2294.9
						Average	2321.4
						Standard deviation	24.38

Fly ash geopolymer ; density at 360 days							
Specimen ID	Weight SSD (gram)	h_1 (mm)	d_1 (mm)	d_2 (mm)	d_{avg} (mm)	Area (mm^2)	Density (kg/m^3)
G15-1-28-E01	3787.4	193.0	103.1	104.0	103.6	8424.5	2329.4
G15-1-28-E02	3788.8	192.3	103.5	103.3	104.4	8394.7	2346.6
G15-1-28-E03	3780.2	193.5	103.8	104.4	104.1	8506.1	2296.7
						Average	2324.2
						Standard deviation	25.35

Fly ash geopolymer ; density at 540 days							
Specimen ID	Weight SSD (gram)	h_1 (mm)	d_1 (mm)	d_2 (mm)	d_{avg} (mm)	Area (mm^2)	Density (kg/m^3)
G15-1-28-E01	3789.4	193.0	103.1	104.0	103.6	8424.5	2330.6
G15-1-28-E02	3791.8	192.3	103.5	103.3	104.4	8394.7	2348.5
G15-1-28-E03	3781.2	193.5	103.8	104.4	104.1	8506.1	2297.3
						Average	2325.5
						Standard deviation	25.96

Appendix C.2 : Density test results of AAS concrete

Standard : AS 1012.12.1 – 1998
Method : Rapid measurement method
Specimen : AAS concrete
Note : Use the same specimens (total 3 specimens) from 28 to 540 days

AAS ; density at 28 days							
Specimen ID	Weight SSD (gram)	h_1 (mm)	d_1 (mm)	d_2 (mm)	d_{avg} (mm)	Area (mm^2)	Density (kg/m^3)
AAS5-1-28-E01	3794.1	195.7	100.0	99.9	99.9	7841.2	2472.9
AAS5-1-28-E02	3780.2	197.6	100.0	100.0	100.0	7856.9	2434.9
AAS5-1-28-E03	3813.6	197.0	100.4	100.2	100.3	7901.4	2450.0
						Average	2452.6
						Standard deviation	19.16

AAS ; density at 56 days							
Specimen ID	Weight SSD (gram)	h_1 (mm)	d_1 (mm)	d_2 (mm)	d_{avg} (mm)	Area (mm^2)	Density (kg/m^3)
AAS5-1-28-E01	3796.3	195.7	100.0	99.9	99.9	7841.2	2474.4
AAS5-1-28-E02	3783.7	197.6	100.0	100.0	100.0	7856.9	2437.1
AAS5-1-28-E03	3814.2	197.0	100.4	100.2	100.3	7901.4	2450.4
						Average	2454.0
						Standard deviation	18.87

AAS ; density at 90 days							
Specimen ID	Weight SSD (gram)	h_1 (mm)	d_1 (mm)	d_2 (mm)	d_{avg} (mm)	Area (mm^2)	Density (kg/m^3)
AAS5-1-28-E01	3803.0	195.7	100.0	99.9	99.9	7841.2	2478.7
AAS5-1-28-E02	3788.6	197.6	100.0	100.0	100.0	7856.9	2440.3
AAS5-1-28-E03	3816.1	197.0	100.4	100.2	100.3	7901.4	2451.6
						Average	2456.9
						Standard deviation	19.75

Appendix C.2 : Density test results of AAS concrete

Standard : AS 1012.12.1 – 1998
Method : Rapid measurement method
Specimen : AAS concrete
Note : Use the same specimens (total 3 specimens) from 28 to 540 days

AAS ; density at 180 days							
Specimen ID	Weight SSD (gram)	h_1 (mm)	d_1 (mm)	d_2 (mm)	d_{avg} (mm)	Area (mm^2)	Density (kg/m^3)
AAS5-1-28-E01	3803.8	195.7	100.0	99.9	99.9	7841.2	2479.2
AAS5-1-28-E02	3790.1	197.6	100.0	100.0	100.0	7856.9	2441.3
AAS5-1-28-E03	3818.0	197.0	100.4	100.2	100.3	7901.4	2452.8
						Average	2457.8
						Standard deviation	19.48

AAS ; density at 360 days							
Specimen ID	Weight SSD (gram)	h_1 (mm)	d_1 (mm)	d_2 (mm)	d_{avg} (mm)	Area (mm^2)	Density (kg/m^3)
AAS5-1-28-E01	3804.4	195.7	100.0	99.9	99.9	7841.2	2479.6
AAS5-1-28-E02	3786.9	197.6	100.0	100.0	100.0	7856.9	2439.2
AAS5-1-28-E03	3821.4	197.0	100.4	100.2	100.3	7901.4	2455.0
						Average	2457.9
						Standard deviation	20.38

AAS ; density at 540 days							
Specimen ID	Weight SSD (gram)	h_1 (mm)	d_1 (mm)	d_2 (mm)	d_{avg} (mm)	Area (mm^2)	Density (kg/m^3)
AAS5-1-28-E01	3806.1	195.7	100.0	99.9	99.9	7841.2	2480.7
AAS5-1-28-E02	3792.8	197.6	100.0	100.0	100.0	7856.9	2443.0
AAS5-1-28-E03	3820.8	197.0	100.4	100.2	100.3	7901.4	2454.6
						Average	2459.5
						Standard deviation	19.34

Appendix D Compressive strength test results of concrete

Appendix D : Compressive strength test results of fly ash geopolymer and AAS concretes

Standard : AS 1012.9 – 1999
Specimen : Fly ash geopolymer and AAS concretes
Loading rate : 20 + 2 MPa/min
Compressive strength : $N / 1/4\pi D^2$

Fly ash geopolymer ; compressive strength at 28 days							
Specimen ID	Max Load (N)	Weight (g)	h_1 (mm)	d_1 (mm)	d_2 (mm)	d_{avg} (mm)	Compressive Strength (MPa)
G15-1-28-A01	177511	3706	199.3	100.0	99.3	99.7	22.75
G15-1-28-A02	174730	3592	199.0	99.3	99.0	99.2	22.62
G15-1-28-A03	167973	3594	199.2	99.3	99.1	99.2	21.73
						Average	22.37
						Standard deviation	0.56

Fly ash geopolymer ; compressive strength at 56 days							
Specimen ID	Max Load (N)	Weight (g)	h_1 (mm)	d_1 (mm)	d_2 (mm)	d_{avg} (mm)	Compressive Strength (MPa)
G15-1-56-A04	198812	3706	199.4	100.2	99.5	99.8	25.40
G15-1-56-A05	198494	3592	199.2	99.4	99.2	99.3	25.62
G15-1-56-A06	189474	3594	199.4	99.6	99.4	99.5	24.37
						Average	25.13
						Standard deviation	0.66

Fly ash geopolymer ; compressive strength at 90 days							
Specimen ID	Max Load (N)	Weight (g)	h_1 (mm)	d_1 (mm)	d_2 (mm)	d_{avg} (mm)	Compressive Strength (MPa)
G15-1-90-A07	203779	3681	199.8	99.0	99.7	99.3	26.29
G15-1-90-A08	208270	3619	199.3	99.2	99.0	99.1	27.01
G15-1-90-A09	215186	3621	199.7	99.4	99.5	99.4	27.72
						Average	27.01
						Standard deviation	0.71

Fly ash geopolymer ; compressive strength at 180 days							
Specimen ID	Max Load (N)	Weight (g)	h_1 (mm)	d_1 (mm)	d_2 (mm)	d_{avg} (mm)	Compressive Strength (MPa)
G15-1-180-A10	246305	3538.5	199.6	99.7	100.0	99.85	31.45
G15-1-180-A11	233870	3740.2	199.8	99.9	100.0	99.95	29.81
G15-1-180-A12	249193	3561.6	199.7	99.6	99.5	99.55	32.01
						Average	31.09
						Standard deviation	1.15

Appendix D : Compressive strength test results of fly ash geopolymer and AAS concretes

Standard : AS 1012.9 – 1999
Specimen : Fly ash geopolymer and AAS concretes
Loading rate : 20 + 2 MPa/min
Compressive strength : $N / 1/4\pi D^2$

Fly ash geopolymer ; compressive strength at 360 days							
Specimen ID	Max Load (N)	Weight (g)	h_1 (mm)	d_1 (mm)	d_2 (mm)	d_{avg} (mm)	Compressive Strength (MPa)
G15-1-360-A13	254274	3583	199.9	99.7	99.5	99.6	32.63
G15-1-360-A14	250278	3603	199.7	99.9	99.3	99.6	32.11
G15-1-360-A15	272747	3730	199.8	100.0	99.4	99.7	34.94
						Average	33.23
						Standard deviation	1.50

Fly ash geopolymer ; compressive strength at 540 days							
Specimen ID	Max Load (N)	Weight (g)	h_1 (mm)	d_1 (mm)	d_2 (mm)	d_{avg} (mm)	Compressive Strength (MPa)
G15-1-540-A16	263736	3580	199.7	99.9	99.7	99.78	33.72
G15-1-540-A17	251236	3778	199.5	99.8	99.8	99.82	32.10
G15-1-540-A18	261523	3556	199.8	99.9	99.7	99.78	33.44
						Average	33.09
						Standard deviation	0.87

AAS ; compressive strength at 28 days							
Specimen ID	Max Load (N)	Weight (g)	h_1 (mm)	d_1 (mm)	d_2 (mm)	d_{avg} (mm)	Compressive Strength (MPa)
AAS5-1-07-A01	321502	3820	199.3	99.9	100.5	100.2	40.74
AAS5-1-07-A02	305621	3862	199.1	99.9	100.1	100.0	38.89
AAS5-1-07-A03	304166	3806	198.5	99.9	100.0	99.9	38.78
						Average	39.47
						Standard deviation	1.11

AAS ; compressive strength at 56 days							
Specimen ID	Max Load (N)	Weight (g)	h_1 (mm)	d_1 (mm)	d_2 (mm)	d_{avg} (mm)	Compressive Strength (MPa)
AAS5-1-28-A04	337577	3820	199.1	99.6	100.4	100.0	42.99
AAS5-1-28-A05	320902	3862	199.1	99.8	100.0	99.9	40.94
AAS5-1-28-A06	319374	3806	198.0	99.6	100.0	99.8	40.83
						Average	41.59
						Standard deviation	1.22

Appendix D : Compressive strength test results of fly ash geopolymer and AAS concretes

Standard : AS 1012.9 – 1999
Specimen : Fly ash geopolymer and AAS concretes
Loading rate : 20 + 2 MPa/min
Compressive strength : $N / 1/4\pi D^2$

AAS ; compressive strength at 90 days							
Specimen ID	Max Load (N)	Weight (g)	h_1 (mm)	d_1 (mm)	d_2 (mm)	d_{avg} (mm)	Compressive Strength (MPa)
AAS5-1-90-A07	314944	3776	199.0	100.1	99.9	100.0	40.10
AAS5-1-90-A08	322981	3795	199.7	99.7	100.0	99.9	41.23
AAS5-1-90-A08	334614	3835	199.8	100.0	100.3	100.2	42.45
						Average	41.26
						Standard deviation	1.18

AAS ; compressive strength at 180 days							
Specimen ID	Max Load (N)	Weight (g)	h_1 (mm)	d_1 (mm)	d_2 (mm)	d_{avg} (mm)	Compressive Strength (MPa)
AAS5-1-180-A10	321025	3788	199.5	99.7	100.2	99.9	40.94
AAS5-1-180-A11	300683	3756	198.5	100.0	100.3	100.2	38.16
AAS5-1-180-A12	332304	3811	199.3	99.7	100.6	100.2	42.18
						Average	40.43
						Standard deviation	2.06

AAS ; compressive strength at 360 days							
Specimen ID	Max Load (N)	Weight (g)	h_1 (mm)	d_1 (mm)	d_2 (mm)	d_{avg} (mm)	Compressive Strength (MPa)
AAS5-1-360-A13	313570	3774	198.8	99.8	99.8	99.8	40.10
AAS5-1-360-A14	320909	3828	198.5	100.2	100.5	100.3	40.59
AAS5-1-360-A15	315889	3799	199.3	99.7	99.9	99.8	40.37
						Average	40.35
						Standard deviation	0.25

AAS ; compressive strength at 540 days							
Specimen ID	Max Load (N)	Weight (g)	h_1 (mm)	d_1 (mm)	d_2 (mm)	d_{avg} (mm)	Compressive Strength (MPa)
AAS5-1-540-A16	282754	3783	199.5	99.8	99.8	99.8	36.13
AAS5-1-540-A17	305827	3779	199.3	99.8	99.9	99.8	39.08
AAS5-1-540-A18	312190	3801	200.2	99.9	100.2	100.1	39.71
						Average	38.31
						Standard deviation	1.91

Appendix E Modulus of elasticity test results of concrete

Appendix E.1 : Calculation of the area and 40% compressive strength of concrete specimen

Test : Modulus of elasticity
Standard : AS.1012.17 – 1997
Specimen : Fly ash geopolymer and AAS concretes

Specimen	d_1 (mm)	d_2 (mm)	d_{avg} (mm)	A (mm^2)	Compressive strength (MPa)	Age (days)	Compressive strength 40% average (MPa)
Fly ash geopolymer concrete							
G15-1-28-B01	97.3	97.7	97.5	7466.4	177511	28	69362
G15-1-28-B02	98.7	98.7	98.7	7646.2	174730		
G15-1-28-B03	97.7	98.0	97.8	7517.6	167973		
G15-1-90-B04	97.7	97.7	97.7	7492.0	203779	90	83631
G15-1-90-B05	98.7	98.0	98.3	7594.6	208270		
G15-1-90-B06	98.3	98.0	98.2	7568.9	215186		
G15-1-180-B07	98.0	98.3	98.2	7568.9	246305	180	97249
G15-1-180-B08	99.0	98.7	98.8	7672.1	233870		
G15-1-180-B09	97.3	97.7	97.5	7466.4	249193		
G15-1-360-B10	97.7	98.3	98.0	7543.2	254274	360	103640
G15-1-360-B11	98.3	98.3	98.3	7594.6	250278		
G15-1-360-B12	98.0	98.3	98.2	7568.9	272747		
G15-1-540-B13	98.7	99.0	98.8	7672.1	263736	540	103533
G15-1-540-B14	97.7	97.7	97.7	7492.0	251236		
G15-1-540-B15	98.0	98.7	98.3	7594.6	261523		
AAS concrete							
AAS5-1-28-B01	97.7	98.0	97.8	7517.6	321502	28	124172
AAS5-1-28-B02	97.3	97.3	97.3	7440.9	305621		
AAS5-1-28-B03	98.7	99.0	98.8	7672.1	304166		
AAS5-1-90-B04	98.3	97.7	98.0	7543.2	314944	90	129672
AAS5-1-90-B05	97.7	97.7	97.7	7492.0	322981		
AAS5-1-90-B06	98.0	98.3	98.2	7568.9	334614		
AAS5-1-180-B07	97.3	97.3	97.3	7440.9	321025	180	127202
AAS5-1-180-B08	97.7	97.7	97.7	7492.0	300683		
AAS5-1-180-B09	98.3	98.3	98.3	7594.6	332304		
AAS5-1-360-B10	97.3	97.7	97.5	7466.4	313570	360	126716
AAS5-1-360-B11	97.0	97.3	97.2	7415.5	320909		
AAS5-1-360-B12	97.3	97.7	97.5	7466.4	315889		
AAS5-1-540-B13	97.7	97.7	97.7	7492.0	282754	540	120103
AAS5-1-540-B14	98.0	97.7	97.8	7517.6	305827		
AAS5-1-540-B15	97.3	97.7	97.5	7466.4	312190		

Appendix E.2 : Calculation of the modulus of elasticity ; existing model

Standard : AS.3600 – 2009 ; Article 3.1.2

: Ng & Foster model from Concrete Institute of Australia, 2011

Modulus of elasticity : $(E_1) = \left(\rho^{1.5}\right) \times \left(0.043\sqrt{f_{cmi}}\right)$ (MPa) AS 3600 – 2009

$(E_2) = E_m = 3710\sqrt{f_{mm}} - 1280$ (MPa) Ng & Foster

Specimen : Fly ash geopolymer concrete

Specimen	Age	Density (ρ) (kg/m^3)	Compressive Strength (f_{cmi}) (MPa)	Modulus of Elasticity AS 3600 Predicted 1 (E_1) (MPa)	Modulus of Elasticity Ng & Foster Predicted 2 (E_2) (MPa)
G15-1-28	28	2297.9	22.37	22403	16267
G15-1-90	90	2289.4	27.01	24480	18001
G15-1-180	180	2282.6	31.09	26147	19406
G15-1-360	360	2278.2	33.23	26954	20106
G15-1-540	540	2275.7	33.09	26853	20061

Specimen : AAS concrete

Specimen	Age	Density (ρ) (kg/m^3)	Compressive Strength (f_{cmi}) (MPa)	Modulus of Elasticity AS 3600 Predicted 1 (E_1) (MPa)	Modulus of Elasticity Ng & Foster Predicted 2 (E_2) (MPa)
AAS5-1-28	28	2452.6	39.47	32317	22028
AAS5-1-90	90	2456.9	41.26	32822	22551
AAS5-1-180	180	2457.8	40.43	32644	22310
AAS5-1-360	360	2457.9	40.35	32748	22287
AAS5-1-540	540	2459.5	38.31	31808	21683

Appendix E.3 : Calculation of the modulus of elasticity ; AS.1012.17 – 1997

Test : Modulus of elasticity
Standard : AS.1012.17 – 1997
Specimen : Fly ash geopolymer concrete

Fly ash geopolymer ; modulus elasticity at 28 days								
Specimen	**Test**	**Test load (kN)**	**Strain**	**Defor-mation strain**	**Applied load at $50x10^{-6}$ m/m (kN)**	**Applied load at $50x10^{-6}$ m/m (MPa)**	**Modulus Elasticity (E) (MPa)**	**Modulus Elasticity (E) average (MPa)**
		(1)		**(2)**	**(3)**	**(4)**	**(5)**	
G15-1-28-B01	3	69.7388	1	0.000405	47.2081	6.3227	8500	6652
			2	0.001922	2.6104	0.3496	4803	
	4	69.9307	1	0.000677	25.0224	3.3513	9593	7690
			2	0.001613	2.3867	0.3197	5788	
	5	69.8780	1	0.000932	11.6305	1.5577	8845	7659
			2	0.001445	2.4620	0.3297	6473	
G15-1-28-B02	3		1					Failed
			2					
	4		1					Failed
			2					
	5		1					Failed
			2					
G15-1-28-B03	3	69.7038	1	0.002015	3.6072	0.4798	4474	8615
			2	0.000719	5.5476	0.7379	12757	
	4	70.2945	1	0.002137	2.0492	0.2726	4350	8894
			2	0.000702	4.4269	0.5889	13438	
	5	69.8613	1	0.002055	2.6029	0.3462	4462	8621
			2	0.000724	5.1064	0.6793	12780	

Fly ash geopolymer ; modulus elasticity at 90 days								
Specimen	**Test**	**Test load (kN)**	**Strain**	**Defor-mation strain**	**Applied load at $50x10^{-6}$ m/m (kN)**	**Applied load at $50x10^{-6}$ m/m (MPa)**	**Modulus Elasticity (E) (MPa)**	**Modulus Elasticity (E) average (MPa)**
		(1)		**(2)**	**(3)**	**(4)**	**(5)**	
G15-1-90-B04	3	93.3233	1	0.000892	6.7991	0.9075	15301	11384
			2	0.001849	2.6774	0.3574	7467	
	4	93.5683	1	0.000925	8.1129	1.0829	14561	11024
			2	0.001848	2.7224	0.3634	7486	
	5		1					Failed
			2					
G15-1-90-B05	3	93.2366	1	0.001186	4.2047	0.5536	11479	11493
			2	0.001060	14.9699	1.9711	11507	
	4	93.5484	1	0.000658	3.4051	0.4484	21688	14490
			2	0.001758	8.9631	1.1802	7292	
	5		1					Failed
			2					
G15-1-90-B06	3	92.9376	1	0.001425	4.0211	0.5313	9409	11076
			2	0.001040	6.4516	0.8524	12743	
	4	93.5382	1	0.001485	2.2401	0.2960	9326	11031
			2	0.001024	9.6501	1.2750	12736	
	5	92.7934	1	0.001297	4.3306	0.5722	10432	10291
			2	0.001303	6.5346	0.8633	10150	

Appendix E.3 : Calculation of the modulus of elasticity ; AS.1012.17 – 1997

Test : Modulus of elasticity
Standard : AS.1012.17 – 1997
Specimen : Fly ash geopolymer concrete

Fly ash geopolymer ; modulus elasticity at 180 days								
Specimen	**Test**	**Test load (kN)**	**Strain**	**Defor-mation strain**	**Applied load at $50x10^{-6}$ m/m (kN)**	**Applied load at $50x10^{-6}$ m/m (MPa)**	**Modulus Elasticity (E) (MPa)**	**Modulus Elasticity (E) average (MPa)**
		(1)		**(2)**	**(3)**	**(4)**	**(5)**	
G15-1-180-B07	3		1					Failed
			2					
	4		1					Failed
			2					
	5		1					Failed
			2					
G15-1-180-B08	3	98.8455	1	0.001031	6.6997	0.8733	12243	12855
			2	0.000964	4.4090	0.5747	13467	
	4	98.6132	1	0.001114	6.5721	0.8566	10395	12477
			2	0.000836	4.8058	0.6264	14559	
	5	98.6700	1	0.001232	5.0999	0.6647	14559	12758
			2	0.000762	6.7531	0.8802	9707	
G15-1-180-B09	3	98.4908	1	0.000812	7.7995	1.0446	15940	15916
			2	0.000848	3.8087	0.5101	15891	
	4	99.5386	1	0.000878	4.9895	0.6683	15294	16553
			2	0.000769	3.9207	0.5251	17811	
	5	98.7715	1	0.000856	3.1697	0.4245	15886	16251
			2	0.000797	6.1009	0.8171	16615	

Fly ash geopolymer ; modulus elasticity at 360 days								
Specimen	**Test**	**Test load (kN)**	**Strain**	**Defor-mation strain**	**Applied load at $50x10^{-6}$ m/m (kN)**	**Applied load at $50x10^{-6}$ m/m (MPa)**	**Modulus Elasticity (E) (MPa)**	**Modulus Elasticity (E) average (MPa)**
		(1)		**(2)**	**(3)**	**(4)**	**(5)**	
G15-1-360-B10	3	118.7008	1	0.002347	2.7251	0.3613	5728	10562
			2	0.000871	5.4981	0.7289	15395	
	4	118.5497	1	0.002432	2.7291	0.3618	8346	12836
			2	0.000907	6.5460	0.8678	17326	
	5		1					Failed
			2					
G15-1-360-B11	3	118.0911	1	0.000621	23.3275	3.0716	21834	13856
			2	0.003799	2.8678	0.3776	5879	
	4		1					Failed
			2					
	5		1					Failed
			2					
G15-1-360-B12	3	118.4462	1	0.000414	61.5273	8.1290	22451	16443
			2	0.001708	2.5087	0.3314	10436	
	4	118.6932	1	0.000397	62.2678	8.2268	22684	16778
			2	0.001726	2.4808	0.3278	10872	
	5	129.4219	1	0.001073	4.9086	0.6485	16081	18186
			2	0.000836	8.7014	1.1496	20292	

Appendix E.3 : Calculation of the modulus of elasticity ; AS.1012.17 – 1997

Test : Modulus of elasticity
Standard : AS.1012.17 – 1997
Specimen : Fly ash geopolymer concrete

Fly ash geopolymer ; modulus elasticity at 540 days								
Specimen	**Test**	**Test load (kN)**	**Strain**	**Defor-mation strain**	**Applied load at $50x10^{-6}$ m/m (kN)**	**Applied load at $50x10^{-6}$ m/m (MPa)**	**Modulus Elasticity (E) (MPa)**	**Modulus Elasticity (E) average (MPa)**
		(1)		**(2)**	**(3)**	**(4)**	**(5)**	
G15-1-540-B13	3	115.0156	1	0.001471	3.2513	0.4238	11942	12965
			2	0.001215	5.1143	0.6666	13989	
	4		1					Failed
			2					
	5		1					Failed
			2					
G15-1-540-B14	3	1149695	1	0.001805	3.6473	0.4868	11915	13253
			2	0.000975	23.4385	3.1285	14591	
	4	117.9459	1	0.001213	5.6142	0.7494	14894	15376
			2	0.001099	3.7197	0.4965	15858	
	5		1					Failed
			2					
G15-1-540-B15	3	114.2513	1	0.000467	30.3894	4.0014	26293	18258
			2	0.002058	2.4438	0.3218	10223	
	4	111.9516	1	0.000512	21.3320	2.8088	26835	17626
			2	0.002191	1.1437	0.1506	8418	
	5	114.9906	1	0.000512	22.3259	2.9397	26103	18175
			2	0.002104	1.9340	0.2547	10248	

Appendix E.3 : Calculation of the modulus of elasticity ; AS.1012.17 – 1997

Test : Modulus of elasticity
Standard : AS.1012.17 – 1997
Specimen : AAS concrete

AAS ; modulus elasticity at 28 days								
Specimen	**Test**	**Test load (kN)**	**Strain**	**Defor-mation strain**	**Applied load at $50x10^{-6}$ m/m (kN)**	**Applied load at $50x10^{-6}$ m/m (MPa)**	**Modulus Elasticity (E) (MPa)**	**Modulus Elasticity (E) average (MPa)**
		(1)		**(2)**	**(3)**	**(4)**	**(5)**	
AAS5-1-28-B01	3	121.7389	1	0.000127	86.1369	11.4580	61504	37531
			2	0.001195	5.0387	0.6703	13558	
	4	121.7866	1	0.000111	91.9876	12.2363	64982	39155
			2	0.001224	4.1651	0.5540	13327	
	5	121.8460	1	0.000111	99.9360	13.2936	47779	30552
			2	0.001223	4.3350	0.5767	13326	
AAS5-1-28-B02	3	122.4214	1	0.000847	28.2374	3.7949	15882	21779
			2	0.000589	11.4211	1.5349	27676	
	4	121.6952	1	0.000797	6.8831	0.9250	20656	23511
			2	0.000610	11.8292	1.5898	26366	
	5	122.0673	1	0.000737	8.8376	1.1877	22150	23061
			2	0.000678	10.0543	1.3512	23971	
AAS5-1-28-B03	3	121.8618	1	0.000764	9.8747	1.2871	20444	21595
			2	0.000705	7.5589	0.9852	22746	
	4	122.7330	1	0.000814	10.3760	1.3524	19169	22467
			2	0.000638	6.5043	0.8478	25765	
	5	122.7724	1	0.000736	11.7715	1.5343	21091	21264
			2	0.000745	8.4619	1.1030	21438	

AAS ; modulus elasticity at 90 days								
Specimen	**Test**	**Test load (kN)**	**Strain**	**Defor-mation strain**	**Applied load at $50x10^{-6}$ m/m (kN)**	**Applied load at $50x10^{-6}$ m/m (MPa)**	**Modulus Elasticity (E) (MPa)**	**Modulus Elasticity (E) average (MPa)**
		(1)		**(2)**	**(3)**	**(4)**	**(5)**	
AAS5-1-90-B04	3	122.2701	1	0.001133	1.7258	0.2288	14756	21163
			2	0.000424	44.4906	5.8981	27570	
	4	123.7223	1	0.001122	2.2223	0.2946	15025	20797
			2	0.000445	44.5617	5.9075	26568	
	5	123.3400	1	0.000896	6.4226	0.8514	18321	22041
			2	0.000647	7.3288	0.9716	25761	
AAS5-1-90-B05	3	123.4742	1	0.001187	9.0511	1.2081	13432	26938
			2	0.000410	14.3909	1.9208	40444	
	4	123.1855	1	0.000798	7.7314	1.0320	20602	20867
			2	0.000779	7.7652	1.0365	21133	
	5		1					Failed
			2					
AAS5-1-90-B06	3		1					Failed
			2					
	4		1					Failed
			2					
	5		1					Failed
			2					

Appendix E.3 : Calculation of the modulus of elasticity ; AS.1012.17 – 1997

Test : Modulus of elasticity
Standard : AS.1012.17 – 1997
Specimen : AAS concrete

AAS ; modulus elasticity at 180 days								
Specimen	**Test**	**Test load (kN)**	**Strain**	**Defor-mation strain**	**Applied load at $50x10^{-6}$ m/m (kN)**	**Applied load at $50x10^{-6}$ m/m (MPa)**	**Modulus Elasticity (E) (MPa)**	**Modulus Elasticity (E) average (MPa)**
		(1)		**(2)**	**(3)**	**(4)**	**(5)**	
AAS5-1-180-B07	3	127.0755	1	0.001491	3.1502	0.4234	11558	19902
			2	0.000541	23.8797	3.2093	28246	
	4	129.5205	1	0.001502	2.3275	0.3128	11773	19308
			2	0.000563	27.0525	3.6357	26844	
	5	129.2436	1	0.001463	2.3031	0.3095	12073	20023
			2	0.000587	17.4734	2.3483	27972	
AAS5-1-180-B08	3	127.7883	1	0.000989	7.7594	1.0357	17062	18321
			2	0.000889	4.7061	0.6282	19581	
	4	129.4908	1	0.001006	7.3076	0.9754	17059	18580
			2	0.000877	4.9426	0.6597	20102	
	5	129.4447	1	0.000989	6.7046	0.8949	17447	19950
			2	0.000788	5.2996	0.7074	22453	
AAS5-1-180-B09	3	129.6267	1	0.000985	5.2430	0.6904	17516	18632
			2	0.000863	7.7017	1.0141	19747	
	4	129.4219	1	0.001073	4.9083	0.6463	16026	18125
			2	0.000836	8.7014	1.1457	20223	
	5	129.1034	1	0.001134	3.9831	0.5245	15198	18044
			2	0.000796	10.7479	1.4152	20890	

AAS ; modulus elasticity at 360 days								
Specimen	**Test**	**Test load (kN)**	**Strain**	**Defor-mation strain**	**Applied load at $50x10^{-6}$ m/m (kN)**	**Applied load at $50x10^{-6}$ m/m (MPa)**	**Modulus Elasticity (E) (MPa)**	**Modulus Elasticity (E) average (MPa)**
		(1)		**(2)**	**(3)**	**(4)**	**(5)**	
AAS5-1-360-B10	3	129.6263	1	0.000499	28.2203	3.7796	30249	20371
			2	0.001670	2.6972	0.3612	10494	
	4	128.7860	1	0.000655	12.8415	1.7199	25668	19025
			2	0.001402	3.7879	0.5073	12383	
	5		1					Failed
			2					
AAS5-1-360-B11	3	128.1658	1	0.001275	7.8899	1.0640	13240	15916
			2	0.000917	8.6359	1.1646	18592	
	4	129.6062	1	0.001287	4.1159	0.5550	13680	16314
			2	0.000874	13.8287	1.8648	18948	
	5	128.9165	1	0.001221	3.8631	0.5209	14401	16662
			2	0.000885	11.7534	1.5850	18922	
AAS5-1-360-B12	3	129.4086	1	0.000578	14.6651	1.9642	29106	18743
			2	0.002026	5.7880	0.7752	8379	
	4	127.9762	1	0.000784	12.6928	1.7000	21036	16137
			2	0.001545	2.5415	0.3404	11237	
	5	128.1631	1	0.000835	9.7131	1.3009	20209	16404
			2	0.001377	3.3415	0.4475	12598	

Appendix E.3 : Calculation of the modulus of elasticity ; AS.1012.17 – 1997

Test : Modulus of elasticity
Standard : AS.1012.17 – 1997
Specimen : AAS concrete

AAS ; modulus elasticity at 540 days								
Specimen	**Test**	**Test load (kN)**	**Strain**	**Defor-mation strain**	**Applied load at $50x10^{-6}$ m/m (kN)**	**Applied load at $50x10^{-6}$ m/m (MPa)**	**Modulus Elasticity (E) (MPa)**	**Modulus Elasticity (E) average (MPa)**
		(1)		**(2)**	**(3)**	**(4)**	**(5)**	
AAS5-1-540-B13	3	117.5371	1	0.000708	17.2893	2.2013	19397	14598
			2	0.001545	2.4777	0.3155	9799	
	4	117.8046	1	0.000760	5.6857	0.7239	20106	16387
			2	0.001198	3.5821	0.4561	12668	
	5	117.8966	1	0.000691	22.2726	2.8357	21018	15507
			2	0.001666	1.1293	0.1438	9996	
AAS5-1-540-B14	3		1					Failed
			2					
	4		1					Failed
			2					
	5		1					Failed
			2					
AAS5-1-540-B15	3	117.7891	1	0.000813	8.6757	1.1046	18207	15536
			2	0.001179	3.7046	0.4717	12866	
	4	118.0764	1	0.000743	11.6487	1.4831	19553	15230
			2	0.001404	2.0862	0.2656	10907	
	5	117.5671	1	0.000830	5.5317	0.7043	18288	15824
			2	0.001144	2.7708	0.3528	13360	

Appendix F Flexural strength test results of concrete

Appendix F.1 : Flexural strength test / modulus of rupture results of fly ash geopolymer concrete

Standard : AS 1012.11 – 2000
Specimen : Fly ash geopolymer concrete
Loading rate : 1 + 0.1 MPa/min
Modulus of rupture : $f_{cf} = PL(1000) / BD^2$

Fly ash geopolymer ; flexural strength at 28 days					
Specimen ID	Max Load (N)	L (mm)	B (mm)	D (mm)	Modulus of Rupture f_{cf} (MPa)
G15-1-28-H01	13893	348.1	102.4	102.0	4.54
G15-1-28-H02	14635	350.0	100.4	99.9	5.11
G15-1-28-H03	13745	346.8	101.5	101.8	4.54
				Average	4.73
				Standard deviation	0.33

Fly ash geopolymer ; flexural strength at 56 days					
Specimen ID	Max Load (N)	L (mm)	B (mm)	D (mm)	Modulus of Rupture f_{cf} (MPa)
G15-1-56H04	15282	348.1	102.4	102.0	4.99
G15-1-56-H05	16830	350.0	100.4	99.9	5.88
G15-1-56-H06	15532	346.8	101.5	101.8	5.13
				Average	5.33
				Standard deviation	0.48

Fly ash geopolymer ; flexural strength at 90 days					
Specimen ID	Max Load (N)	L (mm)	B (mm)	D (mm)	Modulus of Rupture f_{cf} (MPa)
G15-1-90-H07	14721	349.8	99.7	101.4	5.03
G15-1-90-H08	17891	348.0	100.1	98.6	6.40
G15-1-90-H09	16958	347.9	100.1	99.9	5.91
				Average	5.78
				Standard deviation	0.69

Appendix F.1 : Flexural strength test / modulus of rupture results of fly ash geopolymer concrete

Standard : AS 1012.11 – 2000
Specimen : Fly ash geopolymer concrete
Loading rate : 1 + 0.1 MPa/min
Modulus of rupture : $f_{cf} = PL(1000) / BD^2$

Fly ash geopolymer ; flexural strength at 180 days					
Specimen ID	Max Load (N)	L (mm)	B (mm)	D (mm)	Modulus of Rupture f_{cf} (MPa)
G15-1-180-H10	18587	349.0	99.9	100.2	6.48
G15-1-180-H11	19293	348.4	100.4	99.7	6.74
G15-1-180-H12	19035	348.8	100.2	99.8	6.65
				Average	6.62
				Standard deviation	0.13

Fly ash geopolymer ; flexural strength at 360 days					
Specimen ID	Max Load (N)	L (mm)	B (mm)	D (mm)	Modulus of Rupture f_{cf} (MPa)
G15-1-360-H13	21615	346.5	100.5	101.5	7.23
G15-1-360-H14	20117	345.0	100.0	100.5	6.87
G15-1-360-H15	20417	345.8	100.3	100.9	6.91
				Average	7.01
				Standard deviation	0.20

Fly ash geopolymer ; flexural strength at 540 days					
Specimen ID	Max Load (N)	L (mm)	B (mm)	D (mm)	Modulus of Rupture f_{cf} (MPa)
G15-1-540-H16	20231	348.1	99.1	100.5	7.04
G15-1-540-H17	21127	347.1	99.7	100.0	7.36
G15-1-540-H18	20947	347.6	99.3	100.2	7.30
				Average	7.23
				Standard deviation	0.17

Appendix F.2 : Flexural strength test / modulus of rupture results of AAS concrete

Standard : AS 1012.11 – 2000
Specimen : AAS concrete
Loading rate : 1 + 0.1 MPa/min
Modulus of rupture : $f_{cf} = PL(1000) / BD^2$

AAS ; flexural strength at 28 days					
Specimen ID	Max Load (N)	L (mm)	B (mm)	D (mm)	Modulus of Rupture f_{cf} (MPa)
AAS5-1-28-H01	17727	347.0	104.0	100.0	5.91
AAS5-1-28-H02	18592	346.0	101.0	101.5	6.18
AAS5-1-28-H03	18160	346.3	103.0	100.8	6.01
				Average	6.04
				Standard deviation	0.14

AAS ; flexural strength at 56 days					
Specimen ID	Max Load (N)	L (mm)	B (mm)	D (mm)	Modulus of Rupture f_{cf} (MPa)
AAS5-1-56-H04	17372	347.0	104.0	100.0	5.80
AAS5-1-56-H05	18034	346.0	101.0	101.5	6.00
AAS5-1-56-H06	17978	346.3	103.0	100.8	5.95
				Average	5.92
				Standard deviation	0.11

AAS ; flexural strength at 90 days					
Specimen ID	Max Load (N)	L (mm)	B (mm)	D (mm)	Modulus of Rupture f_{cf} (MPa)
AAS5-1-90-H07	17242	347.5	101.8	101.5	5.72
AAS5-1-90-H08	17610	347.0	100.8	102.5	5.77
AAS5-1-90-H09	17426	346.8	104.0	100.2	5.79
				Average	5.76
				Standard deviation	0.04

Appendix F.2 : Flexural strength test / modulus of rupture results of AAS concrete

Standard : AS 1012.11 – 2000
Specimen : AAS concrete
Loading rate : 1 + 0.1 MPa/min
Modulus of rupture : $f_{cf} = PL(1000) / BD^2$

AAS ; flexural strength at 180 days					
Specimen ID	Max Load (N)	L (mm)	B (mm)	D (mm)	Modulus of Rupture f_{cf} (MPa)
AAS5-1-180-H10	15188	349.1	100.1	100.1	5.29
AAS5-1-180-H11	16439	349.7	100.2	100.0	5.74
AAS5-1-180-H12	15814	349.6	100.1	100.2	5.51
				Average	5.51
				Standard deviation	0.22

AAS ; flexural strength at 360 days					
Specimen ID	Max Load (N)	L (mm)	B (mm)	D (mm)	Modulus of Rupture f_{cf} (MPa)
AAS5-1-360-H13	14829	348.3	100.0	100.0	5.16
AAS5-1-360-H14	15618	347.5	99.5	99.3	5.54
AAS5-1-360-H15	15460	347.9	99.8	99.6	5.44
				Average	5.38
				Standard deviation	0.19

AAS ; flexural strength at 540 days					
Specimen ID	Max Load (N)	L (mm)	B (mm)	D (mm)	Modulus of Rupture f_{cf} (MPa)
AAS5-1-540-H16	15231	348.9	100.4	100.8	5.22
AAS5-1-540-H17	14621	349.4	100.0	99.6	5.15
AAS5-1-540-H18	14743	349.2	100.2	100.1	5.13
				Average	5.16
				Standard deviation	0.05

Appendix G Indirect tensile strength test results of concrete

Appendix G.1 : Indirect tensile strength test results of fly ash geopolymer concrete

Standard : AS 1012.10 – 2000
Specimen : Fly ash geopolymer concrete
Loading rate : 1.5 + 0.15 MPa/min
Modulus of rupture : T = 2000P / πLD

Fly ash geopolymer ; indirect tensile strength at 28 days						
Specimen ID	Max Load (N)	L (mm)	d_1 (mm)	d_2 (mm)	d_{avg} (mm)	Indirect tensile strength (MPa)
G15-1-28-F01	125416	283.8	145.3	151.0	148.2	1.90
G15-1-28-F02	141975	288.9	143.2	152.0	147.6	2.12
G15-1-28-F03	156339	285.0	147.3	150.9	149.1	2.34
					Average	2.12
					Standard deviation	0.22

Fly ash geopolymer ; indirect tensile strength at 56 days						
Specimen ID	Max Load (N)	L (mm)	d_1 (mm)	d_2 (mm)	d_{avg} (mm)	Indirect tensile strength (MPa)
G15-1-56-F04	143920	285.3	145.3	151.0	148.2	2.17
G15-1-56-F05	162923	286.8	143.2	152.0	147.6	2.45
G15-1-56-F06	179406	286.0	147.3	150.9	149.1	2.68
					Average	2.43
					Standard deviation	0.26

Fly ash geopolymer ; indirect tensile strength at 90 days						
Specimen ID	Max Load (N)	L (mm)	d_1 (mm)	d_2 (mm)	d_{avg} (mm)	Indirect tensile strength (MPa)
G15-1-90-F07	164890	286.3	148.2	150.1	149.2	2.46
G15-1-90-F08	190016	286.0	149.0	149.9	149.5	2.83
G15-1-90-F09	208732	285.3	149.3	149.8	149.6	3.11
					Average	2.80
					Standard deviation	0.33

Appendix G.1 : Indirect tensile strength test results of fly ash geopolymer concrete

Standard : AS 1012.10 – 2000
Specimen : Fly ash geopolymer concrete
Loading rate : 1.5 + 0.15 MPa/min
Modulus of rupture : T = 2000P / πLD

Fly ash geopolymer ; indirect tensile strength at 180 days						
Specimen ID	Max Load (N)	L (mm)	d_1 (mm)	d_2 (mm)	d_{avg} (mm)	Indirect tensile strength (MPa)
G15-1-180-F10	228794	286.7	148.2	151.0	149.6	3.40
G15-1-180-F11	218324	286.5	148.3	151.2	149.7	3.24
G15-1-180-F12	232440	286.4	148.6	150.7	149.7	3.45
					Average	3.36
					Standard deviation	0.11

Fly ash geopolymer ; indirect tensile strength at 360 days						
Specimen ID	Max Load (N)	L (mm)	d_1 (mm)	d_2 (mm)	d_{avg} (mm)	Indirect tensile strength (MPa)
G15-1-360-F13	249940	285.0	149.2	151.9	150.5	3.71
G15-1-360-F14	276013	285.3	148.3	151.5	149.9	4.11
G15-1-360-F15	245323	285.3	148.5	151.4	149.9	3.65
					Average	3.82
					Standard deviation	0.25

Fly ash geopolymer ; indirect tensile strength at 540 days						
Specimen ID	Max Load (N)	L (mm)	d_1 (mm)	d_2 (mm)	d_{avg} (mm)	Indirect tensile strength (MPa)
G15-1-540-F16	265760	285.3	150.9	151.3	151.1	3.92
G15-1-540-F17	307850	285.3	151.3	151.7	151.5	4.53
G15-1-540-F18	267025	285.7	151.7	151.5	151.6	3.93
					Average	4.13
					Standard deviation	0.35

Appendix G.1 : Indirect tensile strength test results of AAS concrete

Standard : AS 1012.10 – 2000
Specimen : AAS concrete
Loading rate : 1.5 + 0.15 MPa/min
Modulus of rupture : T = 2000P / πLD

AAS ; indirect tensile strength at 28 days						
Specimen ID	Max Load (N)	L (mm)	d_1 (mm)	d_2 (mm)	d_{avg} (mm)	Indirect tensile strength (MPa)
AAS5-1-28-F01	245697	299.0	149.0	150.0	149.5	3.50
AAS5-1-28-F02	214954	299.5	149.5	149.8	149.7	3.05
AAS5-1-28-F03	243077	300.0	149.5	150.0	149.8	3.44
					Average	3.33
					Standard deviation	0.24

AAS ; indirect tensile strength at 56 days						
Specimen ID	Max Load (N)	L (mm)	d_1 (mm)	d_2 (mm)	d_{avg} (mm)	Indirect tensile strength (MPa)
AAS5-1-28-F04	243632	299.0	149.0	150.0	149.5	3.47
AAS5-1-28-F05	213148	299.5	149.5	149.8	149.7	3.03
AAS5-1-28-F06	241034	300.0	149.5	150.0	149.8	3.42
					Average	3.30
					Standard deviation	0.24

AAS ; indirect tensile strength at 90 days						
Specimen ID	Max Load (N)	L (mm)	d_1 (mm)	d_2 (mm)	d_{avg} (mm)	Indirect tensile strength (MPa)
AAS5-1-90-F07	237984	297.5	149.5	150.3	149.9	3.40
AAS5-1-90-F08	228955	298.5	149.6	149.7	149.6	3.26
AAS5-1-90-F09	221322	299.4	150.1	150.1	150.1	3.13
					Average	3.26
					Standard deviation	0.13

Appendix G.1 : Indirect tensile strength test results of AAS concrete

Standard : AS 1012.10 – 2000
Specimen : AAS concrete
Loading rate : 1.5 + 0.15 MPa/min
Modulus of rupture : T = 2000P / πLD

AAS ; indirect tensile strength at 180 days						
Specimen ID	Max Load (N)	L (mm)	d_1 (mm)	d_2 (mm)	d_{avg} (mm)	Indirect tensile strength (MPa)
AAS5-1-180-F10	223719	300.0	149.1	149.0	149.0	3.19
AAS5-1-180-F11	245955	300.2	149.0	148.3	148.7	3.51
AAS5-1-180-F12	215866	299.5	149.3	148.7	149.0	3.08
					Average	3.26
					Standard deviation	0.22

AAS ; indirect tensile strength at 360 days						
Specimen ID	Max Load (N)	L (mm)	d_1 (mm)	d_2 (mm)	d_{avg} (mm)	Indirect tensile strength (MPa)
AAS5-1-360-F13	236584	299.0	149.4	149.2	149.3	3.37
AAS5-1-360-F14	220797	298.1	149.3	149.3	149.3	3.16
AAS5-1-360-F15	216637	298.6	149.3	149.5	149.4	3.09
					Average	3.21
					Standard deviation	0.15

AAS ; indirect tensile strength at 540 days						
Specimen ID	Max Load (N)	L (mm)	d_1 (mm)	d_2 (mm)	d_{avg} (mm)	Indirect tensile strength (MPa)
AAS5-1-540-F16	231650	298.6	149.4	149.4	149.4	3.31
AAS5-1-540-F17	217528	298.5	149.6	149.4	149.5	3.10
AAS5-1-540-F18	216309	298.3	150.0	149.6	149.8	3.08
					Average	3.16
					Standard deviation	0.12

Appendix H Porosity test results of concrete

Appendix H.1 : Porosity test results of fly ash geopolymer concrete

Standard : ASTM C642-97
Specimen : Fly ash geopolymer concrete
Note : Use the same specimens (total 3 specimens) from 28 to 540 days

Porosity at 28 days				
Specimen ID	Mass of surface dry sample (C) gram	Mass of oven-dried sample (A) gram	Apparent mass of sample in water (D) gram	Volume of permeable pore space (voids) (%)
G15-1-G01	3732.9	3480.1	2014.2	14.71
G15-1-G02	3731.7	3486.2	2024.3	14.38
G15-1-G03	3763.4	3516.7	2031.6	14.25
			Average	14.44
			Standard deviation	0.24

Porosity at 56 days				
Specimen ID	Mass of surface dry sample (C) gram	Mass of oven-dried sample (A) gram	Apparent mass of sample in water (D) gram	Volume of permeable pore space (voids) (%)
G15-1-G01	3721.6	3477.1	2011.5	14.30
G15-1-G02	3730.5	3483.7	2022.4	14.45
G15-1-G03	3762.3	3512.1	2028.7	14.43
			Average	14.39
			Standard deviation	0.08

Porosity at 90 days				
Specimen ID	Mass of surface dry sample (C) gram	Mass of oven-dried sample (A) gram	Apparent mass of sample in water (D) gram	Volume of permeable pore space (voids) (%)
G15-1-G01	3716.1	3466.4	2002.6	14.57
G15-1-G02	3722.0	3476.3	2012.0	14.37
G15-1-G03	3748.4	3504.2	2018.8	14.12
			Average	14.35
			Standard deviation	0.23

Appendix H1 : Porosity test results of fly ash geopolymer concrete

Standard : ASTM C642-97
Specimen : Fly ash geopolymer concrete
Note : Use the same specimens (total 3 specimens) from 28 to 540 days

Porosity at 180 days				
Specimen ID	Mass of surface dry sample (C) gram	Mass of oven-dried sample (A) gram	Apparent mass of sample in water (D) gram	Volume of permeable pore space (voids) (%)
G15-1-G01	3703.6	3455.1	1998.4	14.57
G15-1-G02	3710.3	3465.8	2008.6	14.37
G15-1-G03	3739.5	3499.5	2015.8	13.92
			Average	14.29
			Standard deviation	0.33

Porosity at 360 days				
Specimen ID	Mass of surface dry sample (C) gram	Mass of oven-dried sample (A) gram	Apparent mass of sample in water (D) gram	Volume of permeable pore space (voids) (%)
G15-1-G01	3696.2	3454.1	1996.9	14.25
G15-1-G02	3703.3	3465.4	2006.9	14.02
G15-1-G03	3732.4	3494.6	2014.4	13.84
			Average	14.04
			Standard deviation	0.17

Porosity at 540 days				
Specimen ID	Mass of surface dry sample (C) gram	Mass of oven-dried sample (A) gram	Apparent mass of sample in water (D) gram	Volume of permeable pore space (voids) (%)
G15-1-G01	3695.8	3451.7	1992.9	14.33
G15-1-G02	3697.8	3463.6	2002.9	13.82
G15-1-G03	3726.4	3490.2	2010.4	13.76
			Average	13.97
			Standard deviation	0.31

Appendix H2 : Porosity test results of AAS concrete

Standard : ASTM C642-97
Specimen : AAS concrete
Note : Use the same specimens (total 3 specimens) from 28 to 540 days

Porosity at 28 days				
Specimen ID	Mass of surface dry sample (C) gram	Mass of oven-dried sample (A) gram	Apparent mass of sample in water (D) gram	Volume of permeable pore space (voids) (%)
AAS5-1-G01	3794.1	3665.4	2163.7	7.89
AAS5-1-G02	3780.2	3646.2	2148.0	8.21
AAS5-1-G03	3813.6	3675.8	2162.2	8.34
			Average	8.15
			Standard deviation	0.23

Porosity at 56 days				
Specimen ID	Mass of surface dry sample (C) gram	Mass of oven-dried sample (A) gram	Apparent mass of sample in water (D) gram	Volume of permeable pore space (voids) (%)
AAS5-1-G01	3796.3	3660.7	2164.6	8.31
AAS5-1-G02	3783.7	3641.7	2148.8	8.69
AAS5-1-G03	3814.2	3672.9	2163.8	8.56
			Average	8.52
			Standard deviation	0.19

Porosity at 90 days				
Specimen ID	Mass of surface dry sample (C) gram	Mass of oven-dried sample (A) gram	Apparent mass of sample in water (D) gram	Volume of permeable pore space (voids) (%)
AAS5-1-G01	3803.0	3658.2	2166.5	8.85
AAS5-1-G02	3788.6	3637.7	2152.4	9.22
AAS5-1-G03	3816.1	3666.4	2165.4	9.07
			Average	9.05
			Standard deviation	0.18

Appendix H2 : Porosity test results of AAS concrete

Standard : ASTM C642-97
Specimen : AAS concrete
Note : Use the same specimens (total 3 specimens) from 28 to 540 days

Porosity at 180 days				
Specimen ID	Mass of surface dry sample (C) gram	Mass of oven-dried sample (A) gram	Apparent mass of sample in water (D) gram	Volume of permeable pore space (voids) (%)
AAS5-1-G01	3803.8	3642.2	2168.9	9.88
AAS5-1-G02	3790.1	3634.5	2153.1	9.51
AAS5-1-G03	3818.0	3664.7	2166.0	9.28
			Average	9.56
			Standard deviation	0.62

Porosity at 360 days				
Specimen ID	Mass of surface dry sample (C) gram	Mass of oven-dried sample (A) gram	Apparent mass of sample in water (D) gram	Volume of permeable pore space (voids) (%)
AAS5-1-G01	3804.4	3644.4	2173.0	9.81
AAS5-1-G02	3786.9	3630.8	2155.6	9.57
AAS5-1-G03	3821.4	3657.7	2171.7	9.92
			Average	9.77
			Standard deviation	0.18

Porosity at 540 days				
Specimen ID	Mass of surface dry sample (C) gram	Mass of oven-dried sample (A) gram	Apparent mass of sample in water (D) gram	Volume of permeable pore space (voids) (%)
AAS5-1-G01	3806.1	3629.2	2175.3	10.85
AAS5-1-G02	3792.8	3615.9	2156.9	10.81
AAS5-1-G03	3821.8	3649.7	2172.8	10.44
			Average	10.70
			Standard deviation	0.26

Appendix I Water absorption test results of concrete

Appendix I.1 : Water absorption test results of fly ash geopolymer

Standard : AS 1012.21 – 1999
Specimen : Fly ash geopolymer
Note : Use the same specimens (total 4 specimens) from 28 to 540 days

Fly ash	**28 days**					**56 days**			
Geopolymer	**1**	**2**	**3**	**4**		**1**	**2**	**3**	**4**
M_1 (gram)	823.0	825.8	834.0	818.9		820.6	822.2	828.9	816.8
M_{2i} (gram)	888.5	889.7	896.8	882.6		880.8	882.9	890.5	875.4
A_i (%)	7.96	7.73	7.53	7.78		7.33	7.38	7.43	7.16
Average A_i (%)	**7.75**					**7.33**			

Fly ash	**90 days**					**180 days**			
Geopolymer	**1**	**2**	**3**	**4**		**1**	**2**	**3**	**4**
M_1 (gram)	823.1	825.2	832.1	819.6		821.5	824.0	832.0	819.0
M_{2i} (gram)	883.8	885.2	891.4	878.0		879.6	881.2	888.1	874.5
A_i (%)	7.37	7.27	7.14	7.12		7.08	6.94	6.75	6.79
Average A_i (%)	**7.22**					**6.89**			

Fly ash	**360 days**					**540 days**			
Geopolymer	**1**	**2**	**3**	**4**		**1**	**2**	**3**	**4**
M_1 (gram)	821.0	823.6	830.4	825.0		778.1	780.7	787.1	782.0
M_{2i} (gram)	877.8	879.5	886.4	881.3		832.2	833.8	840.3	835.4
A_i (%)	6.93	6.79	6.74	6.82		6.95	6.81	6.76	6.84
Average A_i (%)	**6.82**					**6.84**			

Note :

M_1 : the mass of the specimen from the oven
M_{2i} : the mass of the specimen after immersion in SSD condition
A_i : the immersed absorption of the specimen

Appendix I.2 : Water absorption test results of AAS

Standard : AS 1012.21 – 1999
Specimen : Alkali Activated Slag (AAS)
Note : Use the same specimens (total 4 specimens) from 28 to 540 days

AAS	28 days					56 days			
	1	2	3	4		1	2	3	4
M_1 (gram)	861.0	856.5	863.5	861.2		859.9	855.4	862.8	860.2
M_{2i} (gram)	901.1	897.8	905.7	902.5		901.6	898.6	905.9	903.0
A_i (%)	4.65	4.83	4.89	4.80		4.85	5.05	4.99	4.97
Average A_i (%)	**4.79**					**4.97**			

AAS	90 days					180 days			
	1	2	3	4		1	2	3	4
M_1 (gram)	859.3	854.5	861.3	859.2		859.2	854.2	861.2	859.0
M_{2i} (gram)	902.6	898.9	907.3	903.9		903.4	899.1	907.5	904.3
A_i (%)	5.04	5.20	5.34	5.20		5.14	5.26	5.37	5.27
Average A_i (%)	**5.20**					**5.26**			

AAS	360 days					540 days			
	1	2	3	4		1	2	3	4
M_1 (gram)	859.0	854.1	861.0	858.9		858.5	853.9	860.7	858.6
M_{2i} (gram)	903.5	899.4	907.6	904.5		903.7	899.6	907.7	904.7
A_i (%)	5.18	5.31	5.41	5.31		5.26	5.35	5.46	5.37
Average A_i (%)	**5.30**					**5.36**			

Note :

M_1 : the mass of the specimen from the oven
M_{2i} : the mass of the specimen after immersion in SSD condition
A_i : the immersed absorption of the specimen

Appendix J Ultrasonic Pulse Velocity (UPV) test results of concrete

Appendix J.1 : UPV test results of fly ash geopolymer

Specimen : Fly ash geopolymer
Equipment : TICO ultrasonic instrument / Proceq
Calibration : t = 20.5 μs ; v = 9760 m/s ; Test length = 10 cm
Note : Use the same specimens (total 3 specimens) from 28 to 540 days

Fly ash geopolymer ; Velocity at 28 days						
Test	**Sample No. 1**		**Sample No. 2**		**Sample No. 3**	
	Time (μs)	**Velocity (m/s)**	**Time (μs)**	**Velocity (m/s)**	**Time (μs)**	**Velocity (m/s)**
1	33.9	2810	35.2	2700	32.7	2910
2	33.3	2860	33.5	2840	33.9	2810
3	33.4	2850	32.8	2900	32.9	2890
4	33.8	2810	34.9	2720	32.3	2940
5	34.7	2730	34.0	2800	31.8	2990
6	36.0	2640	34.1	2790	34.1	2790
7	36.3	2620	34.1	2790	32.3	2940
8	36.3	2620	34.3	2770	32.3	2940
9	35.9	2640	34.3	2770	32.7	2910
10	36.6	2590	34.1	2790	32.3	2940
11	35.3	2690	36.3	2620	33.9	2810
12	34.3	2770	38.2	2490	30.4	3110
13	34.4	2770	33.1	2870	30.4	3110
14	33.4	2850	34.3	2770	30.4	3110
15	33.3	2860	34.8	2730	35.2	2700
Mean	**34.7**	**2740.7**	**34.5**	**2756.7**	**32.5**	**2926.7**
Std. dev	1.23	99.46	1.32	100.40	1.41	120.93

Fly ash geopolymer ; Velocity at 56 days						
Test	**Sample No. 1**		**Sample No. 2**		**Sample No. 3**	
	Time (μs)	**Velocity (m/s)**	**Time (μs)**	**Velocity (m/s)**	**Time (μs)**	**Velocity (m/s)**
1	40.4	2840	36.3	2760	38.7	2580
2	39.4	2540	35.6	2816	35.1	2850
3	42.6	2350	34.6	2890	36.3	2760
4	40.5	2470	40.2	2490	33.8	2960
5	39.4	2540	34.5	2900	33.8	2960
6	38.0	2630	37.2	2690	37.5	2670
7	38.5	2600	35.1	2850	35.8	2790
8	39.5	2530	34.7	2880	40.7	2460
9	38.5	2600	36.2	2760	37.4	2670
10	37.6	2660	36.7	2730	33.6	2980
11	36.4	2750	29.4	3400	28.7	3480
12	32.3	3100	32.1	3120	29.5	3390
13	35.6	2810	28.6	3500	29.4	3400
14	32.7	3060	29.0	3450	28.7	3480
15	30.6	3270	28.7	3480	29.5	3390
Mean	**37.5**	**2716.7**	**33.9**	**2981.1**	**33.9**	**2988.0**
Std. dev	3.37	257.26	3.56	326.13	3.95	352.18

Appendix J.1 : UPV test results of fly ash geopolymer

Specimen : Fly ash geopolymer
Equipment : TICO ultrasonic instrument / Proceq
Calibration : t = 20.5 μs ; v = 9760 m/s ; Test length = 10 cm
Note : Use the same specimens (total 3 specimens) from 28 to 540 days

Fly ash geopolymer ; Velocity at 90 days						
Test	**Sample No. 1**		**Sample No. 2**		**Sample No. 3**	
	Time (μs)	**Velocity (m/s)**	**Time (μs)**	**Velocity (m/s)**	**Time (μs)**	**Velocity (m/s)**
1	33.9	2950	33.1	3020	32.4	3090
2	34.2	2930	32.8	3050	34.0	2950
3	33.3	3010	32.7	3060	32.3	3100
4	32.2	3110	32.2	3110	33.3	3010
5	33.0	3030	32.1	3120	31.9	3140
6	33.8	2960	36.8	2720	36.3	2750
7	34.3	2920	36.0	2780	34.8	2870
8	33.1	3020	34.3	2920	35.5	2810
9	33.3	3010	35.4	2820	35.3	2830
10	33.5	2990	34.0	2950	36.3	2750
11	29.3	3410	33.3	3010	33.3	3010
12	28.4	3520	33.1	3020	30.1	3320
13	28.8	3470	33.3	3010	30.7	3260
14	29.6	3380	32.8	3050	31.0	3230
15	27.5	3630	32.0	3130	30.8	3250
Mean	**31.9**	**3156.0**	**33.6**	**2984.7**	**33.2**	**3024.7**
Std. dev	2.41	248.53	1.45	124.66	2.10	193.39

Fly ash geopolymer ; Velocity at 180 days						
Test	**Sample No. 1**		**Sample No. 2**		**Sample No. 3**	
	Time (μs)	**Velocity (m/s)**	**Time (μs)**	**Velocity (m/s)**	**Time (μs)**	**Velocity (m/s)**
1	28.6	3200	34.3	2920	34.3	2920
2	32.2	3110	33.4	2990	33.9	3000
3	30.7	3260	34.5	2900	34.2	2920
4	30.4	3290	34.2	2920	33.7	2970
5	32.6	3070	34.2	2920	32.2	3110
6	32.4	3090	36.6	2730	35.9	2790
7	33.1	3020	36.7	2730	33.8	2960
8	29.5	3390	36.2	2760	34.3	2920
9	30.7	3260	36.0	2780	33.6	2980
10	31.0	3230	36.5	2740	33.2	3010
11	29.6	3380	33.2	3010	28.7	3480
12	32.3	3100	32.2	3110	28.6	3500
13	31.2	3210	31.7	3160	27.7	3610
14	30.7	3260	30.7	3260	27.7	3610
15	31.3	3200	31.4	3190	28.4	3520
Mean	**31.1**	**3204.7**	**34.1**	**2941.3**	**32.0**	**3153.3**
Std. dev	1.27	109.41	2.01	176.99	2.89	295.29

Appendix J.1 : UPV test results of fly ash geopolymer

Specimen : Fly ash geopolymer
Equipment : TICO ultrasonic instrument / Proceq
Calibration : t = 20.5 μs ; v = 9760 m/s ; Test length = 10 cm
Note : Use the same specimens (total 3 specimens) from 28 to 540 days

Fly ash geopolymer ; Velocity at 360 days						
Test	**Sample No. 1**		**Sample No. 2**		**Sample No. 3**	
	Time (μs)	**Velocity (m/s)**	**Time (μs)**	**Velocity (m/s)**	**Time (μs)**	**Velocity (m/s)**
1	29.5	3390	29.2	3420	29.5	3390
2	29.8	3360	28.9	3460	29.0	3450
3	28.6	3600	28.8	3470	29.6	3380
4	29.2	3420	28.4	3520	28.7	3490
5	28.4	3520	27.9	3580	29.1	3430
6	33.8	2960	31.2	3210	29.5	3390
7	33.4	3000	33.3	3010	29.4	3400
8	33.2	3020	31.2	3210	28.3	3530
9	32.4	3090	31.9	3140	29.2	3420
10	32.4	3090	31.7	3160	29.2	3420
11	31.3	3200	28.0	3570	28.6	3500
12	31.2	3210	28.2	3540	27.9	3580
13	30.9	3240	28.0	3570	26.9	3720
14	31.3	3200	27.3	3660	27.8	3590
15	29.9	3350	27.3	3660	28.8	3480
Mean	**31.0**	**3243.3**	**29.4**	**3412.0**	**28.8**	**3478.0**
Std. dev	1.76	193.23	1.91	209.70	0.76	94.81

Fly ash geopolymer ; Velocity at 540 days						
Test	**Sample No. 1**		**Sample No. 2**		**Sample No. 3**	
	Time (μs)	**Velocity (m/s)**	**Time (μs)**	**Velocity (m/s)**	**Time (μs)**	**Velocity (m/s)**
1	31.3	3200	29.9	3350	27.2	3670
2	27.8	3590	30.5	3270	26.4	3780
3	28.5	3510	30.5	3270	26.8	3730
4	27.9	3580	29.6	3380	26.8	3730
5	28.3	3530	30.5	3270	27.1	3690
6	31.6	3170	29.3	3410	31.7	3160
7	32.4	3080	29.3	3410	31.4	3190
8	32.6	3070	28.9	3470	31.9	3140
9	31.2	3200	29.1	3430	32.3	3100
10	31.2	3200	29.4	3400	32.6	3070
11	27.0	3710	27.4	3640	27.0	3700
12	27.3	3670	27.3	3670	26.7	3740
13	26.7	3760	27.7	3610	26.2	3810
14	26.4	3790	27.4	3640	26.3	3800
15	25.6	3910	27.5	3630	26.3	3800
Mean	**29.1**	**3464.7**	**29.0**	**3456.7**	**28.4**	**3540.7**
Std. dev	2.39	284.07	1.20	145.54	2.61	302.88

Appendix J.2 : UPV test results of AAS

Specimen : Alkali Activated Slag (AAS)
Equipment : TICO ultrasonic instrument / Proceq
Calibration : t = 20.5 μs ; v = 9760 m/s ; Test length = 10 cm
Note : Use the same specimens (total 3 specimens) from 28 to 540 days

AAS ; Velocity at 28 days						
Test	**Sample No. 1**		**Sample No. 2**		**Sample No. 3**	
	Time (μs)	**Velocity (m/s)**	**Time (μs)**	**Velocity (m/s)**	**Time (μs)**	**Velocity (m/s)**
1	25.0	4000	31.6	3170	26.5	3770
2	25.6	3910	27.1	3690	27.2	3680
3	25.4	3940	29.4	3400	25.1	3980
4	24.0	4170	27.5	3640	25.8	3880
5	26.7	3750	26.8	3730	25.6	3910
6	25.6	3910	23.8	4200	25.6	3910
7	24.5	4080	25.6	3910	25.0	4000
8	24.8	4030	26.4	3790	25.6	3910
9	25.4	3940	23.5	4260	25.6	3910
10	25.1	3980	26.6	3760	25.4	3940
11	24.8	4030	27.5	3640	24.9	4020
12	25.6	3940	23.5	4260	25.7	3890
13	25.1	3980	25.8	3880	25.8	3880
14	24.9	4020	24.4	4100	25.4	3940
15	25.3	3950	23.7	4220	25.4	3940
Mean	**25.2**	**3975.3**	**26.2**	**3843.3**	**25.6**	**3904.0**
Std. dev	0.61	93.03	2.31	323.68	0.58	85.34

AAS ; Velocity at 56 days						
Test	**Sample No. 1**		**Sample No. 2**		**Sample No. 3**	
	Time (μs)	**Velocity (m/s)**	**Time (μs)**	**Velocity (m/s)**	**Time (μs)**	**Velocity (m/s)**
1	29.8	3360	28.3	3530	25.7	3890
2	26.3	3800	24.9	4020	25.2	3970
3	24.6	4070	24.4	4100	25.6	3910
4	27.3	3660	24.6	4070	25.3	3950
5	24.9	4020	24.4	4100	25.6	3910
6	24.9	4020	27.1	3690	26.0	3850
7	25.2	3970	26.5	3770	24.8	4030
8	24.6	4070	26.6	3760	24.6	4070
9	25.4	3940	24.6	4070	24.9	4020
10	25.3	3950	25.6	3910	24.5	4080
11	27.4	3650	25.3	3950	38.6	2590
12	24.9	4020	24.4	4100	27.8	3600
13	24.5	4080	24.5	4080	29.5	3390
14	25.1	3980	24.2	4130	28.6	3200
15	24.6	4070	24.6	4070	28.3	3530
Mean	**25.7**	**3910.7**	**25.3**	**3956.7**	**27.0**	**3732.7**
Std. dev	1.47	206.62	1.24	184.84	3.58	411.95

Appendix J.2 : UPV test results of AAS

Specimen : Alkali Activated Slag (AAS)
Equipment : TICO ultrasonic instrument / Proceq
Calibration : t = 20.5 μs ; v = 9760 m/s ; Test length = 10 cm
Note : Use the same specimens (total 3 specimens) from 28 to 540 days

AAS ; Velocity at 90 days						
Test	Sample No. 1		Sample No. 2		Sample No. 3	
	Time (μs)	Velocity (m/s)	Time (μs)	Velocity (m/s)	Time (μs)	Velocity (m/s)
1	27.4	3650	29.7	3370	27.5	3640
2	26.2	3820	27.8	3600	26.0	3850
3	28.4	3520	25.5	3920	27.2	3680
4	27.8	3600	30.3	3300	27.8	3600
5	26.7	3750	25.2	3970	25.5	3920
6	27.2	3680	25.5	3920	27.0	3700
7	26.7	3750	27.4	3650	26.6	3760
8	26.4	3750	25.3	3950	25.6	3910
9	26.7	3750	25.2	3970	27.1	3690
10	27.2	3680	27.7	3610	26.2	3820
11	28.2	3550	25.7	3890	26.2	3820
12	26.1	3830	25.2	3970	27.1	3690
13	26.4	3790	26.7	3790	25.7	3890
14	26.7	3750	28.5	3510	25.0	4000
15	25.8	3880	25.1	3980	27.1	3690
Mean	**26.9**	**3716.7**	**26.7**	**3760.0**	**26.5**	**3777.3**
Std. dev	0.76	102.93	1.75	234.86	0.83	118.95

AAS ; Velocity at 180 days						
Test	Sample No. 1		Sample No. 2		Sample No. 3	
	Time (μs)	Velocity (m/s)	Time (μs)	Velocity (m/s)	Time (μs)	Velocity (m/s)
1	27.0	3700	28.4	3520	27.4	3650
2	26.0	3840	27.4	3650	26.1	3830
3	27.8	3600	28.0	3570	28.1	3560
4	27.1	3690	27.1	3690	28.0	3570
5	26.3	3800	25.9	3860	26.1	3830
6	27.3	3660	28.1	3560	28.1	3560
7	28.7	3480	27.4	3650	28.3	3530
8	25.5	3920	26.0	3840	26.1	3830
9	27.5	3630	26.3	3800	27.5	3630
10	26.2	3810	27.4	3650	28.3	3530
11	25.9	3860	26.0	3810	26.7	3740
12	26.4	3780	26.4	3780	27.8	3600
13	26.2	3810	26.1	3830	27.7	3610
14	26.4	3780	25.9	3860	27.3	3660
15	26.1	3830	26.3	3800	28.1	3560
Mean	**26.7**	**3746.0**	**26.8**	**3724.7**	**27.4**	**3646.0**
Std. dev	0.85	116.73	0.88	117.59	0.81	109.92

Appendix J.2 : UPV test results of AAS

Specimen : Alkali Activated Slag (AAS)
Equipment : TICO ultrasonic instrument / Proceq
Calibration : t = 20.5 μs ; v = 9760 m/s ; Test length = 10 cm
Note : Use the same specimens (total 3 specimens) from 28 to 540 days

AAS ; Velocity at 360 days						
Test	**Sample No. 1**		**Sample No. 2**		**Sample No. 3**	
	Time (μs)	**Velocity (m/s)**	**Time (μs)**	**Velocity (m/s)**	**Time (μs)**	**Velocity (m/s)**
1	27.8	3600	25.8	3870	27.7	3610
2	28.2	3540	26.9	3710	27.9	3580
3	27.4	3650	26.3	3800	28.1	3560
4	27.4	3650	26.0	3840	28.6	3500
5	27.2	3670	26.1	3830	28.7	3480
6	25.7	3890	25.6	3900	26.3	3800
7	25.4	3930	26.2	3810	26.0	3840
8	26.1	3830	26.2	3810	27.0	3700
9	25.8	3870	26.0	3840	26.0	3840
10	25.4	3930	26.0	3840	26.1	3830
11	28.4	3520	27.3	3660	28.7	3480
12	29.4	3400	27.9	3580	28.4	3520
13	29.0	3450	27.8	3600	29.2	3420
14	26.9	3710	28.0	3570	28.3	3530
15	26.6	3760	27.9	3580	28.4	3520
Mean	**27.1**	**3693.3**	**26.7**	**3749.3**	**27.7**	**3614.0**
Std. dev	1.29	172.61	0.87	119.43	1.11	147.88

AAS ; Velocity at 540 days						
Test	**Sample No. 1**		**Sample No. 2**		**Sample No. 3**	
	Time (μs)	**Velocity (m/s)**	**Time (μs)**	**Velocity (m/s)**	**Time (μs)**	**Velocity (m/s)**
1	27.2	3670	27.1	3690	27.4	3650
2	28.4	3520	26.4	3790	27.7	3610
3	27.8	3600	27.5	3640	27.1	3690
4	27.4	3650	25.8	3880	27.9	3580
5	29.0	3450	26.7	3790	28.1	3560
6	28.7	3480	27.1	3690	28.3	3530
7	28.4	3520	27.8	3600	27.7	3610
8	29.8	3360	27.4	3650	28.3	3530
9	28.2	3540	25.5	3930	25.9	3850
10	28.2	3550	26.7	3790	27.8	3600
11	28.4	3520	28.4	3520	27.2	3680
12	27.4	3650	28.5	3510	28.4	3520
13	28.7	3480	26.1	3830	28.0	3570
14	28.2	3550	26.9	3710	27.9	3580
15	27.3	3660	27.3	3660	29.5	3390
Mean	**28.2**	**3546.7**	**27.0**	**3712.0**	**27.8**	**3596.7**
Std. dev	0.71	87.64	0.86	122.72	0.78	101.11

Appendix K Water permeability test results of concrete

Appendix K.1 : Water permeability test results of fly ash geopolymer

Equipment : Autoclam Permeability System / Amphora
Note : Use the same specimens (total 2 specimens) from 28 to 540 days

Fly ash geopolymer ; Water Permeability at 28 days					
Time (min)	**√time (√min)**	**Volume (μL)**	**WPI ($m^3/\sqrt{min}$)**	**Volume (μL)**	**WPI ($m^3/\sqrt{min}$)**
		SAMPLE NO. 1		**SAMPLE NO. 2**	
0	0.00	4	---	2	---
1	1.00	1365	13.650	1102	11.016
2	1.41	2121	14.999	1707	12.074
3	1.73	2604	15.037	2621	15.133
4	2.00	2965	14.824	2456	12.280
5	2.24	3254	14.553	2715	12.142
6	2.45	3483	14.221	2926	11.944
7	2.65	3680	13.909	3107	11.744
8	2.83	3847	13.600	3256	11.512
9	3.00	3997	13.322	3389	11.297
10	3.16	4122	13.036	3502	11.076
11	3.32	4232	12.758	3606	10.873
12	3.46	4335	12.515	3690	10.653
13	3.61	4428	12.281	3768	10.451
14	3.74	4505	12.039	3836	10.253
15	3.87	4589	11.849	3898	10.064
	Average 5 – 15 min		**13.099**		**10.987**

Fly ash geopolymer ; Water Permeability at 56 days					
Time (min)	**√time (√min)**	**Volume (μL)**	**WPI ($m^3/\sqrt{min}$)**	**Volume (μL)**	**WPI ($m^3/\sqrt{min}$)**
		SAMPLE NO. 1		**SAMPLE NO. 2**	
0	0.00	2	---	6	---
1	1.00	1583	15.826	1353	13.528
2	1.41	2322	16.417	2037	14.402
3	1.73	2755	15.907	2447	14.129
4	2.00	3229	16.145	2721	13.604
5	2.24	3296	14.741	2903	12.984
6	2.45	3484	14.225	3040	12.411
7	2.65	3649	13.792	3162	11.950
8	2.83	3780	13.364	3257	11.514
9	3.00	3891	12.970	3340	11.134
10	3.16	3995	12.633	3412	10.791
11	3.32	4092	12.339	3485	10.506
12	3.46	4187	12.086	3549	10.246
13	3.61	4267	11.835	3599	9.981
14	3.74	4338	11.593	3652	9.760
15	3.87	4412	11.391	3705	9.566
	Average 5 – 15 min		**12.815**		**10.786**

WPI = Water Permeability Index

Appendix K.1 : Water permeability test results of fly ash geopolymer

Equipment : Autoclam Permeability System / Amphora
Note : Use the same specimens (total 2 specimens) from 28 to 540 days

Fly ash geopolymer ; Water Permeability at 90 days					
Time (min)	**√time (√min)**	**Volume (μL)**	**WPI ($m^3/\sqrt{min}$)**	**Volume (μL)**	**WPI ($m^3/\sqrt{min}$)**
		SAMPLE NO. 1		**SAMPLE NO. 2**	
0	0.00	4	---	2	---
1	1.00	1225	12.250	968	9.679
2	1.41	1927	13.624	1561	11.040
3	1.73	2397	13.840	1987	11.471
4	2.00	2768	13.838	2314	11.570
5	2.24	3058	13.674	2578	11.530
6	2.45	3301	13.475	2798	11.422
7	2.65	3508	13.261	2981	11.269
8	2.83	3687	13.035	3140	11.103
9	3.00	3847	12.825	3279	10.931
10	3.16	3987	12.607	3400	10.753
11	3.32	4120	12.422	3510	10.583
12	3.46	4236	12.227	3611	10.424
13	3.61	4347	12.057	3700	10.263
14	3.74	4447	11.886	3781	10.105
15	3.87	4541	11.726	3862	9.971
	Average 5 – 15 min		**12.654**		**10.682**

Fly ash geopolymer ; Water Permeability at 180 days					
Time (min)	**√time (√min)**	**Volume (μL)**	**WPI ($m^3/\sqrt{min}$)**	**Volume (μL)**	**WPI ($m^3/\sqrt{min}$)**
		SAMPLE NO. 1		**SAMPLE NO. 2**	
0	0.00	2	---	2	---
1	1.00	867	8.670	862	8.618
2	1.41	1373	9.705	1343	9.498
3	1.73	1796	10.366	1697	9.795
4	2.00	2181	10.905	1998	9.990
5	2.24	2534	11.330	2270	10.153
6	2.45	2867	11.702	2522	10.297
7	2.65	3171	11.985	2756	10.418
8	2.83	3458	12.224	2977	10.524
9	3.00	3735	12.450	3184	10.613
10	3.16	3990	12.617	3382	10.694
11	3.32	4244	12.795	3571	10.766
12	3.46	4485	12.947	3753	10.834
13	3.61	4722	13.096	3929	10.896
14	3.74	4953	13.237	4091	10.932
15	3.87	5177	13.366	4250	10.974
	Average 5 – 15 min		**12.523**		**10.695**

WPI = Water Permeability Index

Appendix K.1 : Water permeability test results of fly ash geopolymer

Specimen : Fly ash geopolymer
Equipment : Autoclam Permeability System / Amphora
Note : Use the same specimens (total 2 specimens) from 28 to 540 days

Fly ash geopolymer ; Water Permeability at 360 days					
Time (min)	**√time (√min)**	**Volume (μL)**	**WPI ($m^3/\sqrt{min}$)**	**Volume (μL)**	**WPI ($m^3/\sqrt{min}$)**
		SAMPLE NO. 1		**SAMPLE NO. 2**	
0	0.00	4	---	2	---
1	1.00	920	9.200	811	8.107
2	1.41	1472	10.409	1255	8.874
3	1.73	1930	11.142	1616	9.327
4	2.00	2321	11.607	1928	9.641
5	2.24	2672	11.948	2211	9.888
6	2.45	2985	12.187	2472	10.092
7	2.65	3272	12.368	2713	10.255
8	2.83	3534	12.496	2946	10.416
9	3.00	3782	12.605	3163	10.544
10	3.16	4014	12.694	3378	10.684
11	3.32	4232	12.760	3580	10.793
12	3.46	4444	12.829	3767	10.874
13	3.61	4643	12.876	3954	10.967
14	3.74	4836	12.923	4137	11.058
15	3.87	5018	12.957	4307	11.120
	Average 5 – 15 min		**12.604**		**10.680**

Fly ash geopolymer ; Water Permeability at 540 days					
Time (min)	**√time (√min)**	**Volume (μL)**	**WPI ($m^3/\sqrt{min}$)**	**Volume (μL)**	**WPI ($m^3/\sqrt{min}$)**
		SAMPLE NO. 1		**SAMPLE NO. 2**	
0	0.00	2	---	4	---
1	1.00	835	8.353	699	6.989
2	1.41	1381	9.766	1142	8.073
3	1.73	1819	10.503	1502	8.673
4	2.00	2201	11.006	1829	9.144
5	2.24	2547	11.390	2120	9.482
6	2.45	2885	11.778	2393	9.769
7	2.65	3184	12.033	2661	10.057
8	2.83	3461	12.237	2903	10.264
9	3.00	3725	12.416	3139	10.463
10	3.16	3970	12.556	3366	10.645
11	3.32	4204	12.675	3579	10.790
12	3.46	4430	12.788	3782	10.918
13	3.61	4648	12.891	3978	11.032
14	3.74	4859	12.986	4170	11.144
15	3.87	5062	13.070	4351	11.235
	Average 5 – 15 min		**12.543**		**10.632**

WPI = Water Permeability Index

Appendix K.2 : Water permeability test results of AAS

Specimen : Alkali Activated Slag (AAS)
Equipment : Autoclam Permeability System / Amphora
Note : Use the same specimens (total 2 specimens) from 28 to 540 days

AAS ; Water Permeability at 28 days					
Time (min)	**√time (√min)**	**Volume (μL)**	**WPI ($m^3/\sqrt{min}$)**	**Volume (μL)**	**WPI ($m^3/\sqrt{min}$)**
		SAMPLE NO. 1		**SAMPLE NO. 2**	
0	0.00	2	---	2	---
1	1.00	412	4.120	424	4.240
2	1.41	658	4.653	684	4.837
3	1.73	852	4.919	878	5.069
4	2.00	1022	5.110	1030	5.150
5	2.24	1176	5.259	1156	5.170
6	2.45	1316	5.373	1258	5.136
7	2.65	1446	5.465	1350	5.103
8	2.83	1568	5.544	1428	5.049
9	3.00	1684	5.613	1498	4.993
10	3.16	1792	5.667	1560	4.933
11	3.32	1900	5.729	1620	4.884
12	3.46	2000	5.774	1672	4.827
13	3.61	2106	5.841	1722	4.776
14	3.74	2202	5.885	1764	4.714
15	3.87	2294	5.923	1806	4.663
	Average 5 – 15 min		**5.681**		**4.908**

AAS ; Water Permeability at 56 days					
Time (min)	**√time (√min)**	**Volume (μL)**	**WPI ($m^3/\sqrt{min}$)**	**Volume (μL)**	**WPI ($m^3/\sqrt{min}$)**
		SAMPLE NO. 1		**SAMPLE NO. 2**	
0	0.00	4	---	2	---
1	1.00	416	4.160	452	4.520
2	1.41	670	4.738	750	5.303
3	1.73	880	5.081	988	5.704
4	2.00	1068	5.340	1170	5.850
5	2.24	1230	5.501	1316	5.885
6	2.45	1378	5.626	1440	5.879
7	2.65	1512	5.715	1548	5.851
8	2.83	1642	5.805	1648	5.827
9	3.00	1766	5.887	1740	5.800
10	3.16	1888	5.970	1820	5.755
11	3.32	2000	6.030	1894	5.711
12	3.46	2108	6.085	1964	5.670
13	3.61	2218	6.152	2030	5.630
14	3.74	2318	6.195	2092	5.591
15	3.87	2420	6.248	2150	5.551
	Average 5 – 15 min		**5.971**		**5.726**

WPI = Water Permeability Index

Appendix K.2 : Water permeability test results of AAS

Specimen : Alkali Activated Slag (AAS)
Equipment : Autoclam Permeability System / Amphora
Note : Use the same specimens (total 2 specimens) from 28 to 540 days

AAS ; Water Permeability at 90 days					
Time (min)	**√time (√min)**	**Volume (μL)**	**WPI ($m^3/\sqrt{min}$)**	**Volume (μL)**	**WPI ($m^3/\sqrt{min}$)**
		SAMPLE NO. 1		**SAMPLE NO. 2**	
0	0.00	4	---	4	---
1	1.00	450	4.500	464	4.640
2	1.41	728	5.148	746	5.275
3	1.73	944	5.450	968	5.589
4	2.00	1128	5.640	1162	5.810
5	2.24	1296	5.796	1332	5.957
6	2.45	1448	5.911	1486	6.067
7	2.65	1582	5.979	1618	6.115
8	2.83	1714	6.060	1738	6.145
9	3.00	1840	6.133	1844	6.147
10	3.16	1960	6.198	1934	6.116
11	3.32	2072	6.247	2012	6.066
12	3.46	2180	6.293	2084	6.016
13	3.61	2286	6.340	2144	5.946
14	3.74	2386	6.377	2202	5.885
15	3.87	2488	6.424	2254	5.820
	Average 5 – 15 min		**6.196**		**6.032**

AAS ; Water Permeability at 180 days					
Time (min)	**√time (√min)**	**Volume (μL)**	**WPI ($m^3/\sqrt{min}$)**	**Volume (μL)**	**WPI ($m^3/\sqrt{min}$)**
		SAMPLE NO. 1		**SAMPLE NO. 2**	
0	0.00	2	---	4	---
1	1.00	474	4.740	458	4.580
2	1.41	760	5.374	738	5.218
3	1.73	994	5.739	958	5.531
4	2.00	1192	5.960	1150	5.750
5	2.24	1374	6.145	1316	5.885
6	2.45	1534	6.263	1464	5.977
7	2.65	1684	6.365	1598	6.040
8	2.83	1822	6.442	1730	6.116
9	3.00	1950	6.500	1852	6.173
10	3.16	2068	6.540	1970	6.230
11	3.32	2184	6.585	2082	6.277
12	3.46	2290	6.611	2194	6.334
13	3.61	2392	6.634	2298	6.374
14	3.74	2492	6.660	2402	6.420
15	3.87	2578	6.656	2500	6.455
	Average 5 – 15 min		**6.526**		**6.240**

WPI = Water Permeability Index

Appendix K.2 : Water permeability test results of AAS

Specimen : Alkali Activated Slag (AAS)
Equipment : Autoclam Permeability System / Amphora
Note : Use the same specimens (total 2 specimens) from 28 to 540 days

AAS ; Water Permeability at 360 days					
Time (min)	**√time (√min)**	**Volume (μL)**	**WPI ($m^3/\sqrt{min}$)**	**Volume (μL)**	**WPI ($m^3/\sqrt{min}$)**
		SAMPLE NO. 1		**SAMPLE NO. 2**	
0	0.00	4	---	2	---
1	1.00	478	4.780	474	4.740
2	1.41	768	5.431	768	5.431
3	1.73	1008	5.820	1002	5.785
4	2.00	1216	6.080	1206	6.030
5	2.24	1398	6.252	1388	6.207
6	2.45	1562	6.377	1548	6.320
7	2.65	1722	6.509	1704	6.441
8	2.83	1874	6.626	1846	6.527
9	3.00	2016	6.720	1986	6.620
10	3.16	2156	6.818	2118	6.698
11	3.32	2292	6.911	2244	6.766
12	3.46	2422	6.992	2370	6.842
13	3.61	2540	7.045	2488	6.900
14	3.74	2662	7.114	2606	6.965
15	3.87	2774	7.162	2716	7.013
	Average 5 – 15 min		**6.827**		**6.709**

AAS ; Water Permeability at 540 days					
Time (min)	**√time (√min)**	**Volume (μL)**	**WPI ($m^3/\sqrt{min}$)**	**Volume (μL)**	**WPI ($m^3/\sqrt{min}$)**
		SAMPLE NO. 1		**SAMPLE NO. 2**	
0	0.00	4	---	4	---
1	1.00	606	6.060	592	5.920
2	1.41	966	6.831	948	6.703
3	1.73	1250	7.217	1226	7.078
4	2.00	1500	7.500	1466	7.330
5	2.24	1712	7.656	1674	7.486
6	2.45	1906	7.781	1862	7.602
7	2.65	2086	7.884	2028	7.665
8	2.83	2250	7.955	2184	7.722
9	3.00	2408	8.027	2318	7.727
10	3.16	2550	8.064	2438	7.710
11	3.32	2688	8.105	2542	7.664
12	3.46	2816	8.129	2634	7.604
13	3.61	2938	8.149	2718	7.538
14	3.74	3048	8.146	2788	7.451
15	3.87	3156	8.149	2856	7.374
	Average 5 – 15 min		**8.039**		**7.606**

WPI = Water Permeability Index